Universidade de Aveiro Departamento de Engenharia Mecânica
Ano 2016

CARLOS HENRIQUE LAURO

ESTUDO DO MICRO-CORTE NO ACABAMENTO DE UM BIOMATERIAL DE DIFÍCIL USINABILIDADE

STUDY OF MICRO-CUTTING IN THE FINISHING OF A DIFFICULT-TO-CUT BIOMATERIAL

Universidade de Aveiro Departamento de Engenharia Mecânica
Ano 2016

CARLOS HENRIQUE LAURO

ESTUDO DO MICRO-CORTE NO ACABAMENTO DE UM BIOMATERIAL DE DIFÍCIL USINABILIDADE

MICRO-CUTTING STUDY IN THE FINISHING OF A DIFFICULT-TO-CUT BIOMATERIAL

Tese apresentada à Universidade de Aveiro para cumprimento dos requisitos necessários à obtenção do grau de Doutor em Engenharia Mecânica, realizada sob a orientação científica do Doutor João Paulo Davim Tavares da Silva, Professor Associado com Agregação do Departamento de Engenharia Mecânica da Universidade de Aveiro e coorientação científica do Doutor Lincoln Cardoso Brandão, Professor Associado II do Departamento de Engenharia Mecânica da Universidade Federal de São João del Rei

Apoio financeiro da Coordenação de Aperfeiçoamento de Pessoas do Ensino Superior (CAPES) - Brasil.

Dedico este trabalho ao meu pai, Luiz Antônio.

o júri

presidente

Prof. Doutor Vasile Staicu
Professor Catedrático do Departamento de Matemática da Universidade de Aveiro

Prof. Doutor António Paulo Monteiro Baptista
Professor Associado com Agregação Aposentado da Faculdade de Engenharia da Universidade do Porto

Prof. Doutor João Paulo Davim Tavares da Silva
Professor Associado com Agregação do Departamento de Engenharia Mecânica da Universidade de Aveiro (orientador)

Prof. Doutor Pedro Alexandre Rodrigues Carvalho Rosa
Professor Associado do Instituto Superior Técnico da Universidade de Lisboa

Prof. Doutor Ricardo José Alves de Sousa
Professor Auxiliar do Departamento de Engenharia Mecânica da Universidade de Aveiro

Prof. Doutor Francisco José Gomes da Silva
Professsor Adjunto do Instituto Superior de Engenharia do Porto

agradecimentos

Pela acolhida, à Universidade de Aveiro e seu Departamento de Engenharia Mecânica e o Centro de Tecnologia Mecânica e Automação (TEMA)

Pela ajuda as atividades acadêmicas e de adaptação, sempre com grande afeto, aos bolsistas, docentes e técnicos da Universidade de Aveiro, Departamento de Engenharia Mecânica, Departamento de Engenharia de Materiais e Cerâmica e Departamento de Línguas e Culturas. Sem nomes, para não esquecer de citar alguém.

Por toda a ajuda e compartilhamento de todo o conhecimento aos orientadores Dr. João Paulo Davim e Dr. Lincoln Cardoso Brandão.

Por toda a dedicação aos ensaios e pelos risos, ao Eng. Antônio Festas.

Por autorizar e ajudar nos ensaios eletroquímicos, ao Prof. Dr. Alysson Bueno e o acadêmico Eng. Sérgio Ribeiro Filho. Pelas revisões linguísticas dos artigos e capítulos de livros, ao Dr. Diego Carou.

Por todo o incentivo, aos Profs. Juan Rubio (UFMG), Alessandro Roger (EESC-USP) e Márcio Bacci (UFU) pela ajuda a iniciar esta caminhada. Igualmente aos amigos e professores da UFSJ e IFET Juiz de Fora.

Pela amizade e momentos de descontração, aos amigos que passaram pelo MACTRIB, Ulisses, Telles, Luís Pinho, Celestino, Manuel, Pedro Gaspar, Pedro Cunha, Carlos, Renato, José, Bruno, Rui, Marco, e como os bolsistas brasileiros Paulo e Daniel e suas esposas Fabiane e Juliana.

Por toda generosidade prestada através do auxílio técnico prestado, as Drª Maria Cláudia Brito e Drª Fernanda Albuquerque.

Pela doação da liga de titânio, à empresa TiFast S.R.L. da Itália, em pessoa do Eng. Dr. Marco Costanzi.

Pelo auxílio técnico e financeiro a aquisição das ferramentas, à Sandvik Portugal, em especial a Engª. Dulce Neves.

Pelo fornecimento do termopar, à PCE Instruments da Espanha, em pessoa do Sr. Sergio Lopéz.

Pela concretização do sonho, à Coordenação de Aperfeiçoamento de Pessoa de Ensino Superior (CAPES) do Ministério da Educação do Brasil pelo fornecimento da bolsa de doutorado em âmbito do Programa Ciência sem Fronteiras, especialmente ao Sr. Silvio dos Santos Salles, Sr. Lucas Guimarães de Medeiros Srª Denise Regina Maria Dias pela assessoria.

Por fim, por ter segurado tamanha saudade no coração, a minha mãe, irmãs, sobrinho, tios e primos.

palavras-chave

Micro-corte, acabamento, biomaterial, difícil usinabilidade, alta velocidade de corte, sustentabilidade, corrosão.

resumo

A microusinagem está se tornando um processo de usinagem amplamente usado em indústrias ou pesquisas acadêmicas, pois este processo é uma opção para a miniaturização que apresenta bons resultados. Embora o processo de microusinagem apresente grandes vantagens, existem ainda lacunas há serem preenchidas ou o desenvolvimento de novas aplicações, principalmente para área médica. Este estudo investigou o uso do micro-corte com altas velocidades de corte no acabamento da liga de titânio Ti-6Al-7Nb, para fins de aplicações dentárias. A eficiência desse processo foi analisada através da análise da corrosão dos componentes em *in vitro* testes. Os resultados indicaram que essa técnica pode beneficiar a eficiência dos componentes dentários.

keywords Micro-cutting, finishing, biomaterial, difficult-to-cut, high speed machining, sustainable, corrosion.

abstract The micromachining is becoming a machining process widely used in the industries or academic researchers, because this process is an option to miniaturization that presents good results. In spite of micromachining process presents great advantages, there are still gaps to be filled or discovery of new applications, mainly for the medical applications. This study investigated the use of the micro-cutting with high speed machining in the finishing of the Ti-6Al-7Nb titanium alloy, for purposes of dental applications. The efficiency of this process was analyses through the corrosion analysis of the components in *in vitro* test. The results of experiments indicated that this technique can benefit for the dental components.

CONTENTS

LIST OF FIGURES

LIST OF TABLES

NOMENCLATURE AND SYMBOLS

AI	Artificial Intelligence
AISI	American Iron and Steel Institute
ANOVA	Analysis of Variance
a_p	Depth of cut
CB	Chip-breaker
CNC	Computer Numerical Control
ºC/s	Degree Celsius per second
ETTC	Technical Committee of European Titanium
f	Feed rate
F_C	Cutting force
F_T	Thrust force
F_x	Cutting force component in the direction X (dynamometer reference)
F_y	Cutting force component in the direction Y (dynamometer reference)
F_z	Cutting force component in the direction Z (dynamometer reference)
HSM	High Speed machining
Hz	Hertz (frequency unit)
I/O	Input and output
L_{Rake}	Length of rake plane for the numerical tests
L_{Relief}	Length of relief plane for the numerical tests
LSM	Least Square Method
mm	Millimetre (length unit)
MRR	Material removal rate
N	Newton (force unit)
R_a	Arithmetic average roughness
r_e	Cutting edge radius
rpm	Revolutions per minute
RSM	Response Surface Methodology
R_z	Maximum height of profile
s	Second (time unit)
SBF	Simulated body fluid

UHSM	Ultra-High Speed Machining
VI	Virtual Instrumentation
α	Relief angle
γ	Rake angle
λs	Inclination angle

CHAPTER 1 – INTRODUCTION

The competitive market requires that industries offer services and products with high quality, low price, and as quickly as possible, which makes every day arise new necessities. To attend these necessities, in some time, is need develop new materials and several formats that require of the manufacturer industry develops production techniques that are reliable and economic. As another processes, the machining goes by great evolution, both machines (displacements, precision…) or tools (materials, coatings, geometries…) and operations (milling, turning, grinding…), but to evolution requires many studies to determine the optimal conditions to avoid losses in the production process.

Nowadays, a niche market very explored is the miniaturization of devices and components. The miniaturization has become an important technique for several industrial sectors such as micro-electromechanical systems, micro-sensor systems, micro-electronics, smart communication systems, and biomedical devices (Penchev *et al.*, 2016). The evaluation of this technique, oldest restrict in the wristwatches parts (Masuzawa, 2000), allowed the improvement of many devices, to name a few, likes pressure transducers (Starr *et al.*, 2015). The importance of miniaturization for industry can be understood observing the evolution of the precision in machining. Thus, the standard precision in machining has been evolving increased notably since 1930's (10 μm), lower than 1 μm in the 1980's (Taniguchi, 1983), to the present in 1 nm (Zhang *et al.*, 2014).

The micromachining is a miniaturization technique that arouses certain interest that is the reason why increased the number of paper published in the last years, according to Câmara *et al.* (2012). However, the micromachining requires great attention, such as wear control, referencing tool, size effect, ploughing effect, and others. Saedon *et al.* (2012) cited the disinterest of some investigators in the application of micro-milling due to difficulty in measurement and facilities available. The comparison between the micromachining and the conventional machining processes is not recommended. The reason is because the uncut chip

thickness is on the same order as the material grain size, so the workpiece material cannot be assumed as homogeneous and isotropic (Klocke, Gerschwiler and Abouridouane, 2009).

Ng *et al.* (2006) also affirmed that in micro and nano scale cutting, the edge radius influences the specific cutting energy, being the tool edge geometry the major cause of the size-effect. The relationship between edge radius, feed rate and spindle speed can result in the "cutting" with chip or without chip (ploughing), which the boundary is known as a minimum chip thickness (Afazov *et al.*, 2013). According to Yun *et al.* (2011), it occurs when the uncut chip thickness is greater than the minimum chip thickness avoiding the ploughing effect. The determination of the minimum chip thickness ratio to the cutting edge radius is essential in micromachining in order to avoid or minimize the ploughing effect and achieve a desired material removal (Aramcharoen and Mativenga, 2009).

However, the micro-machined surface presents great results of the surface integrity. Palani, Natarajan and Chellamalai (2013) have worked with micro-turning in tungsten electrode with 0.3 mm diameter and Polycrystalline Diamond (PCD) single point tool as the cutting tool, the surface roughness, Ra, obtained were between 0.029 and 0.58 µm and used speed spindle of 1,000, 1,100 and 1,200. In the micro-milling of AISI H13 steel, Lauro *et al*. (2014) observed a great quality in the micro-machined surface, values of R_z surface roughness between 0.489 and 2.267. Furthermore, the burr in the micro-milling of AISI H13 steel had a shot length (Lauro *et al.*, 2016).

Observing the great quality of the machined surface, the usage of the micro-cutting can provide great advanced in the manufacturing of components that require high accuracy and control of the surface machined, regardless of size. An example of these components are the used in the bioapplications, which require great control in the manufacturing, such as lower surface roughness and burr. This control is important especially in biocomponents that are manufactured in titanium and its alloys.

Jaffery and Mativenga (2009) cited the titanium alloys have high strength, corrosion resistance, fatigue endurance, and biocompatibility. The authors comment that machining is highly expensive because they have poor machinability. Thus, the optimization of the parameters of influence is greater significance for the industry. In their paper, they developed

a wear map for turning the Ti-6Al-4V titanium alloy. The hardness turning require more specific cutting forces than in conventional turning.

According to Trent and Wright (2000), the machinability is a quality or propriety of material that can often be measured in terms of the numbers of components produced per hour. The costs of machining the component or the quality of the finish are critical on a surface quality. However, a material may have good machinability by one criterion, but poor machinability by another, because a different type of operation is being carried out - turning versus milling - or when the tool material is changed. The machinability may be assessed by one or more of the criteria, such as, tool life, limiting rate of metal removal, cutting forces, surface finish and chip shape.

1.1. Objective

The micromachining is a process that has many gaps, mainly in the micro-turning. However, the micromachining provides a great surface quality that is required in biocomponents. Thus, the authors decided to study the advantage and the disadvantage of the usage of the micro-cutting in the finishing operation of biocomponents in titanium alloy, mainly in the dental applications. The reason is to prolong the life, reducing the pain, discomfort, trouble, and avoiding future chirurgic to change the implant, as well as, reduce the cost that become more accessible without causing danger to patients.

In this regard, the Ti-6Al-7Nb titanium alloy was used due to advantage in health issues. As it is a titanium alloy with few studies, the first step was the analysis the mechanical behaviour of this biomaterial in the orthogonal micro-cutting. Furthermore, the usage of the machining sustainable techniques was studied in the micro-cutting of the Ti-6Al-7Nb titanium alloy to obtain the great quality of the micro-machined surface.

In the next steep, the cutting forces, vibration and surface roughness were monitored to understand the behaviour of the micro-cutting as the finishing operation in the biocomponents in different size scales. To evaluate the efficient of the micro-cutting as finishing operation, the manufacturing intelligent technique were employed to define the optimum and worse condition that were used to manufacture workpiece base on dental

application. These workpieces were used *in vitro* tests to analyse the influence of the micro-cutting in the biocorrosion.

1.2. Justification

Nowadays, the health issues have been debated widely to improve the quality of live for the global population that is increasingly living longer and older. The engineering and medicine require there is a necessity for development of alternatives to treat an increasing health issues, such as burden of trauma, congenital abnormalities and degenerative diseases, which human body needs exceed the ability to auto-regenerate due to the original tissue integrity be seriously damaged (Chen and Liu, 2016).

For the bone tissue engineering, the development or improvement of new materials for orthopaedics' reconstruction and implants can eliminate the risk of disease and infection when compared with the auto/allo bone grafts technique. It is because the material and the applied coating are modulated to avoid such sequels and serve as a scaffolding for the growth of the responsive host cells (Burg, Porter and Kellam, 2000).

The replacing the teeth can be presented as another example of significance of development or improvement of the material to serve the health issues. The absence of one or more teeth, seen the Figure 1.1, represents a harm the physical, psychological health and social relationships of the patient due to the imbalance of the bite and the musculature of neighbouring regions that causes problems chewing, speech and pain in the temporomandibular joint and esthetical loss (Barreiros *et al.*, 2011).

Generally, the correction of the dentition is realized by removal dental prosthesis, dentures. According to Att and Stappert (2003), this treatment was the first chosen for centuries, but the dissatisfaction is high, 50% of all complete denture wearers, because the dental prosthesis relies on the residual alveolar ridge and mucosa for support and retention, besides they difficult to consume certain types of food. The authors reported the dissatisfaction of a patient who has trouble eating, talking and embarrassment to meet friends and colleagues. Thus, the use of dental prosthesis requires great attention professional to be well planned and executed to avoid the possibility serious problems to the patient (Silva *et al.*, 2011).

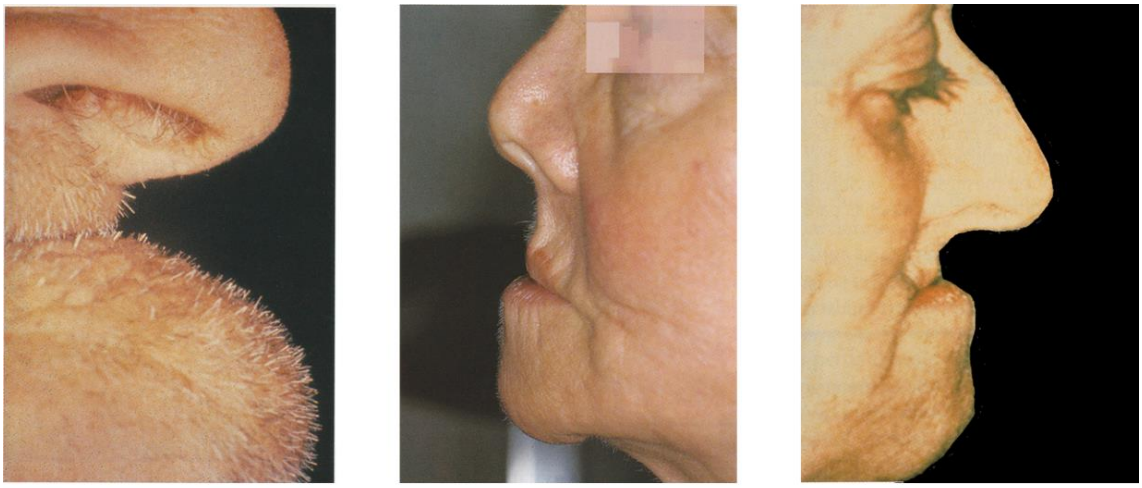

a) Loss of bone height can lead to close bite

b) Loss bone in patient that wears denture for more than 15 year

c) Complete basal bone loss with most of the nasal pine

Figure 1.1 – Examples of damage due to absence of teeth (Misch, 2009).

The implant dentistry, Figure 1.2, is the unique technique that able to offer normal contour, function, comfort, aesthetics, speech, and health for the patient, independently of the atrophy, disease, or injury of the stomatognathic system (Misch, 2014). However, this technique requires the use of the materials that presents an essential characteristic, the biocompatibility. Biocompatibility is the capacity of a material adapt itself to specified application and should not cause inflammatory reaction, allergic, immune, toxic, mutagen, or carcinogenic reactions (Hisbergues, Vendeville and Vendeville, 2009).

Figure 1.2 – Examples of the implants dentistry (Misch, 2014).

1.3. Reading guide

To investigate the behaviour of the Ti-6Al-7Nb titanium alloy, as biomaterial, in the finishing micro-cutting process, was developed a work programme employing reviews and experimental analysis, Figure 1.3. The relevance of each analysis and composition of this work was defined as follows:

CHAPTER 1 – Introduction: this chapter presents a brief script about micro-cutting, the objectives and reason to develop this work.

CHAPTER 2 – Characteristics of the machined and micro-machined surface: this chapter presents a brief review about the main characteristics of the machined surface. This section was developed to determine the emphasis in the improvement of quality micro-cutting.

CHAPTER 3 – Monitoring and signal processing in the machining and micromachining processes: this chapter describes the machining processes and the acquired data treatment used in this study. The reason is that some phenomena in the machining processes, micro or conventional, are identified during the cutting, which can facilitate the comprehension of the results obtained.

CHAPTER 4 – Statistical and Artificial Intelligence for the understanding of the micro-cutting: this chapter presents a brief review about the statistical an Artificial Intelligence techniques employed in the modelling and optimization of the machining processes. This chapter was developed to understand and improve responses obtained in the micro-cutting operation.

CHAPTER 5 – Material and methods: this chapter describes and justified the equipment, cutting tools, and analysis employed in the micro-machined surface study.

CHAPTER 6 – Preliminary analysis of the behaviour of the biomaterial in the micro-cutting: this chapter presents a description of preliminaries analysis in the micro-cutting. The results of preliminaries tests appointed the determination of the micro-cutting parameters and the monitoring and processing techniques to observe the phenomena.

Furthermore, to characterize the micro-surface, the sustainable technique of machining was employed and the surface integrity was analysed via FEM.

CHAPTER 7 – The micro-cutting in the finishing operation of biomaterial: In this chapter presents a dynamic analysis of the finishing micro-cutting operation. The analysis employed the oblique micro-cutting with parameters based on results of the Chapter 6.

CHAPTER 8 – Corrosion behaviour of micro-machined surface in the dental applications: In this chapter is presented the evaluation of the micro-machined surface employing the optimum and worse conditions. This evaluation was developed through the *in vitro* tests for the workpieces with similar geometry of dental implants.

CHAPTER 9 – Conclusions: In this chapter is presented the conclusions about the usage of the micro-cutting in the finishing operation in materials of poor machinability.

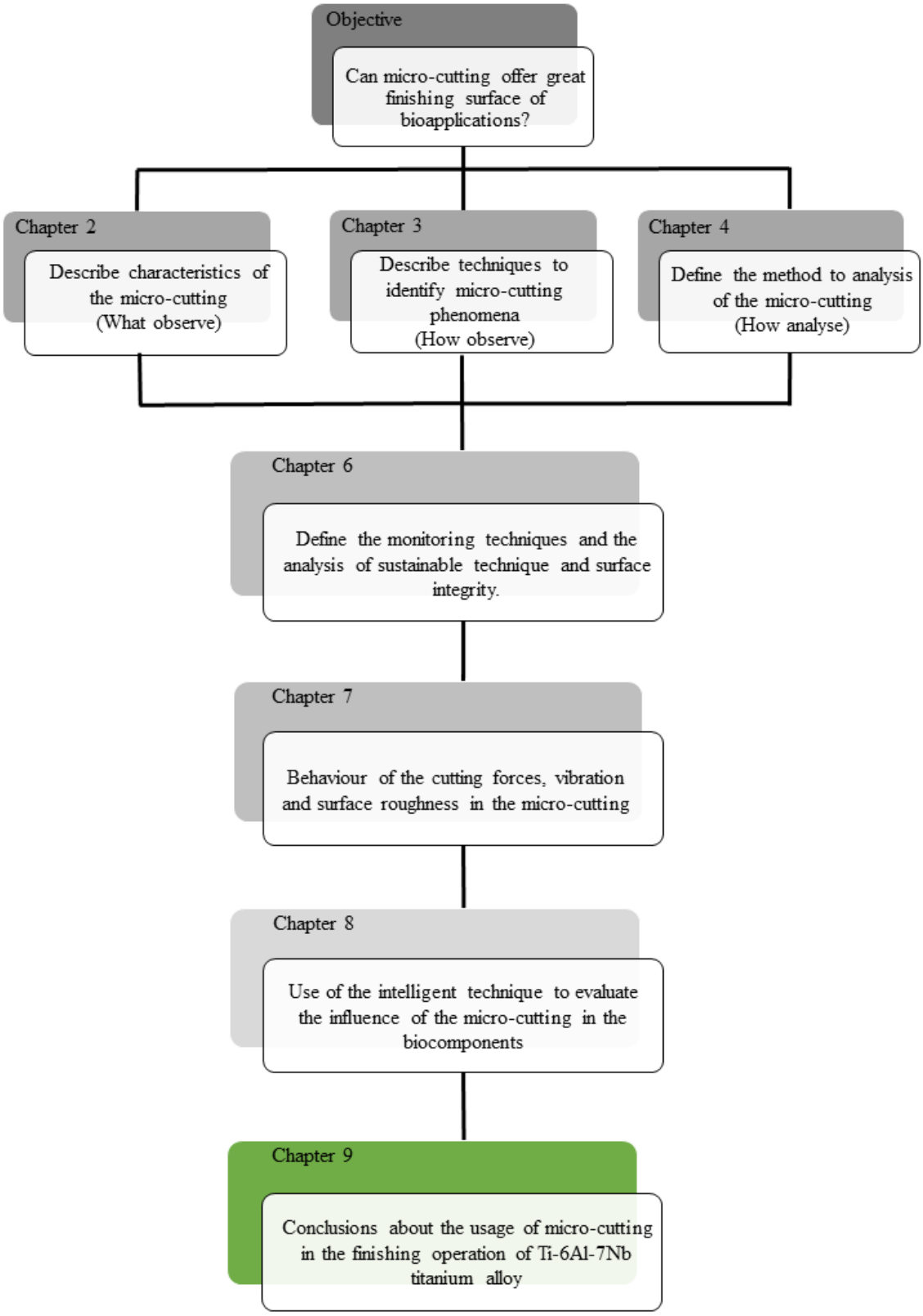

Figure 1.3 – Work programme to investigate the micro-cutting finishing in material with poor machinability.

CHAPTER 2 – CHARACTERISTICS OF THE MACHINED AND MICRO-MACHINED SURFACE

This chapter was developed to indicate the phenomena in machining and micro-machining processes and indicate the responses that should be improved. Portions of this chapter has similarity with:

- LAURO, C. H. *et al*. Quality in the Machining Characteristics and Techniques to Obtain Good Results. in DAVIM, J. P. (Ed.). Manufacturing Engineering: New Research. Hauppauge. Nova Science Publishers, 2015.

- LAURO, C. H. *et al*. Surface integrity in the micromachining: a review. Journal: Review on Advanced Material Science. Vol. 40, 2015, p. 227 – 234.

- LAURO, C. H. *et al*. Finite Element Method in Machining Processes: A Review. in DAVIM, J. P. (Ed.). Modern Manufacturing Engineering Materials Forming, Machining and Tribology. Heidelberg. Springer International Publishing, 2015.

2.1. Introduction

The mechanical components quality should be controlled in all manufacture process, because some parameters in process such as roughness, geometric errors, white layer, and others are essential to ensure a great performance of mechanic components. In finishing process, this control is generally more attentive. Surface finish is one of indicators for the quality control of machining operations directly linked to cutting process conditions (cutting parameters, tool, workpiece material, cooling system, occurring phenomena, machine-tool, and others) (García-Plaza *et al.*, 2013).

An example is the quality of the dies and moulds that directly affect the quality of the produced parts. Moulds used for injection moulding lenses or dies used for precision forging of automotive drive train components need high quality (Altan, Blaine and Yen, 2001).

The goal of quality in engineering is to make products that are robust with respect to all noise factors and the most important stage in the design of an experiment lies in the selection of control factors (Asiltürk and Akkuş, 2011). The developments of new tools through materials, coasting and/or geometry, for example the wiper tools, or procedures, as the use of High Speed Machining, are several researches objects.

Bouzakis, Aichouh and Efstathiou (2003) studied the milling with ball end tools aiming to understand the chip formation mechanisms, the cutting force, the tool deflections, and achieve low roughness values. Tang *et al*. (2009) studied the stability limits of high-speed finishing in end milling of the steel with 0.45% of Carbon, hardness of 24 HR_C, and the spindle speed between 5,000 to 17,000 rpm. Souto-Lebel *et al.* (2011) investigated the defect size distribution induced by ball-end finishing milling in the AISI 4150 with cutting speed of 300 m/min.

According to Suresh *et al.* (2013), the hard turning is used in semi-finishing and finishing in the automobile industry (transmission shafts, axles and engine components), and the aircraft industry (flap gears, landing struts, and aerospace engine components). It can be justified as hard turning when the finishing of gear components is around 60% of reduction in machining time than grinding process. It is the reason that has as trend to replace the grinding process with the turning process to directly rough and finish in the machining of hardened bearing components prior to superfinishing.

2.2. Surface Integrity

Surface Integrity (SI) is important to safety critical industries (as aerospace) or critical to the economics of the processes (as forging dies, plastic moulds, and press tools). The influence of each parameter needs to be known, together with interactions, in order to allow at least, a "pseudo-optimisation" of SI. The parameters, tools, and operation selection are very important on the machining (Axinte and Dewes, 2002).

The constant need for improved the surface integrity and enhanced functional performance of manufactured components has long acted as a driving force in the development of new production methods and high performance manufacturing technologies. Today, new capabilities in machining processes and high precision engineering have enabled the

miniaturization of manufacture of some components. This in turn has required the use of advanced surface characterization methods to assess the nature of the alterations produced in very thin layers of the machined surface (Jawahir *et al.*, 2011).

Ginting and Nouari (2009) researched the surface integrity on the milling of Ti-6242S titanium alloy using uncoated and CVD-coated carbide tools. They found R_a values produced by the uncoated carbide and the CVD-coated carbide tools range from 0.39 to 0.72 μm and from 0.43 to 0.69 μm, respectively.

2.2.1. Surface roughness.

Between the many methods to quantify the surface integrity, the surface roughness is a method widely used and considered as the primary indicator of the quality of the surface finish (Ulutan and Özel, 2011). The surface roughness can be influenced for all parameters and phenomena that occur during the cutting. A set of parameters of influence surface roughness is diagrammatically displayed in the Figure 2.1 (Benardos and Vosniakos, 2003).

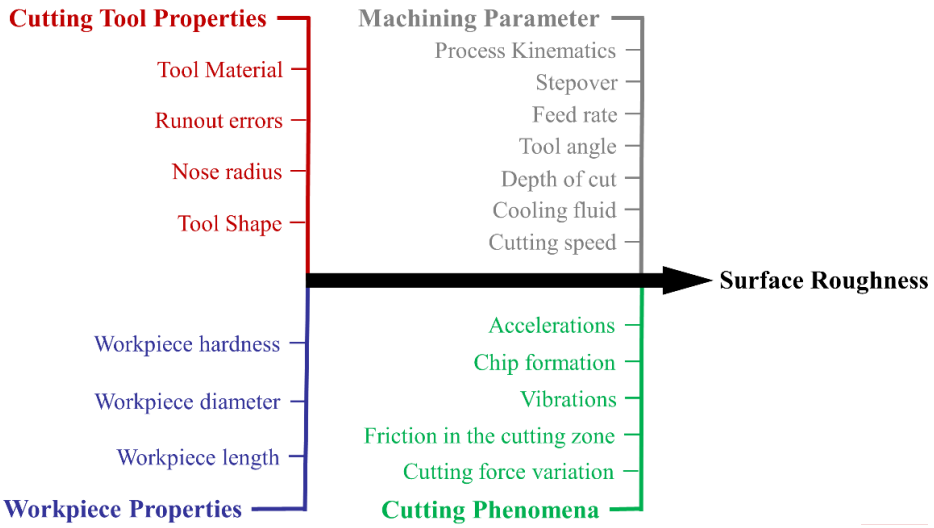

Figure 2.1 – Fishbone diagram with the parameters that affect surface roughness (Benardos and Vosniakos, 2003).

The average roughness (R_a) is the most popular parameter of 2D surface roughness, and for 3D surface, the most popular are the arithmetical mean of the surface (S_a) and surface roughness parameters (S_q) (Mhamdi *et al.*, 2012). Lahiff, Gordon and Phelan (2007) cited that if the surface finish (R_a) was the parameter used to define tool life, the maximum nose

radius is 0.8 mm, because a smaller nose radius has a negative effect on the workpiece surface finish.

Devillez *et al.* (2011) in the turning (dry and wet) of Inconel 718 (44 HR_C) found the surface roughness (R_a) had a tendency to decrease with increase in cutting speed in dry conditions and the wet condition, the values decreased with higher cutting speed values only after the value of 60 m/min. Yazid *et al.* (2011) observed that experiments on the finish turning Inconel 718 using PVD coated TiAIN carbide tool showed that Minimum Quantity Lubrication (MQL) produces better surface roughness than dry condition.

Brandão *et al.* (2013) studied the influence of cooling systems (dry, MQL, cold air) in the surface roughness (R_a) on the turning of Ti-6Al-4V titanium alloy and they observed that the cooling system was lesser influent than the feed rate on surface roughness, but the cooling systems did not show the same influence and they cited the usage of the traditional MQL system is a good choice to provide best surface roughness values.

Pu *et al.* (2012) studied the dry machining and cryogenic machining of AZ31B magnesium alloys that observed the application of liquid nitrogen cooling led to about 20% decrease in surface roughness, the better surface finish in cryogenic machining should be due to the remarkably reduced temperature through effective cooling by applying liquid nitrogen.

Beyond surface roughness and form, the surface finish consists of waviness on surface that is a type of surface inaccuracy of wavelength greater than surface roughness, and with wavelength less than form error. The surface roughness wavelength in the feed direction is equivalent to the feed rate in units of distance (Meyer, Veldhuis and Elbestawi, 2009).

2.2.2. Residual stresses

Residual stress is the stress remaining in that body when there are no external forces applied on the body, inhomogeneous inelastic deformation or during solidification (microscopic level). Residual stress is created at the grain boundary or other nearby imperfections in the material. In machining process, the residual stress is induced by the inhomogeneous inelastic deformation created by the very action of cutting and when the cutting tool is retracted and the workpiece is released. Thus, the stresses that remain in the workpiece, after it is cooled to room temperature (Ee, Dillon and Jawahir, 2005).

In their study about residual stresses, Maranhão and Davim (2012) affirmed that important aspects on machining of materials are:

- Compressive residual stresses generally improve component performance and life;
- The influence of the process parameters on residual stresses is as follows; feed rate, tool nose radius, rake angle;
- Residual stresses are mostly influenced by feed rate and nose radius;
- Increased feed generates significantly higher compressive stresses;
- Residual stress mechanism is influenced by process parameters in a common way.

Tang *et al*. (2009) investigated the influence of residual stresses on the milling of Al 7050-T7451 aluminium alloy. They observed tool flank wear and depth of cut have effect on superficial residual stresses. The use of small depth of cut values produced a lower tensile or compressive stresses on the surface and the thermal load (significantly) and the mechanical load affects the thickness of residual stresses layer.

Madyira *et al*. (2013) studied the residual stresses on the turning of Ti-6Al-4V titanium alloy and observed that maximum principal stress is typically aligned along the main cutting direction and the induced residual stresses by the cutting process are mostly in compression.

Devillez *et al*. (2011) observed that residual stresses in dry and wet conditions appeared when the tensile stress is limited by the use of a lubricant. However, when the lubrication is reduced and the cutting speed also increase, an equivalent tensile stress values occur for a cutting speed of 80 m/min.

2.3. High Speed Machining

Many advantages obtained with the use of HSM were cited by researchers, such as Schulz and Moriwaki (1992). The authors affirm that the main advantages are increase of accuracy in machining, especially in machining of thin webs due to reduced chip load; better surface finish and reduction in the damaged layer; reduced bur formation; better chip disposal; possibility of higher stability in cutting due to stability lobes against chatter vibration;

simplified tooling, etc. The speed applied in the HSM will depend on material and process combination. Kitagawa, Kubo and Maekawa (1997) comments in their paper, that the high-speed machining of Ti-6Al-6V-2Sn titanium alloy using sintered carbide tool with 628 m/min of cutting speed is feasible to end milling and no more than 200 m/min is attainable for continuous turning.

Some of first researches about HSC have sponsored in USA by Defense Advanced Research Project Agency (DARPA), working with a range from 0.0013 m/min to 24,500 m/min, and in Germany by the Ministry of Research and Technology (BMFT). Many of these researches were applied in machining of light alloy, mainly aluminium alloys because the use in the aircraft industry (Schulz and Moriwaki, 1992). The start developed in several companies and laboratories in machining of hardened steel dies, showing that it is possible to obtain better material remove rate than with electrical discharge machining (Tlusty, 1993). The HSM has been applied to a range of applications in the aerospace industry, originally for the machining of aluminium alloys and more recently in titanium alloys and nickel-based super alloys (Coldwell *et al.*, 2003) .

Krajnik and Kopač (2004) cited market exigencies from manufacturing companies to produce high-quality products at acceptable prices with shortest interval of time possible. Thus, manufacturers of mould and die modernize their equipment, processes, and organization, knowing all advantages and disadvantages of rather expensive investments in new technologies, or they can go to bankrupt. They show an evolution of machining time of mould and die manufacturing between 1985's and 2000's, where the manufacturing time improved 43% with HSM in comparison to conventional process. Coldwell *et al*. (2003) affirmed that benefits with HSM approach include significant cost/lead time, reduction through the elimination of multiple processes including hand finishing and a product manufactured using the traditional route can take over 20 weeks.

In the their research using the HSM on the turning of Inconel 718, Pawade *et al*. (2007) observed the surface roughness is lower when the cutting speed increases, and it represents a higher MRR. Gaitonde *et al.* (2010) studied the machinability of tungsten-copper (WCu25) machining with cemented carbide and observed the formation of continuous coiled chips during the machining of tungsten-copper composite and with usage of HSM, the formation of longer and smoother tubular structured chips.

Silva *et al.* (2013) investigated the wear mechanisms of PCD tools when turning Ti-6Al-4V titanium alloy at high speed (175, 200, 230 and 250 m/min) conditions using high pressure coolant supplies. They observed the substantial improvement in tool life and it presented dominant the flank and nose wear and the adhesion and attrition are dominant wear mechanisms.

Small cut depths with intermediate and high cutting speeds may imply a fully tensile surface influence zone and an increase in cutting speed implies a reduction in longitudinal residual stress until tool breakdown starts to occur (Madyira *et al.*, 2013). Arrazola, Arriola and Davies (2009) cited the importance of tool geometry on temperature and tool wear in their research about HSM of hardness steel using tools with uncoated/coated and with or without chip breaker.

Yap, El-Tayeb and Brevern (2013) researched the turning Ti-5Al-4V-0.6Mo-0.4Fe (Ti54) titanium alloy using the HSM (100 m/s). They found surface roughness values 0.236 µm (R_a), 0.305 µm (R_q) and 1.85 µm (R_{max}) in dry condition. When they applied cryogenic liquid nitrogen, the values decreased to 0.208 µm (R_a), 0.272 µm (R_q) and 1.69 µm (R_{max}).

2.4. Micro-cutting

The micro-mechanical machining has strong interest in mechanical cutting processes, because it is a method for creating miniature devices and components with features that range from tens of micrometres to a few millimetres in size (Chae, Park and Freiheit, 2006). This process offers good results, it is reason many researchers are investigated the performance of micromachining and their derivations in several conditions with.

According to Masuzawa (2000) a miniaturization of mechanics devices began with oldest wristwatches parts, the only using in this date. Micro in micromachining indicates “micrometre” and represents the range of 1 µm to 999 µm; despite this definition, the micro conception can vary with time, person, material, process.

There are several definitions for micromachining and micro-cutting. Ng *et al*. (2006) referred to micro/nano scale cutting would be a material removal in smaller undeformed chip thickness values. According to Zhu, Wong and Hong (2009), micromachining is a

precision/ultra-precision machining technology where the tolerances, cutting depths, and even part sizes are in micro-scale.

2.4.1. Size Effect and Ploughing Effect

A difference is the forming chip comprises several grains in conventional machining and in micromachining the chip forms within few or a single grain at a time. When the whole shear deformation occurs within a single grain, the stresses applied to the tool are dependent on individual grain orientation, causing high frequency fluctuations of cutting forces (Bissacco, Hansen and Chiffre, De, 2005).

Another interesting aspect is the chip formation in micromachining. The concept of minimum chip thickness is that the depth of cut or feed must be over a certain critical chip thickness before a chip will form, see as follow: (Chae, Park and Freiheit, 2006)

- If the uncut chip thickness, h, is less than a critical minimum chip thickness, hm, elastic deformation occurs and the cutter does not remove any work piece material, Figure 2.2a.
- As the uncut chip thickness approaches the minimum chip thickness, chips are formed by shearing of the work piece, with some elastic deformation still occurring, Figure 2.2b.
- If the uncut chip thickness is higher than the minimum chip thickness, the elastic deformation phenomena decreases significantly and the entire depth of cut is removed as a chip, Figure 2.2c.

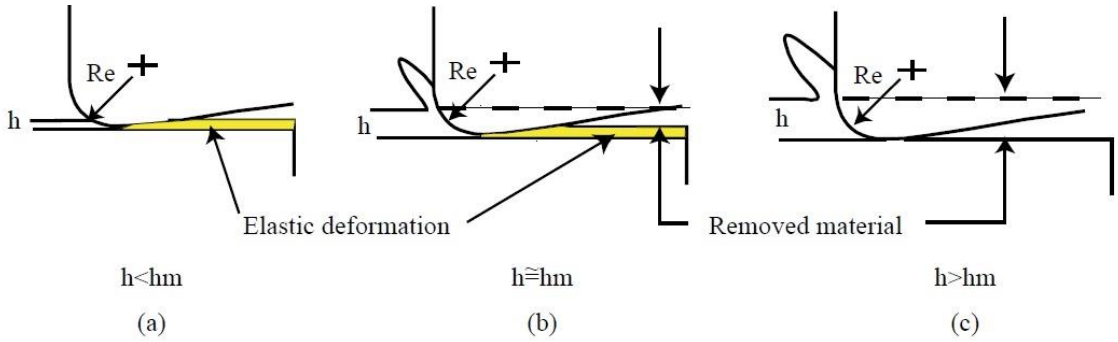

Figure 2.2 – Schematic of the effect of the minimum chip thickness (Chae, Park and Freiheit, 2006).

In micromachining processes although similar to conventional processes, it is cannot be offhand down scaled into the micro range due to size effect, because when the uncut chip thickness is on the same order as the material grain size, the workpiece material cannot any more be assumed as homogeneous and isotropic (Klocke, Gerschwiler and Abouridouane, 2009).

In turning of AISI 1045, occurred continuous chips, Figure 2.3a and Figure 2.3b, when the uncut chip thickness was greater than or equal to the average size of the smallest grain type, in this case ferrite. When the uncut chip thickness is less than the smallest average grain size, the chip is comprised of alternating layers of hard pearlite (grey) and softer ferrite (white), this is interest because it implies that the transition from a continuous to a quasi-shear-extrusion chip could be a function of material microstructure, Figure 2.3c and Figure 2.3d. This result, the chip formation mechanisms and stress state during microscale cutting are more complex than during macroscale cutting, what is presented by the basic models employed for continuous chip formation, because the extensive plastic deformation will occur at the tool tip, which in the case of microscale cutting is entire tool (Simoneau, Ng and Elbestawi, 2006).

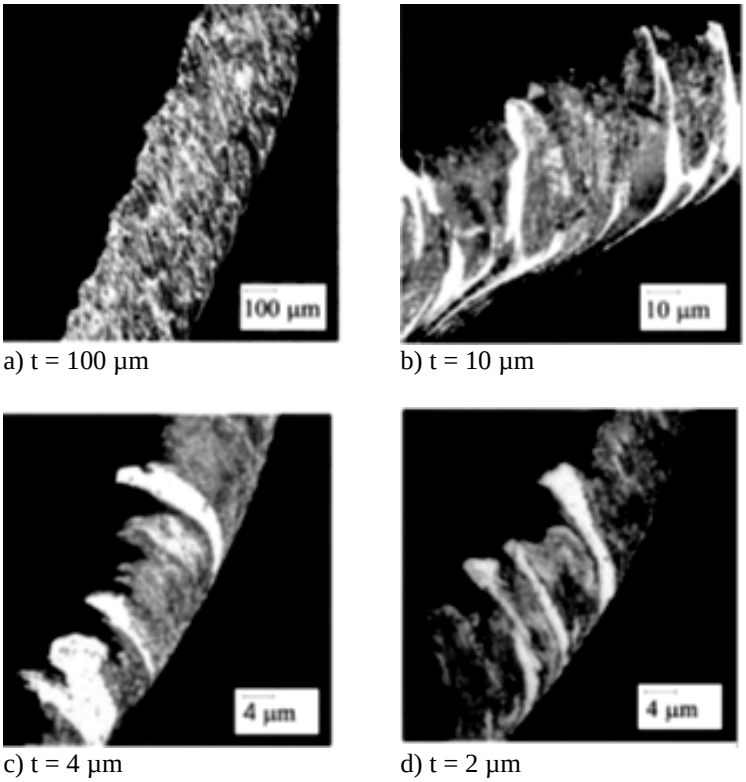

a) t = 100 µm b) t = 10 µm

c) t = 4 µm d) t = 2 µm

Figure 2.3 – Behaviour of chips (Simoneau, Ng and Elbestawi, 2006).

Analysing the specific cutting energy and coefficient of friction, Ng *et al.* (2006) justified that size effect occurred as an undeformed chip thickness is comparable to the cutting edge radius (60 to 100 nm), in both, the values increases nonlinearly with a decrease in the undeformed chip thickness, Figure 2.4.

In 1984, Kopalinsky and Oxley explained that size effect occur when the increase in specific cutting pressure with decrease in the undeformed chip thickness was attributed mainly to the accompanying decrease in shear angle and consequently less than a proportional decrease in cutting force with decrease in undeformed chip thickness (Arsecularatne, 1997).

According to Aramcharoen and Mativenga (2009), specific cutting force is characteristic to determine the size effect. They researched the specific cutting force with the ratio of undeformed chip thickness to cutting edge radius for a feed direction and found that higher specific cutting force is revealed at the lower end of the ratio of undeformed chip thickness to cutting edge radius, when the feed per tooth decrease especially when the feed per tooth is less than the cutting edge radius that supports the size effect phenomenon. Ng *et al*. (2006) also affirmed that in micro and nano scale cutting, the edge radius does influence the specific cutting energy, which considered the tool edge geometry as the major cause of the size-effect.

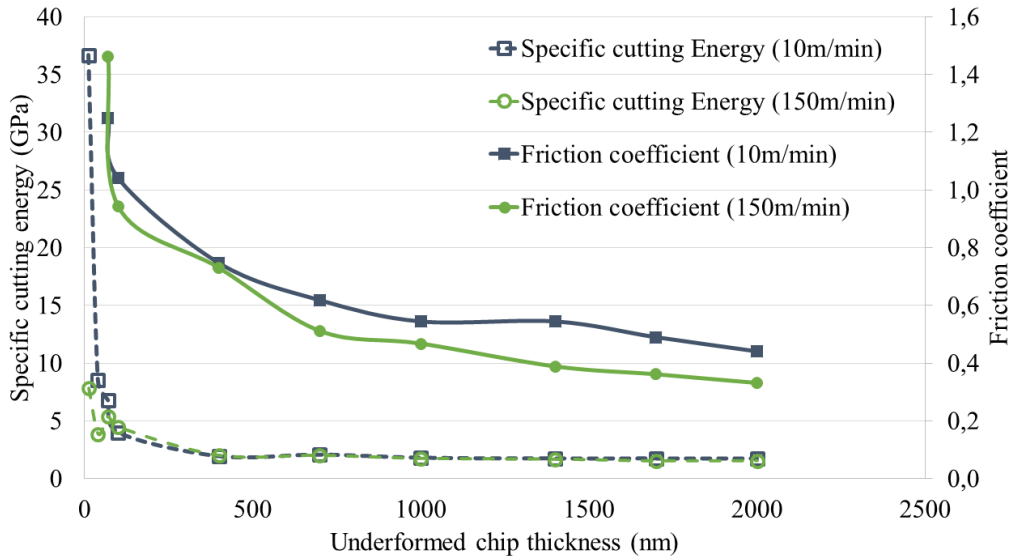

Figure 2.4 – Effect of undeformed chip thickness and cutting speed on the specific cutting energy (Ng et al., 2006).

When a blunt tool edge passes and material is elastically or plastically deformed without the formation of the chip occurs an effect called Ploughing. This effect is related to results in poor surface finish, deteriorated dynamic stability and shortened tool life. According to Yun *et al*. (2011), it occurs when the uncut chip thickness is greater than the minimum chip thickness and to avoid ploughing. The feed per tooth must be higher than the minimum chip thickness. In the micro-milling of copper study, they observed that the surface roughness value is increased when ploughing occurs.

According to Aramcharoen and Mativenga (2009), determine the ratio of minimum chip thickness to the cutting edge radius is essential in micromachining in order to avoid or minimize the ploughing effect and achieve desired material removal, which depends on work and tool material can vary between 0.1 to 0.3.

2.4.2. Applied Techniques in micromachining

Robinson, Jackson and Whitfield (2007) highlighted the interest in micromachining applying high Speed, mainly when speed spindle exceeds of 500 krpm. Cristofaro *et al* (2012) have used the High Speed Machining (HSM), 91 m/min, and Ultra-high Speed Machining (UHSM), 141 m/min, to research influences of seven kinds of coatings on the micro-milling. Many researchers applied High Speed or Ultra-High Speed in their paper, mainly in micro-milling, Table 2.1.

Ding *et al.* (2010) have studied the effect two dimensional vibration-assisted micro-end-milling at hardened tool steel, which observed that it can improve the machinability of hardened tool steel in terms of machined surface improvement and tool wear reduction. Li and Chou (2010) investigated the performance of MQL in micro-milling of SKD 61 steels that resulted in the reducing the flank wear (60%), improvement in the surface roughness and attenuation of burr formation. Lekkala *et al.* (2011) studied the burr in micro-milling and developed a theoretical model predicts the burr height within 0.65 to 25% accuracy. Surmann and Krebs (2012) investigated the tool inclination angles in the five-axis micro-milling. Singh and Melkote (2007) have used the laser-assisted mechanical machining in micro-milling to overcome the limitations of low tool stiffness and bending strength in pure mechanical micro-cutting.

Table 2.1 – High Speed machining (HSM) and Ultra-High Speed Machining (UHSM) in micro-milling.

Researchers	Classification	Material	Tool (mm)	Speed (krpm)
Jahanmir (2011)	UHSM	Al 6061-T6 Aluminium alloy	0.05 to 0.3	150, 250, 300, 350
Nishikawa, Yoshimoto and Somaya (2012)	UHSM	Al 2024 Aluminium alloy	0.4	300, 400
Shin *et al.* (2008)	UHSM	Brass (6:4)	0.2	150
Park and Rahnama (2010)	HSM	Al 7075 Aluminium alloy		10 to 55
Cristofaro *et al.* (2012)	HSM UHSM	AISI O2 steel (62 HR_C)	1.0	29 45
Baldo *et al* (2015)[1]	HSM	Ti-6Al-4V Titanium alloy	0.5	20 and 45
Lauro *et al.* (2015)	HSM	AISI H13 steel (45 HR_C)	0.5	21 and 49

HSM → High Speed Machining UHSM → Ultra High Speed Machining

2.4.3. Surface integrity for the micro-machining process

The micro-milling has more highlight between all micromachining processes, because it has great accuracy, low surface roughness and a high material removal rate, there is directly relation mould and dies manufacturing (Malekian, Park and Jun, 2009). Wang, Kweon and Yang (2005) have studied the surface roughness on the micro-milling of brass and they observed that the surface roughness increased linearly with the increase of tool diameter and spindle speed, but the spindle speed caused a high frequency vibration caused high surface roughness.

According to Filiz *et al*. (2008), only the main effect of the spindle speed was statistically significant, that indicates the possibility of increasing the material removal rate without compromising on surface roughness. Some results of surface roughness, often lower values, can be seeing in the Table 2.2.

According to Liu and Melkote (2006), it been observed that the surface roughness in micro-turning decreases with feed, reaches a minimum, and then increases with further reduction in feed. They developed a kinematic roughness model where the percentage error was less than 15%, to micro-turning of Al 5083-H116 aluminium alloy. It was considered the aspects as account the effect of plastic side flow, tool geometry, and process parameters. They

[1] Self-citation.

observed also that the plastic side flow can cause a discrepancy between the theoretical and measured surface roughness and increases and increase due to the strain gradient-induced strengthening of the material directly ahead of the tool.

Table 2.2 – Roughness in micromachining processes.

Researchers	Material	Process	Roughness (μm)
Palani, Natarajan and Chellamalai (2013)	Tungsten electrode	Turning	R_a = 0.029 to 0.58
Liu and Melkote (2006)	Al 5083-H116 alloy	Turning	R_t = 2.82 to 4.63
Li and Chou (2010)	SKD 61 steels (38 HR_C)	Milling	R_a = 0.1 to 1.2
Wang, Kweon and Yang (2005)	Brass	Milling	R_a = 0.013 to 0.073
Aramcharoen and Mativenga (2009)	AISI H13 steel (45 HR_C)	Milling	R_a = 0.14 to 0.26
Lauro *et al.* (2014)	AISI H13 steel (45 HR_C)	Milling	R_a = 0.088 to 0. 223
Min *et al.* (2008)	Austenitic stainless steel 304	Milling	R_a = 0.190 to 0.300

Bodziak *et al*. (2014) studied the surface integrity of moulds, AISI P20 (29 HR_C) and AISI H13 (45 HR_C), for micro-components manufactured obtained on the micro-milling and EMD process. They observed that EDM presented white layer with irregular thickness with a hardness was about three times higher than the bulk material and in the milled surface alone some plastic deformations with thickness thinner than 5 μm were detected; the milled surface presented compressive residual stress and EDM surface tensile stress and the EDM showed highest surface roughness (R_a), about six times, most aggressive marks and an irregular topography that may increase the polishing time, Figure 2.5.

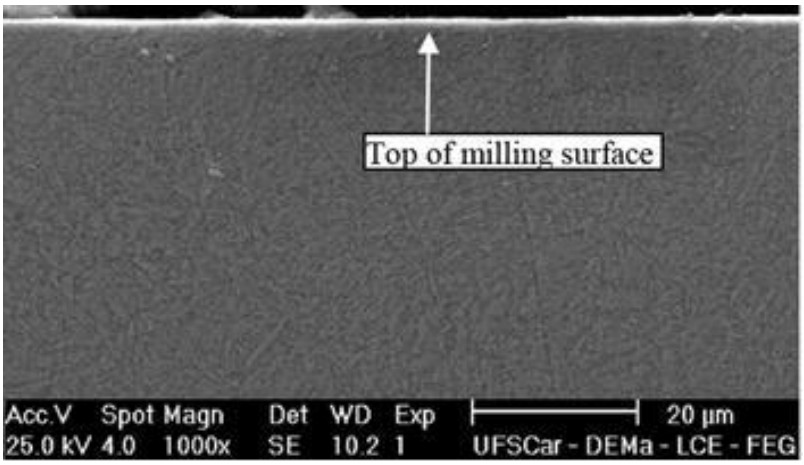

a) micro-milled surface.

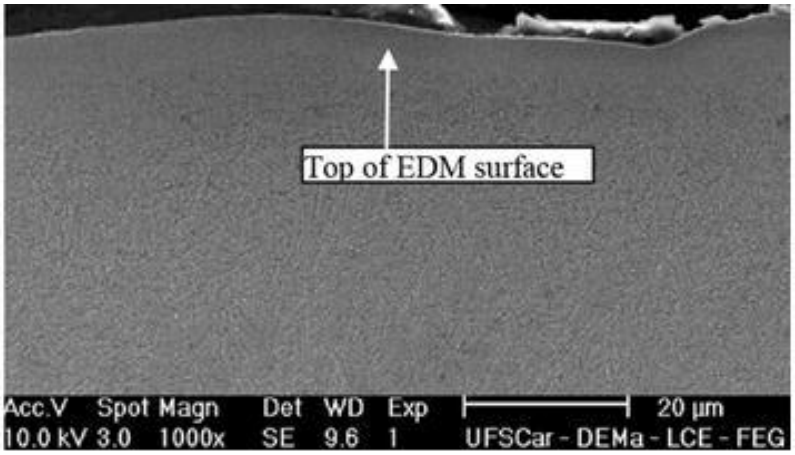

b) EDM surface.

Figure 2.5 – Compared of Top surface obtained between micro-milling and EDM (Bodziak et al., 2014).

The understood of tool wear is important in the micro-cutting, mainly in the hardness materials. Although, the usage of high cutting velocities results in the better surface quality in hardness material, the burrs occur most frequently because of the faster tool wear, see Figure 2.6. It can be reduced by identifying the correct process parameter-material state combination (Weule, Huntrup and Tritschler, 2001).

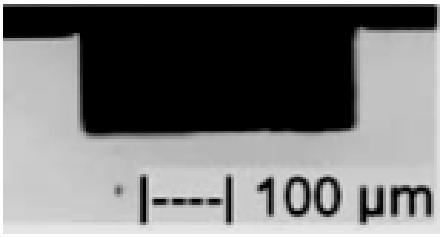

a) SAE 1045 (25 HRC).

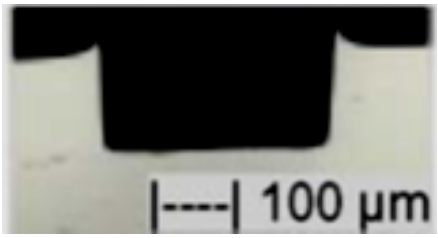

b) SAE 1045 (51 HRC).

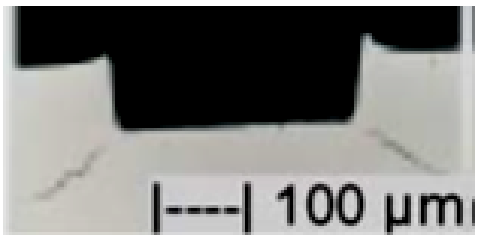

c) SAE 1045 (62 HRC).

Figure 2.6 – Occurrence of burrs in different material states (Weule, Huntrup and Tritschler, 2001).

Zhang *et al*. (2013) developed an accurate prediction model of surface roughness for micro-turning of AISI 1045 based on considering the effect of pile-up formation process, tool geometry and cutting parameters. They observed that the best surface roughness can be obtained when the ratio of feed to cutting edge radius reaches 0.1.

2.5. FEM in the Surface Integrity

Some time, many investigators using the Finites Elements Method (FEM) to study the residual stress behaviour on the machining processes. The use of FEM in cutting processes are emerging as useful techniques for predicting tool temperatures and stresses and for extending tool life (Fallböhmer *et al.*, 2000). According to Arrazola and Özel (2010), it is very costly and difficult to measure stresses and temperatures in high-speed machining using experimental tests. Umbrello *et al*. (2007) cited that the good agreement obtained between the experimental and numerical results indicate that the proposed FEM model appears to be suitable for studying the influence of cutting parameters on residual stress.

Manikandan *et al*. (2012) used orthogonal cutting to analyse plane strain-coupled thermo-mechanical. Buchkremer *et al*. (2013) highlight that the cutting force is the integral representations of the calculated flow stresses in the primary shear zone, showed excellent results for a broad range of cutting conditions.

Weinert and Schneider (2000) affirmed that FEM has proven to be advantageous for describing the thermal and thermo-mechanical stress and can establish a direct link between the thermal stress and the application properties of the tool during grinding.

According to Rizzuti *et al*. (2010), besides the 2D model, the few milliseconds of cutting time are one of the main problem in temperature modelling because there are several problems related to heat generation and diffusion into the tool. In fact, no steady-state conditions are reached during the numerical simulation.

Duan *et al*. (2013) used the FEM simulation to study the thickness of white layer based on phase transformation mechanism. They analysed the effects of mechanical factors on transition temperature were taken into account explicitly. Attanasio *et al*. (2012) used numeric (2D and 3D) and experimental tests to study the formation of layers on the orthogonal hard turning of AISI 52100. They found that the thickness of white and dark layers increases with increasing of tool flank wear and higher cutting speed generates thicker white layers and thinner dark layers.

Ramesh and Melkote (2008) used the FEM to study the white layer formation in orthogonal machining of AISI 52100 (62 HRC) using the cBN tool. They used a model explicitly

incorporates the effects of stress and strain on the transformation temperature, volume expansion and transformation plasticity that showed predicted values and trends of white layer thickness. These effects are in good agreement with the measured values and trends when compared to experimental validation.

Sometime, many investigators using the FEM to study the residual stress behaviour on the machining processes. Thus, for example, Ee, Dillon and Jawahir (2005) used a 2D model to study the residual stresses induced by orthogonal machining. Valiorgue *et al*. (2012) used a 3D model to study the residual stresses in finish turning of AISI 304L stainless steel with a TiN coated carbide tool. They proposed a model that does not simulate the chip formation and the material separation around the cutting edge, but only onto the thermo-mechanical loadings applied onto the machined surface.

Rizzuti *et al*. (2010) affirmed that the residual stresses are generated by the material deformation and by the thermal cycle and both phenomena occur during the cutting process. The components of the residual stresses can be the axial and the circumferential. They measured the circumferential stress using the numerical procedure of orthogonal cutting of AISI 1045, which observed agreement was obtained between the numerical predicted residual stresses and those experimentally measured.

Özel and Zeren (2007) used the FEM to study machining with round edge cutting tools in the HSM of AISI 4340 and they compared with experimentally measured residual stresses obtained from the literature, which indicated an influence the stress and temperature fields greatly. These predictions combined with the temperature field predictions are highly essential to further predict surface integrity and thermos-mechanical deformation related property alteration on the microstructure of the machined surfaces.

2.6. Synthesis

Although the “micro” conception can remind the components of smallest dimensions, the micromachining can be to manufacture components in macro-scale. Through the previous arguments, the use of micromachining can be recommended in the finishing of surfaces that need of high accuracy. A great example is found in the study of Byrne, Dornfeld and

Denkena (2003), which showed the evolution of the ABS system weight, a reduction of 71% between 1989 and 2001.

This technique offers lower surface integrity values that can provide high efficiency and durability. In addition, the surface can show lower error, as form or dimensions. Thus, if there is a demand of high surface quality machining, the usage of micromachining is a great option to obtain these surfaces. However, this technique requires high control and specials or adapted machines.

CHAPTER 3 – MONITORING AND SIGNAL PROCESSING IN THE MACHINING AND MICROMACHINING PROCESSES

This chapter was developed to defined the technique to observe the phenomena during the micro-cutting. A large portion of this chapter has similarity with:

- LAURO, C. H. *et al*. Monitoring and processing signal applied in machining processes – A review. Measurement, v.58, 2014, p. 73 – 86.

3.1. Introduction

The monitoring of machining process can represent economy and practicality due to it help to identify tool wear, surface roughness and anomalies during the cutting metal that can cause waste, damage and other impairing facts in this process. According to Teti *et al*. (2010), the measuring techniques for the monitoring of machining operations have traditionally been categorised into two approaches:

- Direct measurement the actual quantity of the variable is measured and highlight a high degree of accuracy and has been employed extensively in research laboratories (due to the practical limitations caused by access problems during machining, illumination and the use of cutting fluid) to support the investigations of fundamental measurable phenomena during machining processes.
- Indirect measurement actual quantity is subsequently deduced via empirically determined correlations and it is less accurate than direct ones but is also less complex and more suitable for practical applications.

The indirect measurement applied in the tool condition uses an estimate from the measurable signal feature that extracted through signal processing steps, as can be seen in Figure 3.1. It is used for sensitive and robust representation of its corresponding state. Example of this

measurement is the cutting forces, vibrations, acoustic emission, and motor/feed current (Zhu, Wong and Hong, 2009).

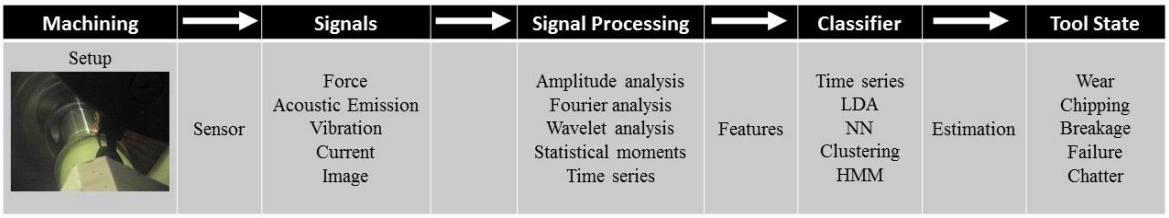

Figure 3.1 – The framework of TCM, adapted from Zhu, Wong and Hong (2009).

According to Dimla (2002), the tool wear monitoring involves the complex and diverse nature, which should provide an indication as to when the cutting tool should be changed, without compromising the workpiece surface finish, the machine integrity, and the manufactured component tolerances.

In their paper, Lee, Lee and Teo (1992) mentioned that the on-line monitoring to tool wear and predict its failure is reliable and able to respond quickly to tool failure. Although the personal computer used (10 MHz 80286) did not offer a good response time. The on-line real-time monitoring (based on cutting forces, sound and vibration, laser scanners, vision systems and computer tomography), even though can supply a surface quality feedback to CNC for on-line adjusting cutting parameters, it has some drawbacks such as some signals may be redundant; measurement errors are not easy to be avoided, resulting in inaccurate prediction; measurement cost is relatively high (Lu, 2008).

3.2. Cutting Forces

The analysis and prediction of cutting forces are very important in research of metal cutting processes and design of cutting tools, which develop in crucial role thermal analysis, tool wear estimation, chatter prediction, chip form categorization, surface roughness prediction, tool condition monitoring and others. Furthermore, large cutting force means more energy consumption that is the aim of studies in reducing of cutting force through appropriate choice of parameters and tools (Deng *et al.*, 2013). According to Kim and Kim (1997), the cutting force is composited by:

- Static force: it is a mean value and have concentrated most of the measurement of cutting force;

- Dynamic force: it is the superposed fluctuation and can satisfy the needs of higher machining accuracy, because it has very useful information on cutting mechanism.

Gok, Gologlu and Demirci (2013) investigated optimum cutting parameter values in the cutting force in the milling of AISI H13 (50-54 HR_C) on convex and concave inclined surfaces using a ball nose tool. They observed that, an absolute difference in percentile of measured and calculated values were lower than 3.57 in both inclined surface types.

According to Childs *et al*. (2000), the cutting forces can be measured in:

- Direct measurements are used when the forces need to be known accurately both in magnitude and direction that involve mounting a tool or the tool or workpiece on a dynamometer, which responds to the forces by creating electrical signals in proportion to them.
- Indirect measurements are less accurate than direct methods, but can be sufficient for monitoring purposes that involve deductions from the machine tool behaviour.

Is common the measurement the motor current as indirect methods, because the phase current waveform varies in the case of feeding while cutting and the phase current signal is a perfect sine wave in the case of feeding without cutting. (Kim and Chu, 1999).

The usage of dynamometer is most popular method to cutting forces measurement, which can be constructed by piezoelectric or stain gauges. The piezoelectric effect is a separation of charge in certain materials that are subjected to mechanical force. Each force component is detected by a separate crystal oriented relative to the force in its piezoelectric sensitive direction. The quartz is usually chosen as the piezoelectric material because of its good dynamic mechanical properties, low loss and piezoelectric constant is approximately $2x10^{-12}$ C/N. A charge amplifier is therefore necessary to create a useful output that must itself have high input impedance. Commercial machining dynamometers are available with natural frequencies from 2 to 5 kHz, depending on size (Childs *et al.*, 2000).

In the study of combined-type tool dynamometer to measure the static and the dynamic cutting force in an ultra-precision lathe, Kim and Kim (1997) used a high-pass filter to eliminate the 60 Hz electrical noise in the dynamic component measurement in the strain gauge dynamometer.

3.3. Vibration

Vibration is a common phenomenon in the finishing machining of the flexible workpiece due to its low rigidity (Zeng *et al.*, 2012). The great industrial interest is avoid the vibrations that produce bad surface finish and may cause some damages on the machine components (Devillez and Dudzinski, 2007).

According to Dimla (2002), the vibration signatures satisfy a robustness, reliability, and applicability conditions and require fewer peripheral instruments than Acoustic Emission. In addition, their signals have the quick response time needed to indicate changes for on-line monitoring. They used an analytical on-line system for TCM based on vibration signature features in the three principal axes to correlate to the tool wear and observed that is possible to identify the trend of the sensor signals, which were affected by the different wear modes. Furthermore, they affirmed the time domain features were deemed to be more sensitive to cutting condition than tool wear, whereas frequency based features correlated well with the tool wear.

Accelerometers are the more used to measure the vibrations. However, Devillez and Dudzinski (2007) mentioned that despite they are very easy to use, accelerometers present a major drawback the acceleration signal that can be used to analyse only the vibration frequency and amplitude. They proposed a method the usage of non-contact displacement measuring system based on eddy current principle with a sensitivity of 30 V/mm, because their interest was to measure directly the tool movement in real time to correlate with the obtained surface finish. This method presented an efficiency to determine the dynamic parameters of the tool system and to obtain the cutting tool displacement signals.

In the monitoring of the vibration in ultra-precision face turning of Al 6061 aluminium alloy with accelerometers fixed on the spindle and tool holders, Meyer *et al*. (2009) observed that waviness errors caused by relative tool/workpiece vibration are a significant source of inaccuracy and the surface finish lobes provide a systematic framework to describe how broadband relative tool/workpiece vibrations manifest themselves on the workpiece surface.

According to Zeng *et al.* (2012), some studies focus on the vibration control of flexible workpiece, but the fixture has importance on the machining, since it has the ability to

suppress the excessive machining vibration of the workpiece and balance the cutting forces. It presents the following advantages:

- It can target the nature of the problem of machining vibration suppression on flexible workpiece because of its clear physical meanings;
- One can easily achieve vibration reduction of flexible workpiece with appropriate fixture layout and the capability of disturbance rejection of the workpiece–fixture–cutter system can be improved using this method;
- The location, the applied forces and the number of fixture elements can be simultaneously optimized.

3.4. Temperature

The power consumed in the cutting is converted into heat near the cutting edge of the tool and many of the economic and technical problems are caused directly or indirectly by this heating action (Trent and Wright, 2000). The two goals of temperature measurement in machining are, mainly, the quantitatively to measure the temperature distribution throughout the cutting region (commonly over 700° C) and to measure the average temperature at the chip/tool contact (Childs *et al.*, 2000).

According to Byrne (1987), the temperature is fundamental to the process of chip removal and perhaps it is the single most important factor influencing the efficiency of the process. The temperature influences following characteristic factors:

- The degree of plastic deformation;
- The extent of tool wear;
- The degree of diffusion and corrosion;
- The fatigue properties;
- Compositional changes in the workpiece material.

According to Sivasakthivel and Sudhakaran (2012), to measure the cutting temperatures is difficult because the temperature is a scalar field which varies throughout the system and cannot be uniquely described by values at a point. Thermocouple is the most widely used method. It can be embedded in the tool or work piece to measure the temperature accurately

with less effort, besides being conductive, operate over a wide temperature range, rugged and inexpensive.

To an improve understanding of work done by a cutting tool in removing metal, O'Sullivan and Cotterell (2001) monitored the temperature in the turning of Al 6082-T6 aluminium alloy tube. They used two thermocouples on the inside of the tube and an infrared thermal camera placed 0.5 m from the workpiece on the opposite side to the cutting tool.

Several experimental methods, as such thermocouple and radiation techniques, can be employed to measure the temperature and the prediction of heat distribution due to extreme difficulty that occur due to a narrow shear band, chip obstacles, and the nature of the contact phenomena where the two bodies, tool and chip, are in continuous contact and moving with respect to each other that became this measurement (Davoodi and Hosseinzadeh, 2012). The Table 3.1 shows some researches that used these methods.

Table 3.1 – Types of temperature measurements.

	Researcher	Material	Method	Target
Drilling	Bagci and Ozcelik (2005)	Al 7075-T651 alloy	Thermocouple	Tool
	Li and Shih (2007)	Ti-6Al-4V alloy	Thermocouple	Tool
	Brandão, Coelho and Lauro (2011)	AISI H13 steel	Thermocouple	Workpiece
Grinding	Ueda *et al*. (1993)	AISI 1055 Annealed and Hardness	Infrared Radiation Pyrometer	Tool
	Wei *et al.* (2010)	Steel with WC-Co coating	Thermocouple	Workpiece
	Mohamed, Warkentin and Bauer (2012)	AISI 4140 steel	Infrared Thermal Camera	Workpiece
Milling	Davoodi and Hosseinzadeh (2012)	Cu–Zn40–Al12	Infrared Sensor	Workpiece
	Sivasakthivel and Sudhakaran (2012)	Al 6063 alloy	Thermocouple	Workpiece
	Lauro, Brandão and Ribeiro Filho (2013)	Al 7050 alloy	Infrared Thermal Camera	Workpiece
Tapping	Brandão and Coelho (2009)	AISI H13 steel	Thermocouple	Workpiece
	Fromentin *et al.* (2010)	AISI 1070 steel	Thermocouple	Workpiece
	Bhowmick, Lukitsch and Alpas (2010)	Al 319 alloy	Infrared Thermometer	Workpiece
Turning	O'Sullivan and Cotterell (2001)	Al 6082-T6 alloy	Thermocouples Infrared Thermal Camera	Workpiece
	Aneiro, Coelho and Brandão (Aneiro, Coelho e Brandão, 2008)	AISI 4340 steel	Thermocouple	Tool
	Hadad and Sadeghi (2013)	AISI 4140 steel	Thermocouples	Tool

Davoodi and Hosseinzadeh (2012) used an infrared sensor to monitor the temperature in the high speed machining that is suitable for dry conditions due to its high response rate. It has ability to provide temperature based on the distance from the cutting zone and is not necessary making hole in the tool or work piece to install the instruments. Moreover, it can be used for all types of materials, but the sensor should be installed as close as possible to the desired surface, because the distance between target surface and sensor is very important and can affect the results. Finally, it is not possible to used liquid cooling and the chip may come between surface and sensor and causes to error.

3.5. Signal Acquisition

To obtain success in the processes monitoring, the choice of devices is very important. The user should check if the measurement resolution and range will attend the process requirements. According to National Instruments (2012), the resolution refers to the number of binary levels an ADC can use to represent a signal; the smallest detectable change in this signal determines the resolution that is required of device, Figure 3.2. The bits per sample will be kept constant and with best quality because this is period of test and already is not possible know if the acquisition in audible sound, between 20 Hz and 20 kHz.

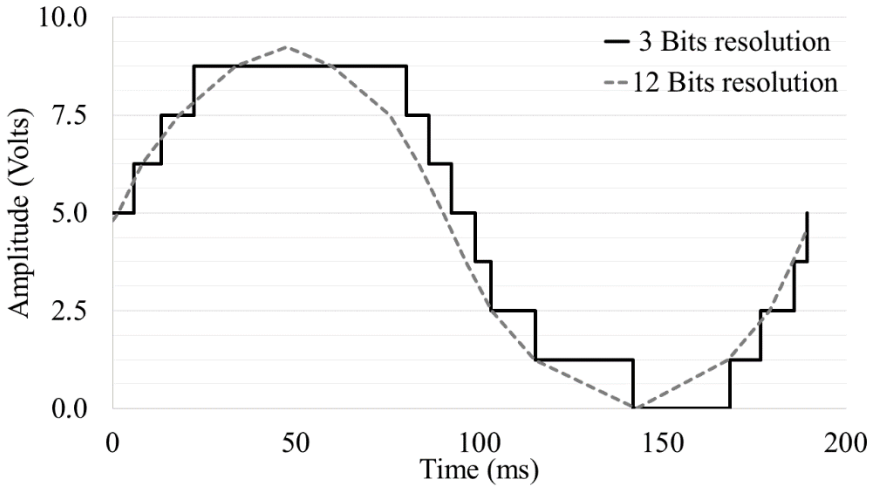

Figure 3.2 – Influence of bits per sample (National Instruments 2012).

Furthermore, the sample frequency is another important aspect. This factor, generally, is related to revolution of operation. The sample frequency should be great definite, because an incorrect value can mask important values that will influence the signal behaviour. Shaw (2004) suggests a sample frequency should be four times more than revolution, a minimum.

Other researchers applied the Nyquist Theorem, should sample at least 10 times the maximum frequency, Figure 3.3 (National Instruments 2012).

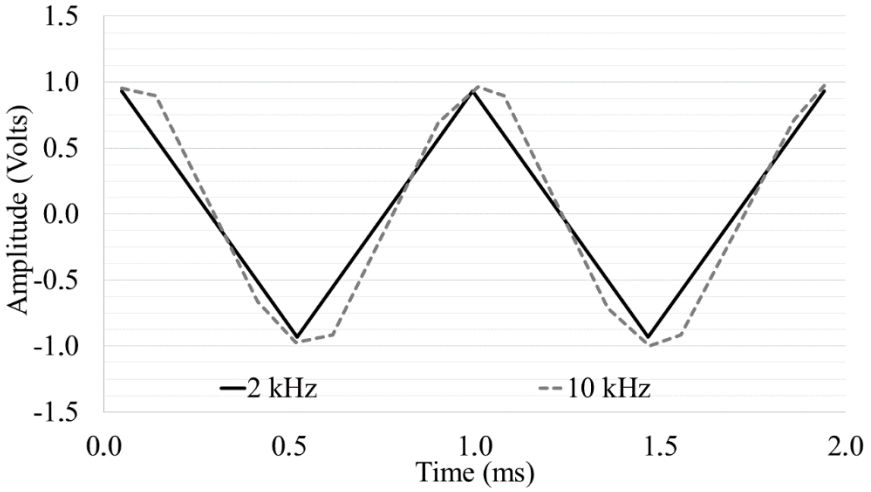

Figure 3.3 – Example of sample rate (National Instruments 2012).

3.5.1. Domain Analysis

The time domain is based on estimating the signal period and subsequent equidistant sampling of one signal period, an integer number of signal periods, or on using measurement time covering many signal periods that are needed to decrease sufficiently the uncertainty of measurement caused by the energy leakage due to non-coherent sampling (Novotny and Sedlacek, 2009).

The time domain signal when processed by the application of the Fourier Transform, see forward, transforms the signal data into the frequency domain, which refers to the display or analysis of data based on frequency. In vibration analysis, the principal advantage is the repetitive nature of the signal and are clearly displaced as peaks in the frequency spectrum at the frequency where the repetition takes place (Bhende, Awari and Untawale, 2011). The use of frequency analysis can verify the monitoring of the tool rotational speed or can detect if the tool is cutting with one or multiple blades (Morska, Matuszak and Waszczuk, 2012).

Analysing the accelerator signal, Bisu *et al*. (2011) realized that the convolution in the time domain is equal to the product in the frequency domain, so the fault signal becomes a modulated signal. They also affirmed that the fault signal can be enlarged more than ten times at the resonant frequency. However, the fault signal is relatively diminished in the

other frequency range due to the character of the wide frequency range of impulsive signal that the average noise signal always contains in the low-frequency range and this situation also applies to the sensor.

Analysing the microphone and accelerometer power spectrum of signals for sharp and worn tools, Lu and Kannatey-Asibu (2002) observed that the energy distribution for sharp and worn tools are easily discernible from the sound and vibration signals. In this regard, ignoring the sound signals below 0.5 kHz, similar peaks were observed in both the sound and vibration signals in the feed and cutting directions.

According to Lamraoui *et al*. (2014), the frequency domain has a drawback due to not providing information in the time domain. A time-frequency analysis is better as it characterises the signal in both the time and frequency domains. In vibration analysis, it manifests in either the frequency or the time domain and thereby gives a compromise between the frequency resolution and the temporal resolution. They acquired the data using the angular-domain because it is more convenient to sample the signal with respect to an angular variable θ, so that the cycle stationary characteristic is preserved.

Zhang and Chen (2007) developed a study of TCM in an CNC end-milling machine based on the vibration signal collected through a microcontroller-based data acquisition system. They observed that displaying vibration signals of the X, Y and Z directions in the time domain is helpful in understanding the cutting condition. The vibration amplitudes in the time domain and the frequency peaks at harmonic frequency bands of the X and Y directions can be used as the key featured signals for monitoring the tool condition.

Sometimes the vibration and sound analysis can be analysed using frequency spectra. More advanced signal-processing techniques needed for system, source, and path identification problems require the computation of frequency spectra. Furthermore, if the data are random in character, a frequency analysis in terms of power quantities per hertz greatly facilitates the desired evaluations of the data signals. For deterministic signals that are periodic, a frequency decomposition or spectrum is directly obtained by computing the Fourier series coefficients of the signal over at least one period of the signal using a Fast Fourier Transform (FFT) algorithm. Line Spectrum or Discrete-frequency Spectrum is represented by the Fourier component magnitudes versus frequency. However, the phase information is

generally retained only in those applications where there may be a need to reconstruct the signal time history or determine peak values. The Power Spectral Density function or Auto Spectral Density function provides a convenient and consistent measure of the frequency composition of random data signals. The power spectrum is most easily visualized as the mean-square value of the signal passed through a narrow-band pass filter divided by the filter bandwidth (Vér and Beranek, 2006).

It is interesting to highlight however, that although the time and frequency domain are more utilized, other domain analysis can also be applied in machining monitoring. In their paper, Ritou *et al*. (2014) studied the radial eccentricity of a new end mill. To study the contribution of each tooth to the cutting force, they applied an angular approach. They acquired the force signals in the time domain associated with the tool angular position. They observed that for every tool revolution, a force peak is extracted for each tooth that passes and hence the cutter eccentricity is estimated.

Lamraoui *et al*. (2014) developed a chatter indicator method to diagnose chatter in high speed milling of Al 7075-T6 aluminium alloy using an angular-frequency domain. They affirmed that analysis in the angular domain is useful for observing the behaviour of cutting forces during each revolution and provides information about the system stability. They acquired the AC motor integrated rotational encoder data using a system with an angular sampling device.

3.6. Signals processing

Sometimes, the acquired signal can have influence by frequency range that is not interest in the analysis and it causes the monitoring be totally impractical. An alternative is to use a non-periodic excitation and statistical signal processing techniques that requires a number of operator decisions: the frequency range, the number of test averages, and choice of windowing procedure (Cheng, 2009).

Kuljanic, Totis and Sortino (2009) mentioned some analysis techniques to the signal processing:

- Time domain analysis (once per revolution sampling, Poincarè sections);
- Frequency domain analysis (Fast Fourier Transform, power spectral density);

- Time–frequency domain analysis (Wavelet Transform);
- Other (entropy, coarse-grained entropy rate, normalized coarse-grained information rate).

Kalvoda and Hwang (2010) affirmed that right data processing technique is one of the most important items for a cutting process that is assumed that to be nonlinear and non-stationary.

3.6.1. Fourier Transform

The Fourier Transform (FT) is commonly applied in the signal processing. The principle of Fourier Transform is to extract the fundamental frequency component of the fringe pattern in the 1D or 2D frequency domain and its inverse transform of the filtered frequency domain signal then provides the modulo 2π phase of the fringe pattern (Huang *et al.*, 2010).

To study the high-precision machining, Kono *et al*. (2008) applied the Fourier series in the frequency domain to analyse geometric errors from other errors using an artefact and a laser displacement sensor. In their study about the analysis using a multi-sensor in high speed machining, Kang, Kim and Kim (2001) monitored the spindle vibration and analysed the rotation frequency and tooth frequency of the acceleration signal transformed by a Fourier transform.

In the literature is possible find the several variations of Fourier Transform applied in machining signal processing. The Discrete Fourier Transform (DFT) and Discrete Cosine Transform (DCT) are efficient forms of the Fourier transform often used in various applications including tool condition monitoring (Liao *et al.*, 2007).

Gabor Transform, also called short-time Fourier Transform (STFT), is a time-frequency technique used to deal with non-stationary signals that has a short data window centered on time and its implementation for AE signal processing is efficient when it is used to locate and characterise events with much defined frequency patterns, not overlapping and long relatively to the window function (Rubio, Teti and Baciu, 2006).

According to Zhu, Wong and Hong (2009), although the Fast Fourier transform (FFT) is the standard method for observing signals in the frequency domain and has been widely studied, it has certain serious theoretical drawbacks in processing machining signals. Liu *et al.* (2005)

used FFT to filter the undesired frequency components in the interpolation points, which guaranteed the exact trajectory generation and shock free motion simultaneously, it to avoid excessive vibrations in machining.

3.6.2. Hilbert-Huang Transform

An option to process the signals is the Hilbert-Huang Transform (HHT) method that, according to Cao, Lei and He (2013), consists in the step following:

- Empirical Mode Decomposition, which a complicated signal is decomposed into a series of simple oscillatory modes, designated as intrinsic mode function (IMF), and a residue;
- Hilbert transform is then invoked for each intrinsic mode function (IMF) to obtain the instantaneous frequencies and the instantaneous magnitudes, which comprise the Hilbert-Huang spectrum of the signal.

The Table 3.2 shows some researchers that used this method. Cao, Lei and He (2013) monitored the vibration signals on the milling aluminium 7050 with a carbide end mill cutter (two flutes) using the spindle speed of 8,500 rpm (1,500 mm/min) and a sampling frequency of 6,400 Hz. They used the Hilbert-Huang Transform (HHT) to analyse the reconstructed signals and obtain the Hilbert-Huang spectrum, which their mean value and standard deviation were used to calculate the chatter indices.

Table 3.2 – Some machining researches using HHT.

	Researcher	Monitored Signal	Material	Spindle Speed (rpm)	Sampling Frequency
Milling	Kalvoda and Hwang (2010)	Vibration	SAE 1045	773, 1345, 2004	2 kHz
	Bassiuny and Li (2007)	Current	SAE 1045	300, 450, 600, 900, 1200	1 kHz
Grinding	Yang *et al.* (2014)	Acoustic emission	AISI 1045	24	2 MHz
		Vibration			2 MHz
		Voltage, Current			10 kHz

Kalvoda and Hwang (2010) used the Hilbert-Huang Transform (HHT) to analyse the cutting forces and vibration on the milling of aluminium alloy using end-mill type in high-speed

steel (HSS-Co), a diameter of 12 mm and four flutes. They used a sampling frequency of 9 kHz to both acquisition signals to a cutting speed of 5,404 rpm. They used the Hilbert-Huang Transform (HHT) to correlate the tool wear/breakage by change in the frequency peak with the change in cutting geometry of the cutter tool that considered the shift of the main frequency peak into lower frequency is a cutter tool wear indicator together with higher frequency fluctuations.

3.6.3. Wavelet Transform

Wavelet transform decomposes a single signal series in the time domain into a two-dimensional function, where each of the decomposed signals is a mixture of source signals. It can be considered as a series of band pass filters, whose results could be regarded as different mixtures of independent source signals (Shao, Shi and Li, 2011).

According to Zhu, Wong and Hong (2009), the wavelet transform was developed in the late 1980's to meet the needs for adaptive time-frequency analysis in applied mathematics, physics, and engineering, which has been used for machinery fault diagnostics and TCM. Its great potential in detecting abrupt changes of tool conditions can be explained by:

- Sparse representation of signal, the wavelet expansion coefficients $c_{j,k}$ and $d_{j,k}$ decay rapidly with increase in j and k, and only a few large coefficients exist while the others are small.
- Setting a suitable threshold, the undesired noise is filtered that is the essence of wavelet denoising, and compression.
- The localization of the time and frequency description of the signal that reveals the signal behaviour in certain time and its corresponding frequency property.

Liao *et al.* (2007) highlighted the properties because the wavelet transforms are more powerful and versatile than the Fourier transform:

- Some wavelet transforms have compact support, thus are able to capture local time-dependent properties of data, whereas Fourier transforms can only capture global properties.
- Wavelet transforms are more efficient even when compared with the FFT.

- The wavelet transform is hierarchical and allows much fine tuning for a variety of applications.
- Unlike the Fourier transform, wavelet transforms have an infinite set of possible basis functions.

The different wavelet features are used in the tools condition monitoring. Continuous Wavelet Transforms (CWT) are recognized as effective tools for both stationary and non-stationary signals, but they involve much redundant information and is computationally very slow. Discrete Wavelet Transform (DWT) has fast algorithm based on the Conjugate Quadratic Filters (CQF) (Zhu, Wong and Hong, 2009).

Wang and Liang (2009) developed a non-dimensional chatter index based on the Wavelet Transform Modulus Maxima (WTMM) and statistical analysis which included as advantages the random and statistical nature of the metal cutting process. The sensibility to chatters that is well known to be effective in detecting singularities; less susceptibility to process changes; it varies between 0 and 1 independents of cutting processes and hence can be used in different machining processes. The Table 3.3 shows some researches that used Wavelet Transform to process monitoring signal.

Table 3.3 – Some machining researches using Wavelet.

	Researcher	Monitored Signal	Material	Spindle Speed (rpm)	Sampling Frequency
Drilling	Tarng and Lee (1999)	Electric Current	S45C steel	1,000, 1200	1 kHz
	Mori *et al.* (1999)	Cutting Force	Stainless steel 316	2,000	1 kHz
	Velayudham, Krishnamurthy and Soundarapandian (2005)	Acoustic Emission	Laminated composite	1762.95	
Grinding	Liao *et al.* (2007)	Cutting Force	Ceramic	4500	4906 Hz
		Vibration,			4906 Hz
		Spindle Power			4906 Hz
		Acoustic Emission			1 MHz
	Yang and Yu (2011)	Acoustic Emission	1045 steel		1 MHz
Milling	Choi, Narayanaswami and Chandra (2004)	Cutting Force	AISI 1018 steel	1,000, 2,000	500 Hz
	Li, Ouyang and Liang (2008)	Electric Current	AISI 1045 steel	300, 450, 600, 900, 1200	1 kHz
	Zhong, Zhao and Wang (2010)	Vibration	Al 7050-T7451 alloy	3,000 - 18000	2 MHz
Turning	Abu-Zahra and Lange (2002)	Vibration	AISI 4140 steel	200 - 1600	100 MHz
		Ultrasound waves			10 MHz
	Morala-Argüello, Barreiro and Alegre (2011)	Image	AISI 6150 steel		
	Bhaskaran *et al.* (2012)	Acoustic Emission	AISI D3 steel	171, 245, 318	8333 Hz

3.7. Monitoring in the micromachining

The micromachining process requires monitoring techniques with great accuracy. According to Taniguchi (1983), the accuracy machining can be classified into Normal, Precision, and Ultra-precision machining. However, this classification depends on its tolerances and its time, the standard precision has been evolving increased notably since 1930 (10 μm), lower than 1 μm in the 1980 (Taniguchi, 1983), to the present in 1 nm (Zhang *et al.*, 2014). A technique suitable at the conventional measuring is the cutting and thrust forces at ranges from several to hundreds of Newtons. At the ultra-precision scale, the Acoustic Emission (AE) is highly desirable due to its ability to detect microscale deformation mechanisms within a relatively "noisy" machining environment, Figure 3.4 (Lee *et al.*, 2006).

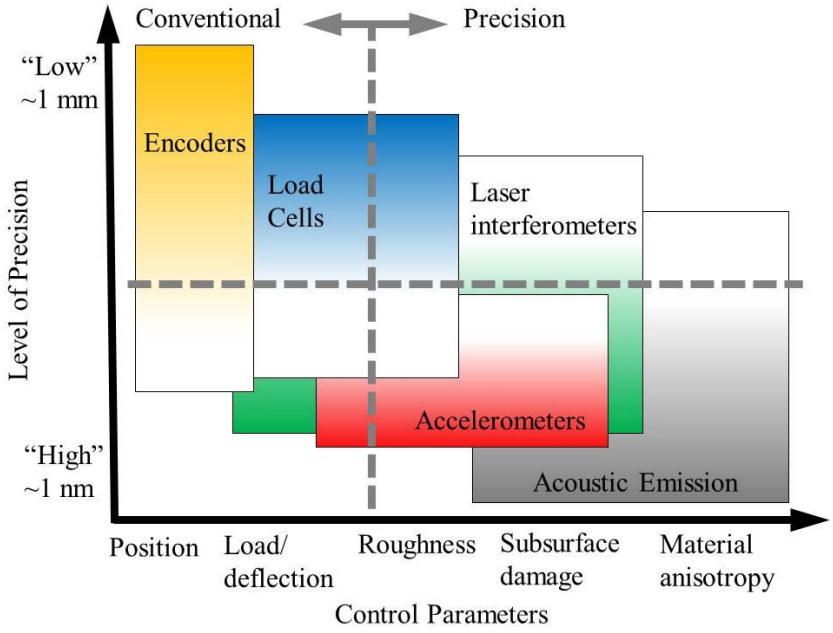

Figure 3.4 – Sensor application vs. level of precision and control parameters (Lee et al., 2006).

Hong, Ha and Cho (2012) used a cutting force monitoring system composed of a micro tool dynamometer, an acceleration sensor and a current hall sensor that affirmed that using current hall sensor and an acceleration sensor can determine the optimum cutting condition. New tasks of TCM used in micro-machining can also cutting edge offset and material structure (Teti *et al.*, 2010).

According to Ren *et al.* (2014) an uncertainty estimation in high precision machining has great meaning for the required continuous improvement in product quality, reliability and manufacturing efficiency in the machining industry. But they found a limitation about the

type-2 fuzzy TCM system based on AE can be the tool life determination is carried out solely.

In their paper Rahman *et al.* (2005) used a microscopic (magnification 10,000 times) to estimate visually surface roughness (less than 0.1 μm) due to their work piece be a micro-pin very small and complex in shape. In the Table 3.4 is exhibited some micromachining researches that used monitoring signals.

Table 3.4 – Monitoring in the micromachining researches.

	Researcher	Monitored Signal	Material	Spindle Speed (krpm)	Sampling Frequency (kHz)
Micro-drilling	Nor *et al.* (1993)	Cutting force	Stainless steel 440F	3	
	Kondo and Shimana (2012)	Acoustic emission, Cutting force, Current electric	AISI 304 steel	10	
	Beruvides *et al.* (2013)	Cutting force, vibration	Tungsten-copper alloy	20, 40, 48	50
	Wang *et al.* (2013)	Cutting force	Laminate Composite	6	
Micro-milling	Ren *et al.* (2014)	Acoustic emission, Cutting force	AISI D2 (50 H_{RC}) steel	36.21	50
	Lauro *et al*. (2015)	Cutting force	AISI H13 (45 H_{RC})	22 and 49	5.6
	Mustapha and Zhong (2013)	Vibration	Al 6061-T6 Alloy	20, 22, 25	
	Zhu, Wong and Hong (2009)	Cutting force	Copper and Steel	18, 20	6
	Kang *et al.* (2008)	Acoustic emission	Al 6061 Alloy	66	400,000
Micro-turning	Palani, Natarajan and Chellamalai (2013)	Image	Tungsten electrode	1.1, 1.2, 1.3	
	Zhang *et al.* (2013)	Cutting force	AISI 1045 steel	0.7	
	Mandal, Kumar and Nagahanumaiah (2013)	Cutting force		2.5, 4.5	
	Silva *et al.* (2008)	Cutting force	Laminate composite	~0.45	

Shin *et al*. (2010) monitored micro-milling of AISI 1045 with a diameter micro-tool of 500 μm using acceleration and current hall sensors with 10 kHz low pass filters to remove high-frequency noise. They used also a micro tool dynamometer to obtain the reference cutting force components in comparison with these signals and FFT to analyse the signal in the Frequency Domain. They calculated the correlations linearity of 98.0% and 94.5% precision with the use of an acceleration sensor and current hall sensors, respectively.

Wang *et al.* (2006) used the wavelet to process the force signal to estimate the tool wear in the micro-milling of POCO-EDM-C3 electrode and aluminium using a carbide tool with diameter of 1/16". They proposed a Wavelet Transform – Pre-processor – Artificial Neural Network (Adaptive Resonance Theory 2 type) combination automatically adjusts the influence of the approximation coefficients one by one by using GA.

To studying the ploughing effect, Yun *et al*. (2011) monitored the cutting force in the micro-milling of copper with a diameter micro-tool of 500 μm. They used a sampling frequency of cutting force of 30 kHz at 45,000 rpm and applied an undecimated wavelet transform. In this study, multi-resolution analysis was used to measure peaks of the cutting force signal that considered a variance of peaks of feed force and normal force is increased under ploughing conditions.

To predict the surface roughness (R_a), tool wear ratio (TWR) and metal removal rate (MRR) on micro-turning of Tungsten electrode, Palani, Natarajan and Chellamalai (2013) developed a prototype system based ANFIS model. They used a surface characterization approach through Machine Vision System applying Image Processing Techniques such as image reduction, histogram equalization, and filtering and analysis algorithms. To attempt to explain surface roughness increases at small feeds, Zhang *et al.* (2013) used a digital camera to measure the material peak-to-valley height and dynamometer to measure the cutting forces.

3.8. Synthesis

Monitoring applied to machining processes can improve the process through an increase in tool life and surface quality with a simultaneous decrease of electric energy and waste material. However, the choice of the monitoring method requires great care due to implementation cost and requirements, besides the objectives to be analysed, i.e., in certain cases, the tool wear monitoring using a dynamometer can be as efficient as the accelerometer, which is more inexpensive. Furthermore, signal interpretation is fundamental. The user should match the best method of analysis to the objective, i.e., if the process uses variable revolution, the vibration or sound monitoring in the frequency domain can be unsuitable if the user does not revise the revolution/frequency ratio. Although

machining monitoring requires great care, its usage brings excellent results for both industrial and academic research.

CHAPTER 4 – STATISTICAL AND ARTIFICIAL INTELLIGENCE FOR THE UNDERSTANDING OF THE MICRO-CUTTING

This chapter was developed to analyse the events, know the phenomena and define the importance of the parameters and the optimum condition in the micro-cutting operation. A large portion of this chapter has similarity with:

- LAURO, C. H. *et al*. Design of Experiments - Statistical and Artificial Intelligence analysis for the improvement of machining processes: A review. in DAVIM, J. P. (Ed.). Design of Experiments in Production Engineering. Heidelberg. Springer International Publishing, 2016.

4.1. Introduction

Nowadays is common to find many investigations that used the statistical and/or Artificial Intelligence analysis in their papers. These methods help to understand the importance of parameter appointed or to define the ideal condition. To obtain a controlled cutting process through the parameter optimisation, a manufacturer should find points in the process that offer the balance of cost and quality (Mukherjee and Ray, 2006). Asiltürk and Akkuş (2011) highlighted that a high number of the cutting variables require a high numbers of experiments, besides, the variables should be studied under controlled conditions.

The usage of these techniques in investigating machinability had the goal of estimating the effects of feed rate, cutting velocity and depth of cut on power consumption and surface finish (Bhattacharya *et al.*, 2008). According to Makadia and Nanavati (2013), in most publications were studied the effect of cutting parameters on surface roughness applying few number of tests. However, they suggested also analyse effect of cutting geometry on surface roughness.

To predict the surface quality, the Artificial Intelligence (AI) methods (artificial neural network, genetic algorithm, and others) has been employed. Its main advantages are models that present most realistic and accurate, a highest level of integration with computers, and an approach that can be used with conventional methods (Lu, 2008).

Paiva *et al*. (2012) used the Multivariate Robust Parameter Design (MRPD) approach to optimise the turning of AISI 52100 using wiper tools due to the moderate to high degree of correlation obtained by multiple responses. The authors observed that MRPD approach showed better results that the individual optimisation routines and minimal variance for each surface roughness profile. Subramanian *et al*. (2013) applied a second-order quadratic model to optimise the milling of Al 7075-T6 aluminium alloy with high-speed steel end mill cutting tool that the deviation is well within the limit of 95% confidence level.

Generally, modelling and monitoring whit statistical methods employ regression-based and time domain techniques (Dey and Stori, 2005). To understand the machinability of tungsten-copper (WCu25) alloy with cemented carbide tool, Gaitonde *et al*. (2010) planned their experiments as per Full Factorial Design (FFD). The adequacy of the quadratic models was verified using the Analysis of Variance (ANOVA) and the analyses used the Response Surface Methodology (RSM).

The trade-offs between energy, production rate and quality were weighed up in a multi-objective optimisation problem by Yan and Li (2013) using grey relational analysis and RSM based method. This approach allowed a reducing of the cutting energy consumption by 18.1% when compared with traditional objective optimisation, satisfying the requirement for sustainable machining. Wang *et al*. (2013) used multi-objective (energy, cost, and machining quality) to optimise the turning of AISI 1045 steel applying Non-dominated Sorting Genetic Algorithm II (NSGA-II).

The present work presents a review of the state of the art on statistical, mathematical and computational techniques applied to machining process planning and analyse. First, statistical methods for design and analyse of experiments are addressed. Subsequently, AI approaches are referenced with focus on machining parameters optimisation. Several papers were covered providing a wide view of methodologies applied to achieve the best results on machining processes.

4.2. Correlations

The correlation between X and Y can be defined as the degree to which the points cluster around the regression line that varies between -1 and 1. The sign of the correlation coefficient has no meaning other than to denote the direction of the relationship, i.e., correlations of 0.75 and -0.75 signify exactly the same degree of relationship (Howell, 2010).

The Spearman's ρ is appropriate to analyse the correlation between some parameters because it identifies monotonic relationships, is resistant to the effect of outliers, and does not assume a specific parametric model or specific distributions for the data (Carou *et al.*, 2014)[2].

4.3. Design of Experiments - DoE

Design of experiments (DoE) comprises a set of statistical techniques to process improvement and planning. Using DoE, the experimenter can adjust the optimum parameter levels to achieve the best output levels and a robust process, that is, a process which has minimum variability.

The DoE strategies can be separated into classical DoE, Response Surface Methodology (RSM) and Taguchi approaches. These methods are commonly jointly applied or with another mathematical and/or computational techniques. There are several statistical packages to apply DoE in machining analysis and planning, facilitating the process improvement.

According to Montgomery (2008) the first statistical concepts to design experiments were based on factorial design and Analysis of Variance (ANOVA). These techniques summarize the classical DoE. Mandal *et al*. (2013) affirmed that the RSM embraces mathematical and statistical techniques to model and analyse the problems in which the objective is to optimise a response that is influenced by the variables.

The Taguchi method is a design of experiments technique, which is useful to reduce the number of experiments and to minimize effects of the not controlled factors, the time of experiments, and costs, besides to present the significant factors in a shorter time. This

[2] Self-citation

technique is focused on determining the parameter settings which produces the best levels of a quality characteristic with minimum variation (Asiltürk and Akkuş, 2011).

Abellan-Nebot and Subirón (2010) affirmed that performing a correct DoE can provide an adjustment of the regression model relatively fine for the machining parameters. In their investigation on turning of AISI 304 stainless steel, Mahdavinejad and Saeedy (2011) used the DoE with full factorial method to analyse the effects of all levels of the parameters.

Krimpenis *et al*. (2004) mentioned that DoE is applied in the manufacturing field to identify the significant parameters that affect the process or product and determine the near-optimum parameter values that increase productivity and machine efficiency. It defines the significant parameters and the ideal values based on the quality characteristics. These authors suggested a series of steps to improve knowledge of the obtained results:

- Choice of parameter levels: each significant parameter has a value out of an extensive field that should be well studied to define the value that are expressive;
- Orthogonal array (OA) issues: is represented by Latin L and number of the array's lines that can be two-level, three-level and mixed-level factors. In this step is chosen the number of parameters and interactions, their levels, and desired experiment resolution between 1 (lowest) and 4 (highest);
- Experiment conduction according to an OA and analysis of results: In this step is applied the statistical analysis. ANOVA is used to define the high influence parameters and draw generic conclusions.

Soshi *et al*. (2012) applied DoE in their investigation to find the best combination of parameters to achieve a smooth surface since there are several important parameters to be considered to produce a high-quality surface in milling operations. In the dry turning of Al 7075-O aluminium alloy study, Agustina *et al*. (2013) used the DoE (24 with 2 replications) to analyse the influence of the cutting parameters on cutting forces in dry turning of an aluminium alloy.

In the investigation of turning of SS202 stainless steel applying cryogenic cooling, Kumar and Choudhury (2008) used the central rotatable composite design of experiments to plan their experiments. This design type allows generating second order models.

Studying the turning of AISI 1045, Hwang and Lee (2010) employed a fractional factorial design with resolution V, widely used in the industry, to analyse the significant effect and two-factor interactions. In this method, generally the significant effects are disconcerted with four factor interactions, and two factor interactions are disconcerted with three-factor interactions, ignoring interactions higher than three factor.

In the electrical discharge machining of AISI D2, Prabhu *et al*. (2013) applied a Full Factorial Design (FFD) using three parameters (pulse current, pulse duration, and pulse voltage) with three levels, amounting to 27 experiments that helped them to found a designed model with 99.7% accuracy.

To find the high influence parameters of the characteristic values in the beginning of the experiment, Park, Kim and Lee (2012), used four factors defined by the FFD and, posteriorly, used the central composite circumscribed design and RSM to optimise the process. They observed that the spindle speed, feed rate, depth of cut, and interval of lubricating oil application presented strong influences in the machinability in ultra-high-speed machining.

4.3.1. Classical DoE (ANOVA)

The influence of some machining parameter can be determined by Analysis of Variance (ANOVA) from a series of results of experiments by the design of experiment approach. ANOVA is the predominant statistical method used to interpret the data (Gopalsamy, Mondal and Ghosh, 2009).

In the 1930's, the Sir Ronald Fisher developed the ANOVA method to understand the results of experiments in the agricultural. He used the sum of the squared deviations from the total mean signal-to-noise ratio, separating its total variability into contributions by each of the design parameters and the error. This method shows the significance of all important factors and their interactions by comparing the mean square against an estimate of the experimental errors at specific confidence levels (Bagci and Ozcelik, 2005).

According to Muthukrishnan and Davim (2009), ANOVA is a technique of portioning variability into identifiable sources of variation and the associated degree of freedom in an experiment. The quality characteristics from the significant effects of the parameters is analysed by Fisher test (F-test). The influence on the result was indicated by the "percent" contribution (P) of each factor.

For some machining processes, especially when the experimenters do not know the factors (controllable or not) affect the outputs, it is necessary to draw a set of screening experiments using fractional factorial designs. Born and Goodman (2001), affirmed that the objective of screening experiments is to diminish a high number of potentially parameters to those that are strong significant since it is not economically practical to perform every possible combination of machining parameters. They studied the tool wear, which observed that the track length, chip size, tool rake angle, and cutting speed had significantly affect in the tested ranges.

In many studies, researchers commonly consider admissible a confidence of 95%, i.e., they use a significance level (α) of 0.05. In Table 4.1 is exhibited some studies that used ANOVA method and the significance level chosen. In the mathematical models developed in turning of AISI 1040, Neşeli, Yaldız and Türkeş. (2011) applied ANOVA and the prediction of surface roughness offered a 96% confident interval.

In the turning AISI 4340 steel with Zirconia Toughened Alumina (ZTA) insert, Mandal, Doloi and Mondal. (2013) used the ANOVA to develop mathematical model that was verified with excellent results. Yu *et al*. (2011) applied ANOVA to find the ideal values of cutting parameters and obtain the better machinability (accuracy and efficiency).

In the Pareto ANOVA the sum of squares of differences (S) for each controlled parameter is calculated as the percentage of sum of squares of differences for each parameter to the total sum of the squares of differences and a Pareto diagram is plotted using the contribution ratio and the cumulative contribution (Sayuti *et al.*, 2011). Hamdan, Sarhan and Hamdi (2012) used Pareto ANOVA method, a very simple alternative to analyse the optimisation exhibiting the influence (percentage) each parameter. This method provided an improvement of cutting forces (25.5%) and surface roughness (41.3%).

Table 4.1 – Significance values used in machining researches.

Researcher	Process	Material	Factors	Significance (%)
Muthukrishnan and Davim (2009)	Turning	Composite	Cutting speed, Feed rate, Depth of cut	5
Gopalsamy *et al.* (2009)	Milling	Tool Steel (55 HR_C)	Cutting speed, Feed, Depth of cut, Width of cut	5
Babu and Chetty (2006)	Waterjet	Al 6063 T6 aluminium alloy	Depth of cut, Top kerf width, Bottom kerf width, Kerf taper, Surface roughness	10
Bagci and Ozcelik (2005)	Drilling	Al 7075-T651 aluminium alloy	Spindle Speed, Feed Rate	5
Carvalho *et al.* (2012)[3]	Tapping	AM60 magnesium alloy	Forming speed, Hole diameter, Type of tool	5
Lin *et al.* (2009)	EDM	AISI H13	Machining polarity, Peak current, Auxiliary current with high voltage, Pulse duration, No-load voltage, Servo reference voltage	5

4.3.2. Response Surface Methodology

The Response Surface Methodology (RSM) is method to optimise and model (empirical approach) a problem to define the relationship between several parameters and the responses with the several desired criteria. For example, this method conjugated with the factorial DoE can predict surface roughness using a small number of experiments (Hessainia *et al.*, 2013).

According to Montgomery (2001), the RSM is a collection of mathematical and statistical techniques that are useful for the modelling and analysis of problems, where, generally, the relationship between the response and the independent variables is unknown. It starts defining an approximation relationship between the response and the variables. The RSM can provide models in linear function (first order), or a polynomial of higher degree (second order) in function of the variables, Equation 4.1 and Equation 4.2, respectively.

$$y = \beta_0 + \beta_1 \cdot x_1 + \beta_1 \cdot x_1 + \cdots + \beta_k \cdot x_k + \varepsilon \qquad \text{Equation 4.1}$$

[3] Self-citation

$$y = \beta_0 + \sum_{i=1}^{k} \beta_i \cdot x_i + \sum_{i=1}^{k} \beta_{ii} \cdot x_i^{\,2} + \sum\sum \beta_{ij} \cdot x_i \cdot x_j + \varepsilon \qquad \text{Equation 4.2}$$

The RSM is used to perform an analysis of the effects of independent variables on the response variables, furthermore, the RSM considers an adjusted surface that were approximately equivalent to the analysis of the process, when adequate (Silva, Ribeiro Filho and Brandão, 2014).

Mandal, Doloi and Mondal (2013) used RSM to model the surface roughness in turning of AISI 4340 and optimised it through desirability function. They optimised the performance of the cutting tool in 92.3% with a combination of cutting parameter, cutting speed (high), feed rate (high), and depth of cut (low). Habib (2009) applied the RSM in the EDM process to determine the relations between the parameters (material removal rate, electrode wear ratio, gap size and the surface finish) for developing mathematical models, in a manner very simple, powerful and flexible.

In the study of turning on the AISI 410 steel, Makadia and Nanavati (2013) applied the RSM and found a quadratic model to analyse the influence of cutting parameters in Ra that presented an error value of 6%. They affirmed that 3D surface counter plots allow determine the ideal combination to optimise the surface roughness. Neşeli, Yaldız and Türkeş (2011) mentioned that in RSM shall have at least three levels for each factor to avoid uncertainties due to estimated values for the combinations of not tested factor.

4.3.3. Multiple Comparisons

The multiple comparisons are used to analyse the statistical significance of differences between means using a set of confidence intervals, a set of hypothesis tests or both. It is because an individual error rates are exact in all cases, and a family error rates are exact for equal group sizes. In general, the null hypothesis of no difference between means is rejected if and only if zero is not contained in the confidence interval (Minitab, 2016). The multiple comparison method can be essential to define an optimal combination of cutting parameter through the response, such as cutting conditions, chip breaker type, and others (Pereira *et al.*, 2013).

According to Montgomery and Runger (2003), the Fisher LSD method, that is easy and very widely used, can be consider to be a very "liberal" procedure in that although each test is at significance level α, the type I error for the entire set of comparisons (called the experimentwise error rate) is much greater than α. The Tukey confidence intervals are a set of simultaneous confidence intervals that hold with probability 1- α. Tukey's method is a very conservative procedure relative to Fisher's LSD because it requires a larger observed difference in treatment averages to declare the pair of means different.

4.4. Artificial Intelligence Analysis

Artificial Intelligence (AI) is related intelligent machines, especially intelligent computer programs that use similar the human intelligence. It is more used in the engineering to resolve problems normally requiring human intelligence due to a number of powerful tools, such as Ant colony optimisation (ACO), Artificial Neural Network (ANN), Expert System (ES), Fuzzy Logic (FL), Genetic Algorithm (GA), Simulated Annealing (SA), Particle Swarm Optimisation (PSO) and various swarm intelligence (Mohd Adnan *et al.*, 2015).

Ramesh, Jyothirmai and Lavanya (2013) cited in their paper the usage of artificial intelligence techniques to develop a thermal error compensation module using temperature values at different locations of the machine. They developed a positioning accuracy measured and surface finish automatically controlled by adjusting the operating parameters using artificial intelligence based regression techniques to build the prediction model between vibration and surface finish.

According to Abellan-Nebot and Subirón (2010), AI technique had been applied to monitoring systems due to need consistent models that can learn complex non-linear relationships between variables and its adequate selection is crucial to develop reliable machining models. Several AI techniques, mainly ANN, fuzzy logic systems and the ANFIS, have been widely used for monitoring machining systems and modelling (surface roughness and tool wear).

4.4.1. Genetic algorithms

Genetic algorithm (GA) can be considered an optimisation technique, indifferently of physical substance, used to resolver a complex problem similar to Darwinian theories of

evolution. Its principle is optimising an objective function in complex multi-modal space that occurs indifferently of the nature of the phenomenon (Vosniakos and Krimpenis, 2002).

According to Wang *et al*. (2006), the GA is based in the theory of biological evolution that include the natural selection. The survival of the fittest uses the parameters, rules, and switches of the problem that are represented by binary combination. This combination is called chromosome that optimises an objective function through the following step:

- Designing of the parents;
- Designing of the hereditary chromosome;
- Gene crossover;
- Gene mutation;
- Creation of the subsequent generation.

In the temperature milling study of Al-6063 aluminium alloy, Sivasakthivel and Sudhakaran (2012) applied GA to optimise the machining parameters to obtain the minimum temperature rise. They found a result that optimised the helix angle, spindle speed, feed rate, axial and radial depth of cut. Rao *et al*. (2009) studied a relationship between the input parameters and surface roughness using GA, which was observed a significant decrease in mean square error when GA is used to optimise an ANN. Non-dominated Sorting Genetic Algorithm II (NSGA II) is a very famous multi-objective optimization algorithm and it was applied in this study because of its coverage and strength (Deb *et al.*, 2002).

The development of GA was based on the LSM (least Square Method) mathematic model. The LSM searches the best fit into a data group, minimizing the sum of the squared differences between the estimated and observed values (generally, this difference is called residual). The least-square method can be linear or non-linear, and the response is a linear function of the independent variables. Thus, the relation between “y” and the three predictor variables can be written as a Taylor series, seen and.

When using a database with 3 input variables and 27 observations, Equation 4.3, the model can be written in matrix form, as follows.

$$\begin{pmatrix} y_1 \\ y_2 \\ y_3 \end{pmatrix} = \begin{pmatrix} 1 & x_{11} & x_{21} & \ldots & x_{271} \\ 1 & x_{12} & x_{22} & \ldots & x_{272} \\ 1 & x_{13} & x_{23} & \ldots & x_{273} \end{pmatrix} \cdot \begin{pmatrix} \beta_1 \\ \beta_2 \\ \ldots \\ \beta_{27} \end{pmatrix} + \begin{pmatrix} \varepsilon_1 \\ \varepsilon_2 \\ \varepsilon_3 \end{pmatrix} \quad \text{Equation 4.3}$$

Where x_{ji} is the value of the j^{th} variable of the i^{th} observation, which can therefore be written in the short form as in Equation 4.4

$$y = x \cdot \beta + \varepsilon \quad \text{Equation 4.4}$$

The solution of LSM can be reached using the minimization of the sum of the square of the errors, Equation 4.5, and it should be rewritten as ε'ε. Thus, replacing ε with y-xβ, we get the following Equation 4.6.

$$\sum_{i=1}^{n} \varepsilon_i^2 \quad \text{Equation 4.5}$$

$$S(\beta) = (y - x \cdot \beta)' \cdot (y - x \cdot \beta) \quad \text{Equation 4.6}$$

The minimization occurs when the derivation S (β) is carried out in relation to (β) and when it is equal to zero, instead of can be seen in Equation 4.7

$$\beta = (2x' \cdot y)^{-1} \cdot 2x' \cdot x\beta \quad \text{Equation 4.7}$$

4.5. Modelling and optimisation for machining process

In the literature, several papers employed models to understand, predict, or optimise the parameters or events that occur in the machining processes. Campos *et al*. (2013) affirmed that the modelling and optimisation are employed by researchers due to it has an important influence in the total cost of the product. It is need due to increase the number of cutting parameters that require high number of tests, consuming several means. These authors suggest the employ of the following methods to model bellow:

- Taguchi and ANOVA: efficient techniques to control the effect on tool wear and surface roughness.

- Response surface methodology (RMS): to optimise the relationship between the several inputs and outputs.
- Adaptive Neuro-Fuzzy Inference System (ANFIS): to provide or optimise the cutting parameter and phenomenon such as surface roughness and tool wear.
- Artificial neural networks (ANN): to predict the phenomenon such as the surface roughness, tool wear.
- Genetic algorithm (GA): to find the factors of a model and optimise the outputs.

Akkuş and Asilturk (2011) affirmed that time, material and labour work may be saved by predicting surface roughness without experimental testing for intermediate values. They developed accurate models to predict the surface roughness in the turning of AISI 4140 applying ANN, Fuzzy logic and statistically multi-regression methods for the used input parameters, cutting speed, feed rate and depth of cut.

Hessainia *et al*. (2013) classified the surface roughness (R_a) modelling techniques into three groups: experimental; analytical; and AI models. They proposed a model using the RSM for the hard turning of AISI 4140 (56 HR_C), which found a quadratic model of RMS with correlation coefficient of 99.9% and 96.4% for models Ra and Rt respectively.

According to Upadhyay, Jain and Mehta (2013), to predict the surface roughness using machining parameters was useful only to define the parameters for finishing due to the vibrations/cutting forces. They developed this model using multiple regression method as a function of vibration in radial, axial and tangential directions. They tested the prediction using an ANN model that was trained with the Levenberg-Marquardt. These developed models can be effect to predict the surface roughness with average error of 4.11% and maximum error of 6.42%.

Lopes *et al*. (2013) presented a model considering the multivariate uncertainty as weighting matrix for the principal components. In the study of turning of AISI 52100 hardened steel with wiper tools was implemented a Central Composite Design using three factors, cutting parameters, for a set of five correlated metrics, different surface roughness profile. The results showed that the developed technique presented an excellent predictability.

4.6. Synthesis

The objective of the manufacturers is obtaining a production that be economic, ecological, efficient and reliable. Thus, in the machining sector, there are several developments in tools (example the geometry, material, and coatings) and machines (example power, spindle speed, and accuracy). However, the definition of the cutting parameters is more important to obtain a condition that results in desired objectives. The users can be several parameters as outputs, as the tool wear, chip removal volume, cutting forces, vibration and others. After, the users should analyse the outputs and define the cutting parameters to obtain the desired objective, as the maximum production, low time, or quality of product, and others.

Meantime, the machining processes are composed of several operations, as turning, milling, drilling, broaching, and others, that have variables, as cutting speed, feed rate, depth of cutting, cooling system, and others. Sometimes, the users ignore or forget that some variable can be influence the process, as the brands, room temperature, material structure, and others. Thus, the users should realize randomly all tests at least twice (repeat and replications), to reduce the influence of the not assigned variables and the randomness of responses. Furthermore, the analysis will be more reliable and easily to comprehend the influence of the parameters.

The analysis of the outputs using Statistical and/or Artificial Intelligence methods provides results about the cutting parameter and their interaction that facilitate the comprehension of machining phenomena. These methods employed to model the process can indicate the best cutting parameter combination to obtain a product with maximum quality, minimum losses (time, material, and others) among the tested condition. The usage of the one or both methods will depend of the user's goal, i.e., if the user want an analysis simplest, the statistical analysis using the ANOVA can be the ideal method. However, if the research employs the several factors, levels, and other or the previse results, the usage of the Artificial Intelligence analysis, as the Artificial Neural Network (ANN), can be the ideal method. Furthermore, the planning of experiments is more important in the research because it can reduce the cost and the time need to execute the experimental.

CHAPTER 5 – MATERIAL AND METHODS

In this chapter is presented the material and equipment used to investigate the behaviour of the biomaterial with poor machinability when employed the micro-cutting in the finishing operation. Furthermore, it is presented and justified the choice of the monitoring, processing, statistical and artificial intelligence techniques to observe and identify the events in the micro-cutting. Some portions of this chapter has similarity with:

- LAURO, C. H. *et al*. Analysis of behaviour biocompatible titanium alloy (Ti-6Al-7Nb) in the micro-cutting. Measurement, v. 93, 2016, p. 529-540.

- LAURO, C. H. *et al*. Analysis of the tool wear influence in the micro-cutting in the Ti-6Al-7Nb titanium alloy. IX National Congress of Mechanical Engineering - CONEM. Fortaleza. 2016.

5.1. Biomaterial and the Ti-6Al-7Nb titanium alloy

The biomaterials are synthetic or natural substances (single or combination) to prolong or improve the quality of life of the individual, augmenting or replacing tissue, organ, or function of the body (Bergmann and Stumpf, 2013). Biomaterials have enhanced the osseointegration and regeneration, however, the engineering should be seeking or improving biomaterials continuously because the growing bone tissue is a dynamic process and changing requirements appear every day (Agarwal and García, 2015). Several materials classes can be employed as biomaterials, an example, for odontology is employed the largest range of materials, as polymers, surgical cements, ceramics, and others (Hisbergues et al., 2009).

Metal biomaterial, that should be biocompatible, non-immunogenic and good osseointegration, are applied where the mechanical properties are required, which should be bind strongly to bones to minimize the looseness and guarantee the physiological function, such as the femur, tibia, and others. The titanium (pure and alloys) and stainless steel are the

most used metal. Although the stainless steel has been used for over 100 years due to excellent mechanical properties and resistance to corrosion, with an emphasis on the 316 L, the titanium and its alloys have gained significant interest in recent years. It is because booth materials have a similar strength, but the titanium (pure and alloy) is much lighter than the stainless steel (Agarwal and García, 2015).

Several in-vivo and in-vitro studies for the titanium and its alloy have been developed throughout the world for the last 50 years. It may be justified because these materials are the most attractive metallic biomaterials, whether in medicine or in dentistry. Its important biocompatibility characteristics are the low level of electronic conductivity, high corrosion resistance, thermodynamic state at physiological pH values, low ion-formation tendency in aqueous environments, and an isoelectric point of the oxide (Elias et al., 2008).

Among the metallic biomaterials, the commercially pure titanium can be considered as the best biocompatible due to surface properties result in the spontaneous build-up of a stable and inert oxide layer (Elias *et al.*, 2008). However, the titanium alloy has higher resistance to repeated stress loading that is ideal for load-bearing orthopaedic applications, besides, the modulus of elasticity is lower and is more conducive to minimize stress at interfaces (Agarwal and García, 2015). In the literature can be found several studied that analysed the biocompatibility between commercial pure titanium and titanium alloys (Andrade *et al.*, 2015; Fernandes, Elias and Valiev, 2015; Zhang and Liu, 2015).

When compared the commercial pure titanium and Ti-6Al-4V titanium alloy, Shah *et al*. (2016) gathered on literature information about surfaces machined, osseointegration, and bacterial interactions. The surface machined were similar (morphology, topography, phase composition and chemistry). For the bacterial adhesion to surfaces, in vitro tests, some papers fail to disclose differences, others pointed a favouring one material over the other depending on the bacterial species under test and the methodological design. The osseointegration in rabbits was similar in both biomaterials after 8 weeks, although a research group observed a higher biomechanical capacity of commercial pure titanium. According to these authors, the choice between these materials (pure or alloy), that is indisputable, is based on the mechanical properties, strongly, then biology for the implant material.

The Ti-6Al-4V titanium alloy is the most employed titanium-based biomaterial used in the medical/dental applications that require the replacing of hard tissues, likes artificial hip joints and dental implants (Niinomi, 2003). A notion of this fact can be observed through the high number of researches of the Ti-6Al-4V titanium alloy found in the Engineering Village database (2016), which can correspond about 90% of publications in titanium alloy on the, Figure 5.1. However, new titanium alloys have been developed to replace the Ti-6Al-4V titanium alloy due to the presence of vanadium (V), which are called of V-free. This is because the vanadium be a toxic element (Gallego *et al.*, 2012; Santos *et al.*, 2016). Although vanadium is not clastogenic, it is cytotoxic and mitogenic and can modify several cell functions involved in mitosis and the formation of DNA–protein. Meanwhile, the degree of toxicity depends on several aspects, the chemical form, the oxidation state, the route of exposure, the period of dosing, and the dose administered (Domingo, 2002).

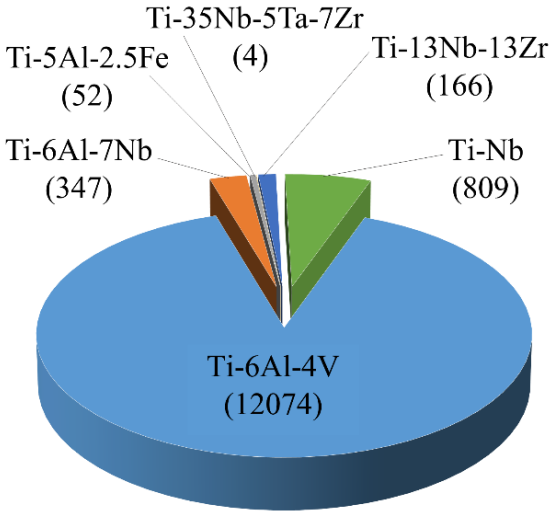

Figure 5.1 – Number of papers about titanium-based biomaterial (Engineering Village, 2016).

Several alloys have been studied to obtain a substitute of the Ti-6Al-4V, such as Ti-10Cu (Zhang and Liu, 2015), Ti-Mo-Sn-Zr (Nunome *et al.*, 2015), Ti-Mn (Santos *et al.*, 2016), and others. In addition to these alloys, the Ti-6Al-7Nb has strong emphasis in the bioapplications researches. Ashida *et al*. (2015) studied the superplasticity in the grain refinement of the Ti-6Al-7Nb titanium alloy using the high-pressure torsion. When using values from the literature to compare with Ti-6Al-4V titanium alloy, the authors observed an increasing in the superplastic elongation of 575% and 676%.

Gallego *et al*. (2012) investigated the microstructural of the Ti-6Al-7Nb titanium alloy after equal channel angular pressing (ECAP) followed by thermomechanical treatment. Chlebus *et al*. (2011) investigated the influence of laser melting in the mechanical properties and microstructure of the Ti-6Al-7Nb titanium alloy, which observed layered microstructure with thin plates of α′ martensite hardened by evenly distributed dispersive phase, discontinuities at low ductility indicates the initiation of fatigue cracks. The authors recommended a thermal treatment for increasing the resistance for the bioapplications of this material.

In this study, the bars of Ti-6Al-7Nb titanium alloy provided by TiFast S.R.L., were used. The material was annealed, their structure composed by fine dispersion of the α and β phases (A4 as per ETTC 2 Ed 2), Figure 5.2. The internal microstructure of Alpha-Beta phase can be classified between A1 and A24, however, only the microstructure between A1 to A10 is considered adequate for the manufacturing of orthodontic mini-implants (Cotrim-Ferreira *et al.*, 2010). The mechanical proprieties and chemical composition are showed in the Table 5.1 and Table 5.2, according to TiFast quality certificate, seen the Annex A. The Table 5.3 shows the physical properties of the Ti-6Al-7Nb titanium alloy.

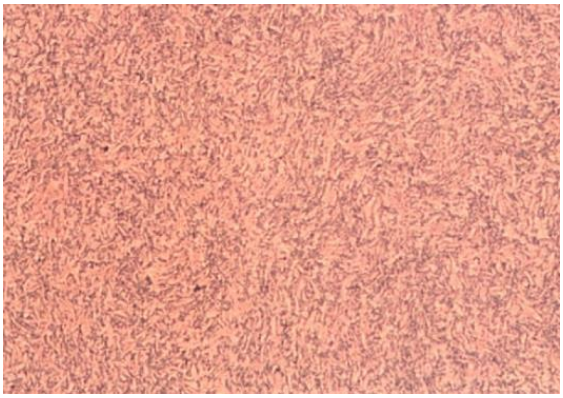

Figure 5.2 – Ti-6Al-7Nb titanium alloy microstructure (magnification 200x) (courtesy TiFast S.R.L.).

Table 5.1 – Chemical composition of the Ti-6Al-7Nb titanium alloy.

Element	**Maximum (%)**	**Element**	**Maximum (%)**
Al	5.94 - 6.02	Nb	6.83 - 6.90
C	0.013	O	0.169 - 0.178
Fe	0.15 - 0.16	Ta	0.05
H	0.003	Ti	In balance
N	0.005		

Table 5.2 – Mechanical properties of Ti-6Al-7Nb titanium alloy.

Property	**Reference standard (minimum)**	**Measured (ASTM E8/E8M-09)**
Tensile Strength (MPa)	900	995
Yield Strength 0.2% (MPA)	800	910
Reduction of area (%)	25	49.6
Elongation (%)	10	15.4

Table 5.3 – Physical properties of Ti-6Al-7Nb titanium alloy (AZO Material, 2016).

Property	Unit	Value
Density	kg/m^3	4510 - 4530
Latent heat of Fusion	kJ/kg	360 - 370
Melting temperature	K	1800 - 1860
Resistivity	$\Omega \cdot m$	126×10^{-8} - 158×10^{-8}
Specific heat	$J/kg \cdot K$	540 - 560
Thermal conductivity	$W/m \cdot K$	7 - 8
Thermal expansion	K^{-1}	8×10^{-6} - 9.8×10^{-6}

5.2. Machine and equipment for the micro-machined surface investigation

This section describes the machines (as such the lathe), the equipment (dynamometer, accelerometer, thermos-couple, and other), and the cutting tools that were used in the micro-cutting tests.

5.2.1. Lathe

A Kingsbury™ MHP 50 CNC lathe with 18 kW power and maximum spindle speed of 4,500 rpm, was used, Figure 5.3. However, the spindle speed was limited at 3,000 rpm due avoid excessive vibrations during the cutting.

Figure 5.3 – Kingsbury™ MHP 50 CNC lathe used for the tests.

5.2.2. Cutting tools

To develop the micro-cutting, were employed different cutting tools setting, which depended of the objective of the experimental tests. A setting was composed by TPGN 16 03 04 H13A cutting inserts, Figure 5.4, and CTGPL 2020 K16 (ISO) tool holder, Figure 5.5, both supplied by Sandvik Coromant™. The tool holder has a rake angle of 6º, tool cutting edge angle of 91º, and cutting edge inclination angle of 0º. The characteristics of the cutting insert is shown in the Table 5.4.

Figure 5.4 – TPGN 16 03 04 H13A inserts used in the micro-cutting tests.

Figure 5.5 – CTGPL 2020 K16 tool holders used in the micro-cutting tests.

Table 5.4 – Geometry data of the TPGN 16 03 04 H13A inserts used micro-cutting tests (Sandvik Coromant, 2012).

Material	Coating	Tool noise radius (mm)	Edge radius (µm) *	Clearance angle (º)	Chip-breaker
cemented carbide	No	0.3969	20	11	No
* Edge radius was measured by the author.					

The other settings were employed three kind of V-inserts and two kind of tool holder provide by Sandvik Coromant™, Figure 5.6 and Figure 5.7. The selected tool holders were SVJBL

2020K 16 and DVJNL 2020K16, both tool holder have the tool cutting edge angle is 93º. The Table 5.5 and Table 5.6 show the geometry data of the tool holders and inserts, respectively.

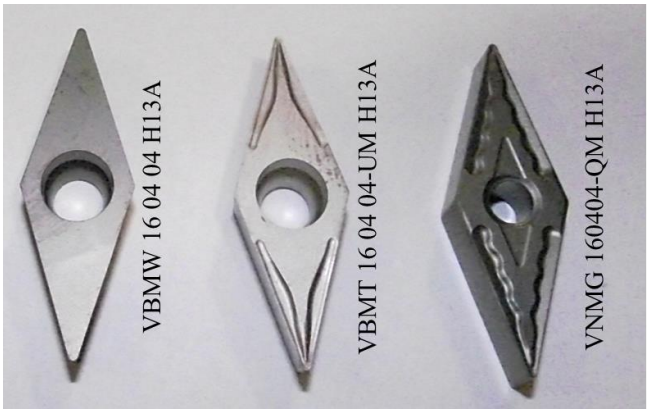

Figure 5.6 – Inserts used in the cylindrical micro-cutting tests.

a) Tool holder SVJBL 2020K 16.

b) Tool holder DVJNL 2020K16.

Figure 5.7 – Tool holders used in the cylindrical micro-cutting tests.

Table 5.5 – Geometry data of the tool holders used in the micro-cutting tests (Sandvik Coromant, 2012).

Tool holder	Orthogonal rake angle (º)	Inclination angle (º)
SVJBL 2020K 16	0	0
DVJNL 2020K 16	-4	-13

Table 5.6 – Geometry data of the inserts used micro-cutting tests (Sandvik Coromant, 2012).

Insert	Material	Coating	Tool noise radius (mm)	Edge radius (µm)	Clearance angle (º)	Chip-breaker
VBMW 16 04 04 H13A	cemented carbide	No	0.3969	15	5	No
VBMT 16 04 04-UM H13A	cemented carbide	No	0.3969	15	5	Yes
VNMG 160404-QM H13A	cemented carbide	No	0.3969	25	0	Yes

* Edge radius was measured by the author.

5.2.3. Minimum Quantity Lubrication System

For the cooling/lubrication in the micro-cutting tests, was used an Unist™ Minimum Quantity Lubrication (MQL) system model Coolubricator JR, Figure 5.8, with the biodegradable oil Coolube™ 2210.

Figure 5.8 – MQL system used in the micro-cutting tests.

5.2.4. Piezoelectric dynamometer

In turning operation exist the three force components that generally are defined as the Cutting forces (force occurs along the direction of cutting speed, tangential to turned surface), Feed

or Thrust force (force occurs along the direction of the tool feed whereas radial force acts perpendicular to the turned surface) and Depth force, among these forces, the Cutting force and feed force plays major role in determining the machinability of any material (Thakur, Ramamoorthy and Vijayaraghavan, 2009). To acquire the cutting forces, a setting was composed by a Kistler™ piezoelectric dynamometer model 9121 (Figure 5.9a), a Kistler™ charge amplifier model 5019B (Figure 5.9b), and the Dynoware™ software, was used.

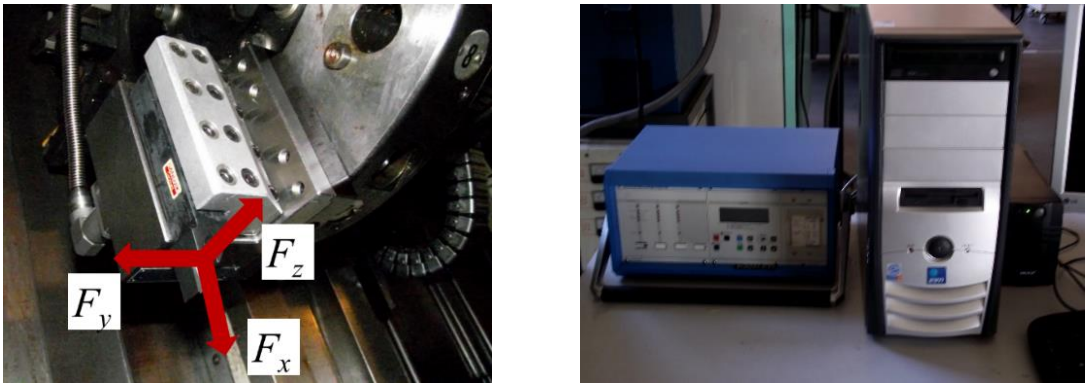

a) Piezoelectric dynamometer. b) Change amplifier.

Figure 5.9 – Setting to acquire the cutting forces during the micro-cutting tests.

5.2.5. Accelerometer

The vibration during the cutting was acquired using a Dytran™ shock accelerometer model 3200B (Figure 5.10a) and a signal conditioners/vibration meters Dytran™ model 4102C (Figure 5.10b). The signal was monitored using a National Instrument™ connector block model BNC-2120 (Figure 5.11), a National Instrument™ I/O card PC 6034, and a Virtual Instrument (VI) developed on the software Labview™, Figure 5.12.

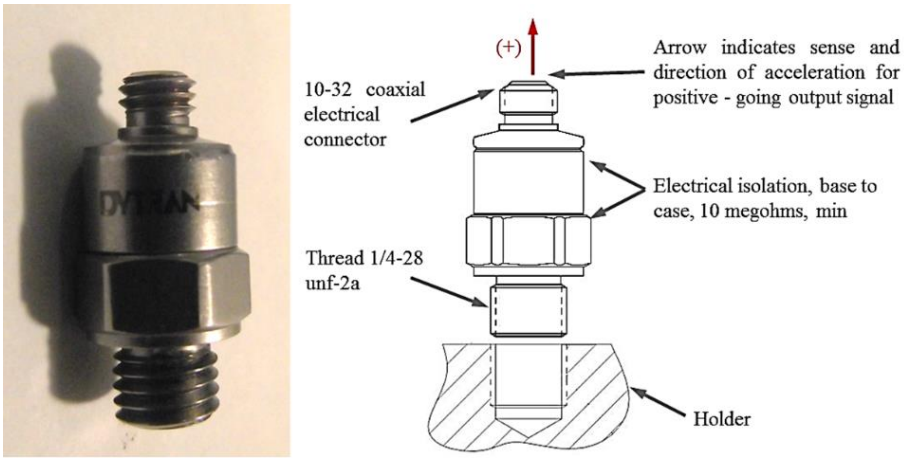

a) shock accelerometer (photo and diagram).

b) Signal conditioner.

Figure 5.10 – Setting to acquire the vibration during the micro-cutting tests.

Figure 5.11 – Connector block used in the monitoring of the vibration signals.

Figure 5.12 – Virtual instrument used to acquire the vibration signal.

5.2.6. Temperature

The temperature in the tool can be considered a most important parameters to improve the cutting conditions, understand the tool wear and obtain acceptable surface integrity (Coz *et al.*, 2012). To observe the evaluation of the temperature in the tool, during the cutting, a thermos-couple K from Thermo-electra™ provided by PCE Ibérica, was used. The signal was monitored also using the National Instrument™ connector block model BNC-2120 and the I/O card PC 6034, described in the section 5.2.5. Another VI was developed to monitoring the temperature signal, Figure 5.13.

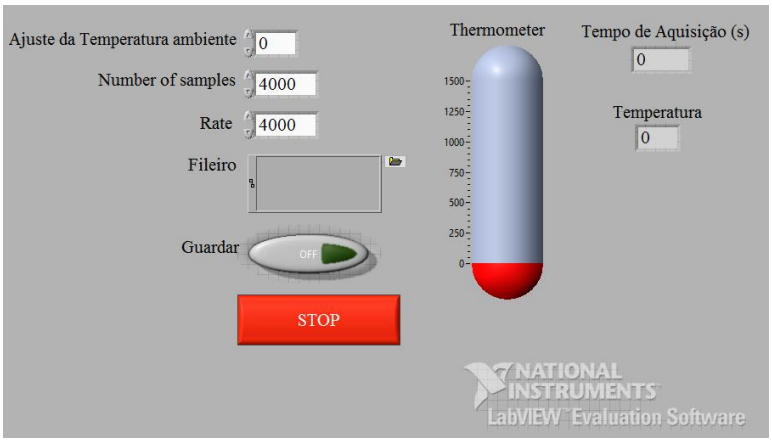

Figure 5.13 – Virtual instrument used to acquire the temperature signal.

5.2.7. Surface roughness

To measure the surface roughness, seen the section 2.2.1, in the workpieces during the micro-cutting tests, a portable surface tester Hommel™ T 500, was used, Figure 5.14. To measure the surface roughness in the machined components with complex geometry, was used a Taylor Hobson™ profilometer model Talyrond 131c, Figure 5.15.

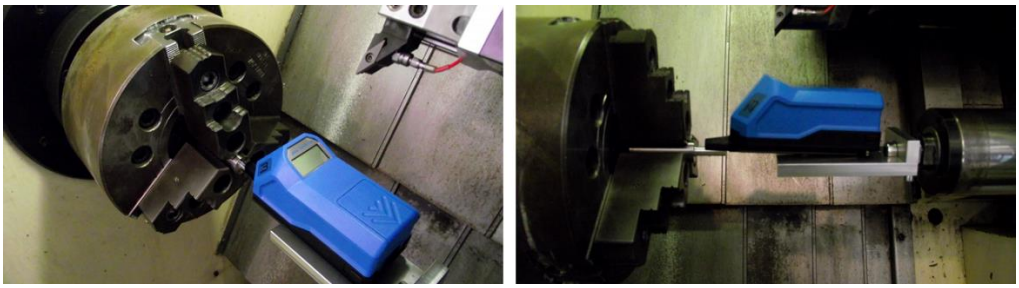

Figure 5.14 – Portable surface tester used in the micro-cutting tests.

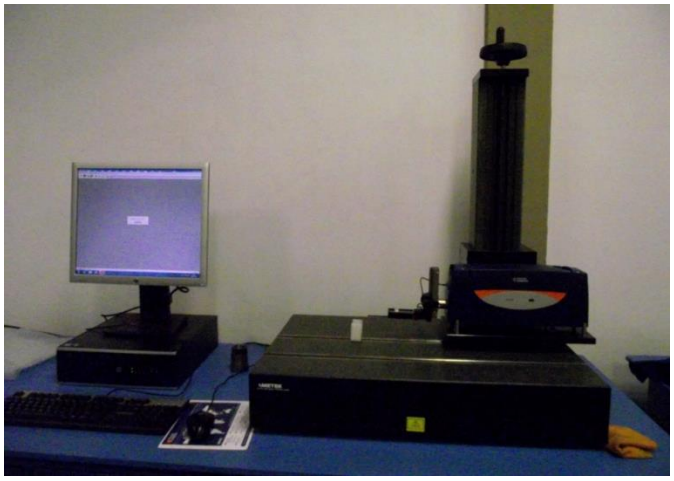

Figure 5.15 – Taylor HobsonTM profilometer model Talyrond 131c used in micro-cutting tests.

5.2.8. Electrochemical tests

Several studies have been developed to characterize and improve the biomaterials, such as the machining, mechanical properties, design. Among the analysis of mechanical characteristics, the corrosion is a big significance in biomaterial property. A brief search in the Engineering Village (2016) database indicated that when combined the "CORROSION" and "BIOMATERIAL", the results corresponded to 3.2% of the result when use only "BIOMATERIAL", Figure 5.16.

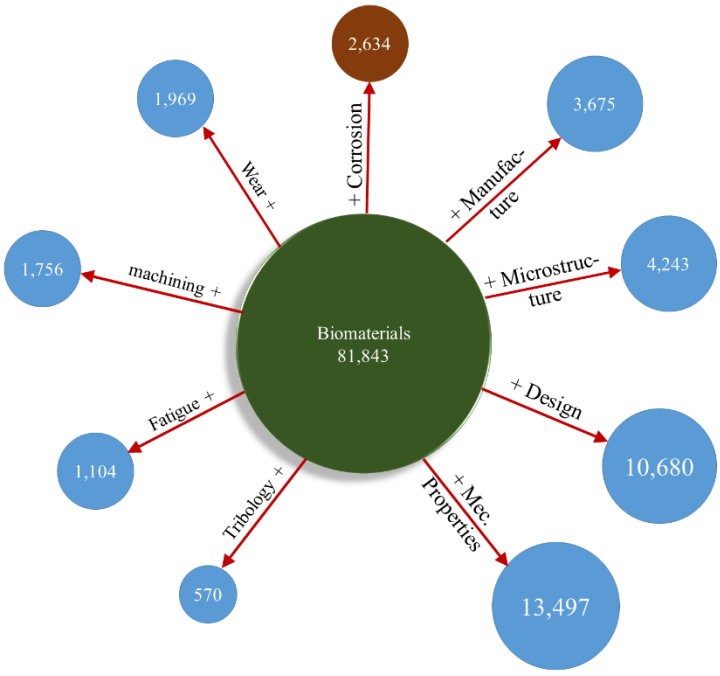

Figure 5.16 – Type of analysis in the biomaterial (Engineering Village, 2016).

The corrosion, gradual degradation, of biomaterials is a complex multifactorial phenomenon that are related to several aspects, such as geometric, metallurgical, mechanical and solution-chemistry. This is important due to metallic implant is placed in the hostile electrolytic environment provided by the human body. The degradation of metallic implants is undesirable because it can decrease their structural integrity and elicit an adverse biological reaction due to the release of degradation products. It can occurs due to electrochemical dissolution phenomena, wear or a synergistic combination of both (Balamurugan *et al.*, 2008). The tolerable corrosion rate is estimated about $2.5x10^{-4}$ mm per year, on maximum (Callister and Rethwisch, 2012).

Basiaga *et al*. (2015) analysed the corrosive behaviour of the Ti-6Al-7Nb titanium alloy under simulated of blood. The workpieces were coated with a SiO2 layer and exposed for 28 days, which was observed functional implant application and coating structure for the thickness adequate. Ribeiro Filho (2016, 2016b)[4] investigated the influence of the machining processes in the corrosion behaviour of the Ti-6Al-4V using the simulated body fluid (SBF). For turning process, the authors observed the significant influence of the feed rate and depth of cut in the corrosion rate. The combination of the lowest feed rate and depth of cut improved the biocompatibility due to the formation of the passive layer more quickly.

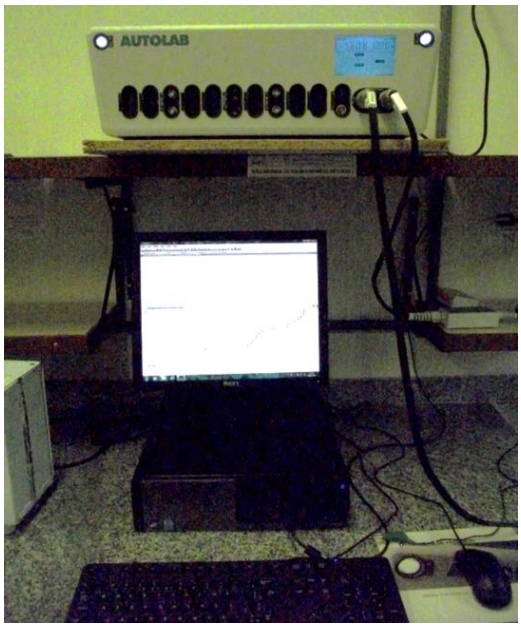

Figure 5.17 – Potentiostat/galvanostat used in electrochemical tests.

[4] Self-citations.

A modular line potentiostat/galvanostat instruments Model PGSTAT 128N from Metrohm Autolab™, was used to develop the electrochemical tests, Figure 5.17. The NOVA™ 1.11 software was used to control the tests. The reference electrode was a saturated calomel electrode and the counter-electrode was a platinum wire. To steady the temperature of the solution during the electrochemical analysis, was used a Novainstrument™ thermostatic bath model NI 1235, Figure 5.18. The measure of the pH of the solution was made by a Hanna Instruments™ pH meter model HI 2221, Figure 5.19.

Figure 5.18 – Thermostatic bath to steady the temperature in electrochemical tests.

Figure 5.19 – The pH meter to measure the pH of the solution of electrochemical tests.

5.2.9. Scanning electron microscope

A Hitachi^{TM} scanning electron microscope (SEM) model SU-70, Figure 5.20, was used to observe the machined surface, chip and tools used in the investigation.

Figure 5.20 – Scanning electron microscope, DEMAC (2015).

5.3. Preliminaries studies of micro-cutting in the biomaterial

In the literature is found few studies of the machining in the Ti-6Al-7Nb titanium alloy, it was decided to develop preliminaries tests to understand the behaviour of this biomaterial in micro-cutting, and define the measurements techniques. Thus, were developed orthogonal micro-cutting tests in the Ti-6Al-7Nb titanium alloy. The orthogonal cutting, Figure 5.21, is a type of cutting that has been applied in many machining processes studies. Because the simplicity, it can help understand the basic mechanics of the machining process, many researchers employing this process to develop their models (Cheng, 2009). The orthogonal cutting is a simplified cutting operation that is employed as the first stages of investigations (Trent and Wright, 2000). The existence of only two cutting force components or the uncut chip thickness (t) can be considered equal to feed rate are some aspects that simplified the orthogonal cutting.

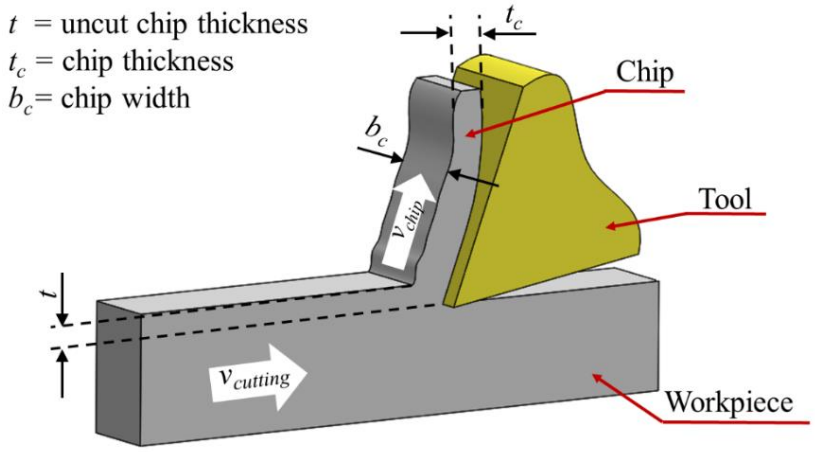

Figure 5.21 – Schematic of orthogonal cutting.

The orthogonal cutting was employed to study several machining phenomena in the AISI 1045 (Guohe, Cai and Bing, 2010) steel, Ti-6Al-7Nb titanium alloy (Ducobu, Rivière-Lorphèvre and Filippi, 2016), or bone (Liao and Axinte, 2016). To compare with orthogonal cutting, macro-scale, Fromentin *et al*. (2016) developed a laboratory machine to study of fundamental of micro-cutting. The authors performed some micro-cutting tests to observe models of micro-cutting, such as the influence of the lubrication in the cutting forces, chip, and the nominal value of depth of cut in the micro-cutting of 316L stainless steel with a tungsten carbide (WC) insert. Liu and Melkote (2007) developed a FEM model to study the influence of tool edge radius on size effect in orthogonal micro-cutting process, which observed a nonlinear growth of the specific cutting energy when the uncut chip thickness and closed to the edge radius.

Schneider *et al*. (2016) used the orthogonal micro-cutting to study the influence of the rake angle in micro-cutting of titanium commercial pure. They observed that an increase of the rake angle can improve the quality of the surface due to it reduce the plastic deformation in chip formation, independent of the uncut chip thickness. Ducobu *et al*. (2016) observed that the thrust force is larger than the cutting force, which go against the conventional cutting theory.

5.3.1. Material and methods

The workpieces of Ti-6Al-7Nb titanium alloy was machined, in wet condition, to obtain the "tube" shape with wall thickness of 0.8 mm and 1.1 mm, Figure 5.22. The tests were done using the Kingsbury^{TM} MHP 50 CNC lathe, described in the section 5.2.1, and the

piezoelectric dynamometer with the setup described in the section 5.2.4. The cutting tool setting was composted by the inserts TPGN 16 03 04 H13A and a tool holder CTGPL 2020 K16, described in the section 5.2.2, were used. The cutting was performed without the tool noise radius, i.e., the depth of penetration of the tool was more than the thickness of workpiece, Figure 5.23. The tests were carried out randomly and repeated twice.

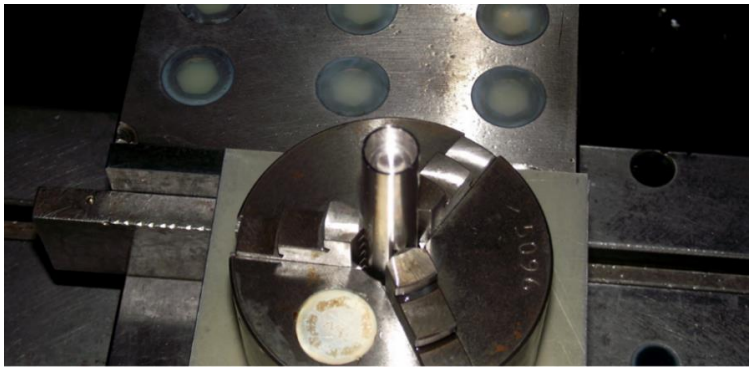

Figure 5.22 – Workpieces for the orthogonal micro-cutting tests in the titanium alloy.

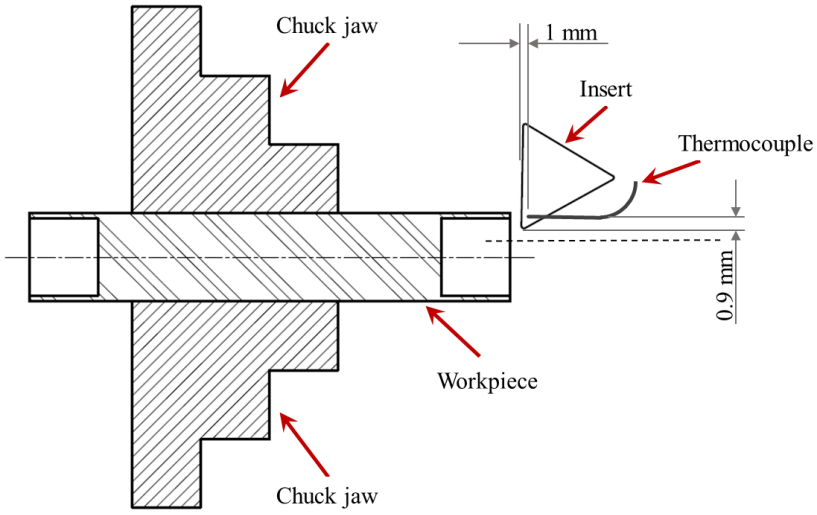

Figure 5.23 – Orthogonal micro-cutting tests in the titanium alloy.

5.3.2. Measurement techniques and analysis

The cutting force were monitored using the setting described in the section 5.2.4. The set was configured as a sample frequency of 4 kHz, an acquisition time of 300 seconds and manually triggered. To study the phenomena that occur in machining processes, the several researchers have been employed the signal processing techniques (Lauro *et al.*, 2014). One of these techniques is the Wavelet Transform, seen the section 3.6.3, which was employed

in micro (Lauro *et al.*, 2015; 2006; Yun *et al.*, 2011) and macro (Sevilla-Camacho *et al.*, 2015; Yang and Yu, 2011) scales in machining process. The Wavelet Transform was employed to classify the signal in all tested conditions with the same refinement level, as can be seen in Figure 5.24. To define the forces, a small section in the beginning and end of the acquired signal, the same for each component, was discarded due to the inertia. Furthermore, the maximum and minimum values of the cutting forces were defined by the average of the peaks, Figure 5.25.

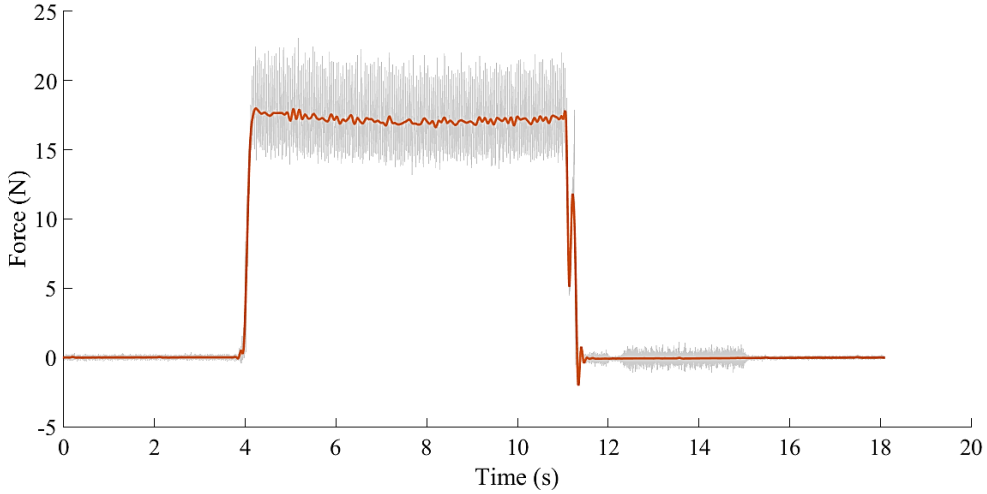

Figure 5.24 – Processing of the acquired force signals of micro-cutting tests.

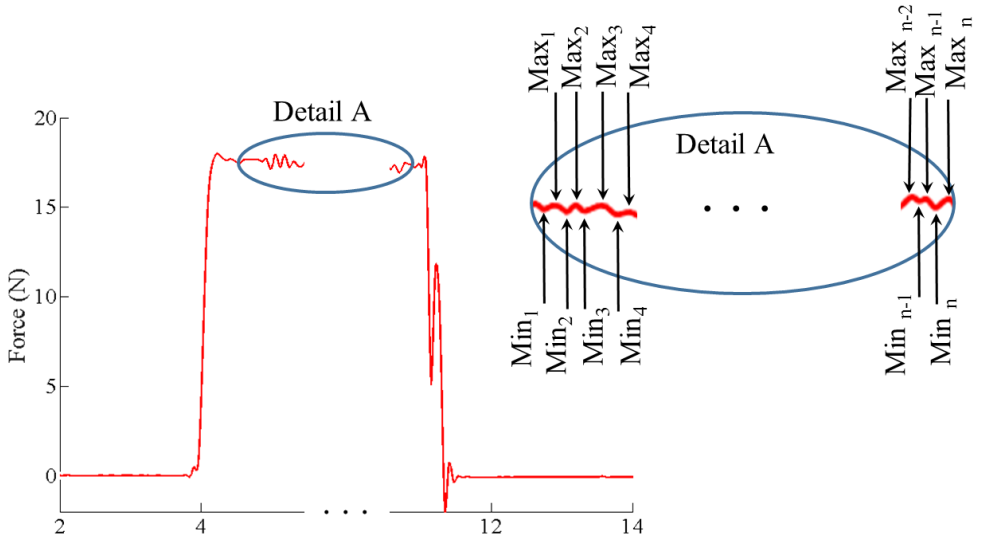

Figure 5.25 – Definition of maximum and minimum values of micro-cutting force.

The same section used to define the cutting forces was used to calculate the friction coefficient (μ), specific cutting energy (u_c), and the shear plane. The values of the friction

coefficient, specific cutting energy were calculated by the average of acquired points, Equation 5.1 and Equation 5.2, respectively.

$$\mu = \frac{\sum_{1}^{n} \frac{F_{T_i} + F_{c_i} \cdot \tan\gamma}{F_{c_i} - F_{T_i} \cdot \tan\gamma}}{n} \qquad \text{Equation 5.1}$$

Where,

F_T ↔ thrust force (N)
F_c ↔ cutting force (N)
i ↔ time increment
γ ↔ tool rake angle (º)
n ↔ number of increments

$$u_c = \frac{\sum_{1}^{n} \frac{v_c}{V_{rem}} \cdot \sqrt{F_{T_i}^{\ 2} + F_{C_i}^{\ 2}} \cdot \Delta t}{n} \qquad \text{Equation 5.2}$$

Where,

u_c ↔ specific cutting energy (J/mm^3)
F_T ↔ thrust force (N)
F_c ↔ cutting force (N)
v_c ↔ cutting speed (m/s)
V_{rem} ↔ removed chip volume (mm^3)
Δt ↔ interval of time equally spaced (s)

To calculate the shear plane angle (φ), the experimental (Equation 5.3), Merchant (Equation 5.4), and Lee - Shaffer (Equation 5.5) models were used. The Merchant model employs the derivative of the shear stress with respect to φ considering its value zero; and the Lee - Shaffer model assumes that the material was an ideal rigid-plastic solid and the shear plane approaches of the direction of maximum shear, ignoring the work of separation (Silva *et al.*, 2012).

$$\varphi_{Experimental} = \arctan\frac{\cos\gamma}{\zeta - \text{sen}\gamma} \qquad \text{Equation 5.3}$$

$$\varphi_{Merchant} = \frac{\pi}{4} - \frac{1}{2}\cdot\left(\arctan\mu - \gamma\right) \qquad \text{Equation 5.4}$$

$$\varphi_{Lee-Shaffer} = \frac{\pi}{4} - \arctan\mu + \gamma \qquad \text{Equation 5.5}$$

Where,

γ ↔ tool rake angle (º)

μ ↔ friction coefficient (Equation 5.1)

ζ ↔ chip compression ratio

The measurement of the chip thickness (t_c) was performed with a Mitutoyo™ digital micrometre model MDC-25SB. The value of the chip thickness was the mean value of the values measured for ten specimens, which were cleaned and dried before the measurement. These measures were used to calculate the chip compression ratio (ζ), Equation 5.6, and the chip deformation (ε), Equation 5.7. The uncut chip thickness (t) was considered equal to feed rate (f) because the process was an orthogonal cutting.

$$\zeta = \frac{t_c}{t} \qquad \text{Equation 5.6}$$

Where,

t_c ↔ chip thickness (mm)

t ↔ uncut chip thickness (mm)

$$\varepsilon = \frac{\zeta^2 - 2\zeta\cdot\sin\gamma + 1}{\zeta\cdot\cos\gamma} \qquad \text{Equation 5.7}$$

To observe the temperature in the tools, a “type K” thermocouple, described in the 5.2.6, was used, which was positioned at 1 mm of the cutting edge to avoid interference in the chip outlet. To reduce the noise, in the holders was applied insulating tape. The acquisition was made using a sample frequency of 4 kHz and manually started and stopped. To denoise the signal, the Wavelet Transform was employed, seen the section 3.6.3. To define the criterion for comparison of temperature, was used the mean of the maximum peak in the monitored temperature each condition. The Figure 5.27 exemplifies the maximum peak of temperature for comparison.

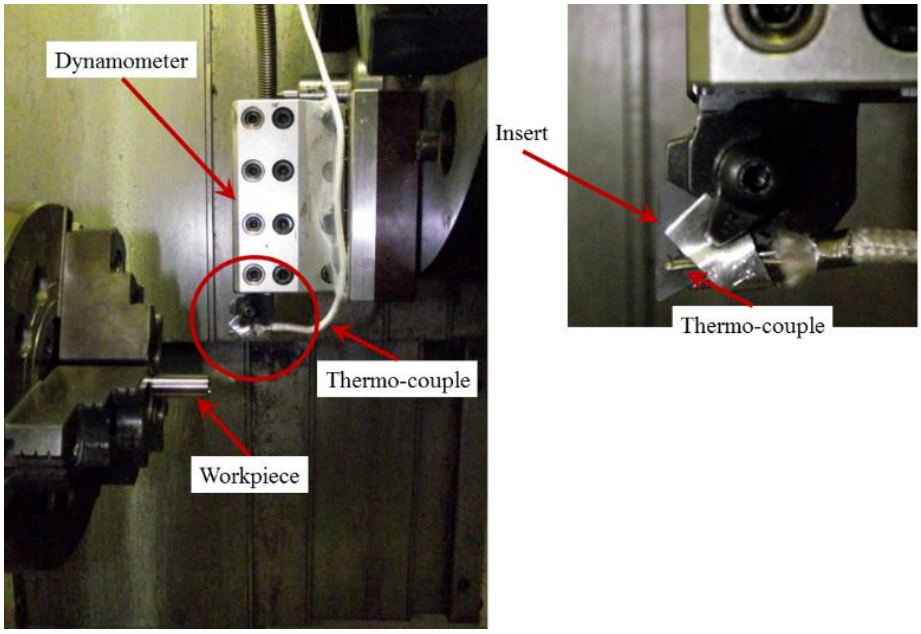

Figure 5.26 – Acquisition of the temperature in the orthogonal micro-cutting of titanium alloy.

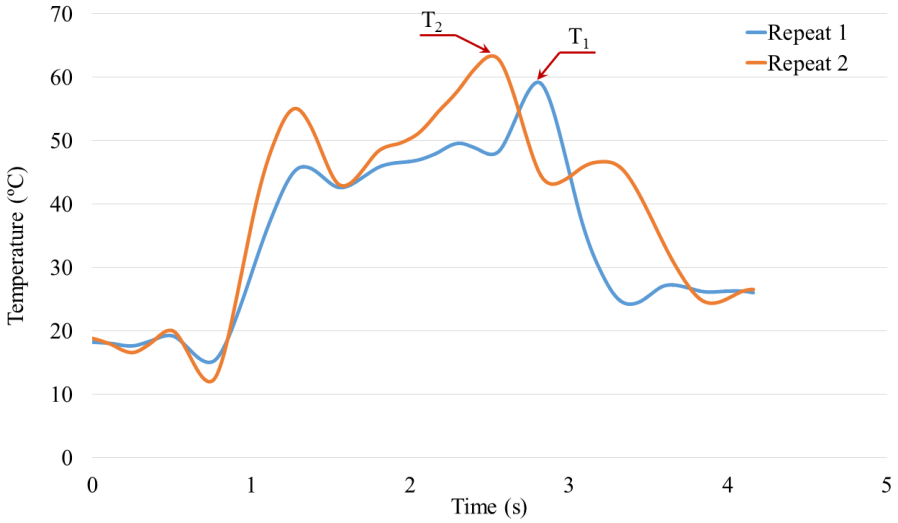

Figure 5.27 – Example of the acquired temperature in the orthogonal micro-cutting of the titanium alloy.

For this analysis, were used the workpiece with wall thickness of 0.8 mm. The cutting parameters were determined based on the manufacture catalogue and the geometry of the tool. Thus, the cutting speed were defined at 60 m/min, the mean of values suggested by the manufacturer, 30 m/min (low speed), and 120 m/min (high speed). The feed rate were defined at 10, 25, and 50 µm/rev, which were based on the cutting edge radius, Figure 5.28, about of 20 µm. Furthermore, cutting speed with two levels of the spindle speed were used. The low level was defined when the spindle speed was lower than 1,500 rpm, and high level of spindle speed was higher than 1,500 rpm. The Table 5.7 is shown the design of experiments used in this study.

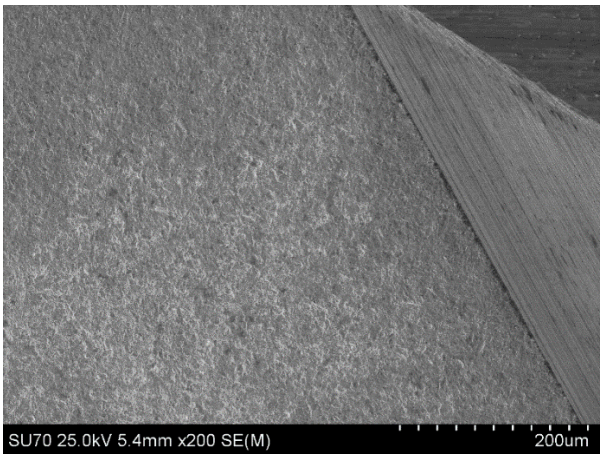

Figure 5.28 - Cutting edge radius used in the micro-cutting of titanium alloy.

Table 5.7 – Cutting parameters employed in the validation tests.

Cutting speed (m/min)	Feed rate (µm/rev)	Spindle speed (rpm) (approach)	Depth of cut (mm)
30	10	1,500	0.800
30	10	750	0.800
30	50	750	0.800
60	10	1,500	0.800
60	10	3,000	0.800
120	10	3,000	0.800
120	25	3,000	0.800
120	50	3,000	0.800

5.3.3. Influence of the HSM and MQL.

In this analysis, to understand the influence of the cooling/lubrication in the orthogonal micro-cutting, three two-level factors were analysed (cutting speed, feed rate and cooling

condition) with two levels. The cutting speed (v_c) was fixed at 30 m/min (low speed) and 120 m/min (high speed). The feed rate (f) was defined at 10 µm/rev ($f/r_e < 1$) and 50 µm/rev ($f/r_e > 1$). For these tests, were used the wall thickness of 1.1 mm, it is because to obtain a section to measure the surface roughness. The Table 5.8 shows the factors and levels used in this study.

Table 5.8 – Experimental planning in the micro-cutting tests.

Factor	Level	
	Low	High
Cutting speed (v_c) (m/min)	30	120
Feed rate (f) (µm/rev)	10	50
Cooling condition	Dry	MQL
Depth of cut (mm)	1.1	

The dry and cooling/lubrication cutting were employed to analyse the influence of the cooling/lubrication in the ploughing effect. The MQL system, described in the section 5.2.3, was adjusted with a flow rate fixed at 2.6 ml/min and pressure of 6 bar. In the Figure 5.29 is shown the experimental set-up for the micro-cutting tests. To measure the surface roughness, a Taylor Hobson™ profilometer, described in the section 5.2.7, was used. The surface was characterized through the R_a, R_z and R_t profiles using four sampling length (cut-off of 0.8 mm), seen the section 2.2.1. In each test, three surface roughness measures with 120º angular separation, were taken to reduce the experimental errors, see Figure 5.30. The micro-machined surfaces and the chips were observed using a Hitachi™ SEM, described in the section 5.2.9.

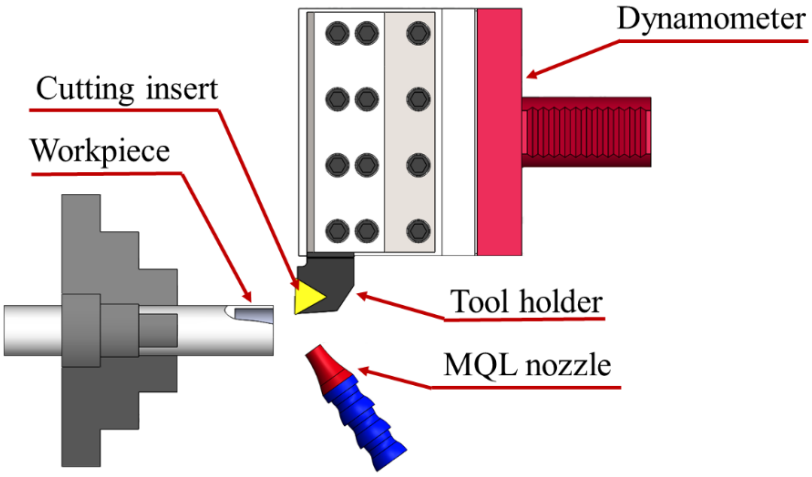

Figure 5.29 – Experimental set-up for use of the MQL in the micro-cutting.

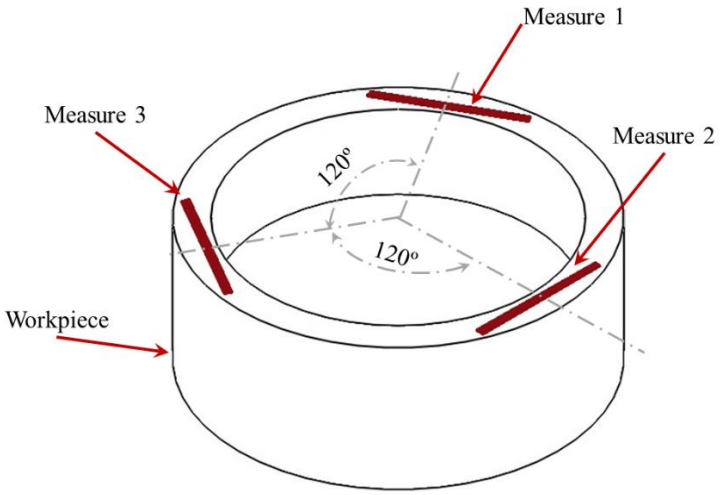

Figure 5.30 – Surface roughness measures diagram of the orthogonal micro-cutting tests.

5.3.4. Material modelling of Ti-6Al-7Nb titanium alloy to surface integrity via FEM

To analyse the residual stresses and the microstructural alteration in the micro-cutting of the Ti-6Al-7Nb titanium alloy, was developed a numeric model. A 2D model was developed to predict the force, temperature, and stresses using the AdvantEdge™ version 7.3014, Figure 5.31. This software was chosen because it shows great results and reliability to simulate the machining processes. The adaptive meshing that is employed in the AdvantEdge™ improves the quality and precision of the output results (Maranhão and Davim, 2012).

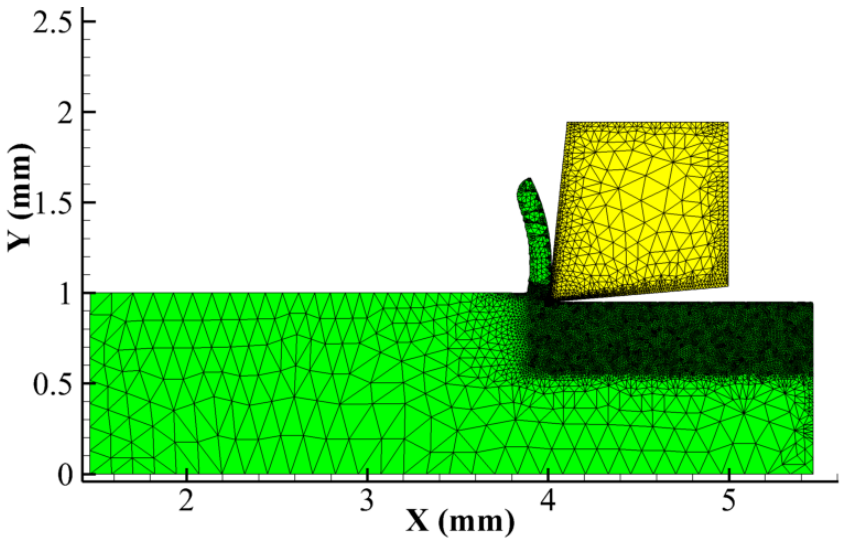

Figure 5.31 – Schematic of the simulation of the orthogonal micro-cutting.

The uncoated cemented carbide insert was designed with rake angle (γ) of 6º, relief angle (α) of 5º. The mesh size was fixed at 0.01 to 0.1 mm, and length and width of tool, L_{Refief} and

L_{Rake}, respectively, were defined at 1 mm, Figure 5.32. The workpiece was rectified and considered only length of 4 mm, thickness of 1 mm, and width were equal to feed rate, 0.010, 0.025, and 0.050 mm. The meshing size varied between 0.01 mm, cutting zone, and 0.1 mm, encastre region. To model the biomaterial, Ti-6Al-7Nb titanium alloy, the Johnson-Cook equation were employed, Equation 5.8. The values of the constants to model this material were defined based on study of Lee and Chen (2013), Table 5.9.

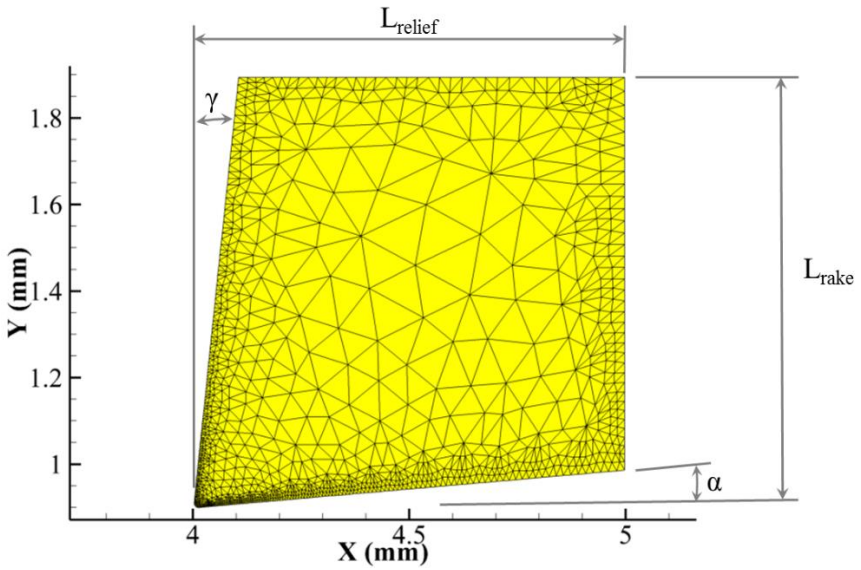

Figure 5.32 – Dimensions and meshing of tool in the orthogonal micro-cutting.

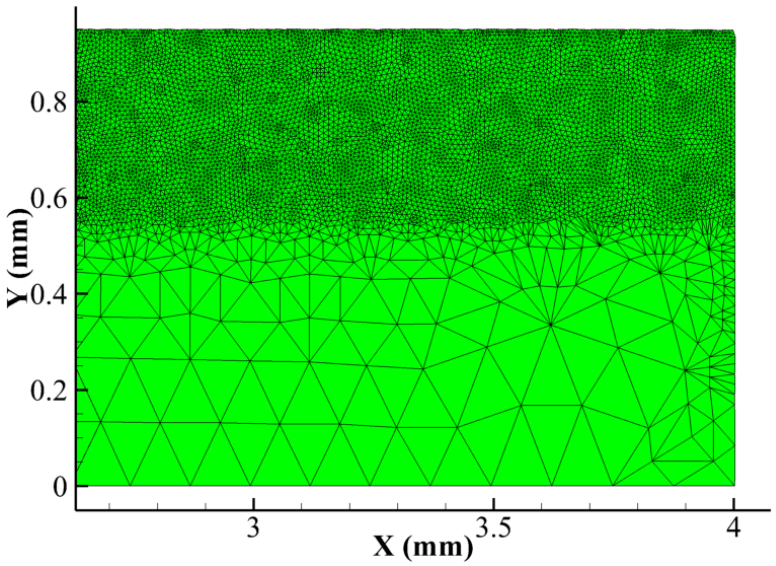

Figure 5.33 – Dimensions and meshing of workpiece in the orthogonal micro-cutting.

$$\bar{\sigma} = \underbrace{\left[A + B \cdot \varepsilon^{n}\right]}_{\text{Elasto-Plastic term}} \cdot \underbrace{\left[1 + C \cdot \ln\left(\frac{\dot{\varepsilon}}{\dot{\varepsilon}_0}\right)\right]}_{\text{Viscosity term}} \cdot \underbrace{\left[1 - \left(\frac{T - T_{room}}{T_{melt} - T_{room}}\right)^{m}\right]}_{\text{Thermal softening term}} \qquad \text{Equation 5.8}$$

Where,

A	↔	yield stress of the material under reference deformation conditions (MPa)
B	↔	strain hardening constant (MPa)
n	↔	strain hardening coefficient
C	↔	strain rate strengthening coefficient
m	↔	thermal softening coefficient
T	↔	deformation temperature
T_{room}	↔	room temperature
T_{melt}	↔	melting temperature of the material
$\dot{\varepsilon}_0$	↔	reference strain rate (1/s)
$\dot{\varepsilon}$	↔	equivalent plastic strain normalized with a reference strain rate
ε	↔	plastic equivalent strain

Table 5.9 – Johnson-Cook constants for the Ti-6Al-7Nb titanium alloy.

Constant	Value
A	802 MPa
B	556.2 MPa
n	0,26
m	15,4
C	$22{,}4\times10^{-15}$
ε	1,000
T_{room}	20º C
T_{melt}	1660º C

The initial temperature was considered of 20º C and the simulated cutting length was defined to 4 mm. The friction coefficient used in the numerical tests were based on the values of friction coefficient obtained in the experimental tests, section 6.1.3. The responses of the numerical tests were treated similar to experimental tests. The beginning and end of the results obtained due to inertia of the process and the wavelet transform was employed to fit the results. The average of feed and cutting forces in the section selected were used to

compare to average of cutting forces, maximum and minimum, obtained in the experimental tests, section 6.1.1. To valid the numerical tests, the deviations between results of numerical and experiments tests could not be higher than 45%, Equation 5.9.

$$Deviation = \frac{\left|F_{num} - F_{exp}\right|}{F_{exp}} \times 100 \qquad \text{Equation 5.9}$$

Where,

F_{num} ↔ Force values obtained in the numerical tests

F_{exp} ↔ Force values obtained in the experimental tests

To analyse the efficiency of the condition employed in this study, the power and the material removal rate, Equation 5.10, were compared. The heat flux during the micro-cutting was analysed through the temperature in the radial direction and the temperature in the elements in the beginning of cutting were analysed, Figure 5.34. In the same direction of the radial heat flux, the residual stress was extracted.

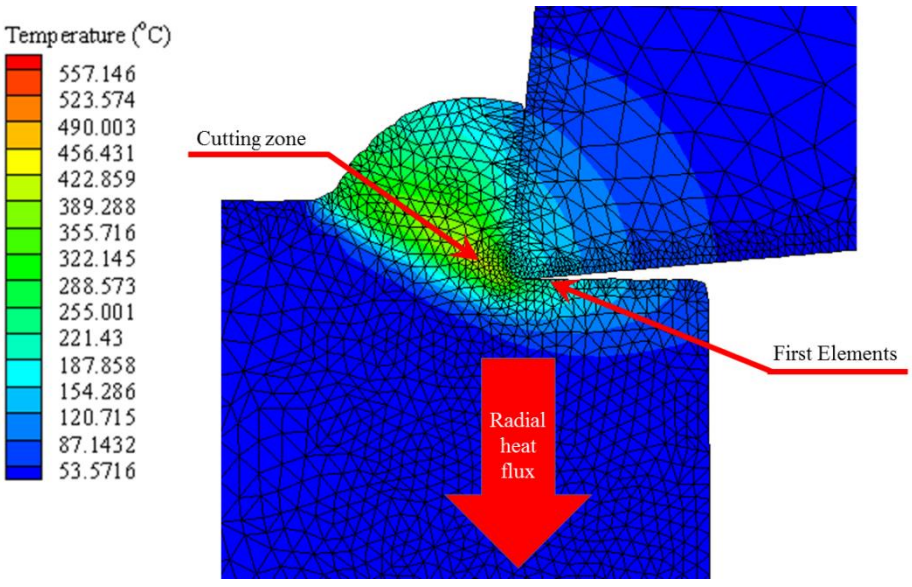

Figure 5.34 – Methodology of analysis of the temperature during the orthogonal micro-cutting.

$$MRR = \frac{f \cdot a_p \cdot v_c}{10^{12}} \times 60 \qquad \text{Equation 5.10}$$

Where,

MRR	↔	Material removal rate (m^3/h)
f	↔	Feed rate (μm/rev)
a_p	↔	Depth of cut (μm)
v_c	↔	Cutting speed (m/min)

5.4. The micro-cutting in the finishing operation of biomaterial

Generally, in the paper about micromachining, the cutting speed is related to spindle speed. In many study, the cutting speed is low, but the high number of revolutions per minute (rpm) allows that the processes be considered processes in high speed machining or ultra-high speed machining. However, these papers studied the micro-cutting developed in the milling or drilling processes. Thus, this section analysed the influence of spindle speed in the micro-cutting on the turning process.

5.4.1. Micro-cutting parameters

The cutting parameters was based on the catalogue of the tool manufacture and the results of the orthogonal micro-cutting tests. The cutting speed were kept at 60 m/min, average value, 30 m/min (low speed), and 120 m/min (high speed). Based on preliminaries tests, seen the section 5.3, and Ng *et al.* (2006), the feed rate was defined to obtain a feed rate and edge radius ratio is more than 1, to avoid the ploughing effect. Thus, the feed rate was fixed at 25, 50, and 100 μm/rev. The depth of cut was selected at 25, 50, and 100 μm. The tests were performed in dry conditions to obtain the better surface quality due to particle and slip of tools during the cutting, see the section 6.2.5.

To performance this analysis, three range of the spindle speed, three types of geometry of inserts, three feed rate, and three depth of cut were employed in each diameter scale, Table 5.10, and the cutting forces, vibration, and surface roughness were monitored. In these tests, was select the Ti-6Al-7Nb titanium alloy, due to it be commonly employed in components on different scales, and a same machined length of 25 mm.

Table 5.10 – Parameters and tools employed in the analysis of the spindle speed in the cylindrical micro-cutting tests.

Range of diameter (mm)	Range of spindle Speed (rpm)	Cutting speed (m/min)	Feed rate (µm/rev)	Depth of cut (µm)	Insert
> 10 (macro-scale)	0 - 1,000	30, 60, and 120 (macro-scale)	25	25	VBMW 16 04 04 H13A
5 – 8 (transition scale)	1,000 - 2,000	15, 30, and 60 (transition scale)	50	50	VBMT 16 04 04-UM H13A
2 – 4.5 (meso-scale)	2,000 - 3,000	7, 15, and 30 (meso-scale)	100	100	VNMG 160404-QM H13A

5.4.2. Micro-cutting monitoring

The methodology for the acquisition and classification of the cutting forces signals was based on section 5.3. The cutting force setting was adjusted to a sample frequency was defined at 4 kHz and manually triggered and stopped. In the signal was processed employing the Wavelet Transform, to denoise. The value of each component was defined in function of the average of the peaks, maximum and minimum, discarding a small section in the beginning and end of the acquired signal.

To monitoring the vibration during the cutting, was used the accelerometer described in the section 5.2.5. The accelerometer was assembled in the tool holder on vertical and horizontal to analyse the behaviour of the vibration in the cutting and feed direction, respectively, Figure 5.35. To reduce the noise, in the holders was applied insulating tape and avoid variation in the fixation, due to force of jaw chuck, the diameter to fix the workpiece was the same for all workpiece. To reduce the stress concentration, was made a cam for each range of diameter, Figure 5.36, except in the macro-scale. The Figure 5.37 shows the experimental setup for the micro-cutting tests.

a) axial direction.

b) SVJBL 2020K 16.

Figure 5.35 – Position of the accelerometer in the axial and tangential direction.

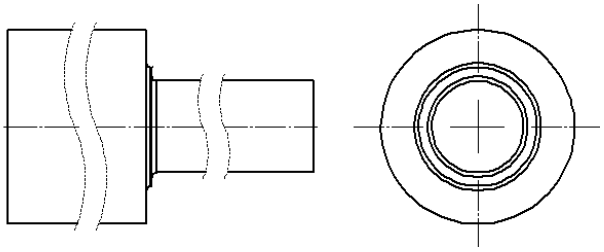

a) Workpiece of titanium alloy for the transition scale in the cylindrical micro-cutting tests.

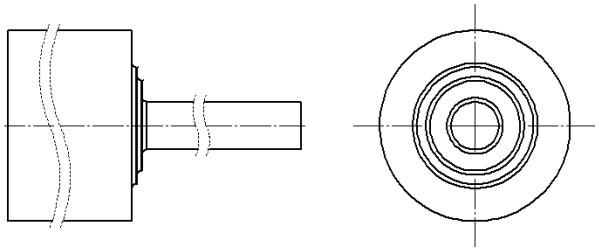

b) Workpiece of titanium alloy for the meso scale turning tests.

Figure 5.36 – Workpieces of titanium alloy in the spindle speed tests.

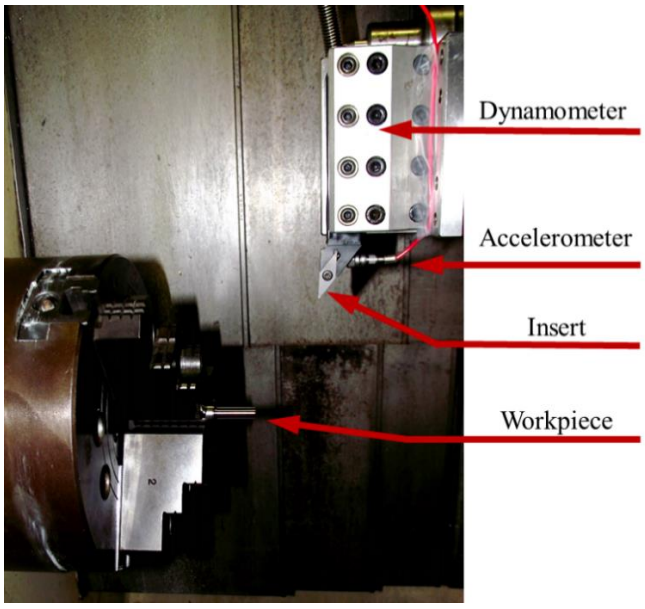

Figure 5.37 – Experimental setting for the finishing micro-cutting.

The sample frequency also was defined 4 kHz and manually triggered. Initially, the vibration signals were acquired and recorded without a filter, to observe the particular features that could occur in the micro-cutting. In the next stage, was developed a new VI applying a high-pass type Butterworth filter to remove the signal disturbances, Figure 5.38. To observe the phenomena of the vibration during the micro-cutting, the vibration signal was filtered using a pass-low filter type Finite Impulse Response (FIR), at 0.1 kHz and 0.8 kHz, based on the section 3.3.

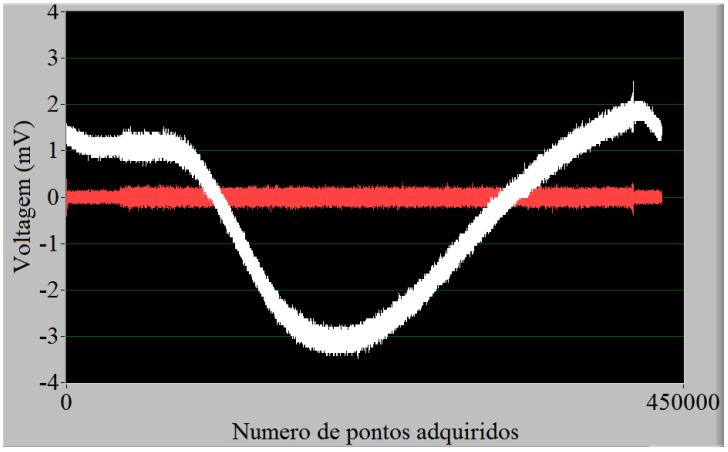

Figure 5.38 – Virtual instrumentation developed to filter the vibration signal.

For the time domain analysis, the root mean square (RMS) method was employed, which is calculate through the Equation 5.11. The frequency domain was used to compare the condition, which was developed by the Fast Fourier transform, seen the section 3.6.1, Equation 5.12, that was employed to find the frequency components of a signal and the Hilbert transform (HT), seen the section 3.6.2, Equation 5.13, that was used to develop the envelope technique, Equation 5.14.

$$X_{RMS} = \sqrt{\frac{1}{n}\sum_{1}^{n}\left|Xn\right|^2} \qquad \text{Equation 5.11}$$

$$X = \sum_{i=1}^{n} X(i) W_n^{(i-1)(k-1)} \qquad \text{Equation 5.12}$$

$$\hat{x}(t) = H\left[x(t)\right] = \frac{1}{\pi}\int_{-\infty}^{\infty}\frac{x(\tau)}{t-\tau}d\tau \qquad \text{Equation 5.13}$$

$$u(x) = \sqrt{\hat{x}(t) \cdot \bar{z}}$$ Equation 5.14

To compare the vibration among the different micro-cutting conditions employed in this study, were considered only the lengths where the cutting was stable. The Figure 5.39 is exemplified the vibration signal acquisition. For this acquisition, the section between 0 (cutting start) and 10 was discarded due to the instability that occurred because the diameter had smaller dimension.

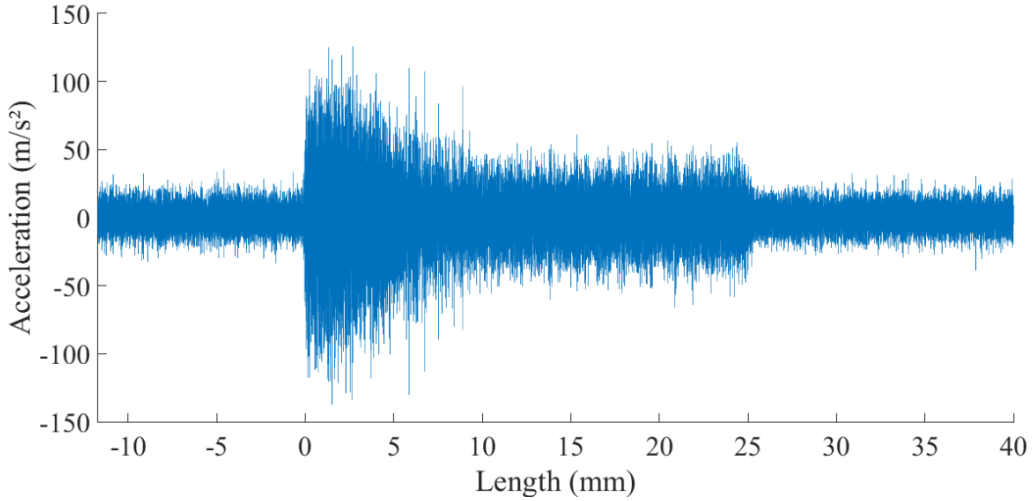

Figure 5.39 – Example of the vibration signal acquired during the micro-cutting.

5.4.3. Geometric deviation

In the micro-turning, Lu and Yoneyama (1999) analysed the deflection that as the diameter was decreasing, the stress and deflection were increasing, Figure 5.40. Thus, the minimum deflection was calculated to compare the micro-turning in different scales. To calculate this deflection, was employed the Equation 5.15.

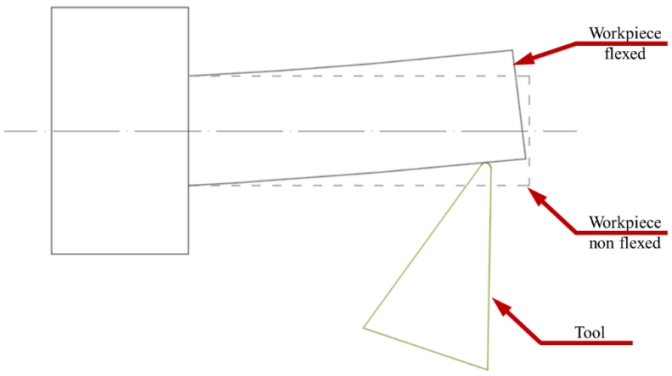

Figure 5.40 – Deflection of workpiece, adapted from Lu and Yoneyama (1999).

$$\delta = \frac{F_d \cdot l^3}{3 \cdot E \cdot I} \times 1{,}000 \qquad \text{Equation 5.15}$$

Where;

δ	↔	deflection (μm)
F_d	↔	depth force (N)
l	↔	cutting length (mm) (30 to macro; 25 to transition and meso)
E	↔	tensile strength (MPa)
I	↔	area moment of inertia (mm^4)

To characterize was used the portable surface tester, describe in the section 5.2.7. The profilometer was configured to a cut-off of 0.8 mm, and the profiles R_a and R_z was analysed, seen the section 2.2.1. The surface roughness, was considered the average of the three measurements, rounding it 120º around the contour, for each test. Furthermore, the measurements were performed neared end of cut jaw chuck due to the stability of cutting, Figure 5.41.

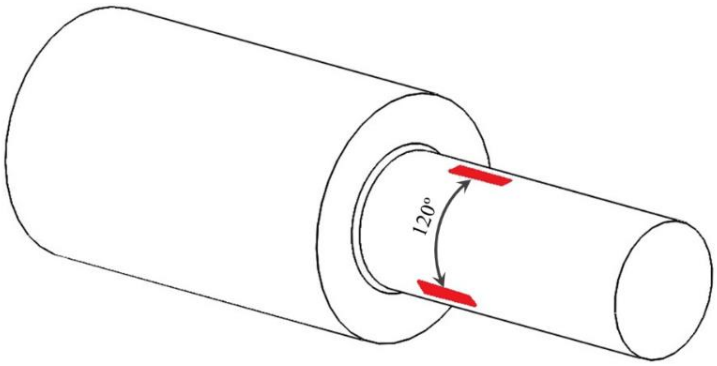

Figure 5.41 – Surface roughness measures diagram of the oblique micro-cutting tests.

5.5. Corrosion behaviour of micro-machined surface in the dental applications

In this section was analysed the influence of the micro-cutting in the finishing operation of dental components. In this regard, three different workpieces were manufactured based on geometries and dimensions of some dental components (Misch, 2009). These geometries used in the electrochemical tests are shown in the Figure 5.42 and the area analysed are shown in the Table 5.11. The dimensions of the workpieces can be seen in the Annex C. In

the roughness operation, the workpieces were machined using the TPGN 16 03 04 H13A cutting inserts mounted in the CTGPL 2020 K16 tool holder to reduce the influence of the cutting geometry. The cutting parameters used were a feed rate of 0.1 mm, depth of cut of 0.5 mm, and cutting speed was limited at 60 m/min or 3,000 rpm. The cut was performed in wet condition to reduce the metallurgic alterations, tool wear, and others unforeseen events that influenced the analysis.

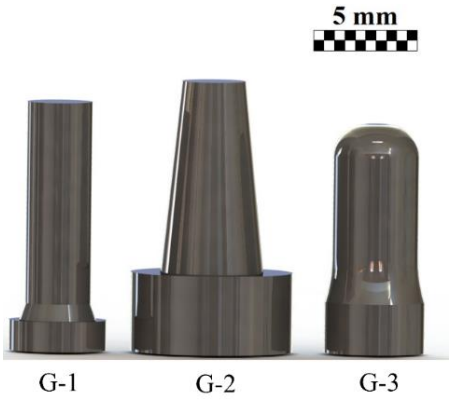

Figure 5.42 – Workpieces geometries developed for electrochemical tests.

Table 5.11 – Area of workpieces used in the electrochemical tests.

Workpiece	Area (mm^2)
G1	95.99
G2	116.23
G3	116.25

5.5.1. Definition of the micro-cutting parameters

To analyse the performance of the micro-cutting as finishing operation, the first step was find the optimum and worse condition. Thus, values obtained of cutting force and surface roughness for micro-cutting in the meso-scale diameter in the section 5.4, were used. The V inserts shape were selected to obtain the lower cutting section, the VBMW 16 04 04 H13A and VBMT 16 04 04-UM H13A mounted in a tool holder SVJBL 2020K 16; and VNMG 16 04 04-QM H13A mounted in a tool holder DVJNL 2020K 16.

To design and implement an effective process control for metal cutting operation by parameter optimization, a manufacturer seeks to balance between quality and cost at each stage of operation resulting in improved delivery and reduced warranty or field failure of a product under consideration (Mukherjee and Ray, 2006). Sometimes, the ideal cutting

parameters combination can be developed to optimize just one output, but, sometimes the ideal cutting parameters combination should involve several outputs. Maiyar *et al.* (2013) employed a technique to predict the optimal cutting parameters during the milling of Inconel 718 alloy, which resulted in the reducing of the surface roughness (9.5%) and the increasing of the material removal rate (65%), simultaneously.

In many cases, there are a complexity due to high number of inputs and outputs, which can be determined through the Artificial Intelligence (AI) methods. The AI methods is more used in the engineering to solve difficult problems normally requiring human intelligence due to a number of powerful tools (Mohd Adnan *et al.*, 2015).

To optimize the results of this work, a Genetic Algorithm (GA) based on the Least Square Method (LSM), it was developed, seen the section 4.4. This choice was because the high number of outputs analysed, like the cutting forces, surface roughness, manufacturing time and other. To verify the adequacy of the LSM models, Analysis of Variance (ANOVA) was used, with a confidence interval of 95%. The ANOVA was carried out to verify whether the main and/or the interaction factors were statistically significant.

The optimum condition was found using a Genetic Algorithm (GA) based on the Least Square Method (LSM) that is the best fit into a data group. Similar method was employed to find the worse condition, meanwhile the models were inverted. The initial population of the model was formed by 1,000 individuals who evolved during 1,000 interactions. The weights of the responses to find the optimum and worse conditions were defined at 0.5 for the cutting forces and 0.5 for the surface roughness profiles. To model the responses of the micro-cutting finishing tests was employed the Response Surface Method, seen the section 4.3.2, based in the study of Silva *et al*. (2014).

5.5.2. Electrochemical analysis

In this analysis were used the equipment described in the section 5.2.8. After the manufacturing, the workpieces were cleaned and dried, to avoid influences in the electrochemical test, joined a wire, and mounted on polyester resin base, Figure 5.43. The electrochemical tests were developed using the simulated body fluid (SBF) based on studies of Kokubo and Takadama (2006) on thermostatic bath at temperature of 37 °C, Figure 5.43.

The simulated body fluid (SBF) is a reproduction of *in vivo* apatite formation, whose the ion concentrations is similar to human blood plasma, that has been employed to develop new biomaterials with great success (Kokubo and Takadama, 2006). The reagents and their weights for preparing 1,000 ml of SBF are presented in the Table 5.12. The pH of the SBF used in the electrochemical tests varied between 7.23 and 7.31.

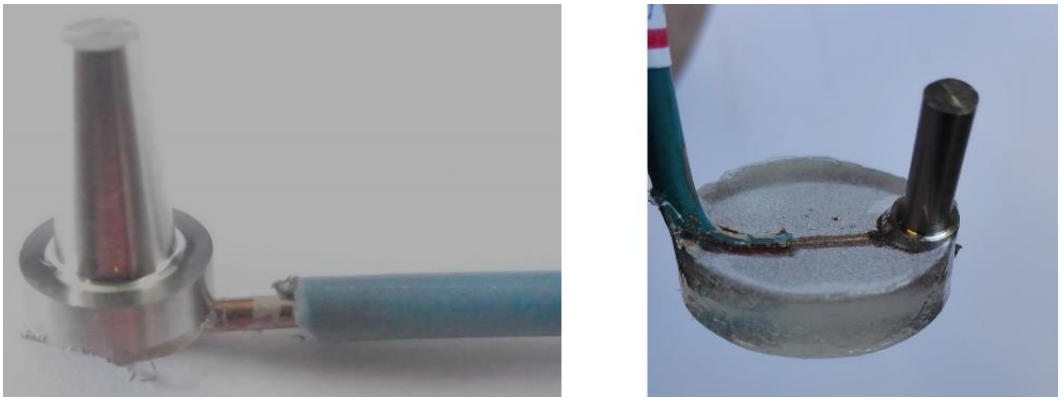

Figure 5.43 – Preparation of the workpieces for electrochemical tests.

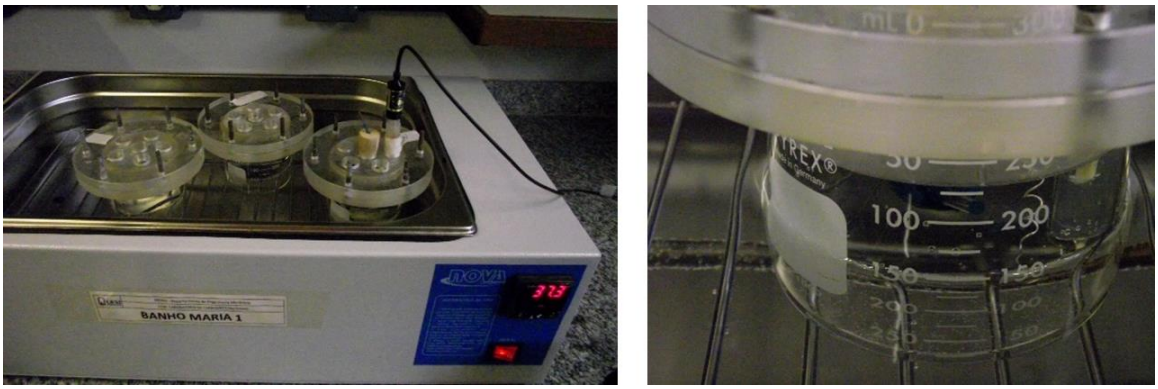

Figure 5.44 – Workpieces on thermostatic bath during the electrochemical tests.

Table 5.12 – Reagents and weights for 1,000 ml of SBF to corrosion tests (Kokubo and Takadama, 2006).

Reagents	Weight (g)
sodium chloride (NaCl)	8.035
sodium hydrogen carbonate ($NaHCO_3$)	0.355
potassium chloride (KCl)	0.255
di-potassium hydrogen phosphate trihydrate ($K_2HPO_4.3H_2O$)	0.231
magnesium chloride hexahydrate ($MgCl_2.6H_2O$)	0.311
1m (mol/l) Hydrochloric Acid (HCl)	39 ml
calcium chloride ($CaCl_2.H_2O$)	0.292
sodium sulfate Na_2SO_4	0.072
tris-hydroxymethyl aminomethane: ($(HOCH_2)3CNH_2$) (Tris)	0.118
pH standard solution	7.2 – 7.4

The NOVA 1.11 software was used to control the tests that were adjusted at scan rate of 10 mHz to 100 kHz (electropositive direction), disturbance of 10 mV, and acquisition rate of 0.05 mV/s. To analyse the impedance, the bode and phase curves were obtained at OPC, 0.75 V, 1.5 V, and 2.0 V. The reference electrode was a saturated calomel electrode and the counter-electrode was a platinum wire. Initially, the samples were kept in solution for 3,600 s and then the ECORR was determined.

CHAPTER 6 – PRELIMINARY ANALYSIS OF THE BEHAVIOUR OF THE BIOMATERIAL IN THE MICRO-CUTTING

In this chapter is analysed the measurements techniques developed to observe the behaviour of the Ti-6Al-7Nb titanium alloy when employed the in the micro-cutting. Furthermore, it is analysed the behaviour of the micro-machined surface using the High Speed Machining (HSM) and the Minimum Quantity Lubrication (MQL). Large portion of the section 6.1 has similarity with:

- LAURO, C. H. *et al*. Analysis of behaviour biocompatible titanium alloy (Ti-6Al-7Nb) in the micro-cutting. Measurement, v. 93, 2016, p. 529-540.

6.1. Development of measurements techniques and analysis

6.1.1. Cutting Forces

In this section, the thrust (F_T) force, cutting (F_C) force, and their variation are compared. The Figure 6.1 shows the maximum and minimum feed force values obtained in the micro-cutting of the Ti-6Al-7Nb titanium alloy. The results of experiments showed that the feed force tends to increase with the increase of the feed rate (37.6% on average) and decrease of the spindle speed (27.0% on average). The increase of the cutting speed caused a reduction, from 30 to 60 m/min, and an increase, from 60 to 120 m/min, considering the feed force range. The variation between the maximum and minimum values was the same for all tested conditions, practically, 1.05% on average. When performed the Analysis of Variance (ANOVA), feed rate (linear and square), the square of the cutting speed, and the interaction of these parameters were significant sources of variation, Table 6.1. The Equation 6.1 shows the feed force model for these tested conditions. A clear understanding of the influence of the parameters can be observed in the contour plots, Figure 6.2.

$$F_{T_{th}} = 22.91 - 0.2344 \cdot v_c + 1 \cdot f - 7.67 \cdot n + 1.706 \times 10^{-3} \cdot v_c^2 - 8.37 \times 10^{-3} \cdot f - 1.615 \times 10^{-3} \cdot v_c \cdot f + 53.8 \times 10^{-3} \cdot v_c \cdot n$$

Equation 6.1

Where,

v_c ↔ cutting speed (30 to 120 m/min)

f ↔ feed rate (10 to 50 µm/rev)

n ↔ spindle speed (0 to low and 1 to high)

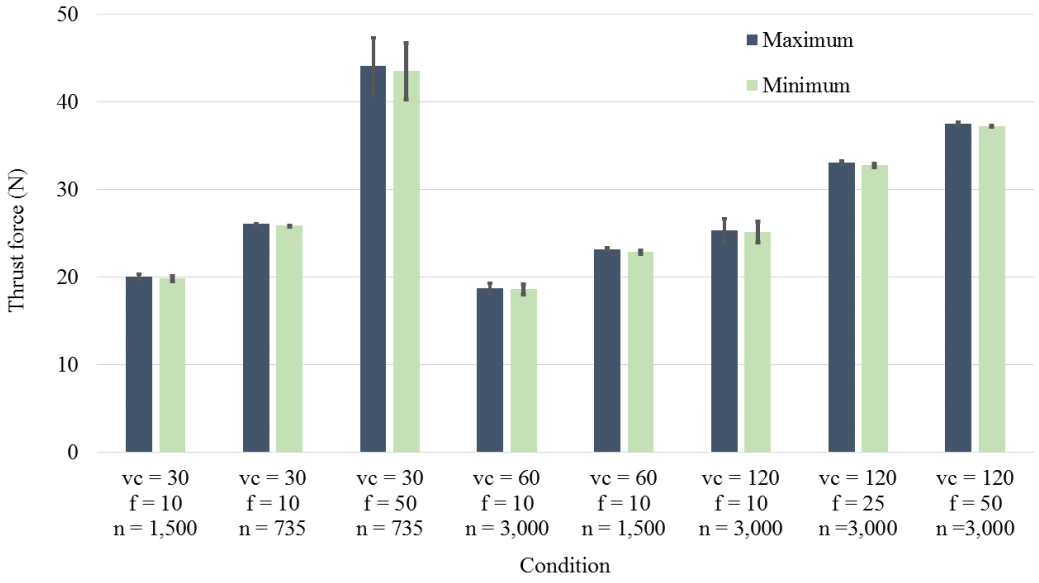

Figure 6.1 – Maximum and minimum values of thrust force for the micro-cutting in titanium alloy.

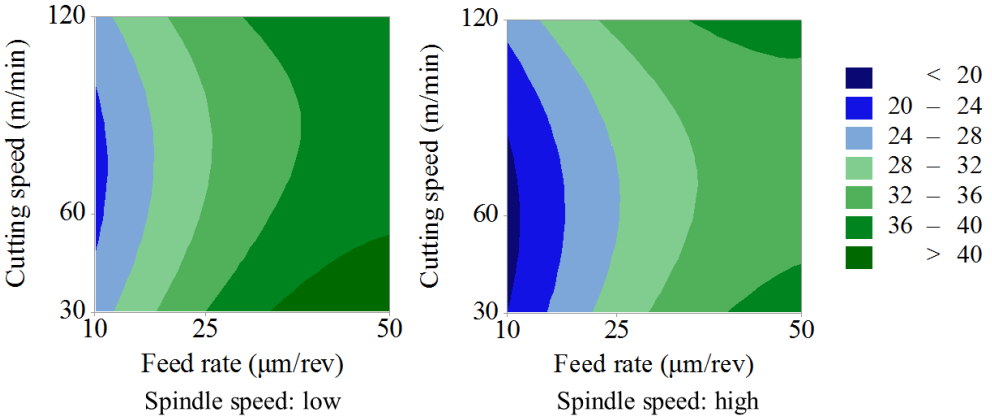

Figure 6.2 – Contour plot of the F_T in function of the feed rate and cutting speed.

Table 6.1 – ANOVA for the feed force in the micro-cutting of titanium alloy.

Source	F-Value	P-Value
Model	101.32	0.000
Linear	102.35	0.000
Cutting speed	0.00	0.997
Feed rate	*289.88*	*0.000*
Spindle speed	3.39	0.103
Square	9.23	0.008
*Cutting speed*Cutting speed*	*7.75*	*0.024*
*Feed rate*Feed rate*	*8.23*	*0.021*
2-Way Interaction	7.01	0.017
*Cutting speed*Feed rate*	*10.81*	*0.011*
Cutting speed*Spindle speed	0.83	0.389
R^2 = 98.88%	R^2_{adj} = 97.91%	

The results of the cutting force (F_c) in the micro-cutting of Ti-6Al-7Nb titanium alloy are shown in Figure 6.3. The increase of the feed rate caused an increase of the cutting force, 79.0%, and the increase of the spindle speed resulted in a reduction of this force, 21.5% on average. The increase from 30 to 60 m/min in the cutting speed presented a reduction of the cutting force, 10.2% on average. The increase from 60 to 120 m/min caused a small increase of the cutting force, 1.7%. However, when compared the cutting force for the increase from 30 to 120 m/min, the force reduced on average of 4.7%. Analysing the variation between the maximum and minimum values, the cutting force was more stable employing the high level of the inputs, Figure 6.4.

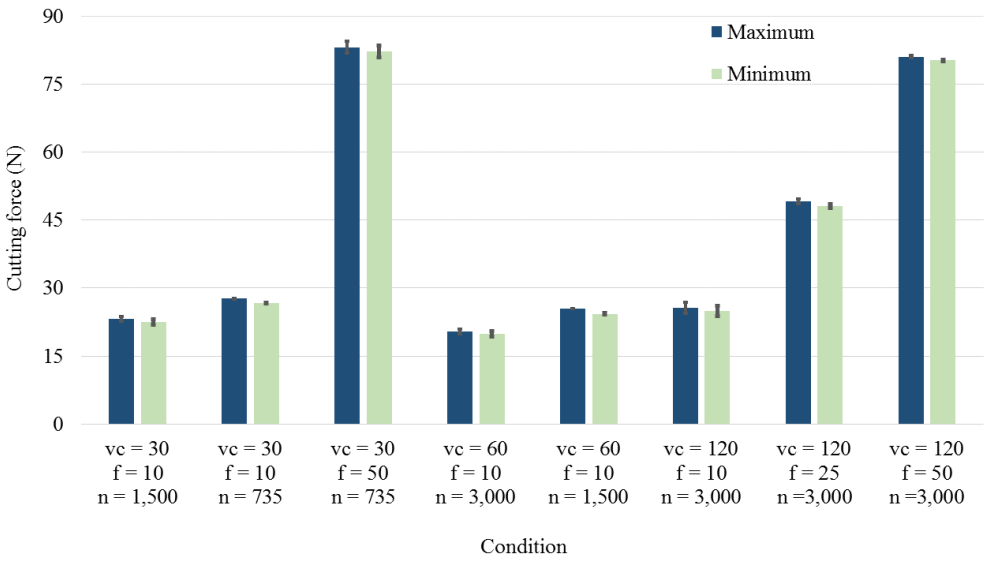

Figure 6.3 – Maximum and minimum values of the cutting force for the micro-cutting in titanium alloy.

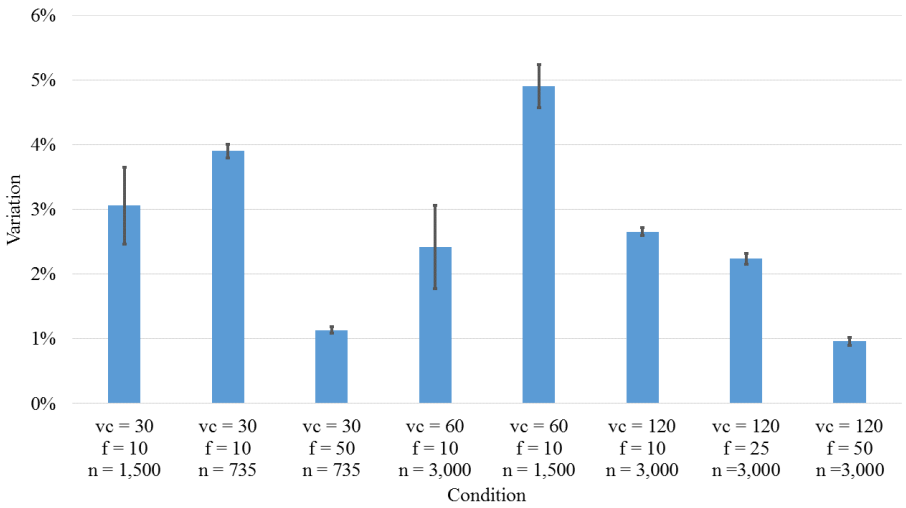

Figure 6.4 – Variation of the cutting force for the micro-cutting in titanium alloy.

The Table 6.2 shown the ANOVA for the cutting force. The ANOVA showed that all inputs were significant in the cutting force, but their interactions were not significant. The Equation 6.2 shows the modelling for the cutting force for the tested conditions. The Figure 6.5 shows the contours plot for the cutting force in the micro-cutting of Ti-6Al-7Nb titanium alloy, which can be the influence of parameters.

Table 6.2 – ANOVA for the cutting force in the micro-cutting of titanium alloy.

Source	F-Value	P-Value
Model	2703.11	0.00
Linear	4031.31	0.000
Cutting speed	*6.61*	*0.033*
Feed rate	*12026.33*	*0.000*
Spindle speed	*22.73*	*0.001*
Square	29.83	0.000
*Cutting speed*Cutting speed*	*33.08*	*0.000*
*Feed rate*Feed rate*	*18.77*	*0.003*
2-Way Interaction	0.18	0.837
Cutting speed*Feed rate	0.00	0.980
Cutting speed*Spindle speed	0.35	0.572
R^{2} = 99.96%	R^{2}_{adj} = 99.92%	

$$F_{C_{th}} = 16.04 - 0.2554 \cdot v_c + 1.821 \cdot f - 3.90 \cdot n + 2.016 \times 10^{-3} \cdot v_c^2 - 7.23 \times 10^{-3} \cdot f^2 - 7 \times 10^{-6} \cdot v_c \cdot f - 0.0199 \cdot v_c \cdot n$$

Equation 6.2

Where,

v_c ↔ cutting speed (30 to 120 m/min)

f ↔ feed rate (10 to 50 µm/rev)

n ↔ spindle speed (0 to low and 1 to high)

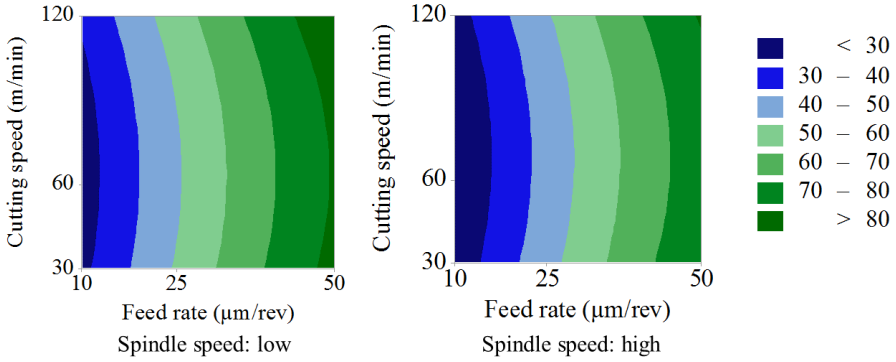

Figure 6.5 – Contour plot of the F_c in function of the feed rate and cutting speed.

6.1.2. Specific cutting energy

The Figure 6.6 shows the values of the specific cutting energy in the micro-cutting tests. The specific cutting energy presented a fall when both the feed rate and spindle speed were increased, 36.2% and 15.3% on average, respectively. However, when the cutting speed increased from 30 to 60 m/min, proportional to spindle speed, the specific cutting energy presented a reduction of 8.2% on average. However, it can be noted an increase of 2.2% for the variation from 60 to 120 m/min. Moreover, when the cutting speed was varied from 30 to 120 m/min, the specific cutting energy decreased 4.9% on average. The ANOVA showed that all parameters were significant, but their interaction was not significant in this process, Table 6.3.

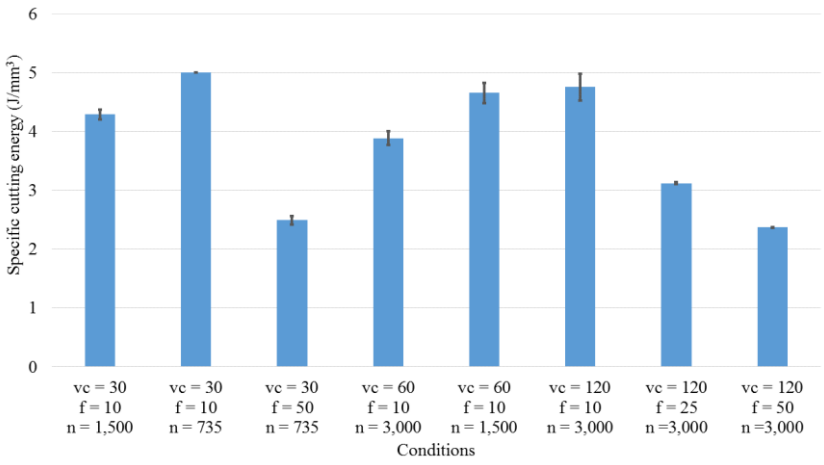

Figure 6.6 – Specific cutting energy in the micro-cutting in titanium alloy.

Table 6.3 – ANOVA for the specific cutting energy in the micro-cutting of titanium alloy.

Source	F-Value	P-Value
Model	160.63	0.000
Linear	320.85	0.000
Cutting speed	*8.74*	*0.018*
Feed rate	*892.68*	*0.000*
Spindle speed	*19.06*	*0.002*
Square	36.93	0.000
*Cutting speed*Cutting speed*	*30.20*	*0.001*
*Feed rate*Feed rate*	*53.12*	*0.000*
2-Way Interaction	0.43	0.666
Cutting speed*Feed rate	0.53	0.489
Cutting speed*Spindle speed	0.14	0.717
R^2 = 99.29%	R^2_{adj} = 98.68%	

6.1.3. Friction coefficient

The results of the friction coefficient are showed in Figure 6.7. The feed rate was the unique input parameter that presented uniform behaviour. The increase of the feed rate reduced the friction coefficient in 30.1% considering mean values. Using the data of the ANOVA, in Table 6.4, it is possible to observe that only the square of the cutting speed was not significant in this process.

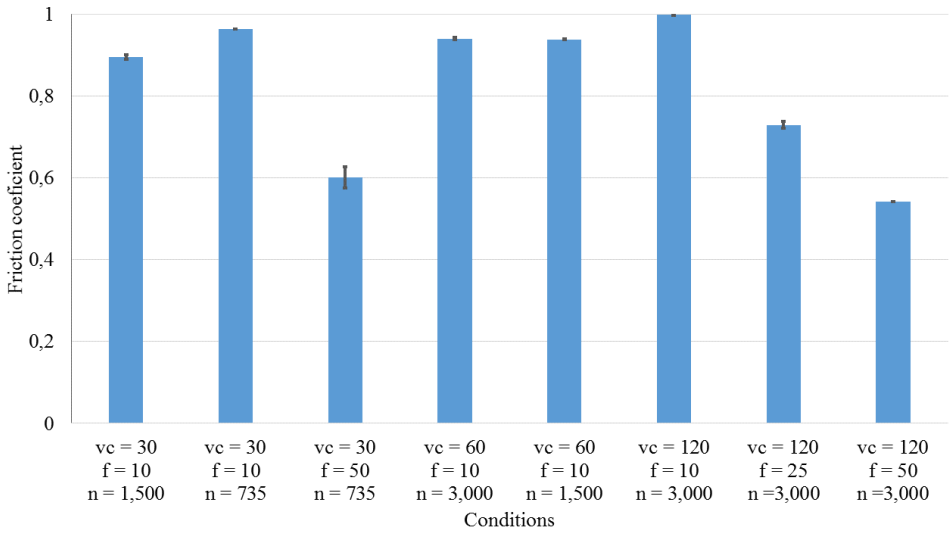

Figure 6.7 – Friction coefficient in the micro-cutting in titanium alloy.

Table 6.4 – ANOVA for the friction coefficient in the micro-cutting of titanium alloy.

Source	F-Value	P-Value
Model	620.79	0.000
Linear	1113.21	0.000
Cutting speed	*7.56*	*0.025*
Feed rate	*3317.44*	*0.000*
Spindle speed	*5.46*	*0.048*
Square	65.10	0.000
Cutting speed*Cutting speed	1.46	0.262
*Feed rate*Feed rate*	*122.76*	*0.000*
2-Way Interaction	45.02	0.000
*Cutting speed*Feed rate*	*43.34*	*0.000*
*Cutting speed*Spindle speed*	*24.72*	*0.001*
R^2 = 99.82%	R^2_{adj} = 99.66%	

6.1.4. Temperature

The values of the temperature in the tool obtained in the micro-cutting of Ti-6Al-7Nb titanium alloy are exhibited in the Figure 6.8. The temperature presented, practically, a fall with the increase of all the input parameters. The increase of the feed rate, spindle speed, and cutting speed presented a reduction of 15.5%, 12.7%, and 10.9% on average, respectively. From the ANOVA in Table 6.5, it can be concluded that only the feed rate was significant. The temperature model for tested conditions is shown in the Equation 6.3.

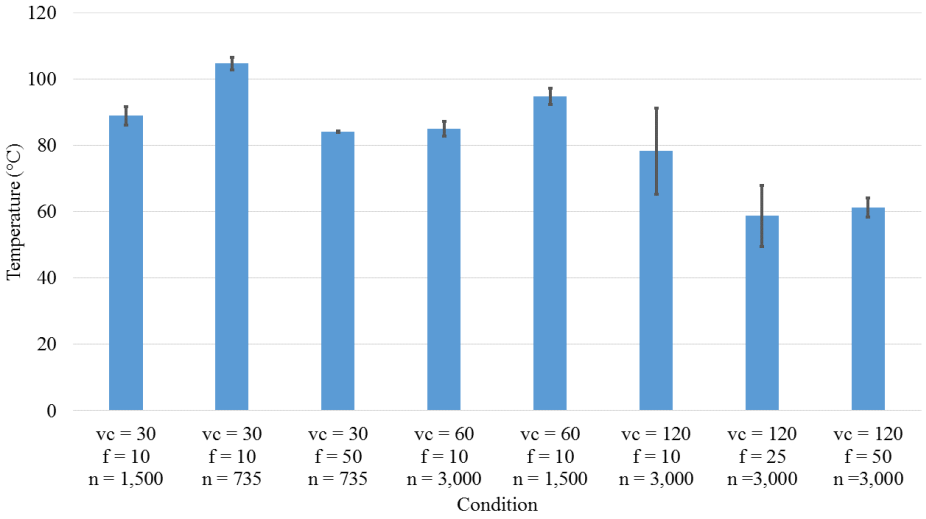

Figure 6.8 – Temperature in the micro-cutting in titanium alloy.

$$T_{th} = 138.1 - 0.361 \cdot v_c - 2.652 \cdot f - 21.9 \cdot n + 0.20 \times 10^{-3} \cdot v_c^2 + 35.1 \times 10^{-3} \cdot f^2 + 0.99 \times 10^{-3} \cdot v_c \cdot f + 0.204 \cdot v_c \cdot n$$

Equation 6.3

Where,

v_c ↔ cutting speed (30 to 120 m/min)

f ↔ feed rate (10 to 50 μm/rev)

n ↔ spindle speed (0 to low and 1 to high)

Table 6.5 – ANOVA for the temperature in the micro-cutting of titanium alloy.

Source	F-Value	P-Value
Model	13.86	0.001
Linear	19.21	0.001
Cutting speed	2.80	0.133
Feed rate	*19.87*	*0.002*
Spindle speed	0.50	0.499
Square	3.23	0.094
Cutting speed*Cutting speed	0.00	0.948
*Feed rate*Feed rate*	*6.38*	*0.036*
2-Way Interaction	0.29	0.754
Cutting speed*Feed rate	0.18	0.684
Cutting speed*Spindle speed	0.52	0.490
R^2 = 92.38%	R^2_{adj} = 85.71%	

6.1.5. Chip

The values of the chip compression ratio are exhibited in Figure 6.9. The increase of the feed rate was the parameter that presented a significant reduction with 18.9%, followed by the cutting speed with a reduction of 5.5%. It is worth pointing out that the increase of the feed rate from 10 to 25 μm/rev presented a decrease of the chip compression ratio in 20.6%, while the increase of feed rate from 25 to 50 μm/rev resulted in a reduction of 5.4%. The increase of the spindle speed reduced the chip compression in 5.3% (735 to 1,500 rpm) and 0.4% (1,500 to 3,000 rpm). The ANOVA for the chip compression ratio is shown in Table 6.6. It is observed in the ANOVA that the feed rate (linear and square), the cutting speed (linear) and the interaction between both parameters were significant for the chip compression ratio. The chip compression ratio for the tested condition was modelled by Equation 6.4.

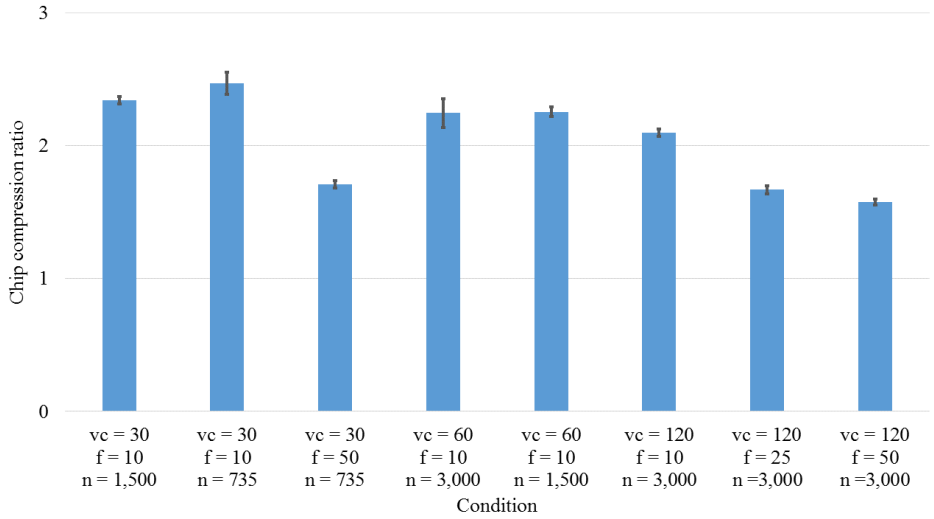

Figure 6.9 – Chip compression ratio in the micro-cutting in titanium alloy.

$$\varepsilon_{th} = 3.224 - 8.57\times10^{-3}\cdot v_c - 0.05875\cdot f - 0.250\cdot n + 8\times10^{-6}\cdot v_c^2 + 0.63\times10^{-3}\cdot f^2 + 66\times10^{-6}\cdot v_c\cdot f + 4\times10^{-3}\cdot v_c\cdot n$$

Equation 6.4

Where,

v_c ↔ cutting speed (30 to 120 m/min)

f ↔ feed rate (10 to 50 μm/rev)

n ↔ spindle speed (0 to low and 1 to high)

Table 6.6 – ANOVA for the chip compression ratio in the micro-cutting of titanium alloy.

Source	F-Value	P-Value
Model	80.97	0.000
Linear	109.63	0.000
Cutting speed	*9.59*	*0.015*
Feed rate	*281.30*	*0.000*
Spindle speed	0.34	0.574
Square	12.56	0.003
Cutting speed*Cutting speed	0.10	0.761
*Feed rate*Feed rate*	*24.99*	*0.001*
2-Way Interaction	5.15	0.036
*Cutting speed*Feed rate*	*9.63*	*0.015*
Cutting speed*Spindle speed	2.47	0.155
R^2 = 98.61%	R^2_{adj} = 97.39%	

The chip deformation in the micro-cutting is showed in the Figure 6.10. The analysis of the chip deformation presented a similar behaviour to the chip compression ratio. The increase of the feed rate from 10 to 25 μm/rev varied the chip deformation in -13.0%, while the

increase of feed rate from 25 to 50 µm/rev resulted in -2.7% in the chip deformation. The increase of the cutting speed reduced the chip deformation in 4.0%, on average. The spindle speed presented a variation of -4.0% (735 to 1,500 rpm) and -0.3% (1,500 to 3,000).

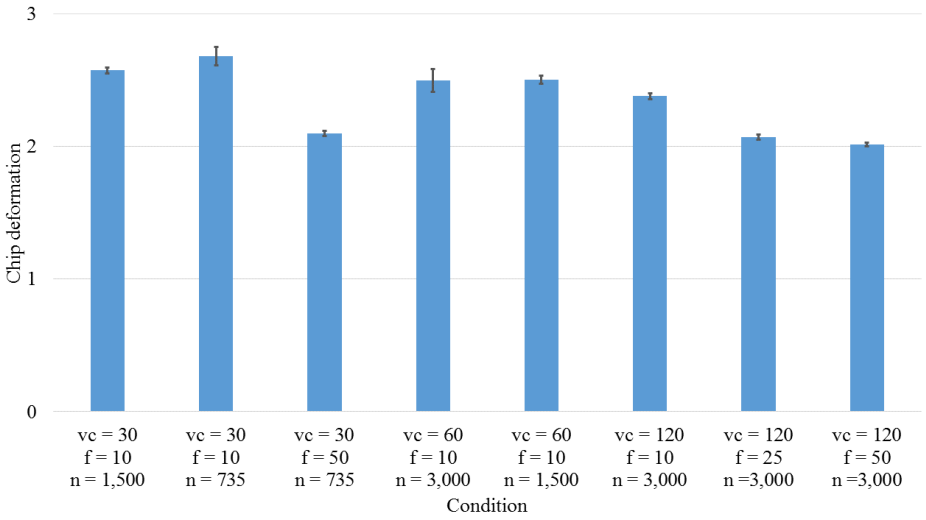

Figure 6.10 – Chip deformation in the micro-cutting in titanium alloy.

The ANOVA appointed the same influence of the parameters than that of the chip deformation, as can be seen in the Table 6.7.

Table 6.7 – ANOVA for the chip deformation in the micro-cutting of titanium alloy.

Source	F-Value	P-Value
Model	69.71	0.000
Linear	93.96	0.000
Cutting speed	*9.03*	*0.017*
Feed rate	*239.24*	*0.000*
Spindle speed	0.39	0.551
Square	10.41	0.006
Cutting speed*Cutting speed	0.11	0.747
*Feed rate*Feed rate*	*20.74*	*0.002*
2-Way Interaction	6.52	0.021
*Cutting speed*Feed rate*	*12.42*	*0.008*
Cutting speed*Spindle speed	2.69	0.140
R^2 = 98.39%	R^2_{adj} = 96.98%	

6.1.6. Shear plane angle

In Figure 6.11 is shown the values of the shear plane angle of the micro-cutting. When analysing the cutting speed, only in the experimental model, the increase of the cutting speed caused an increase of the shear plane angle value, 5.4% on average. The other models, the

shear plane angle increased, from 30 to 60 m/min, or decreased, from 60 to 120 m/min. For the variation of the feed rate, the increase of the feed rate caused an increase of the shear plane angle for all models, on average 22.2% in experimental, 18.4% in Merchant, and 127.4% in Lee - Shaffer models. In the analysis of the spindle speed, the variation from 735 to 1,500 rpm presented an increase for all models, 5.1% in experimental, 4.1% in Merchant, and 30.1% in Lee - Shaffer models. However, for the variation from 1,500 to 3,000 rpm, the influence was lower, 0.5% in experimental, -0.1% in Merchant, and -0.7% in Lee - Shaffer models.

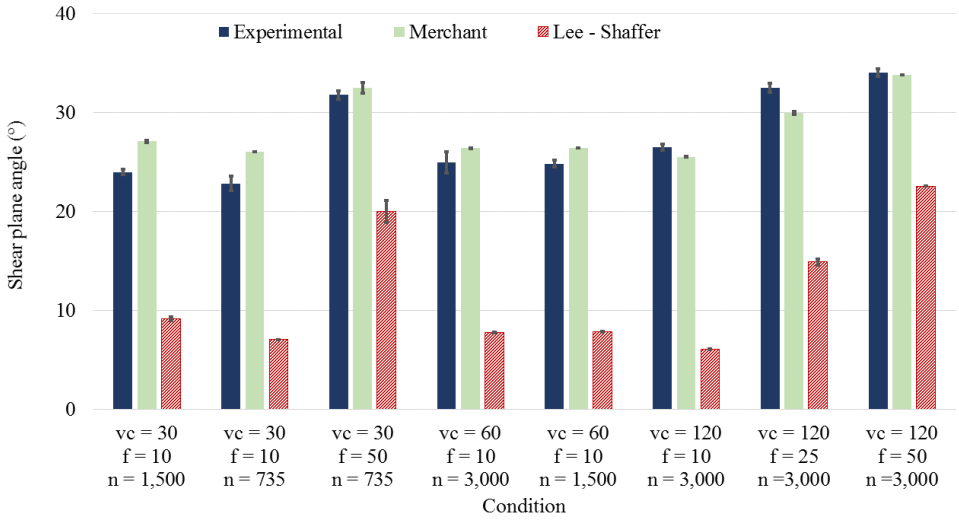

Figure 6.11 – Shear plane angle in the micro-cutting in titanium alloy.

6.1.7. Discussion

Although the low feed rate resulted in low values of the cutting forces, the feed rate used in these experiments caused high values of the specific cutting energy and friction coefficient. It can be related to the ploughing effect due to the feed rate/cutting edge radius (f/r_e) ratio, lower than 1. Ng *et al*. (2006) observed that the specific cutting energy and coefficient of friction increased nonlinearly with the decrease of the undeformed chip thickness/cutting edge radius ratio. In Figure 6.12, it can be seen the influence of the feed rate/cutting edge radius ratio in the micro-cutting of the Ti-6Al-7Nb titanium alloy. The ploughing effect can be also one of the causes of the high variation of the cutting force, as well as the temperature, when it was employed the feed rate of 10 μm/rev.

The ploughing effect caused an increase of the chip compression ratio. In Figure 6.13 is presented the chip compression ratio in the micro-cutting at 120 m/min and high level of the spindle speed. In this figure, it can be observed that the chip compression ratio rises sharply when the f/r_e is lower than 1. When analysing the effect of the cutting speed, the increase of the cutting speed reduces the difference of the chip compression ratio between the feed rates used, see Figure 6.14. To know this is important because it can facilitate the optimization of the metal cutting process (Astakhov and Shvets, 2004).

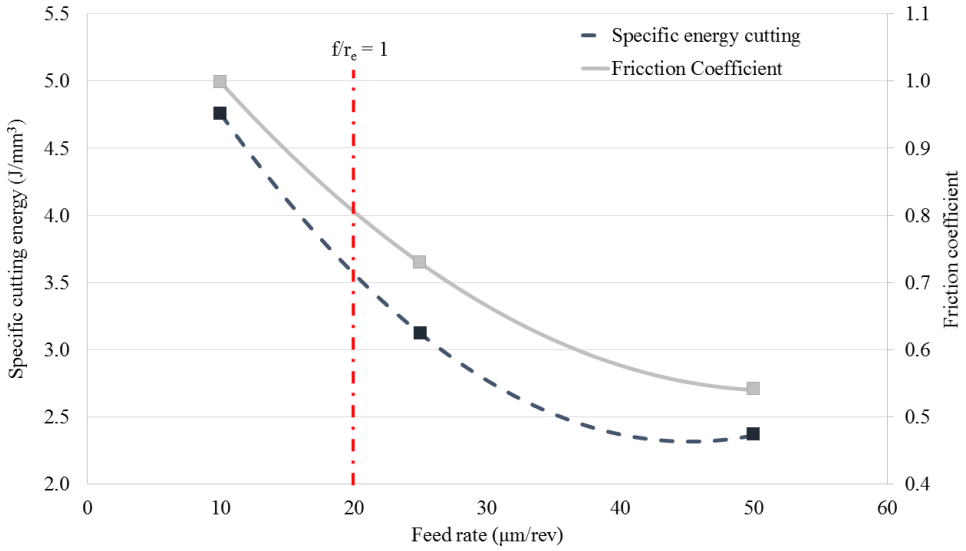

Figure 6.12 – Influence of the f/r_e in the micro-cutting at 120 m/min and high level of spindle speed.

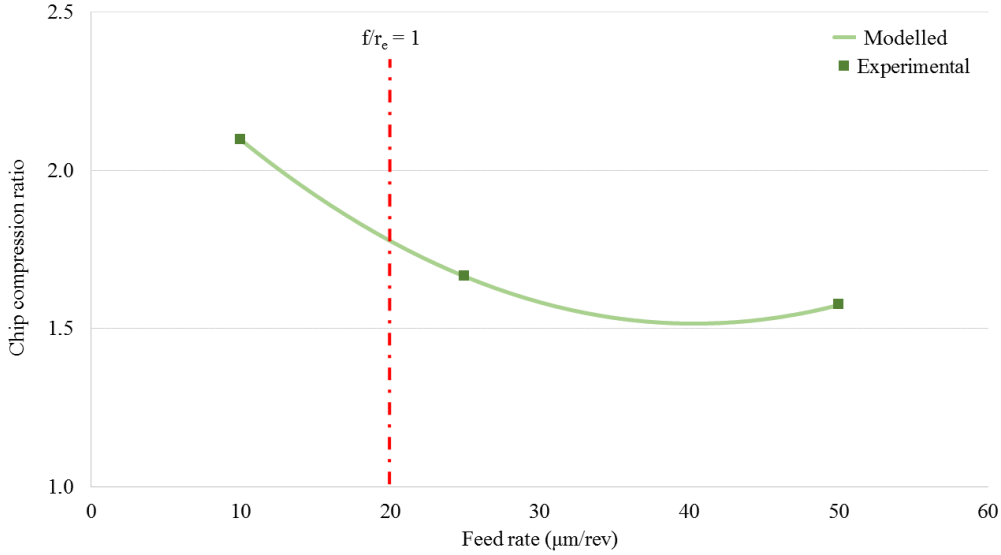

Figure 6.13 – Influence of the ploughing effect in the chip compression ratio at 120 m/min and high level of spindle speed.

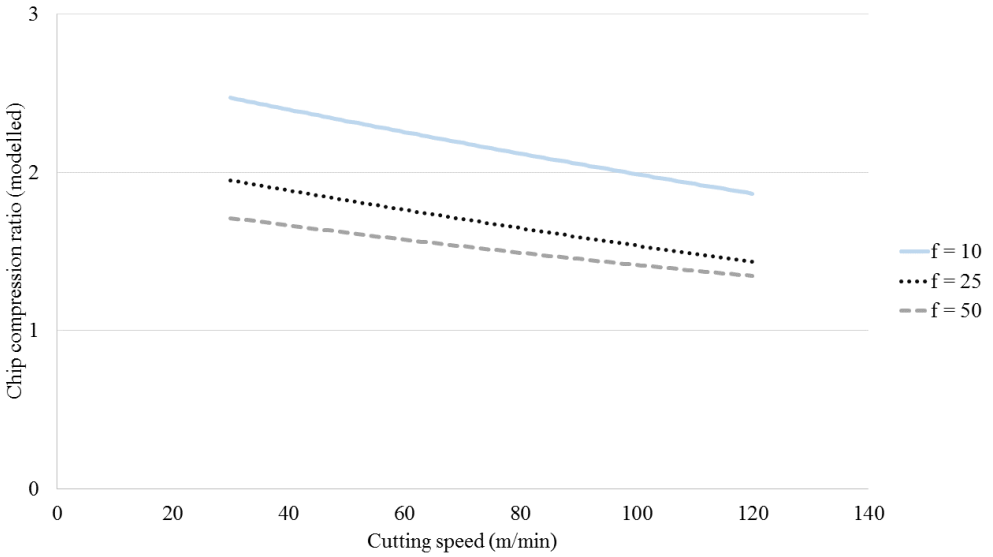

Figure 6.14 – The behaviour of the chip compression ratio in function of the cutting speed for various feed rate and low level of spindle speed.

The results of the experiments for the shear plane angle can also indicate the ploughing effect. A small shear plane angle means that the chip moves away slowly, while a large shear plane angle means a thin, high-velocity chip (Trent and Wright, 2000). Furthermore, a small shear plane angle requires more energy for the same shear stress than an optimum condition (Rowe, 2009). In Table 6.8, it is presented the Spearman's ρ correlation for the micro-cutting of the Ti-6Al-7Nb titanium alloy. The Merchant and Lee - Shaffer models presents the better monotonic correlation with both the friction coefficient and specific cutting energy. However, the Lee - Shaffer model presents a better comparison. The condition that indicated the ploughing effect for the shear plane angle according the Lee - Shaffer model was to have a value lower than 10º. In the Figure 6.15, it is plotted the comparison between the specific cutting energy and Lee - Shaffer shear plane angle model.

Table 6.8 – Spearman's ρ correlation for analysis of the micro-cutting in titanium alloy.

	Cutting speed	Feed rate	Spindle speed	Specific cutting energy	Friction coeff.	Temp.	Experimental	Merchant
Feed rate	0.218							
Spindle speed	*0.974*	0.149						
Specific cutting energy	-0.266	*-0.861*	-0.287					
Friction coeff.	-0.063	*-0.861*	-0.067	*0.888*				
Temperature	*-0.658*	*-0.676*	*-0.683*	*0.809*	*0.600*			
Experimental	*0.689*	*0.820*	*0.635*	*-0.791*	*-0.665*	*-0.871*		
Merchant	0.063	*0.861*	0.067	*-0.888*	*-1.000*	*-0.600*	*0.665*	
Lee-Shaffer	0.063	*0.861*	0.067	*-0.888*	*-1.000*	*-0.600*	*0.665*	1.000

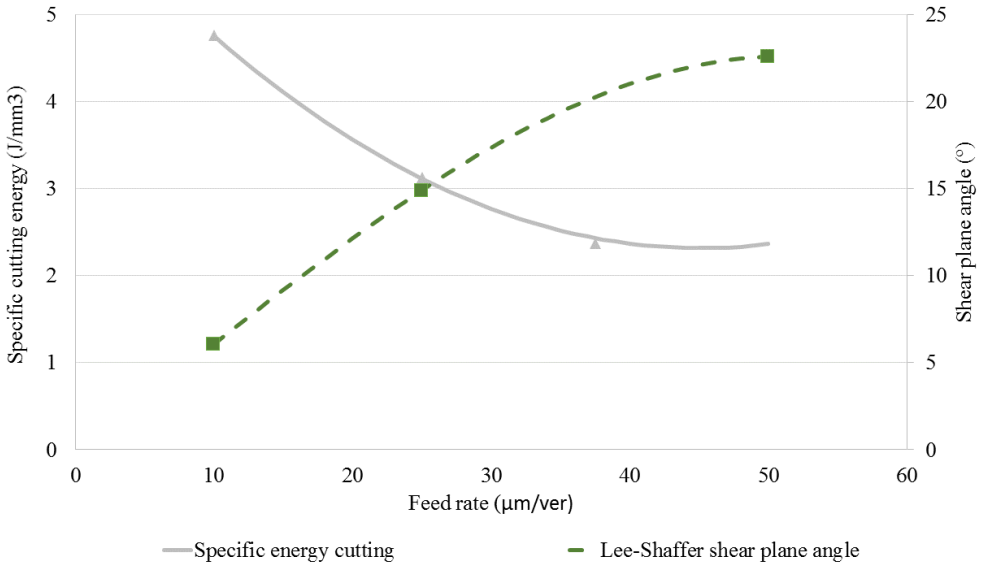

Figure 6.15 – Behaviour of the specific cutting energy and Lee - Shaffer shear plane angle model in the micro-cutting in titanium alloy at 120 m/min.

Thus, the knowledge of the behaviour of biomaterial material in the micro-cutting is very important because it can avoid damage to component or patient. The ploughing effect is undesirable because it causes a machined surface of poor quality, which requires techniques restricted by the price or damages on the microstructures (Afazov *et al.*, 2013; Schueler *et al.*, 2010). It is worth mentioning that the biomedical components requires burr height too small, about 25 nm is acceptable (Fang and Liu, 2004).

6.1.8. Conclusion of the section

This section provides an experimental investigation on the micro-cutting of the Ti-6Al-7Nb titanium alloy for biomedical application. The main conclusions drawn from the study are the following:

- ✓ The increase of the cutting speed, used in this study, caused a growth of the cutting forces, however, it was verified a reduction in the other response, which may indicate an improvement of the cutting and the component quality.

- ✓ Although the lower level of feed rate provided lower values of the cutting forces. For this value occurred the ploughing effect, which was accounted for the increase of the specific energy, friction coefficient, temperature in the tool, and other.

- ✓ The variation of the spindle speed was significant for the cutting force, specific energy, and friction coefficient. Although it was not significant for the temperature in the tool, it was observed that a higher spindle speed caused a lower tool heating.
- ✓ The ploughing effect caused a reduction in the shear plane angle. This event was more notable in the Lee - Shaffer model that were lower than 10º.

6.2. Influence of the HSM and MQL in the micro-cutting

6.2.1. Cutting forces

In the Figure 6.16 is shown the values of the F_T (feed) force in the orthogonal micro-cutting in dry and cooling/lubricated conditions for different cutting parameters. The increase of the feed rate increased the values of the F_T force in both conditions, 82.8% (MQL) and 66.3% (dry). The increase of the cutting speed decreased the F_T force in all condition practically, 10.9% in average. The use of the MQL system varied the F_T force in -18.9% and 3.3% for the cutting speed of the 30 and 60 m/min, respectively. The Figure 6.17 shows the effect Pareto chart for the F_T force. The use of the cooling/lubrication reduced the magnitude of effect for all parameters and the "*Feed rate*" remained important for the F_T force.

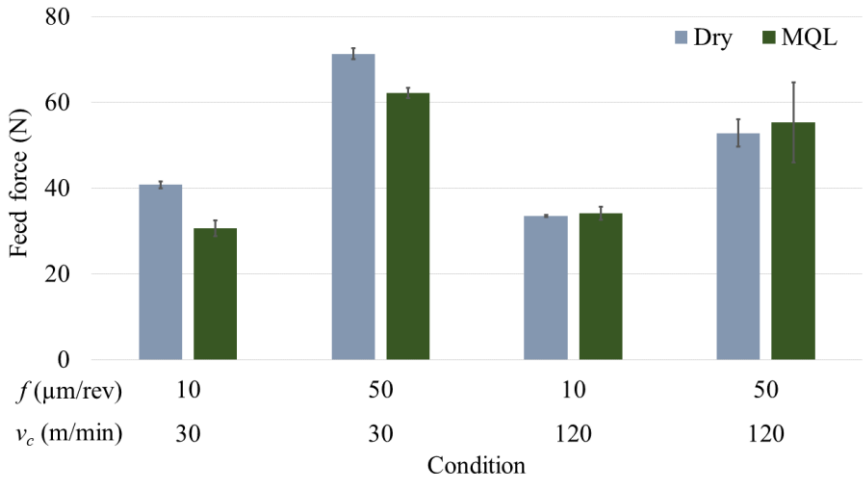

Figure 6.16 – Comparison of F_T forces in the dry and cooling/lubricated micro-cutting.

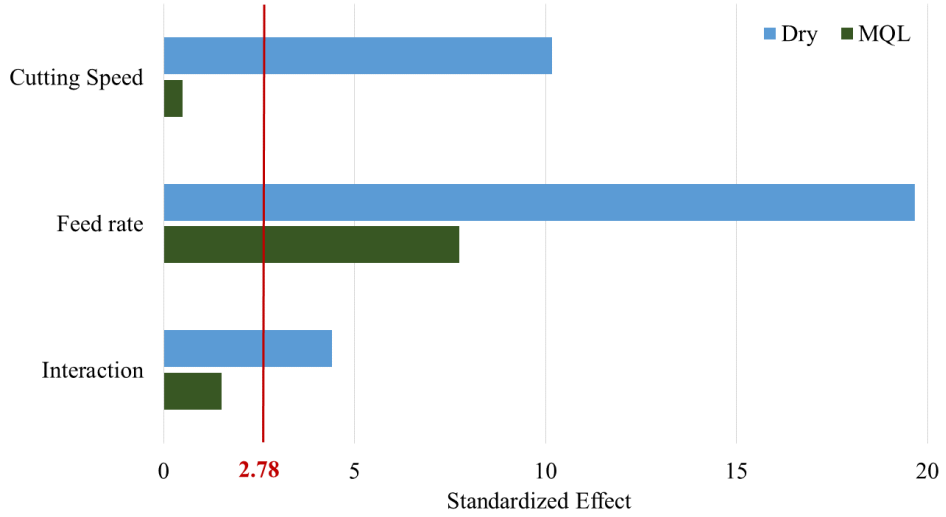

Figure 6.17 – Effect Pareto chart for the F_T forces in the micro-cutting tests.

The F_C (cutting) force for the micro-cutting is shown in the Figure 6.18. The increase of the feed rate caused a growth of 65.4% (Dry) and 82.6% (MQL) in the F_C force, in average. The increase of the cutting speed reduced the F_C force in all conditions practically, 10.9% in average. The use of the MQL system decreased, for v_c of 30 m/min, or increased, for v_c of 120 m/min, in the F_C force. The effect Pareto chart for the F_C force is shown in the Figure 6.19. The employed of the MQL system reduced the magnitude of the "*Feed rate*" and the "*Cooling*" become no importance for the F_C force.

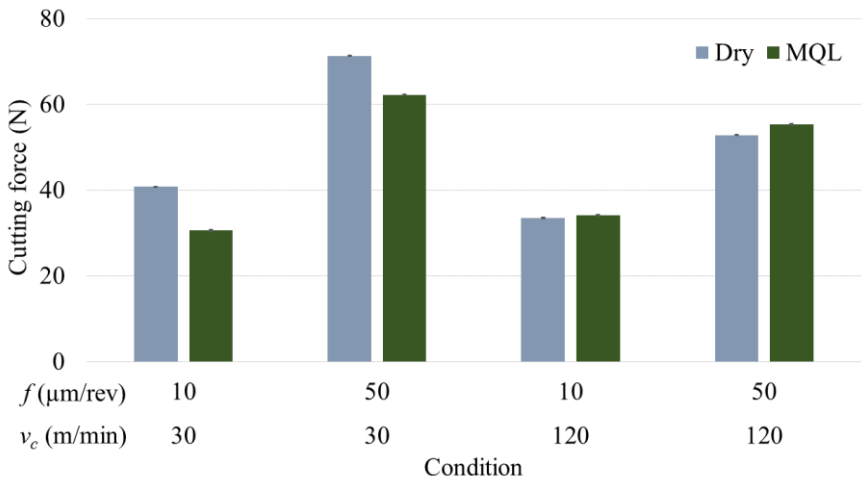

Figure 6.18 – Comparison of F_C forces in the dry and cooling/lubricated micro-cutting.

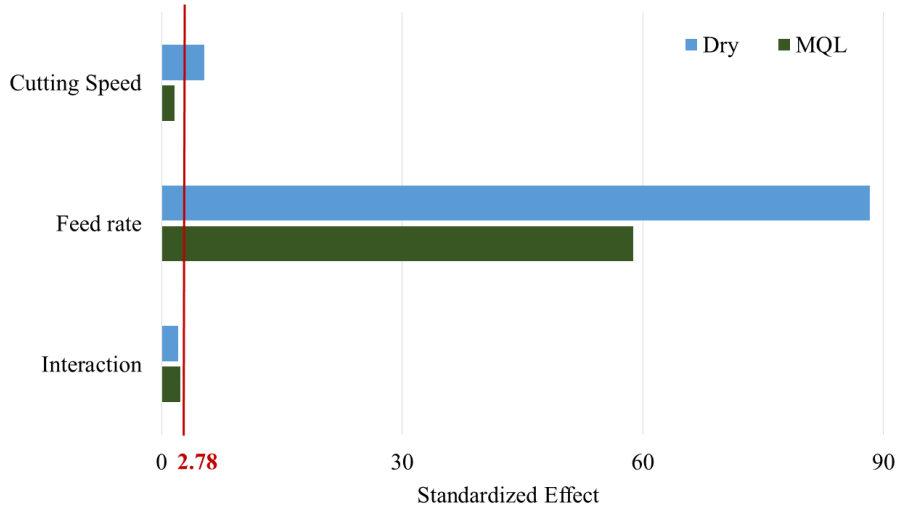

Figure 6.19 – Effect Pareto chart for the F_C forces in the micro-cutting tests.

The Figure 6.20 shows the values of the F_R (machining) force calculated in the dry and cooling/lubricated micro-cutting. The increase of feed rate rose the F_R force in 160.4% (dry) and 194.0% (MQL), on average. The increase of the cutting speed reduced the F_R force in 13.0% (dry) and 2.0% (MQL). For the usage of the MQL system, the most reduction employing the MQL system, was in the condition with lower level (v_c = 30 m/mim and f = 10 µm), 22.3%. For the cutting speed of 120 m/min and feed rate of 10 µm, the reduction was 3.7%. In the meantime, when compared the dry cutting (v_c = 120 m/mim and f = 10 µm) and the cooling/lubricated condition (v_c = 30 m/mim and f = 10 µm), the values of F_R force were lower, 6.1% in average. The reduction of the F_R force for the feed rate were 3.4% (30 m/min) and 1.2% (120 m/min), on average.

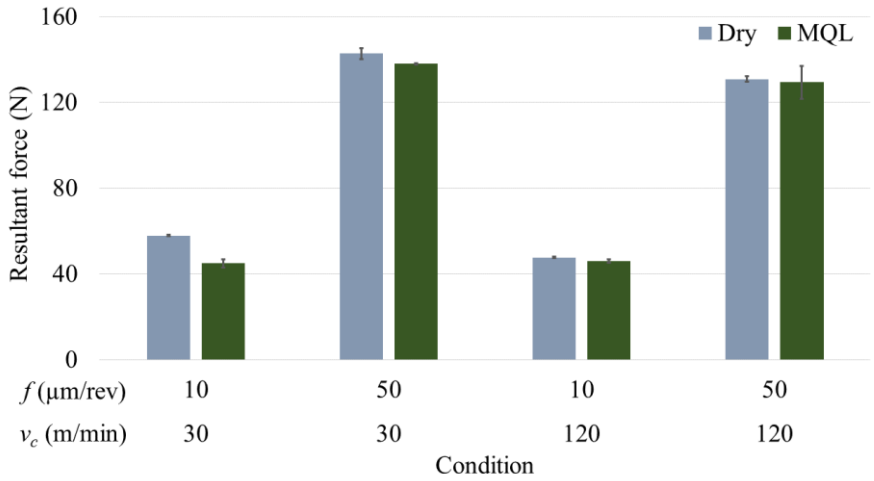

Figure 6.20 – Comparison of the F_R forces in the dry and cooling/lubricated micro-cutting.

The Figure 6.21 shows the effect Pareto chart for the F_R force. The "*Cutting speed*" was no important and the magnitude of the "*Feed rate*" was reduced for the F_R force when used the MQL system.

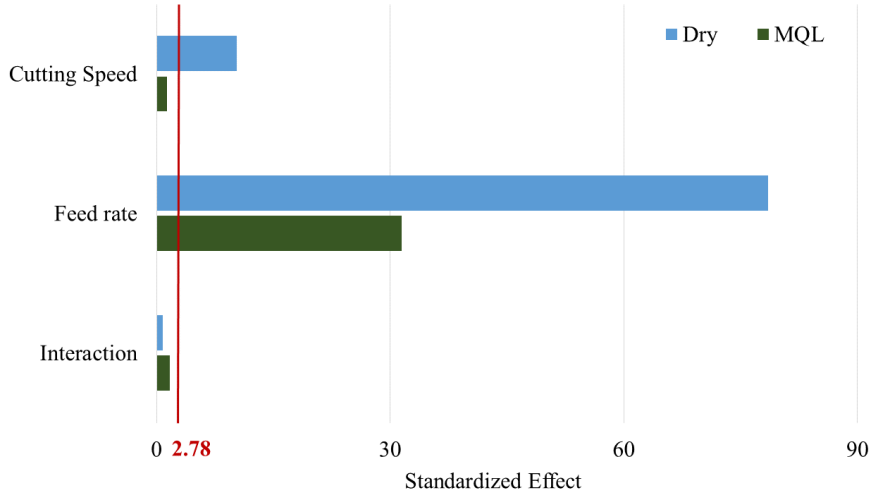

Figure 6.21 – Effect Pareto chart for the F_R forces in the micro-cutting tests.

6.2.2. Specific cutting energy and Friction coefficient

The comparison of the specific cutting energy for dry and cooling/lubricated cutting is shown in the Figure 6.22. The increase of the cutting speed and the feed rate decreased the specific cutting energy in, respectively, 13.0% and 47.9%, for dry cutting, and 2.0% and 41.2%, employing the MQL, on average. The use of the MQL system, the reduction was higher in the low cutting speed (22.3% and 3.4%) than high cutting speed (3.7% and 1.2%), for the feed rate of 10 and 50 µm respectively.

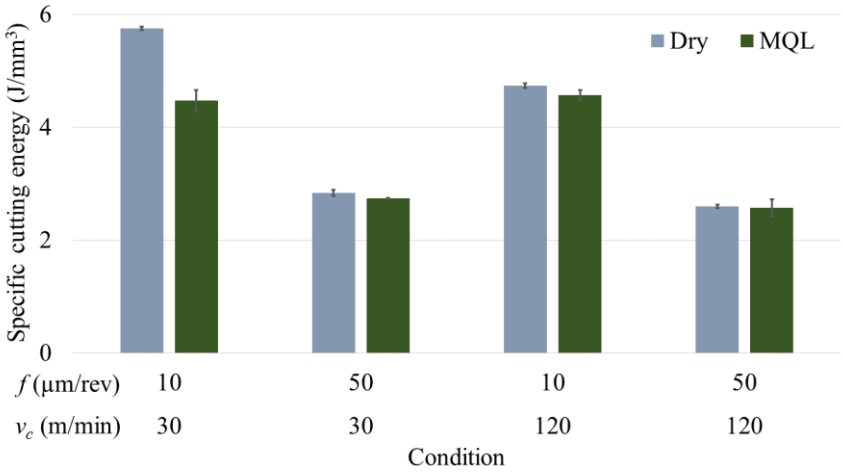

Figure 6.22 – Comparison of the specific cutting energy in the dry and cooling/lubricated micro-cutting.

The effect Pareto chart for the specific cutting energy is shown in the Figure 6.23. For the specific cutting energy, the all parameters were important in the dry condition, and only the "*Feed rate*" was important in the cooling/lubricated condition.

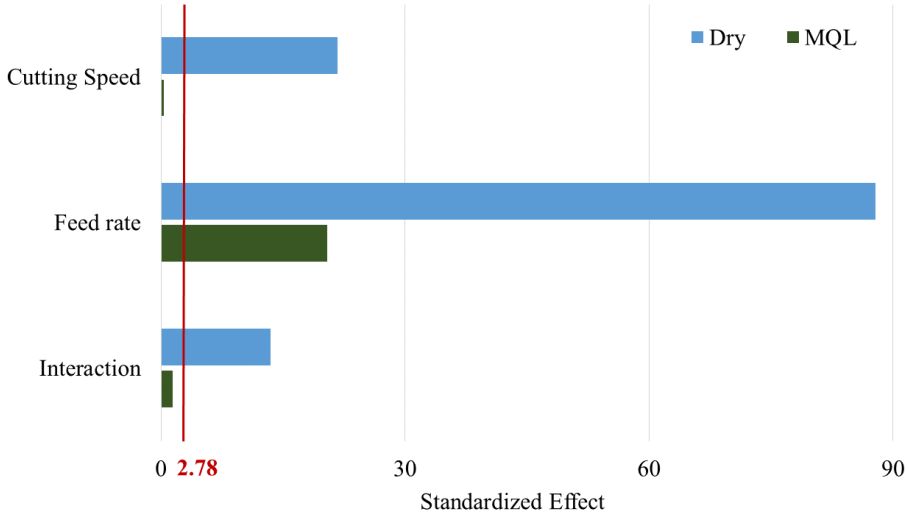

Figure 6.23– Effect Pareto chart for the specific cutting energy in the micro-cutting tests.

The Figure 6.24 shows the values of the friction coefficient between tool and chip in the micro-cutting. The increase of the feed rate caused a reduction in the friction coefficient in in the MQL (42.9%) and dry (41.1%) conditions. Except for the condition using MQL and low feed rate, the increase of the cutting speed decreased the friction coefficient in all condition, 8.2% on average. The employed of the MQL system varied the friction coefficient of -8.2% (v_c = 30 m/min) and 5.6% (v_c = 120 m/min).

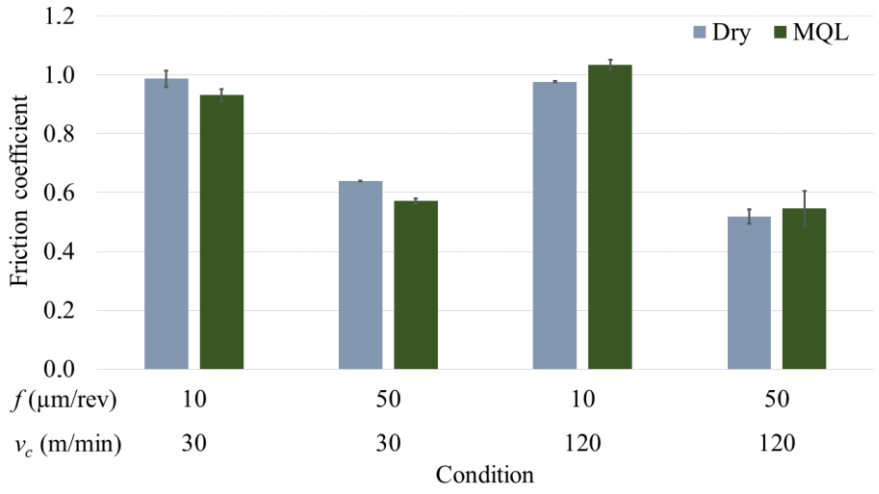

Figure 6.24 – Comparison of the friction coefficient in in the dry and cooling/lubricated micro-cutting.

The effect Pareto chart for the friction coefficient is shown in the Figure 6.25. When employed the MQL system, only the *"Feed rate"* become important for the friction coefficient.

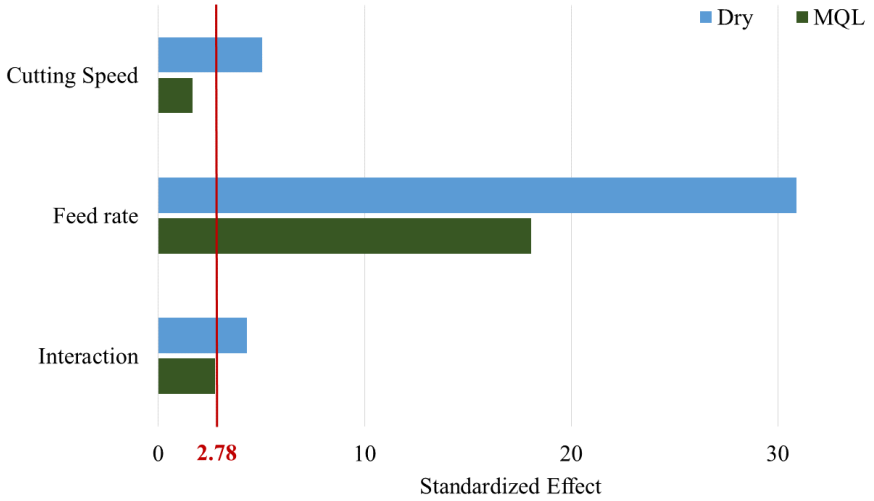

Figure 6.25 – Effect Pareto chart for the friction coefficient in the micro-cutting tests.

6.2.3. Shear plane angle

The values of the shear plane angle calculated by the Lee - Shaffer model is shown in the Figure 6.26. The increase of the feed rate rose sharply the shear plane angle in 221.4% (dry) and 254.3% (MQL). The variation of the cutting speed, from 30 to 120 m/min, increased the shear plane angle for all conditions, practically, at least 4.2%. The use of the MQL system caused an increase (20.8% for the v_c = 30 m/min) or a reduction (14.8% for the v_c = 30 m/min).

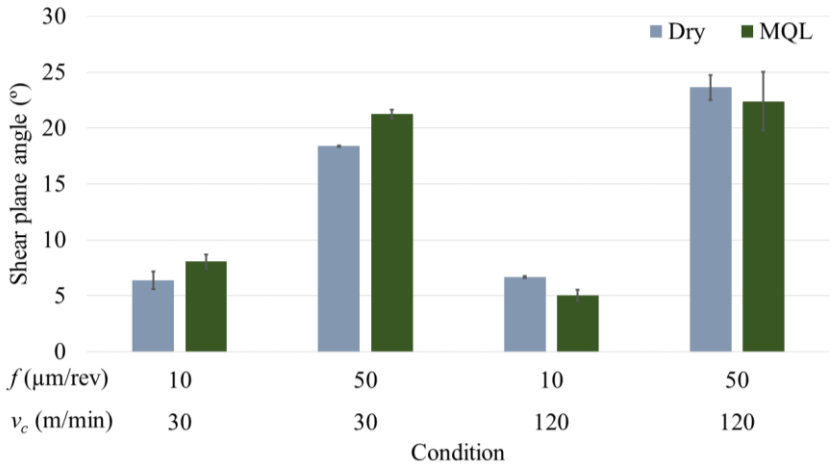

Figure 6.26 – Comparison of the Lee – Shaffer shear plane angle in the dry and cooling/lubricated micro-cutting.

The Figure 6.27 shows the effect Pareto chart for the shear plane angle. All parameters presented reduction of the magnitude of the standardized effect, however, only *"Feed rate"* was important in this response when used the MQL system.

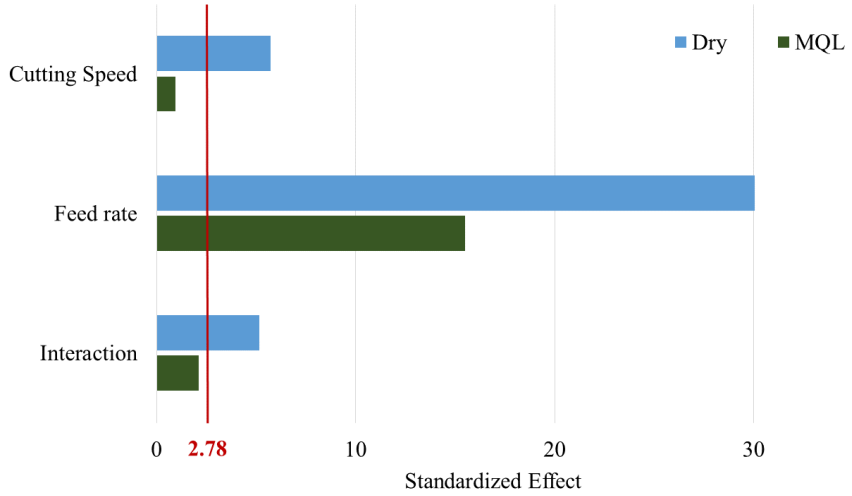

Figure 6.27 – Effect Pareto chart for the Lee – Shaffer shear plane angle in the micro-cutting tests.

6.2.4. Chips

The comparison between dry and cooling/lubricated condition for the chip compression ratio is shown in the Figure 6.28. The increase of the feed rate went down the chip compression ratio in 33.5% (dry) and 27.6% (MQL). Similar evolution was observed for the cutting speed, a reduction of 18.8% (dry) and 9.5% (MQL), on average. The usage of cooling/lubrication in the micro-cutting varied the values of the chip compression ratio in -3.2% (v_c = 30 m/min) and 7.8% (v_c = 120 m/min), on average.

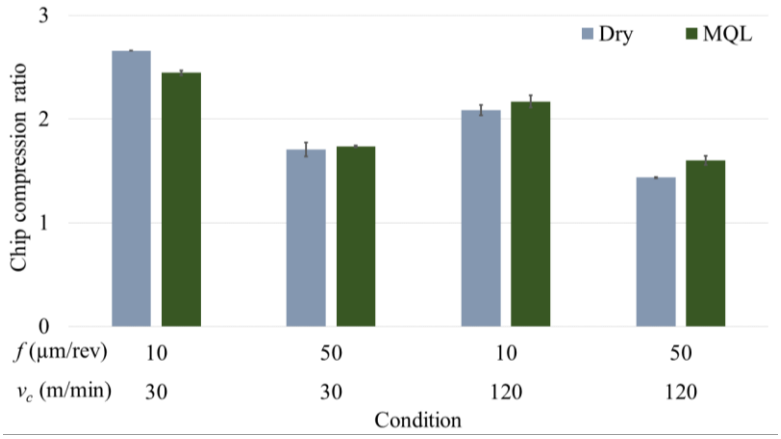

Figure 6.28 – Comparison of chip compression ratio in the dry and cooling/lubricated micro-cutting.

In the Figure 6.29 is shown the effect Pareto chart for the chip compression ratio. When used the MQL system, the importance of the "*Feed rate*" and "*Cutting speed*" presented reductions, however, the interaction presented the increase of the magnitude for the chip compression ratio.

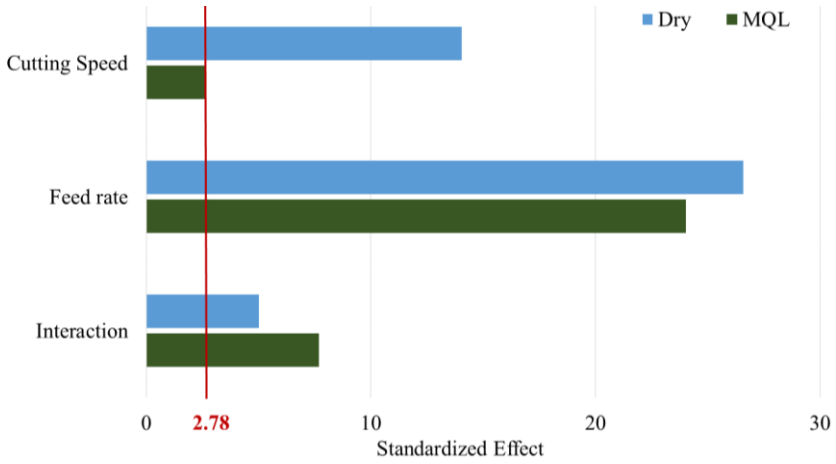

Figure 6.29 – Effect Pareto chart for the chip compression ratio in the micro-cutting tests.

In the d) f = 50 μm/rev and vc = 120 m/min

Figure 6.30 is shown the chip morphology of micro-cutting for the feed rate of 10 and 50 μm/rev. For the free surface of chip, the lamellar structures were more spaced for the increase of the feed rate and the cutting speed. When analysing the effect of the cooling/lubricated, the spacing increased for the v_c of 30 m/min and decreased for the v_c of 120 m/min.

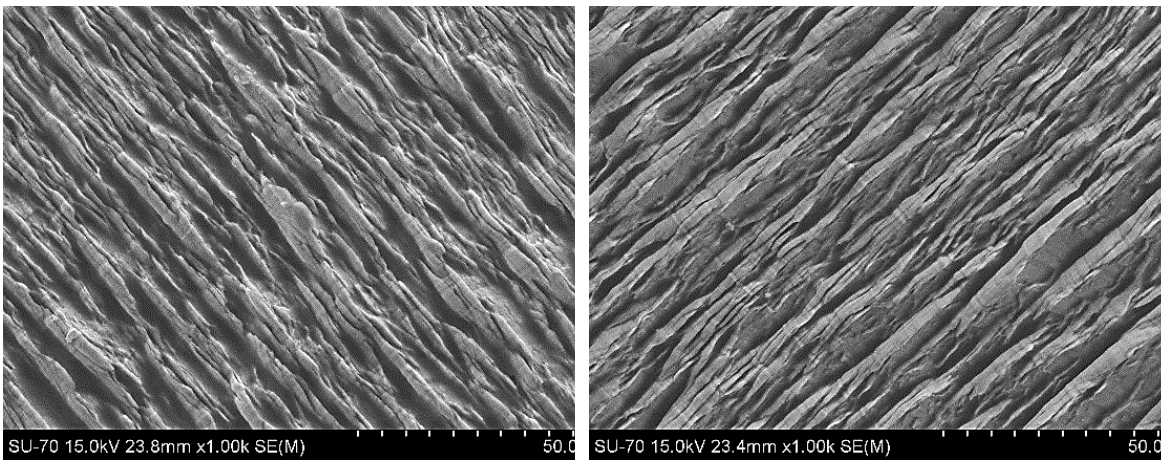

Dry Cooling/lubricated

a) f = 10 μm/rev and vc = 30 m/min

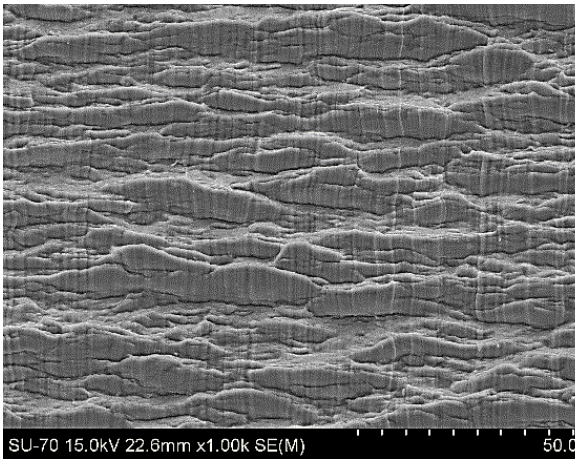

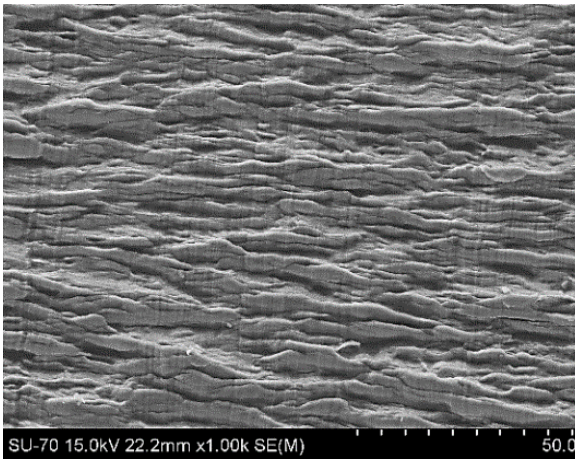

Dry Cooling/lubricated

b) f = 10 μm/rev and vc = 120 m/min

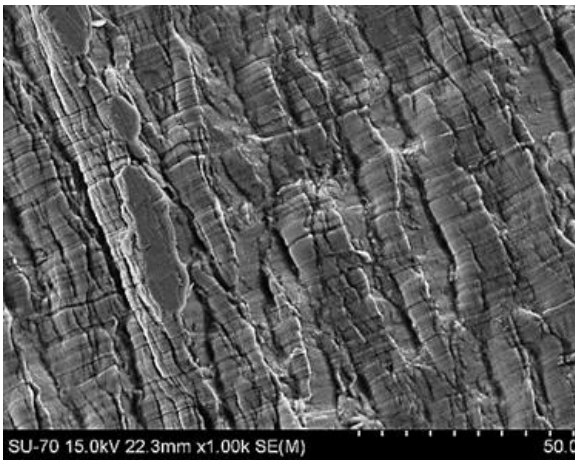

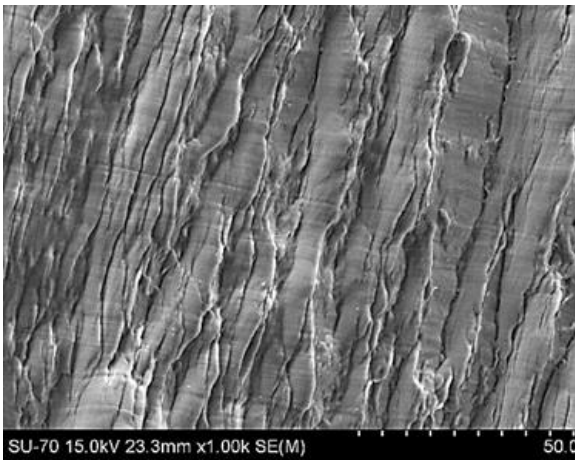

Dry Cooling/lubricated

c) f = 50 μm/rev and vc = 30 m/min

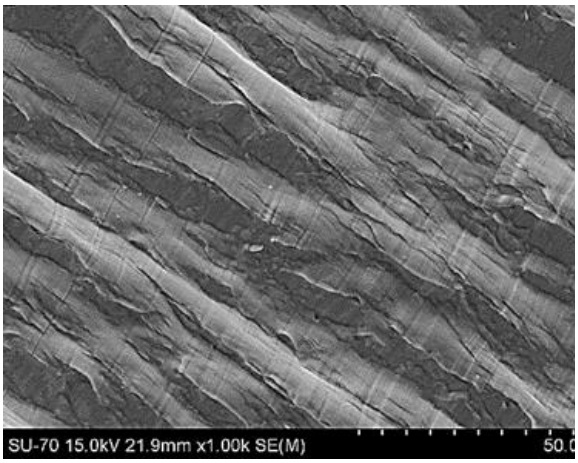

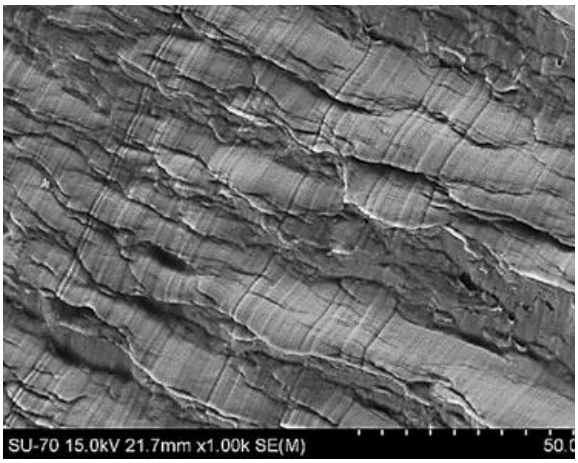

Dry Cooling/lubricated

d) f = 50 μm/rev and vc = 120 m/min

Figure 6.30 – Chip morphology in the micro-cutting tests.

6.2.5. Surface roughness

The values of R_a, R_z and R_t surface roughness obtained in the micro-cutting are showed in the Figure 6.31a and Figure 6.31b, respectively. The values of the surface roughness for the feed rate of 50 µm/rev were low than the feed rate of 10 µm/rev, on average, 28.8% (dry) and 34.3% (MQL). It can be justified because the feed rate of 10 µm/rev suffered the ploughing effect, $f/r_e < 1$, that provided surface with poor quality. In general, the application of the cooling/lubrication in the micro-cutting increased the values of the surface roughness, on average, 17.1% (v_c = 30 m/min) and 148.1% (v_c = 120 m/min). The increase of the cutting speed caused an increase, when used the MQL system, or a decrease, for the dry condition, in the values of the surface roughness.

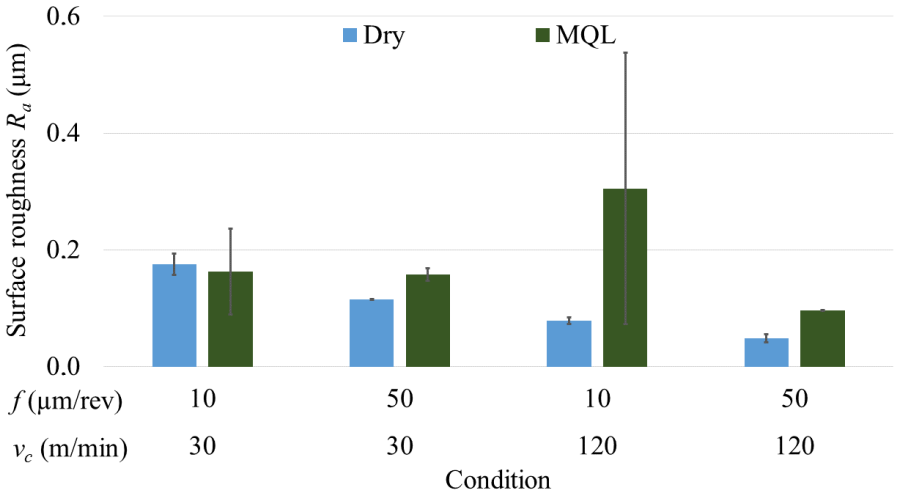

a) Values of R_a surface roughness in the micro-cutting.

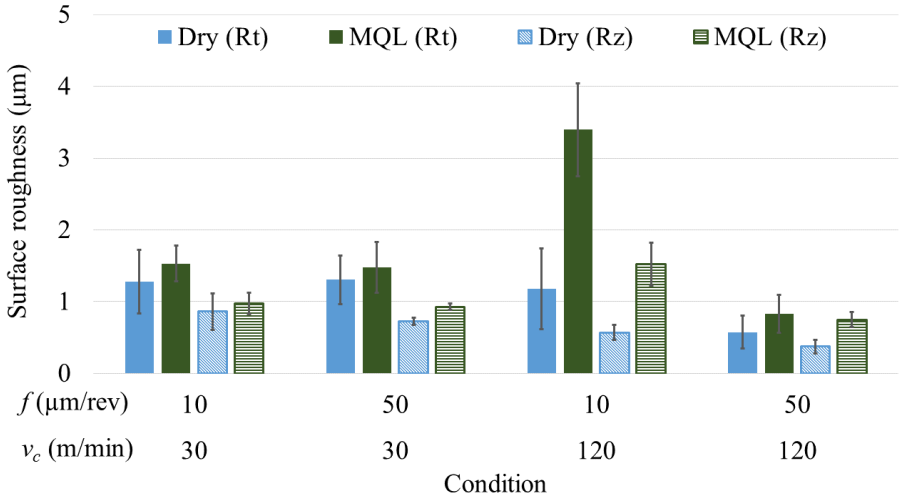

b) Values of R_t and R_z surface roughness in the micro-cutting.

Figure 6.31 – Comparison of surface roughness in the dry and cooling/lubricated micro-cutting.

In the conditions that were employed the cooling/lubrication, was observed a larger number of scratches in the micro-machined surface, Figure 6.32a, than condition without cooling/lubrication, Figure 6.32b. It can be justified because the use of the MQL allowed further adhesion of micro-chips and the slip of the tool during the cutting, seen Figure 6.33.

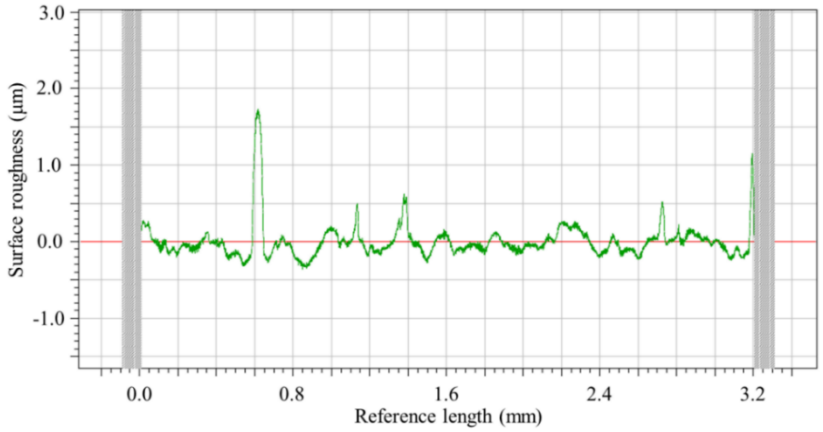

a) Cooling/lubricated cutting

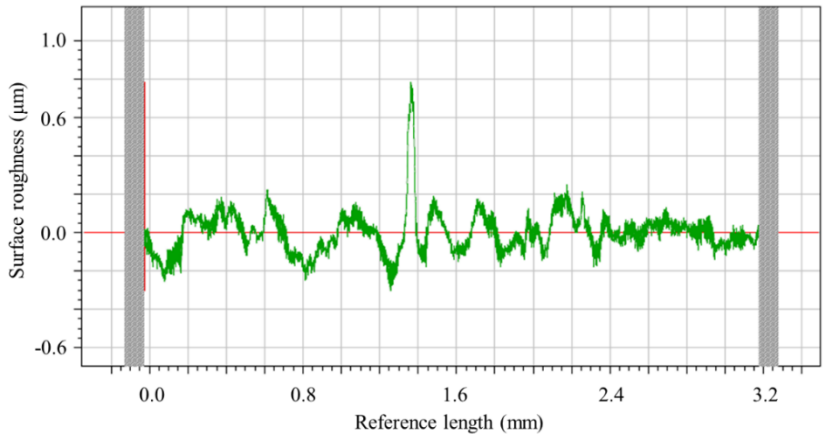

b) Dry cutting

Figure 6.32 – Surface roughness outline for the dry cutting (v_c = 120 m/min and f = 10 µm/rev).

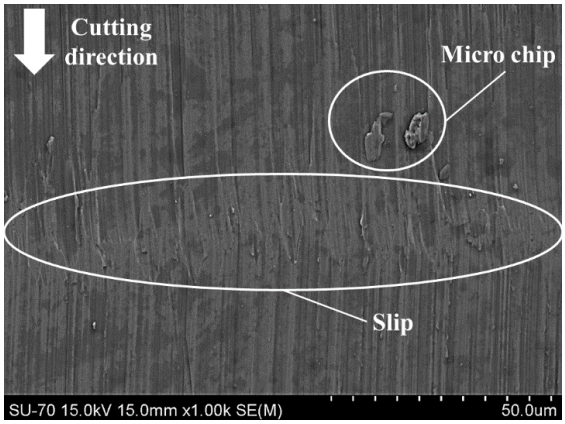

Figure 6.33 – SEM of the micro-machined surface for the cooling/lubricated micro-cutting.

6.2.6. Burr

In the Figure 6.34 is shown the comparison of the burr length in the dry and cooling/lubricated conditions. The increase of the feed rate caused an increase of burr length in 124.9% (dry) and 100.3% (MQL), on average. The increase of the cutting speed decreased the burr length in 48.5% (dry) and 65.8% (MQL). When compared the dry and cooling/lubricated conditions, the use of the MQL system caused a great reduction of the burr formation, 75.9% (f = 10 µm/rev) and 68.8% (f = 50 µm/rev), on average. The reduction of the burr formation when employed the MQL system, can be observed in the Figure 6.35. In the Figure 6.36 is shown the effect Pareto chart for the burr formation. The magnitude both parameters and their interaction were increased for burr formation when employed the cooling/lubricated condition.

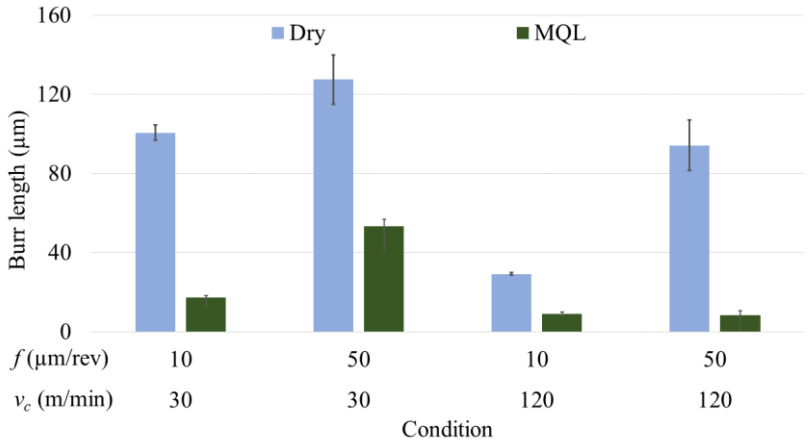

Figure 6.34 – Comparison of burr in the dry and cooling/lubricated micro-cutting.

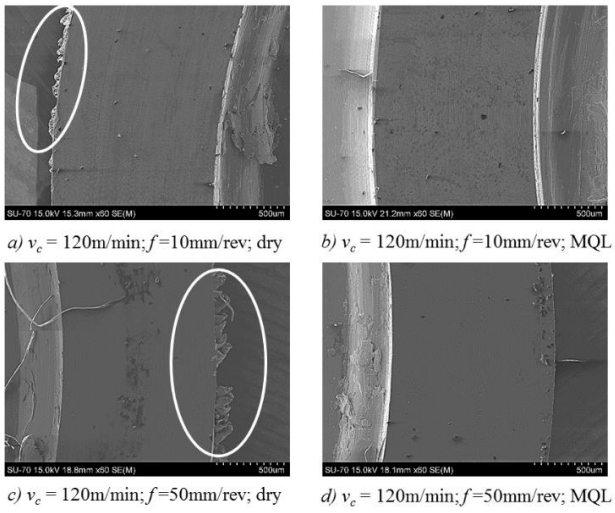

Figure 6.35 – SEM to observe the burr formation in micro-cutting of the titanium alloy.

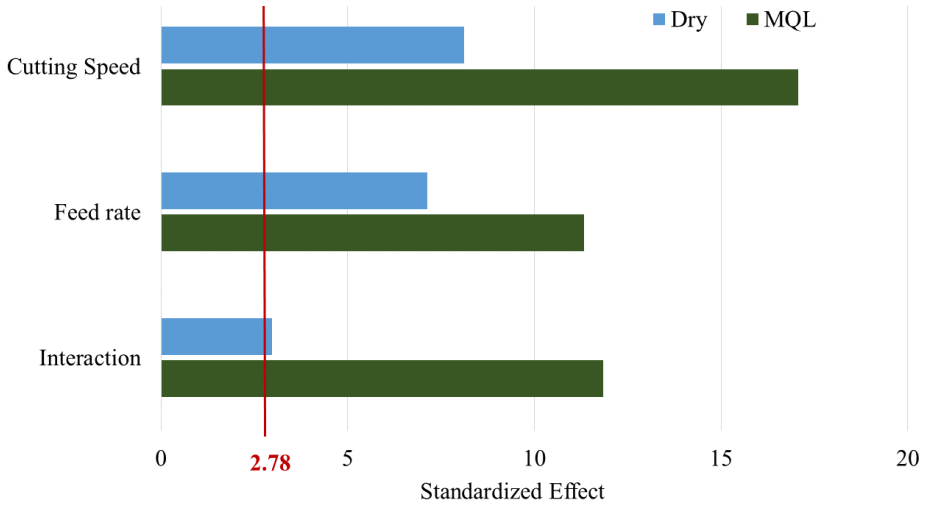

Figure 6.36 – Effect Pareto chart for the burr formation in the micro-cutting tests.

6.2.7. Discussion

In this section is debated the influence of the cooling/lubrication in the micro-cutting in the Ti-6Al-7Nb titanium alloy. The higher influence of the feed rate in all response, practically, can be justified because the relation between depth of cutting and feed rate with the cutting area, the feed rate was the main factor because the depth of cutting was constant during the experiments. Thus, the feed force was affected directly by increase of cutting section due to the feed rate variation. Furthermore, should be considered a similar phenomenon as well as in macro turning where the feed rate is important to change the chip geometry, this changing occurs of long chips when low feed rates are used to small chips when higher feed rates are fixed.

When compared the dry and the cooling/lubricated conditions, the results for the cutting speed of 30 m/min were improved when employed the MQL system. However, the use of the MQL system for the cutting speed of 120 m/min, provided the negative impact or neglect improvement. The exceptions were the burr formation, which was strongly reduced when employed the cooling/lubricated condition.

According to Childs (2006), the use of the cutting fluids can influence differently the low speeds (friction) and the high speed (thermal flow at the chip–tool contact area). It can be the reason for the cutting speed was more significant in dry condition than MQL system, as observed in the Pareto charts, for the cutting forces and specific cutting energy, it was observed that. The temperature in the cutting is strongly influence by cutting speed and the

increase of temperature can reduce the cutting forces. Leppert (2011) and Hadad and Sadeghi (2013) observed that the MQL system was not efficient for cutting speed more than 100 m/min. Simunovic *et al*. (2015) did not observe different between dry and wet conditions in the analysis of the surface roughness. The use of the MQL system presented prominent efficiency for in the burr formation. It occurs because the use of the MQL system produces a minimum burr due to the absence of build-up edge or a thermal chemical reaction, when compared to flood and dry machining (Kajaria *et al.*, 2012). However, it should be noted that in the micro-milling of Inconel 718, dry and MQL conditions presented no significant difference for the burr formation (Ucun, Aslantas and Bedir, 2014).

Considering the relationship between cutting edge radius and the undeformed chip thickness during a machining process, in this paper, the ratio h/reis was greater than 1. Based on this, this situation provided, according to Balogun *et al*. (2016), a cutting mechanism tends to be value adding and sustainable machining. Thus, it can be considered that the elastic deformation of the workpiece during machining process decreased quickly and a perfect chip was generated. Moreover, the shearing phenomenon can be considered perfect because not occurred the ploughing effect and the increase of feed rate changed of the cutting mechanism from the rubbing/ploughing phenomenon to the shearing phenomenon.

According to Singaravel and Selvaraj (2016) the main cutting force components have higher magnitude than feed force and radial force components as occurred in these experimental tests. Thus, it can be considered that the main cutting force decreased at high cutting speed and this phenomenon occur due to high cutting speed that increases the shear angle and generates a minimum shear plane area. The simultaneous increase of cutting speed and feed rate provides an increase of the contact area between the cutting tool and workpiece.

The Figure 6.37 shows the comparison influence of the cooling/lubrication using the Minimum Quantity Lubrication (MQL) system, High Speed Machining (HSM) and both technique, although the average of the response analysed in this study. The HSM provided similar or betters results than the MQL system. For the response used to identify the ploughing effect, like the Lee – Shaffer shear plane angle model, the employed of HSM was better than MQL and both techniques joints. Besides, in the chip compression ratio, the use of the MQL was disadvantageous. Thus, when possible, the use of the HSM, only, can be more advantageous than the use of the MQL system, only, for the micro-cutting orthogonal

in the Ti-6Al-7Nb titanium alloy for all criteria analysed in this study, except for the burr formation.

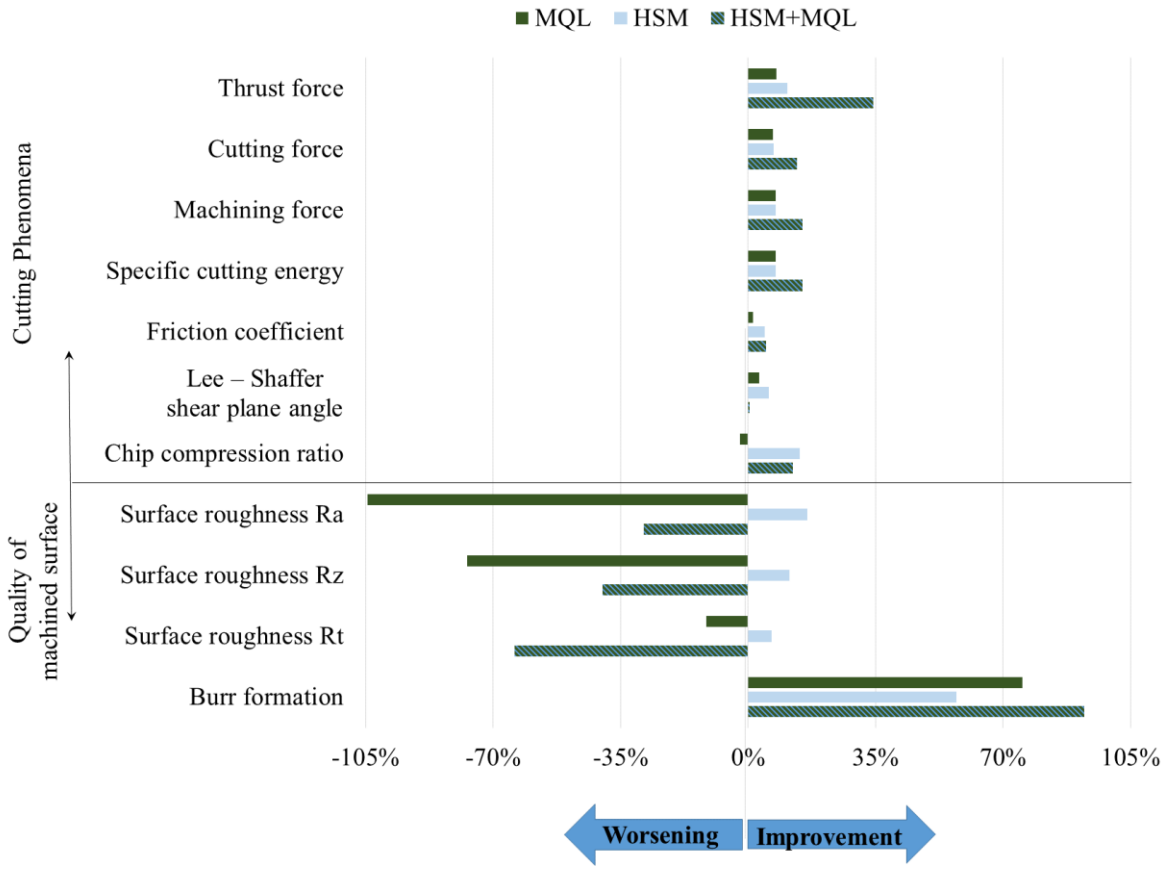

Figure 6.37 – Summary of the influence in the response of the micro-cutting tests.

6.2.8. Conclusion of the section

Based on the results of the orthogonal micro-cutting in the Ti-6Al-7Nb titanium alloy, the main conclusions drawn from the study are the following:

✓ For the cutting forces (thrust, cutting and machining), the use of the MQL system reduced the magnitude of these forces only when employed in the low cutting speed. For the combination of HSM and MQL system increased the magnitude of these cutting forces.

✓ When analysed the specific cutting energy, the use of the MQL system was efficient for all conditions. However, the use of the MQL did not present good performance for the friction coefficient and shear angle plane for the combined use with the HSM.

✓ For the analysis of the chip, chip compression ratio and the morphology, the great result was obtained for the use of the HSM, while the use of the MQL system caused a worsening independently of the cutting speed.

✓ For the quality of the micro-machined surface, the use of the MQL caused the increase of the surface roughness due to the high adherence of number of micro-chip and the slip of tool during the cutting, although the MQL was responsible for the great reduction of the burr formation.

6.3. Material modelling of Ti-6Al-7Nb titanium alloy to surface integrity via FEM

In the Table 6.9 is shown the comparison between the results of experimental and numerical tests and the material removal rate for the micro-cutting of Ti-6Al-7Nb titanium alloy. The numerical tests showed more deviation for the thrust force (F_T), which can be justified due to the displacement in the feed direction is not controlled. In the Figure 6.38 are shown the values of power obtained in the numerical tests. Though the responses may appear similar, the power differed the conditions. For example, the condition with v_c of 30 m/min and f of 50 µm/rev presented the cutting forces about 3 and 4 higher than the condition with v_c of 120 m/min and f of 10 µm/rev, however, the powers were similar for both condition. Furthermore, the condition with low level of parameters required 20 times less than the condition with high level of parameters, however, the condition with high level of parameters presented a material remove rate 16 times higher than the condition with low level of parameters.

Table 6.9 – Comparison between experimental and numeric tests for cutting forces

Parameter			MMR	Thrust force (F_T)			Cutting force (F_C)		
Cutting speed (m/min)	Feed rate (µm/rev)	Depth of cut (µm)	(m^3/h)	Exp. (N)	Num. (N)	Deviation	Exp.	Num. (N)	Deviation (N)
30	10	800	0.02	25.96	19.77	23.8%	27.16	25.32	6.8%
30	50	800	0.12	43.78	58.40	33.4%	82.70	107.51	30.0%
120	10	800	0.10	25.24	19.68	22.0%	25.28	25.04	1.0%
120	50	800	0.48	37.35	53.16	42.3%	80.69	103.52	28.3%

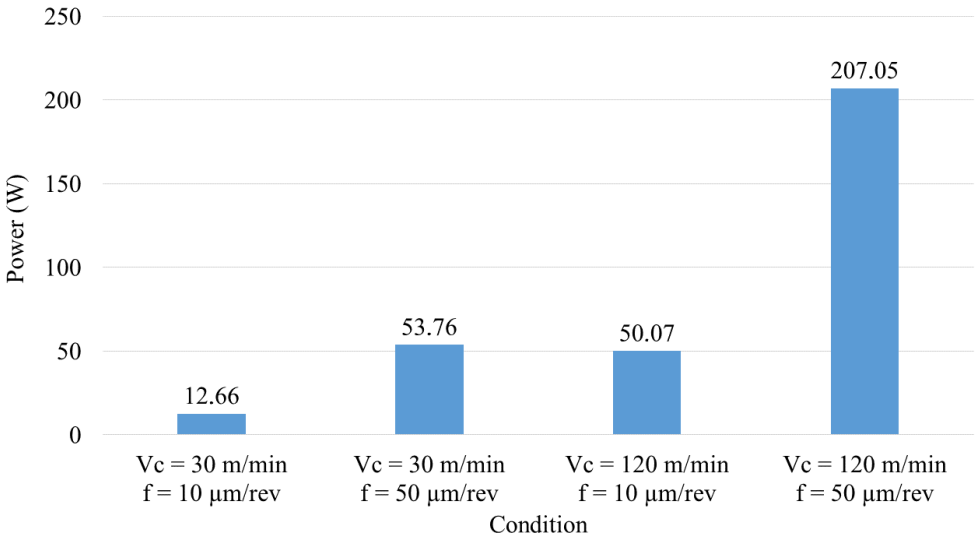

Figure 6.38 – Power in the numerical tests of orthogonal micro-cutting tests.

The Figure 6.39 shows the temperature during the micro-cutting. When compared the relation between the temperature in the chip and the cutting zone, the combination of high parameters presented the greater approximation. For the relation between the temperature in the machined surface and the cutting zone, the combination of high parameters presented the greater approximation the combination of high feed rate and low cutting speed presented smaller approximation.

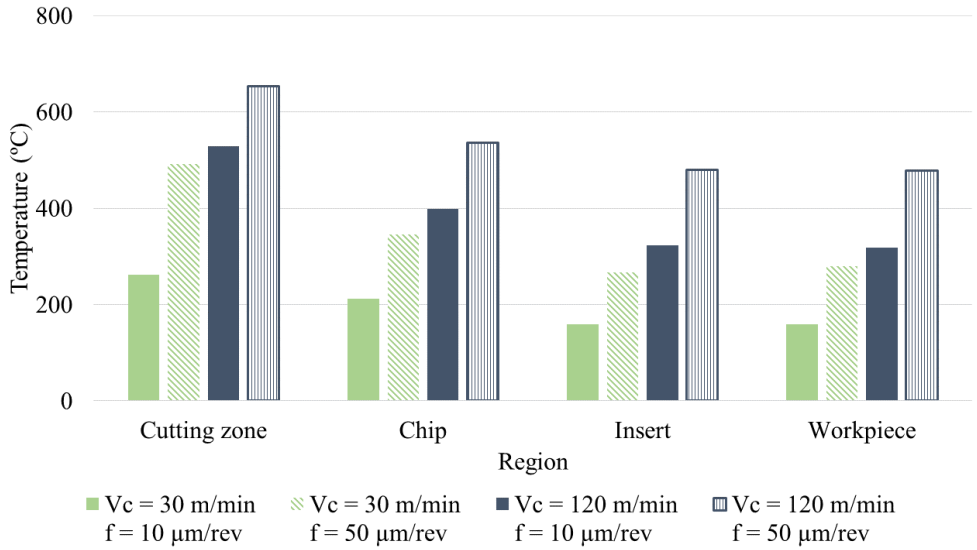

Figure 6.39 – Distribution of temperature during the orthogonal micro-cutting.

The heat flux in the radial direction is shown in the Figure 6.40. The high cutting speed caused more heating in the machined surface than the low cutting speed, however, the temperature reached a smaller depth. It can be justified because the heat source moves quickly that hampers spread of the heat. The Figure 6.41 shows the temperature in the first elements. The high cutting speed caused higher temperature than the low cutting speed, however, the cooling was faster than one.

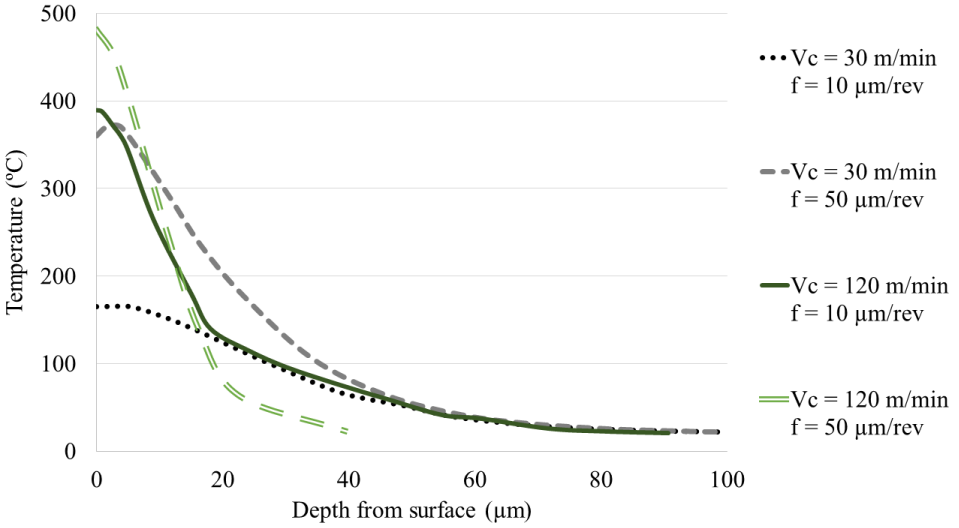

Figure 6.40 – Heat flux in the radial direction for the orthogonal micro-cutting.

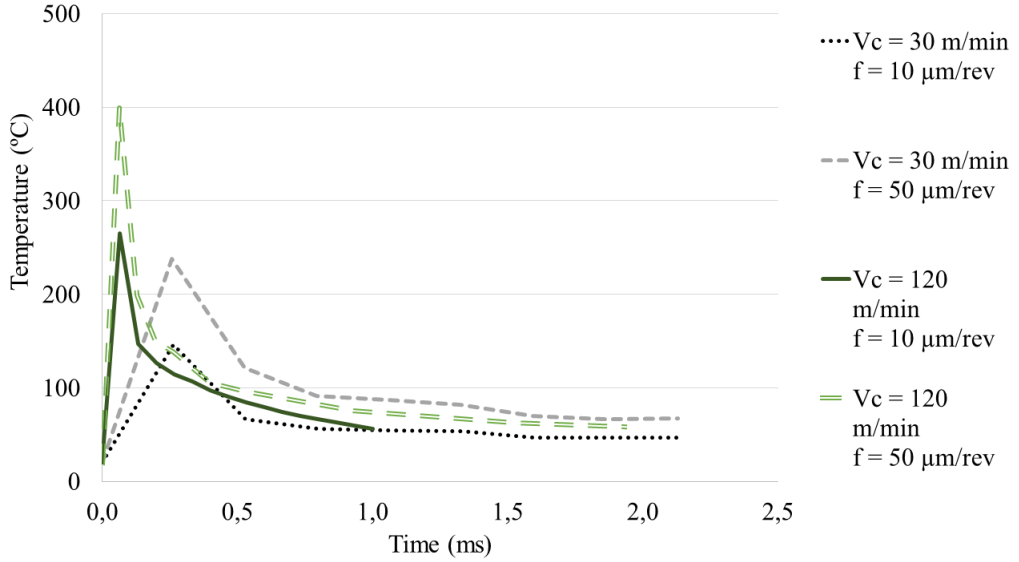

Figure 6.41 – Temperature in the first elements in the orthogonal micro-cutting.

For the Ti-6Al-7Nb titanium alloy, heating range between 800º C and 900º C causes a microstructure that is clearly fine-grained. The grains of the α phase can precipitates a new

phase originated due to the alloy heating directly after the plastic deformation. They can result from the α' phase recrystallization or the α phase coalescence. At higher temperatures the growth of this phase is observed (Dąbrowski, 2012).

Pilehva *et al*. (2016), the martensitic α (α′) is generated due to the quenching right after preheating from the single-phase β regions. The deformation temperatures and prior to the hot compression testing, the microstructure can be consisted by only beta grains. Moreover, the average grain size can increase from 163 ± 6 μm at 1050 °C to 236 ± 13 μm at 1100 °C, approximately.

Meanwhile, according to Sieniawski *et al*. (2013), a cooling rate higher than 18 °C/s, when the Ti-6Al-2Mo-2Cr and Ti-6Al-4V titanium alloys are above β transus temperature, leads to formation of martensitic microstructure consisting of α' (α") phases. A cooling rate less than 3.5 °C/s, the martensitic transformation is accompanied by diffusional transformation β for α + β and the volume fraction of martensitic phases decreases to the benefit of stable α and β phases. Cooling rates below 2 °C/s lead to a diffusion controlled nucleation and growth of stable α and β phases in the shape of colonies of parallel α-phase lamellae in primary β-phase grains.

Although the cutting temperature were lower than 500 ºC in the machined surface during the micro-cutting, little metallurgic alterations in the material can occur because during the cutting, the machined surface is under pressure. In the milling of Ti-6242S titanium alloy, Ginting and Nouari (2009) observed that the effect of activation energy to produce cyclic heating/cooling for internal work hardening is gradually dissipated; therefore. Thus, the microstructure below the machined surface, for some micrometres, suffers a plastic deformation that is caused by the high pressure at the elevated cutting temperature.

In the is shown the residual stress of the orthogonal micro-cutting. The feed rate of the 10 μm/rev caused a tractive residual stress in the machined surface, while, the feed rate of the 50 μm/rev caused a compressive residual stress, that according to Hua *et al*. (2006) is beneficial. The variation of the cutting speed did not cause great variation.

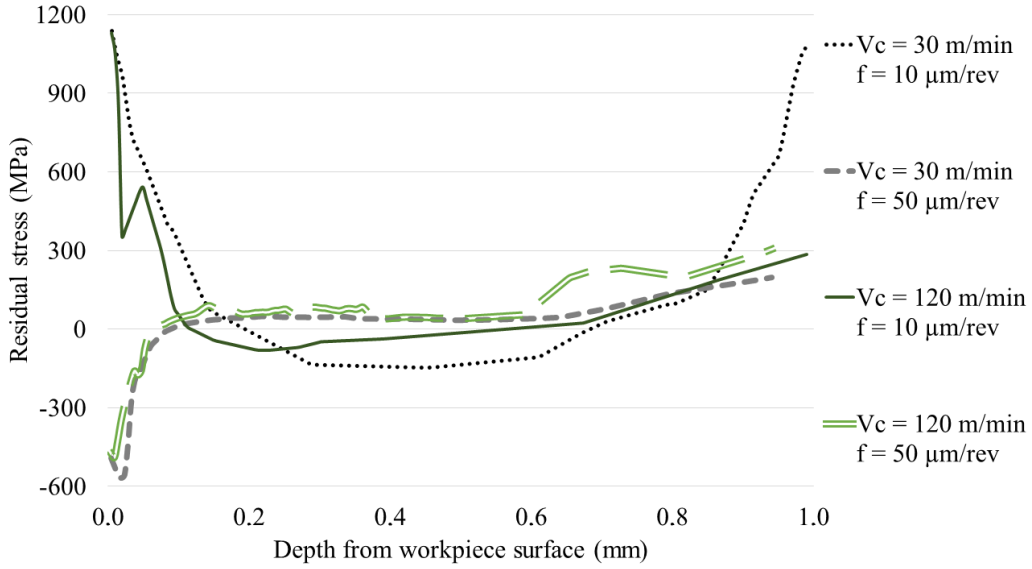

Figure 6.42 – Residual stress in the orthogonal micro-cutting.

6.3.1. Conclusion of the section

When observed the results of the numerical tests of orthogonal micro-cutting in the Ti-6Al-7Nb titanium alloy, the following conclusions can be drawn:

✓ The use of the micro-cutting can represent a great economy of cost due to the lower cutting forces and power, however, the process presented a very low material removal rate. Thus, this process can be beneficial in the finishing operation.

✓ The temperature in the micro-cutting were lower than 960º C, phase transformation of Ti-6Al-7Nb titanium alloy. This temperature evolution can reduce the metallurgic alteration in the machined surface that can prolong the life of the components.

✓ Although the micro-cutting presented the lower values for the cutting forces, power and temperatures, the use of the feed rate of 10 µm/rev caused a tractive residual stress, which can influence in the life of the component.

CHAPTER 7 – THE MICRO-CUTTING IN THE FINISHING OPERATION OF BIOMATERIAL

In this chapter, the cutting forces, vibration and surface roughness in the micro-cutting were analysed to quality of the micro-cutting as finishing operation for different diameter scales. This study was performed to understand the influence of the deflection and compare the relationship between spindle speed and cutting speed in the micro-cutting.

7.1. Cutting forces in the micro-cutting

7.1.1. F_x force

The values of F_x force using the flat inserts for the spindle speed range of 0-1,000, 1,000-2,000, and 2,000-3,000 rpm are shown in the Figure 7.1. The increase of the feed rate and depth of cut caused an increase of the F_x force, on average, for the macro (14.5% and 42.2%), transition (15.3% and 36.9%), and meso-scale (9.6% and 30.4%), respectively. The rise in the spindle speed range reduced the F_x force in the transition (3.7%) and meso (3.9%) scales, on average. For the macro scale, the rise in the spindle speed range caused increase of the F_x force, 8.0%, on average.

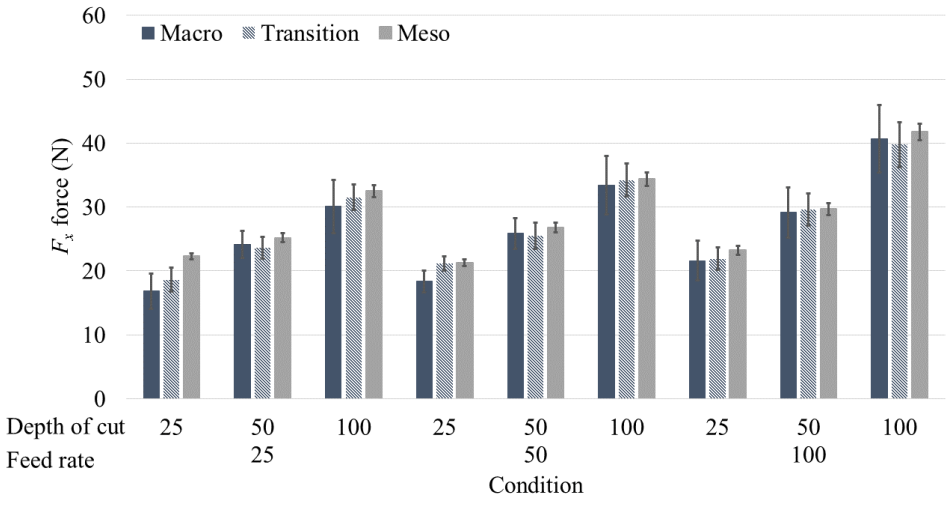

a) Spindle speed range of 0 to 1,000 rpm.

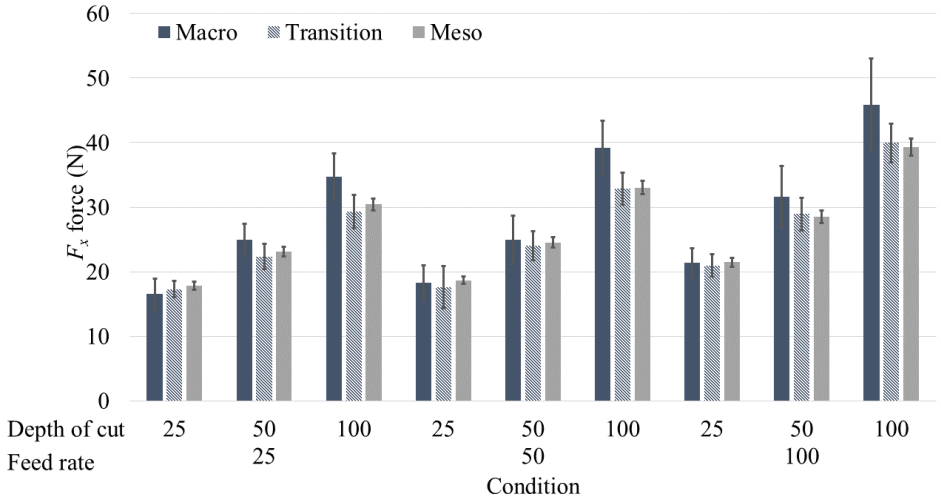

b) Spindle speed range of 1,000 to 2,000 rpm.

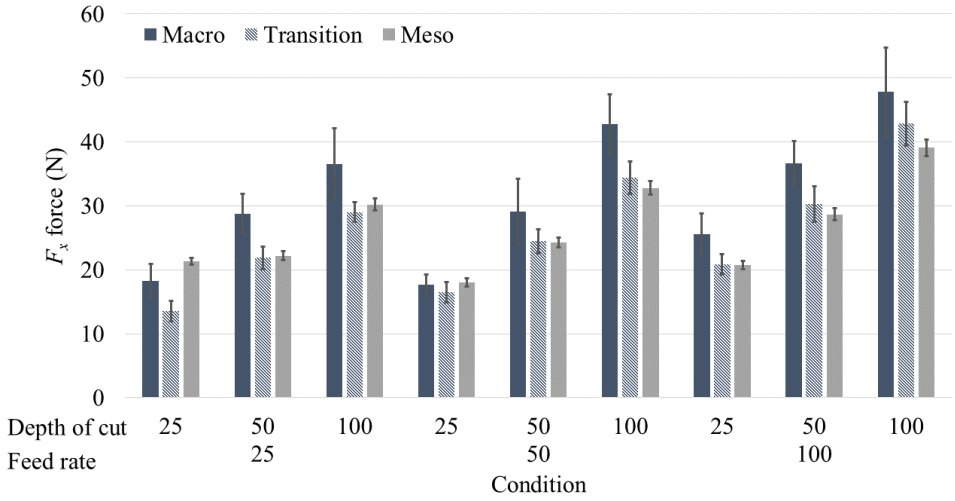

c) Spindle speed range of 2,000 to 3,000 rpm.

Figure 7.1 – F_x force for different the spindle speed range with flat inserts.

For the chip-breaker inserts, the values of F_x force are shown in the Figure 7.2 for the spindle speed range of 0-1,000, 1,000-2,000, and 2,000-3,000 rpm. The increase of the feed rate and the depth of cut increased the F_x force, which was higher for the macro scale (14.6% and 39.4%) than the transition (13.4% and 34.6%) and meso (16.6% and 34.8%), on average, respectively. The rise in the spindle speed range dropped the F_x force transition (4.6%), and meso (1.0%) scales, but, increased in the macro scale, 1.8%, on average.

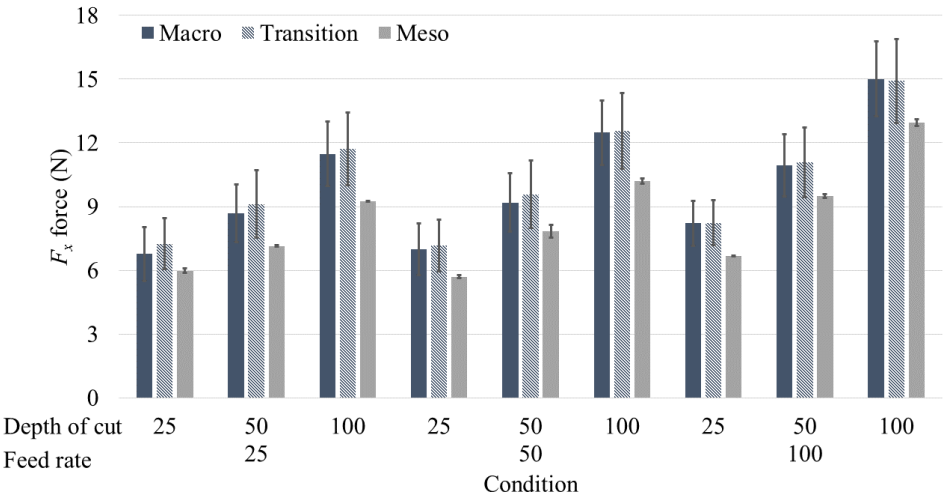

a) Spindle speed range of 0 to 1,000 rpm.

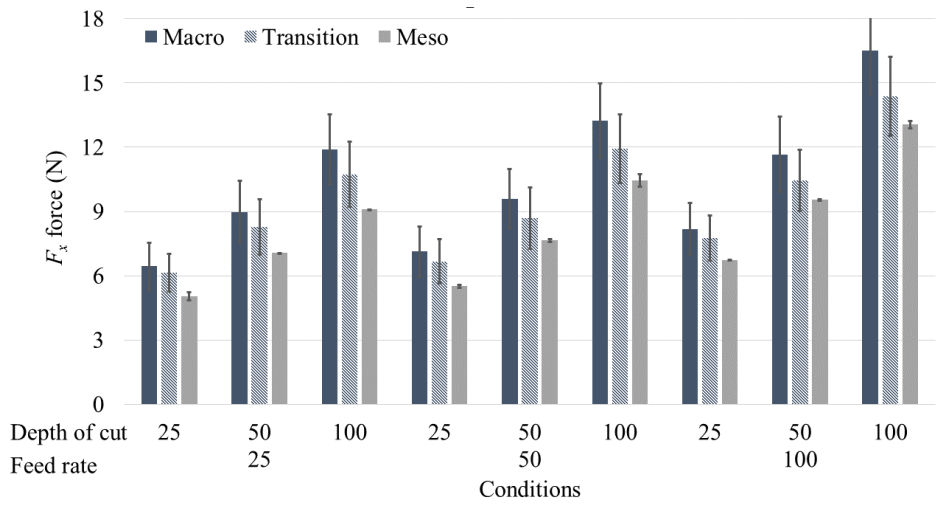

b) Spindle speed range of 1,000 to 2,000 rpm.

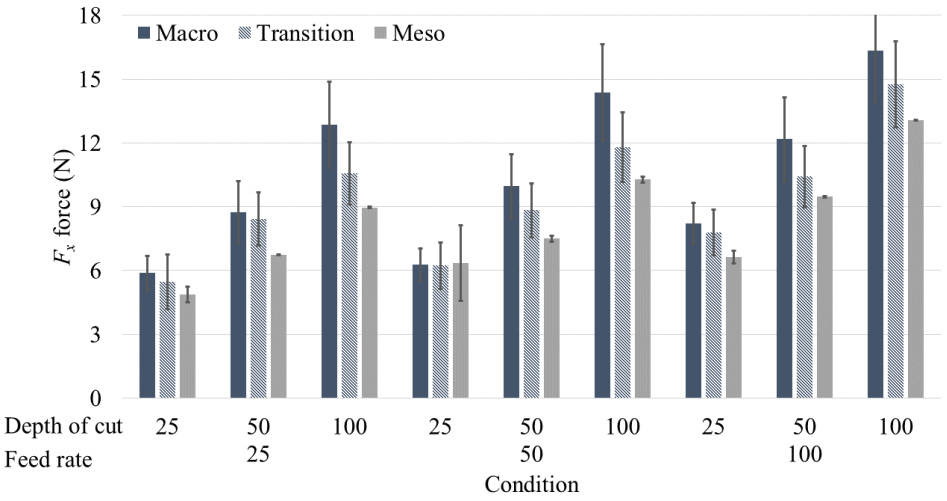

c) Spindle speed range of 2,000 to 3,000 rpm.

Figure 7.2 – F_x force for different the spindle speed range with chip-breaker.

Figure 7.3 shows the F_x force for the spindle speed range of 0-1,000, 1,000-2,000, and 2,000-3,000 rpm using dual negative inserts. The increase of the feed rate and depth of cut increased the F_x force in the macro (18.5% and 38.0%), transition (16.4% and 37.3%), and meso (12.6% and 31.5%) scales, on average, respectively. The rise in the spindle speed range fell the F_x force in the transition (2.5%) and meso (1.9%). For macro scale, generally, the rise of spindle speed range increase of F_x force, 2.6%, on average.

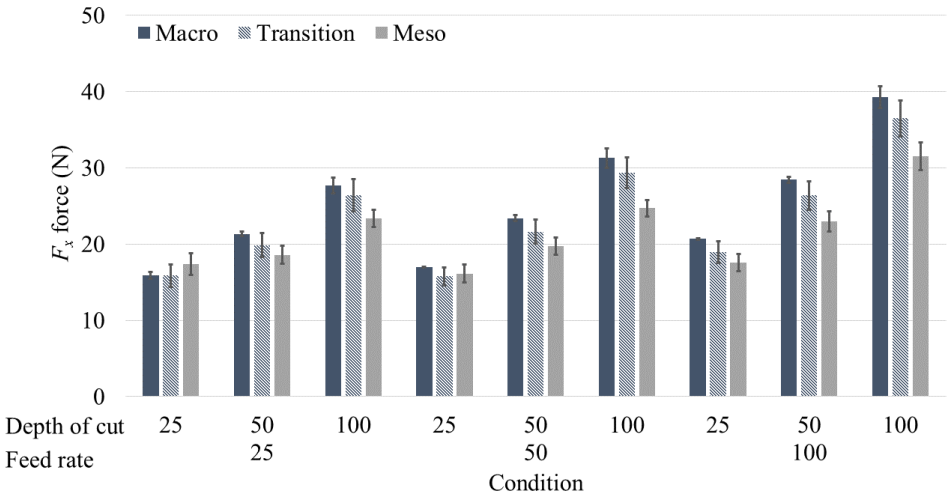

a) Spindle speed range of 0 to 1,000 rpm.

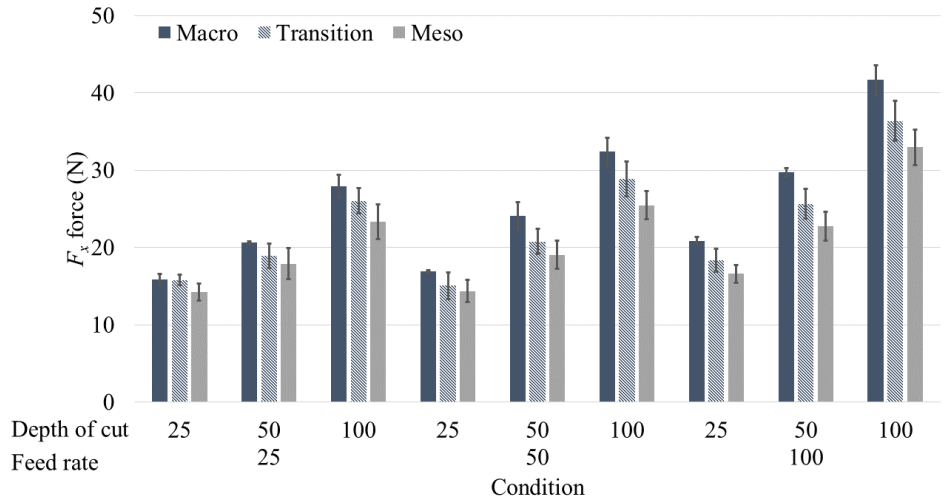

b) Spindle speed range of 1,000 to 2,000 rpm.

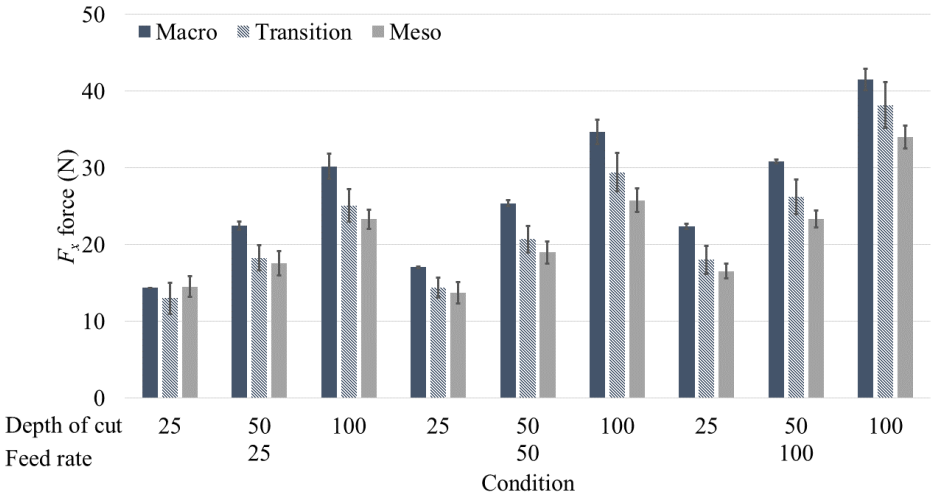

b) Spindle speed range of 2,000 to 3,000 rpm.

Figure 7.3 – F_x force for different the spindle speed range with dual negative inserts.

When compared the change of the diameter scale, the F_x force reduced for the reduction of scale for the chip-breaker (9.9%) and dual negative (8.9%) inserts. For the flat inserts, the F_x force decreased when compared the reduction from macro to transition scale, 7.3% on average, but, the F_x force increased when compared the reduction from transition to meso scale, 4.4% on average. The Table 7.1 is shown the ANOVA of the F_x force for all scales and individual scale. Excepting the spindle speed range when analysed the all scales, transition and meso, all factors were significant for the F_x force in the micro-cutting. The Figure 7.4 shows the multiple comparisons of the "scale", Tukey and Fisher. In both methods, the "scale" were significantly different.

Table 7.1 – ANOVA of the F_x force for different scales.

Source	All scales		Macro		Transition		Meso	
	F-Value	P-Value	F-Value	P-Value	F-Value	P-Value	F-Value	P-Value
Spindle speed range	1.38	0.252	*5.84*	*0.004*	2.35	0.099	1.39	0.255
Feed rate	*100.05*	*0.000*	*30.51*	*0.000*	*58.22*	*0.000*	*32.57*	*0.000*
Depth of cut	*460.70*	*0.000*	*147.74*	*0.000*	*250.09*	*0.000*	*155.07*	*0.000*
Chip-breaker	*1883.95*	*0.000*	*633.87*	*0.000*	*905.17*	*0.000*	*673.07*	*0.000*
Inclination angle	*1172.06*	*0.000*	*305.64*	*0.000*	*624.84*	*0.000*	*563.68*	*0.000*
Scale	*22.62*	*0.000*						
	R^2	R^2_{adj}	R^2	R^2_{adj}	R^2	R^2_{adj}	R^2	R^2_{adj}
	89.58%	89.31%	89.41%	88.74%	91.55%	91.11%	93.29%	92.70%

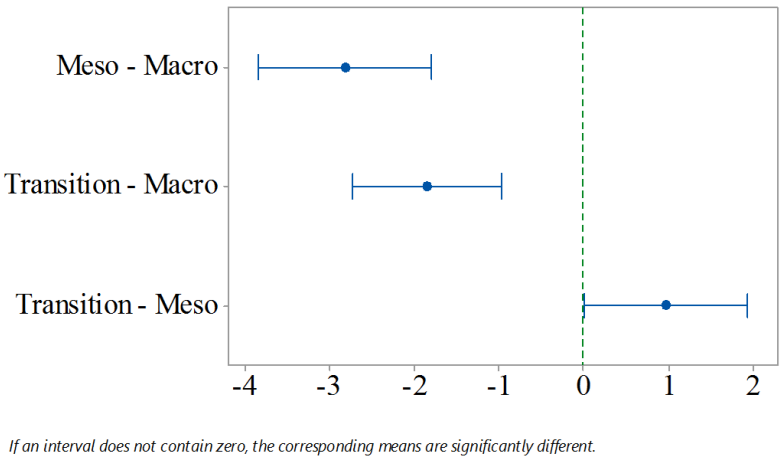

a) Tukey test.

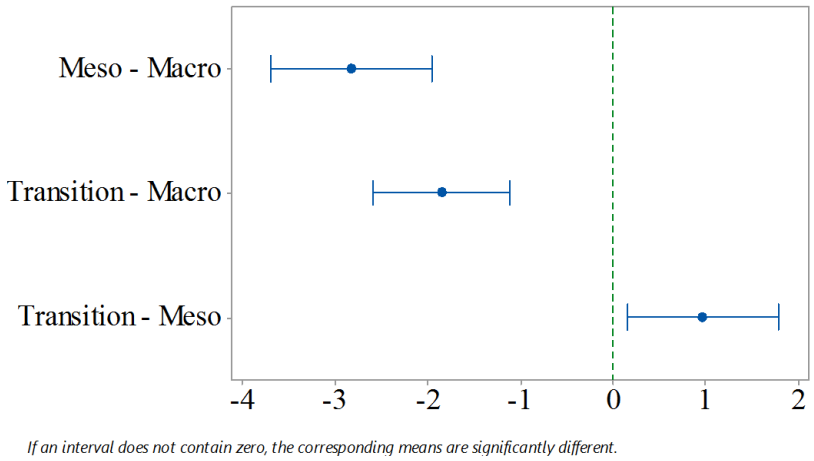

b) Fisher test.

Figure 7.4 – Comparison test of the F_x force for different scales.

The Table 7.2 shows the ANOVA for the same cutting speed and same spindle speed range for different scales. In the comparison of the same cutting speed (30 m/min), all factors were significant. For the same spindle speed range, only in the range of 0 to 1,000 rpm, the factor "scale" was not significant for the F_x force in the micro-cutting.

Table 7.2 – ANOVA of the F_x force for same cutting speed.

Source	v_c 30 m/min		n 0-1,000 rpm		n 1,000-2,000 rpm		n 2,000-3,000 rpm	
	F-Value	P-Value	F-Value	P-Value	F-Value	P-Value	F-Value	P-Value
Feed rate	*36.45*	*0.000*	*32.29*	*0.000*	*34.15*	*0.000*	*38.10*	*0.000*
Depth of cut	*173.68*	*0.000*	*160.61*	*0.000*	*155.55*	*0.000*	*165.89*	*0.000*
Chip-breaker	*715.74*	*0.000*	*814.60*	*0.000*	*518.81*	*0.000*	*638.05*	*0.000*
Inclination angel	*483.18*	*0.000*	*479.13*	*0.000*	*405.73*	*0.000*	*357.68*	*0.000*
Scale	*3.99*	*0.021*	1.41	0.247	*10.99*	*0.000*	*18.36*	*0.000*
	R^2	R^2_{adj}	R^2	R^2_{adj}	R^2	R^2_{adj}	R^2	R^2_{adj}
	90.95%	90.38%	91.05%	90.49%	90.13%	89.46%	90,13%	89.51%

In the Figure 7.5 show the Tukey and Fisher tests for same cutting speed. In these comparison, it was observed that the only macro and meso scales was not differ among themselves. The Tukey and Fisher tests for spindle speed range of 1,000-2,000 rpm are shown in the Figure 7.6, respectively. In the Tukey test, the F_x force in transition and meso scale was not differ among themselves. Figure 7.7 show the Tukey and Fisher tests for spindle speed range of 2,000-3,000 rpm. In both tests, the F_x force in transition and meso scales were not significantly different.

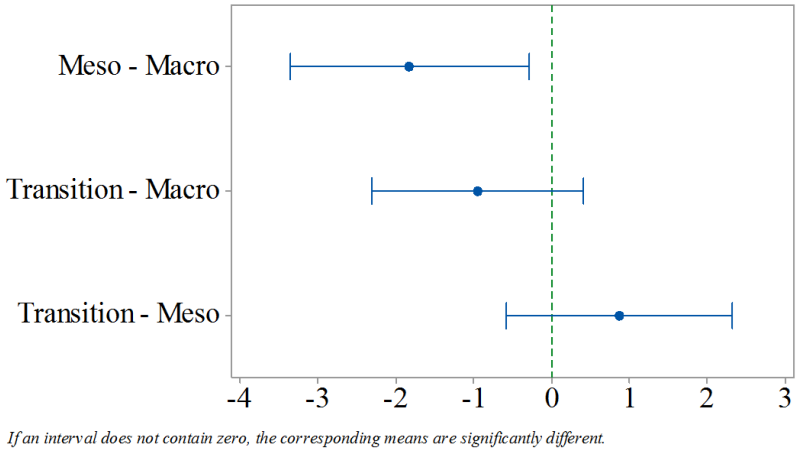

a) Tukey test.

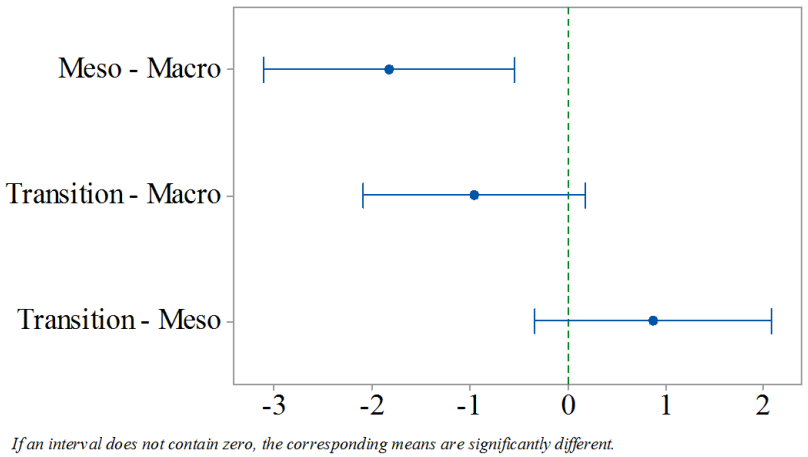

b) Fisher test.

Figure 7.5 – Comparison tests of the F_x force for same cutting speed in different diameter scales.

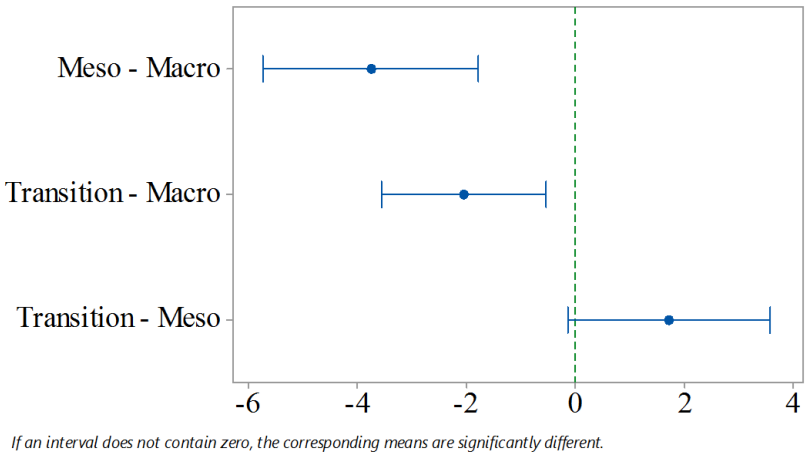

a) Tukey test.

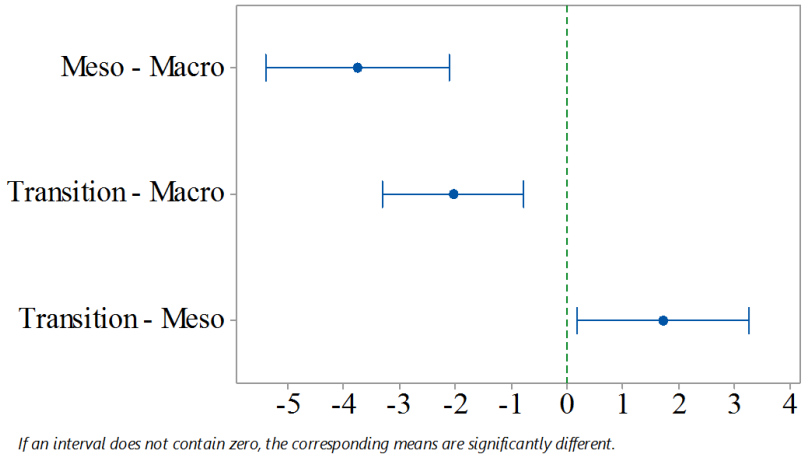

b) Fisher test.

Figure 7.6 – Comparison tests of the F_x force for spindle speed range of 1,000 to 2,000 rpm.

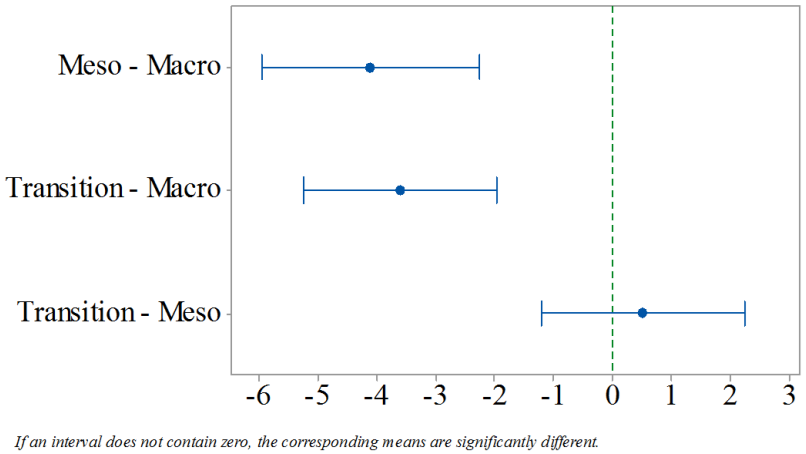

a) Tukey test.

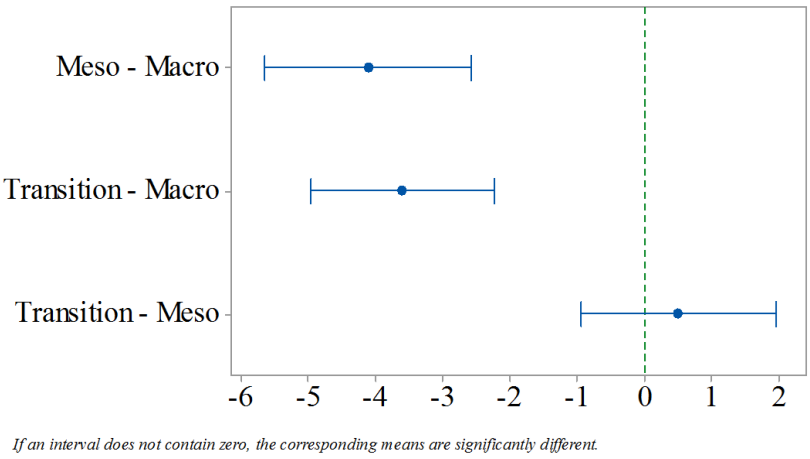

b) Fisher test.

Figure 7.7 – Comparison tests of the F_x force for spindle speed range of 2,000 to 3,000.

7.1.2. F_y force

The values of F_y force using flat inserts are shown in the Figure 7.8 for the spindle speed range of 0-1,000, 1,000-2,000, and 2,000-3,000 rpm. The increase of the feed rate increased of the F_y force in 1.7% for the macro and 5.4% for the transition scales, on average, however, for the meso scale, was observed a reduction of 8.4%, on average. The increase of the depth of cut increased the F_y force in 120.5%, on average, for all scales. The rise of the spindle speed range, generally, grown the F_y force in 6.0% for the macro, and reduced in 3.8% for the transition and 1.0% for meso scales, on average.

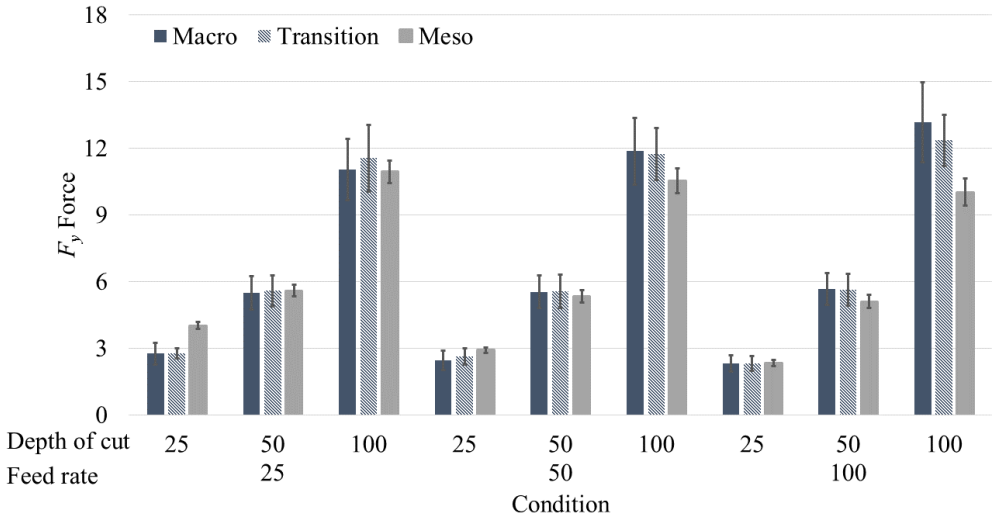

a) Spindle speed range of 0 to 1,000 rpm.

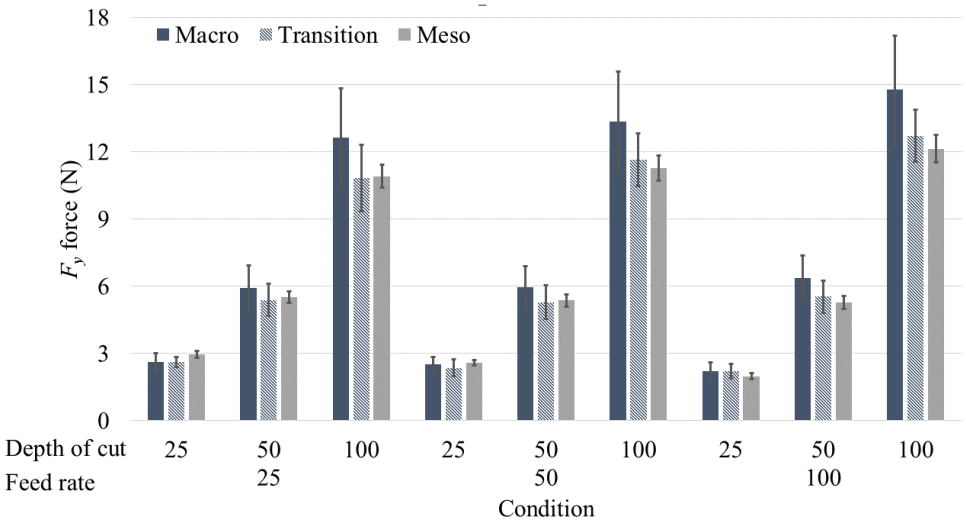

b) Spindle speed range of 1,000 to 2,000 rpm.

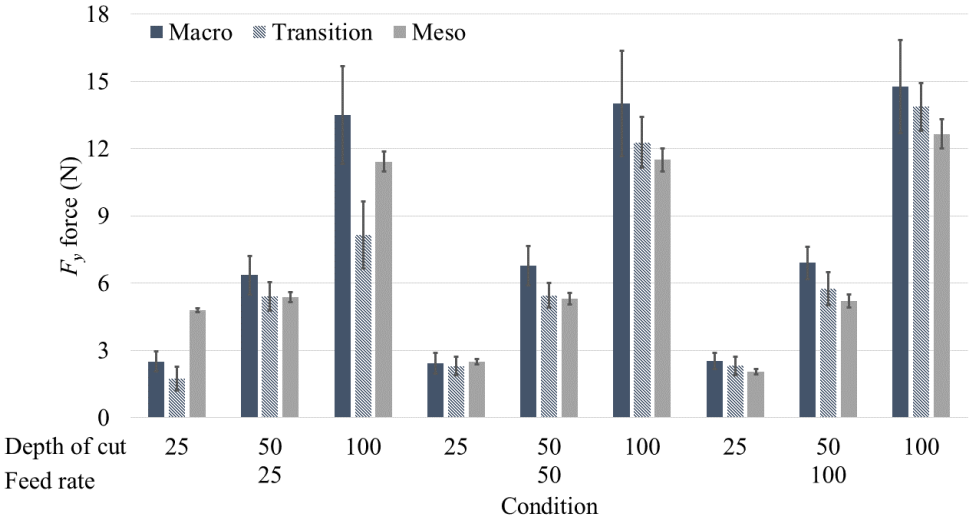

c) Spindle speed range of 2,000 to 3,000 rpm.

Figure 7.8 – F_y force for different the spindle speed range with flat inserts.

The Figure 7.9 shows for the spindle speed range of 0-1,000, 1,000-2,000, and 2,000-3,000 rpm, the evolution of the F_y force employing the chip-breaker inserts. The increase of the feed rate increased the F_y force in 6.3% for the macro, 7.6% for the transition, and 6.8% for the meso scale, on average. For the increase of the depth of cut, an increase was observed for scales, 120.7%, on average. The rise of the spindle speed range caused increase for macro scale (3.2%) and a reduction for transition (3.7%) and meso (5.9%), on average.

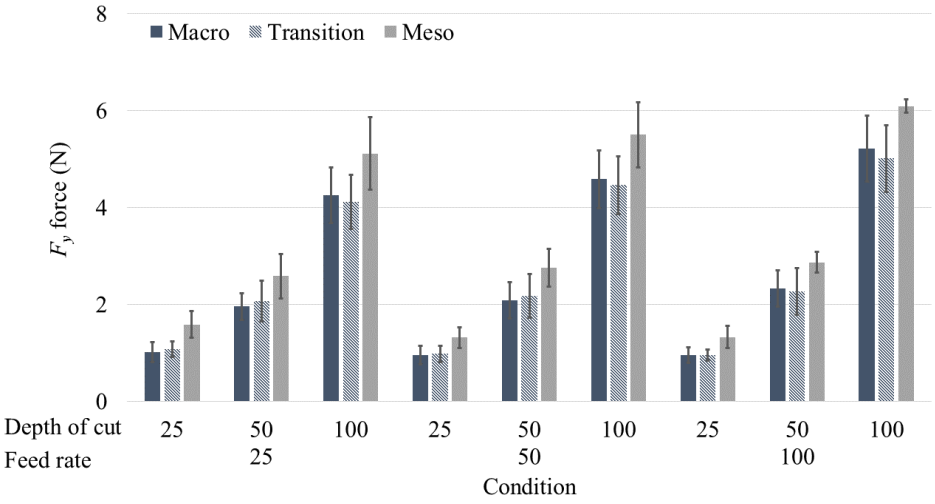

a) Spindle speed range of 0 to 1,000 rpm.

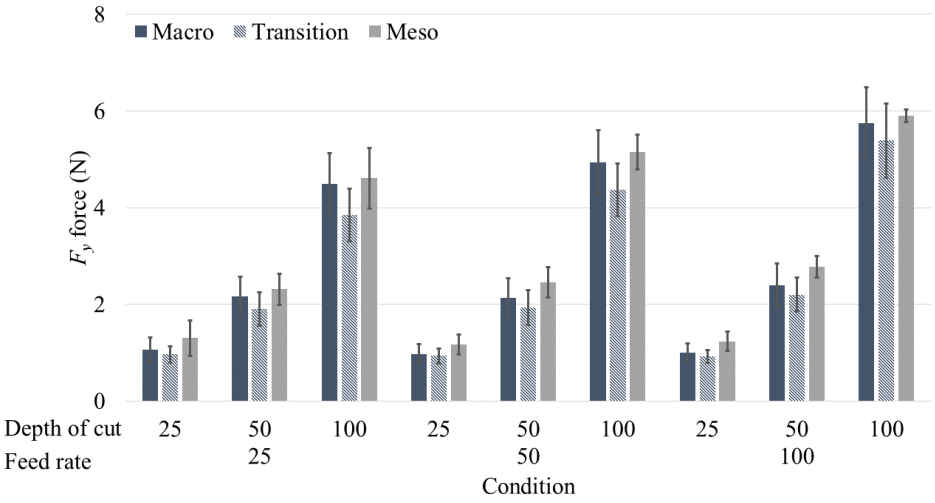

b) Spindle speed range of 1,000 to 2,000 rpm.

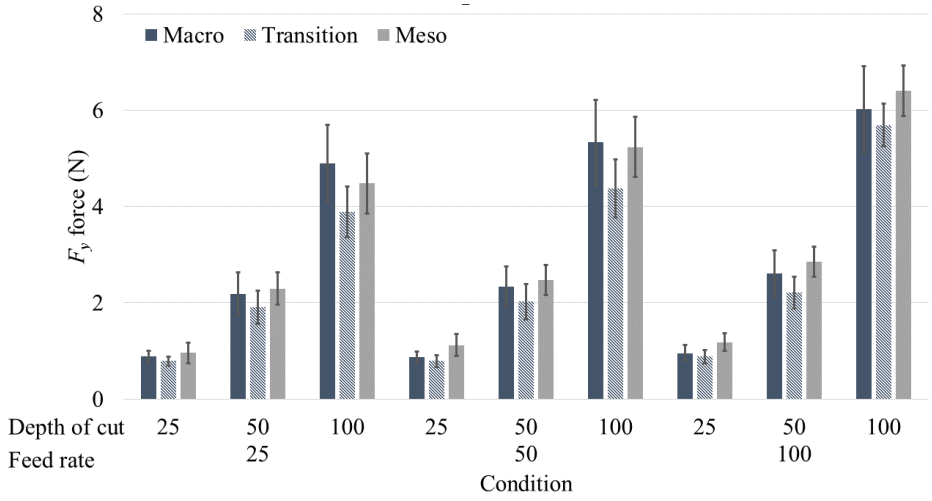

c) Spindle speed range of 2,000 to 3,000 rpm.

Figure 7.9 – F_y force for different the spindle speed range with chip-breaker inserts.

The values of F_y force for the dual negative are shown in the Figure 7.10, for the spindle speed range of 0-1,000, 1,000-2,000, and 2,000-3,000 rpm. The increase of the feed rate and the depth of cut caused increase in the F_y force in macro (7.0% and 121.3%), transition (7.4% and 116.4%) and meso (2.7% and 101.4%) scales, respectively, on average. The rise of the spindle speed range fell the F_y force in the macro (1.2%), transition (3.2%), and meso (2.4%) scales, on average.

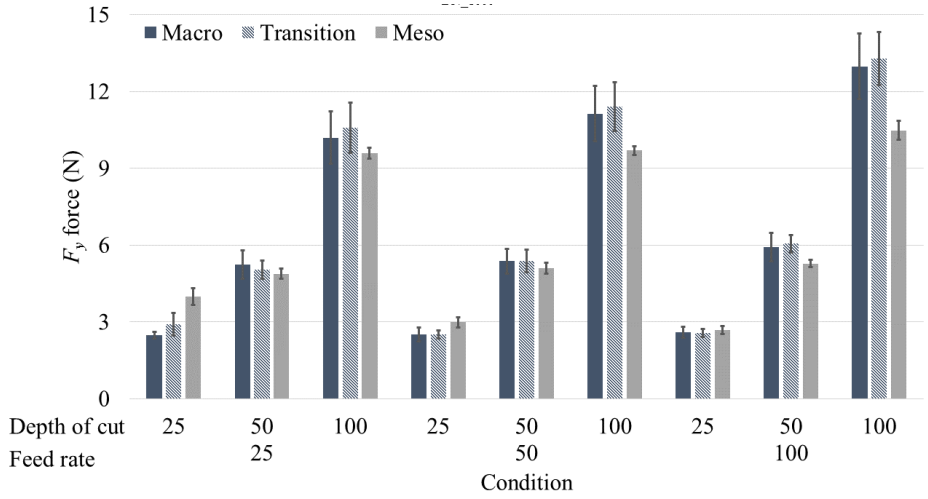

a) Spindle speed range of 0 to 1,000 rpm.

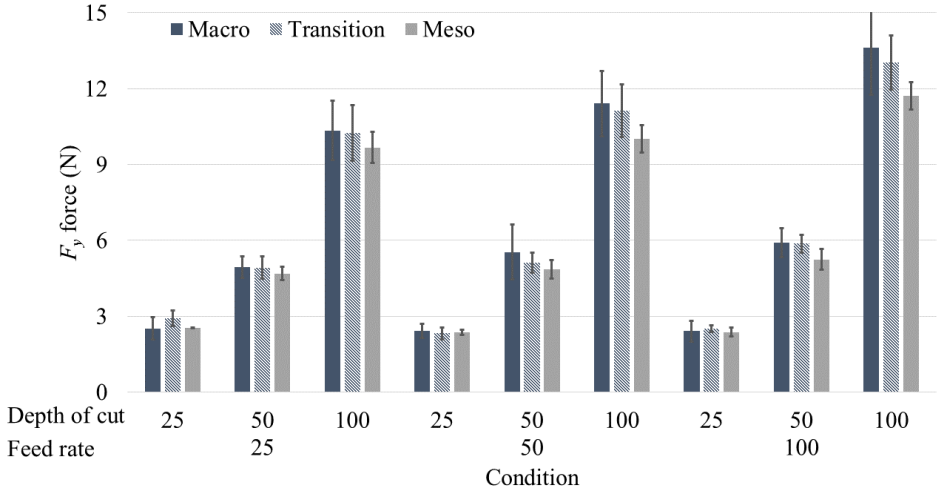

b) Spindle speed range of 1,000 to 2,000 rpm.

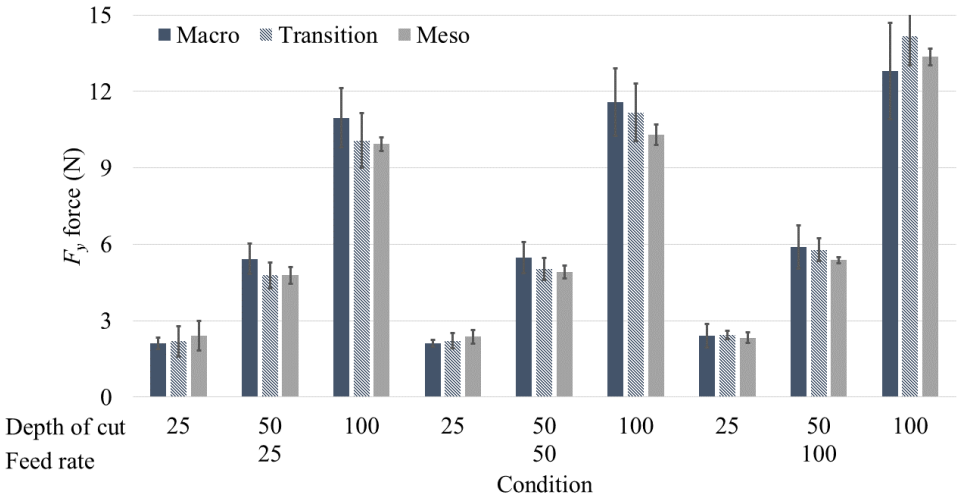

c) Spindle speed range of 2,000 to 3,000 rpm.

Figure 7.10 – F_y force for different the spindle speed range with dual negative insert.

When compared the reduction of the scale, the dual negative inserts presented a decrease of the F_y force, 1.3%, on average. For the flat and chip-breaker inserts, a reduction was observed for the reduction from macro to transition, 8.4% and 6.9%, and an increase for the reduction from transition to meso, 7.4% and 25.8%, on average, respectively. Table 7.3 shows ANOVA of the F_y force for all scales and individual scales. The factor "scale" was not significant for the F_y force. Furthermore, the "spindle speed" was not significant for all or individual scales, and feed rate was not significant for the macro and meso scales.

Table 7.3 – ANOVA of F_y force for all and individual scales.

Source	All scales		Macro		Transition		Meso	
	F-Value	P-Value	F-Value	P-Value	F-Value	P-Value	F-Value	P-Value
Spindle speed range	0.35	0.708	1.71	0.186	0.25	0.777	0.20	0.821
Feed rate	*9.24*	*0.000*	2.16	0.120	*6.39*	*0.002*	1.90	0.155
Depth of cut	*1013.26*	*0.000*	*289.99*	*0.000*	*429.00*	*0.000*	*404.54*	*0.000*
Chip-breaker	*559.33*	*0.000*	*216.40*	*0.000*	*222.53*	*0.000*	*121.29*	*0.000*
Inclination angle	*507.45*	*0.000*	*106.32*	*0.000*	*247.25*	*0.000*	*225.27*	*0.000*
Scale	2.58	0.077						
	R^2	R^2_{adj}	R^2	R^2_{adj}	R^2	R^2_{adj}	R^2	R^2_{adj}
	87.23%	86.92%	86.77%	85.93%	88.68%	88.08%	90.23%	89.56%

The ANOVA for same cutting speed and spindle speed are shown in the Table 7.4. The factor "scale" was not significant for the cutting speed and the spindle speed range. Besides, in the spindle speed range of 0 to 1,000 rpm, the feed rate was not significant.

Table 7.4 – ANOVA of the F_y force for same cutting speed and spindle speed.

Source	v_c 30 m/min		n 0-1,000 rpm		n 1,000-2,000 rpm		n 2,000-3,000 rpm	
	F-Value	P-Value	F-Value	P-Value	F-Value	P-Value	F-Value	P-Value
Feed rate	*3.65*	*0.029*	1.31	0.274	*3.20*	*0.044*	*5.11*	*0.007*
Depth of cut	*381.23*	*0.000*	*374.56*	*0.000*	*310.54*	*0.000*	*333.15*	*0.000*
Chip-breaker	*206.93*	*0.000*	*217.31*	*0.000*	*157.73*	*0.000*	*185.19*	*0.000*
Inclination angel	*201.20*	*0.000*	*207.36*	*0.000*	*159.99*	*0.000*	*147.72*	*0.000*
Scale	0.22	0.806	0.03	0.972	1.10	0.335	2.85	0.061
	R^2	R^2_{adj}	R^2	R^2_{adj}	R^2	R^2_{adj}	R^2	R^2_{adj}
	88.63%	87.95%	88.73%	88.05%	87.28%	86.48%	87.10%	86.33%

7.1.3. F_z force

The values of F_z force for the spindle speed range of 0-1,000, 1,000-2,000, and 2,000-3,000 rpm are shown in Figure 7.11, for the flat inserts. The increase of the feed rate and the depth of cut went up the F_z force, on average, 30.6% and 55.0% for the macro, 29.5% and 53.4% for the transition, and 49.1% and 79.9% for meso scales, respectively. The rise of the spindle speed range caused a reduction in macro (2.5%), transition (9.7%), and meso (11.3%) scales.

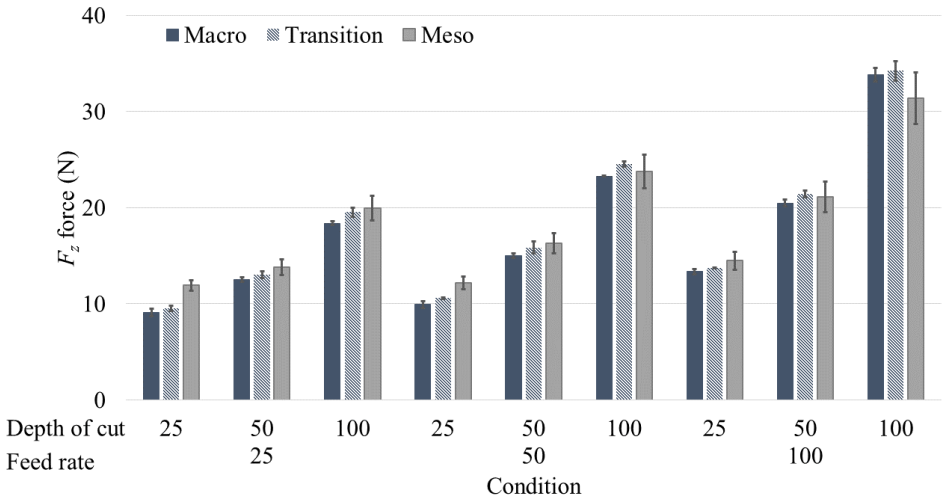

a) Spindle speed range of 0 to 1,000 rpm.

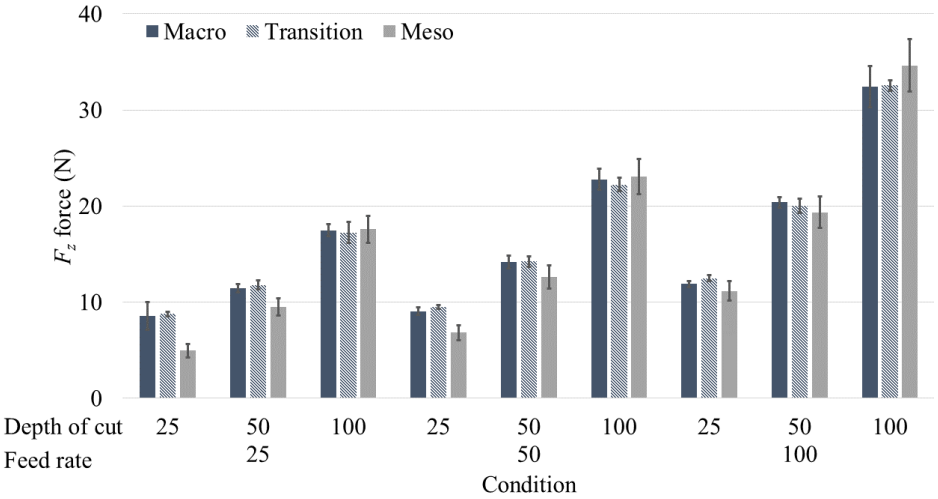

b) Spindle speed range of 1,000 to 2,000 rpm.

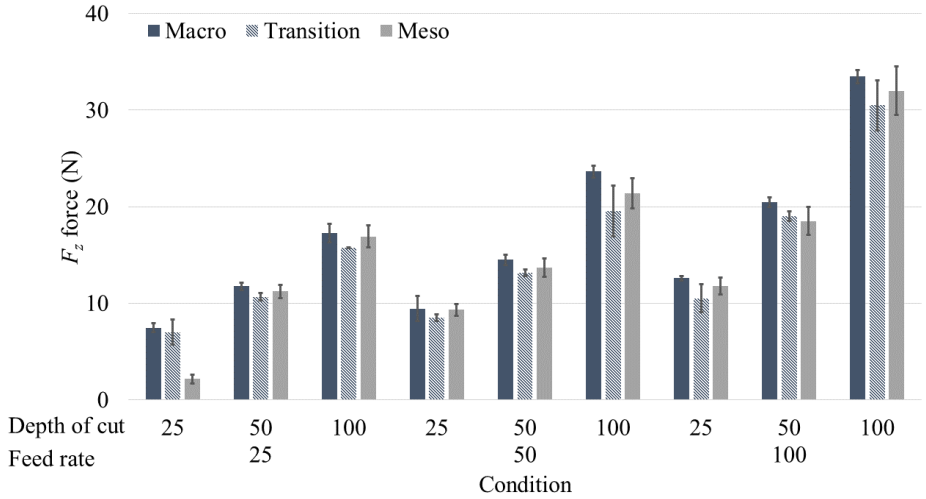

c) Spindle speed range of 2,000 to 3,000 rpm.

Figure 7.11 – F_z force for different the spindle speed range with the flat inserts.

Figure 7.12 shows the F_z force, for the spindle speed range of 0-1,000, 1,000-2,000, and 2,000-3,000 rpm with chip-breaker inserts. The increase of the feed rate caused a similar increase of the F_z force in the macro, (43.6%), transition scale (42.8%), meso (38.6%) scales, on average. A similar evolution was observed for the depth of cut, the increase of 65.2% for macro, 62.5% for transition, and 59.0% for meso scales, for the increase of the depth of cut. The rise of the spindle speed range dropped the F_z force in macro (4.9%), transition (7.6%), and meso (9.2%).

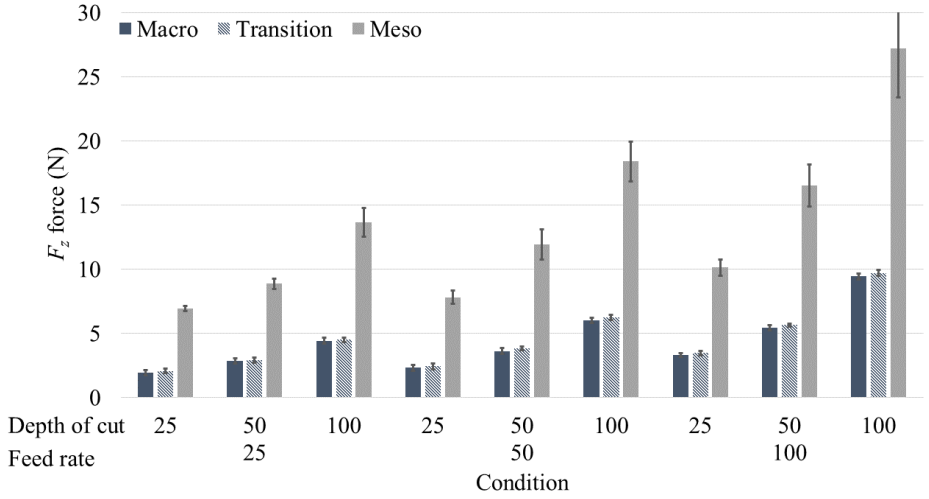

a) Spindle speed range of 0 to 1,000 rpm.

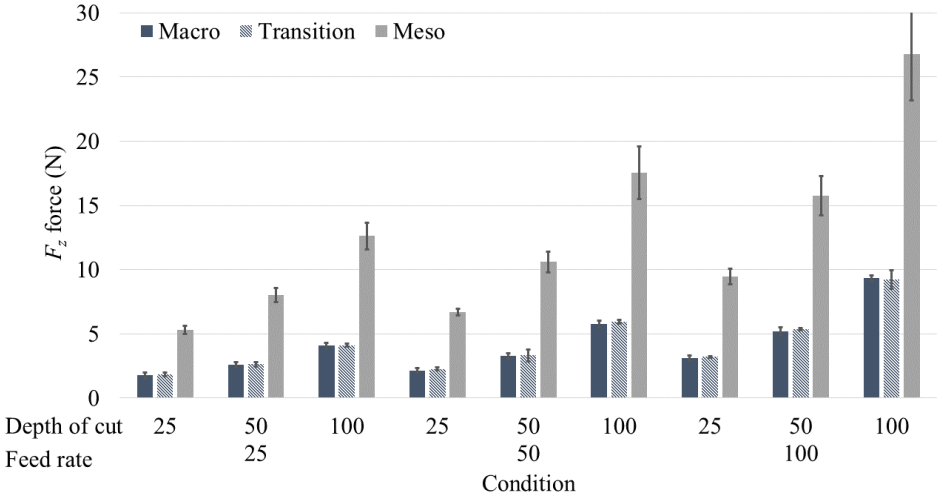

b) Spindle speed range of 1,000 to 2,000 rpm.

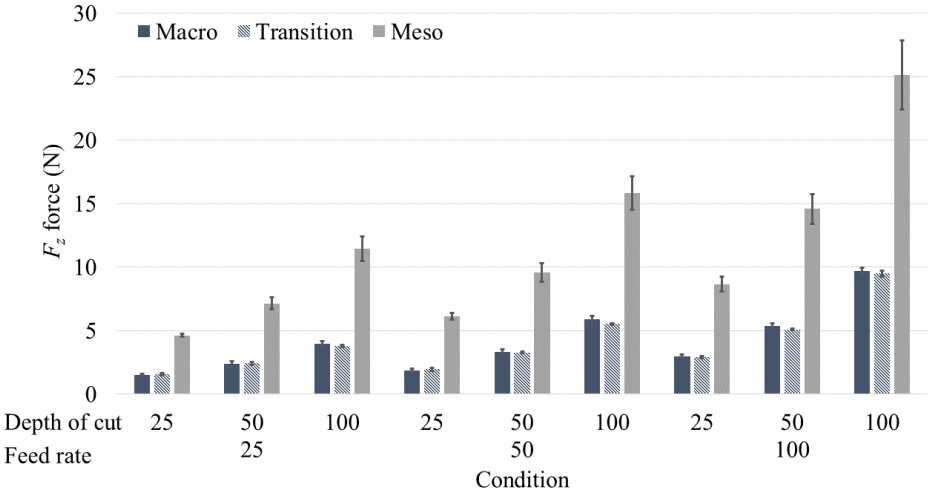

c) Spindle speed range of 2,000 to 3,000 rpm.

Figure 7.12 – F_z force for different the spindle speed range with chip-breaker inserts.

The values of F_z force for the use of the dual negative inserts for the spindle speed range of 0-1,000, 1,000-2,000, and 2,000-3,000 rpm are shown, in the Figure 7.13. The increase of the feed rate and depth of cut went up the F_z force in macro (34.4% and 56.9%), transition (30.5% and 54.3%), and meso (25.2% and 50.4%) scales. The rise of the spindle speed range decreased, on average, the F_z force in the macro (5.4%), transition (11.1%), and meso (11.8%) scales.

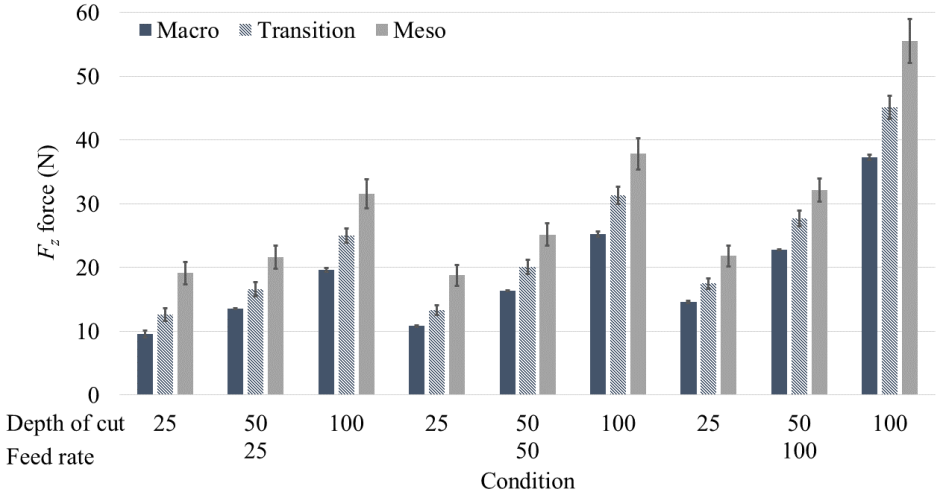

a) Spindle speed range of 0 to 1,000 rpm.

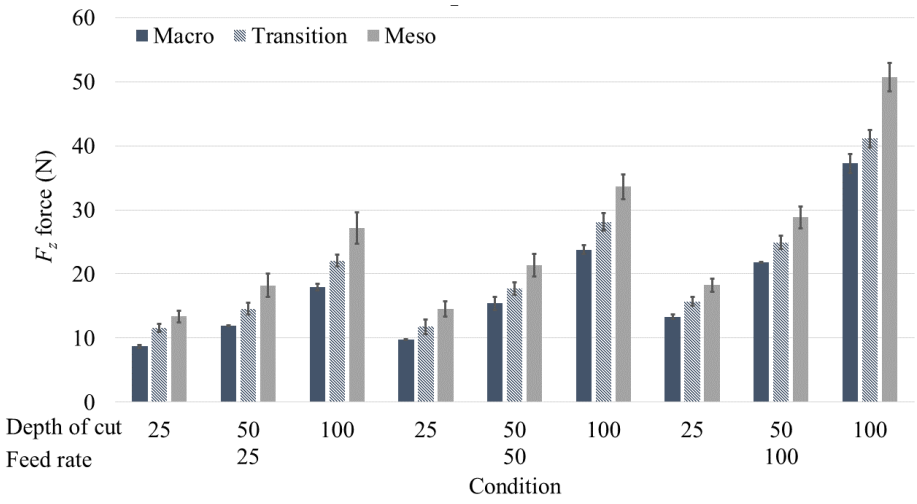

b) Spindle speed range of 1,000 to 2,000 rpm.

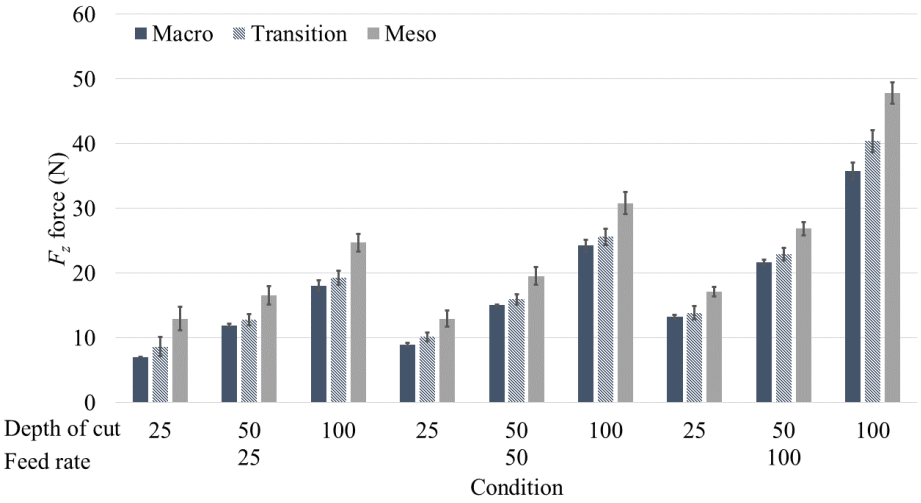

c) Spindle speed range of 2,000 to 3,000 rpm.

Figure 7.13 – Fz force for the dual negative inserts at spindle speed range of 2,000 to 3,000 rpm.

In the comparison among scales, generally, it was observed increase on the F_z force for flat inserts, 2.3% on average. For the chip-breaker and dual negative inserts, the reduction of the scale increased the F_z force in 62.3%. The ANOVA for the F_z force is shown in the Table 7.5. The all factors were significant for the F_z force in the micro-cutting. Only in the macro scale, the feed rate was not significant. The Tukey and Fisher tests are shown in the Figure 7.14. The comparison between macro and transition scales did not presented difference.

Table 7.5 – ANOVA of the F_z force for all and individual scales.

Source	All scales		Macro		Transition		Meso	
	F-Value	P-Value	F-Value	P-Value	F-Value	P-Value	F-Value	P-Value
Spindle speed range	*10.76*	*0.000*	0.38	0.682	*5.48*	*0.005*	*12.38*	*0.000*
Feed rate	*133.73*	*0.000*	*45.32*	*0.000*	*47.53*	*0.000*	*77.13*	*0.000*
Depth of cut	*299.71*	*0.000*	*87.93*	*0.000*	*107.57*	*0.000*	*183.08*	*0.000*
Chip-breaker	*331.08*	*0.000*	*302.58*	*0.000*	*181.42*	*0.000*	*13.29*	*0.000*
Inclination angle	*946.09*	*0.000*	*312.73*	*0.000*	*506.48*	*0.000*	*337.31*	*0.000*
Scale	*83.07*	*0.000*						
	R^2	R^2_{adj}	R^2	R^2_{adj}	R^2	R^2_{adj}	R^2	R^2_{adj}
	85.18%	84.78%	87.48%	86.53%	86.93%	86.11%	88.47%	87.68%

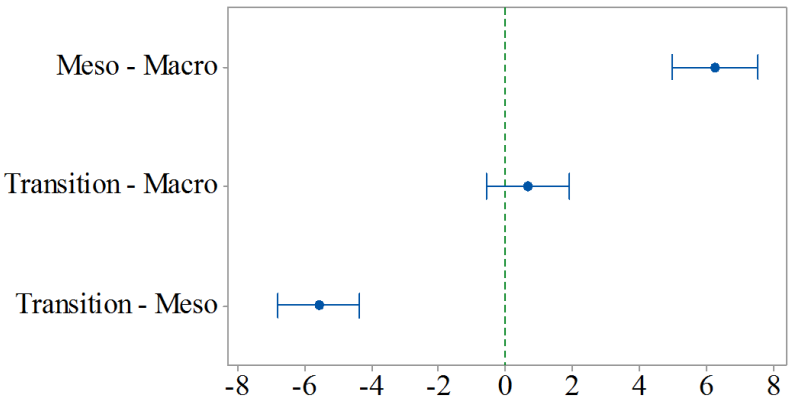

a) Tukey test.

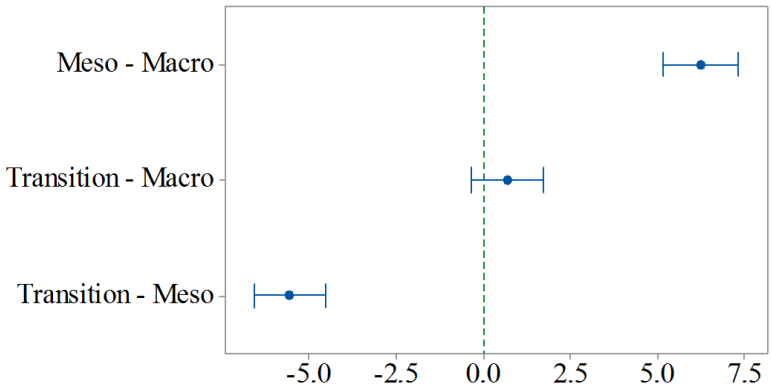

b) Fisher test.

Figure 7.14 – Comparison tests of the F_z force for different scales.

The Table 7.6 shows the ANOVA for cutting speed of 30 m/min in all scales and the same spindle speed range. For all factor were significant for the F_z force in the micro-cutting with same cutting speed or same spindle speed range. The Tukey and Fisher tests are shown in the Figure 7.15, Figure 7.16, Figure 7.17, and Figure 7.18 for the cutting speed of 30 m/min, spindle speed range of 0-1,000, 1,000-2,000, and 2,000-3,000 rpm, respectively. In all tests, for the comparison between macro and transition scale were not observed significance difference.

Table 7.6 – ANOVA of the F_z force for same cutting speed and spindle speed.

Source	v_c 30 m/min		n 0-1,000 rpm		n 1,000-2,000 rpm		n 2,000-3,000 rpm	
	F-Value	P-Value	F-Value	P-Value	F-Value	P-Value	F-Value	P-Value
Feed rate	*44.64*	*0.000*	*39.21*	*0.000*	*42.91*	*0.000*	*54.14*	*0.000*
Depth of cut	*97.36*	*0.000*	*95.33*	*0.000*	*95.52*	*0.000*	*112.21*	*0.000*
Chip-breaker	*98.24*	*0.000*	*104.98*	*0.000*	*111.72*	*0.000*	*114.72*	*0.000*
Inclination angel	*305.79*	*0.000*	*363.27*	*0.000*	*316.38*	*0.000*	*276.32*	*0.000*
Scale	*11.80*	*0.000*	*36.18*	*0.000*	*32.73*	*0.000*	*19.18*	*0.000*
	R^2	R^2_{adj}	R^2	R^2_{adj}	R^2	R^2_{adj}	R^2	R^2_{adj}
	84.47%	83.40%	86.43%	85.51%	86.59%	85.60%	84.38%	83.36%

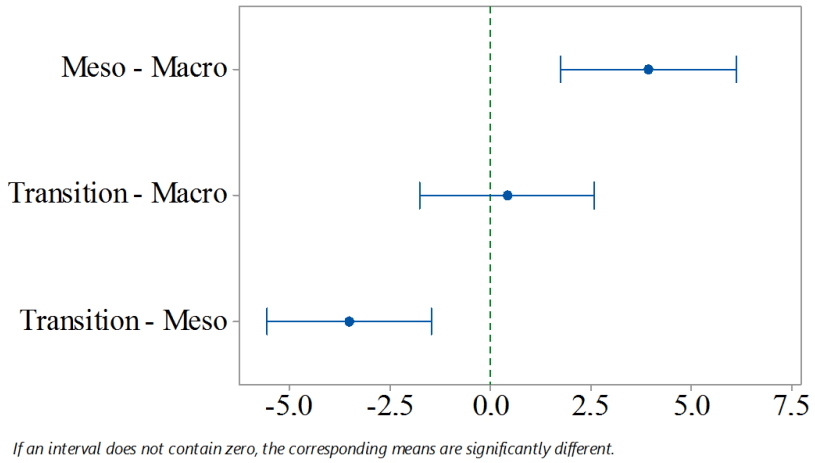

a) Tukey test.

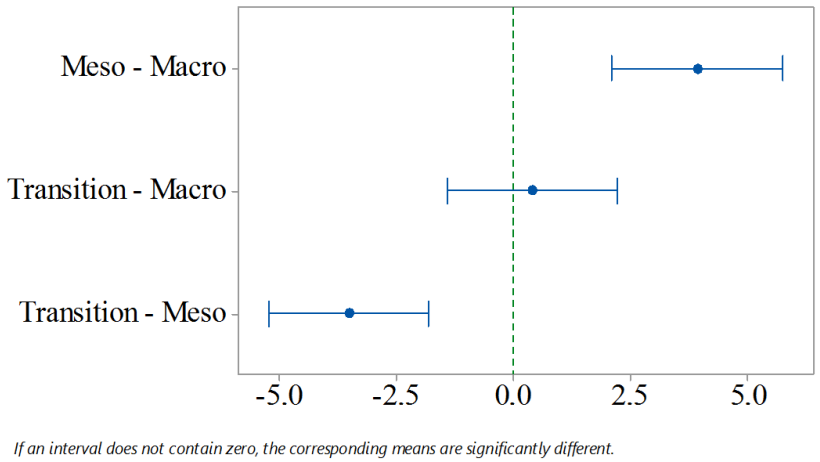

b) Fisher test.

Figure 7.15 – Comparison tests of the F_z force for same cutting speed in different diameter scale.

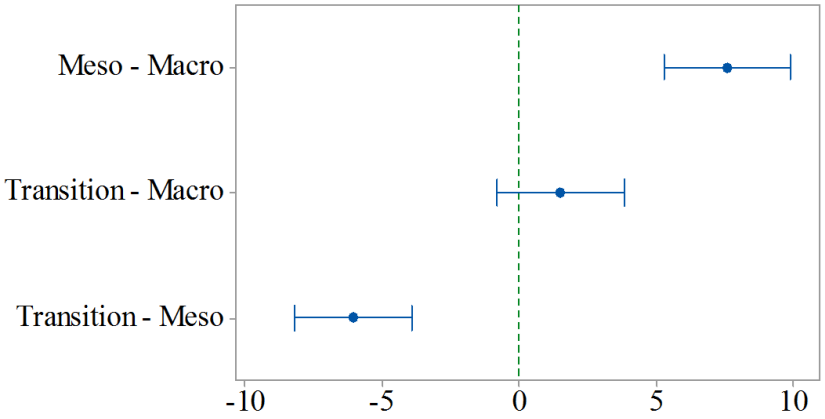

a) Tukey test.

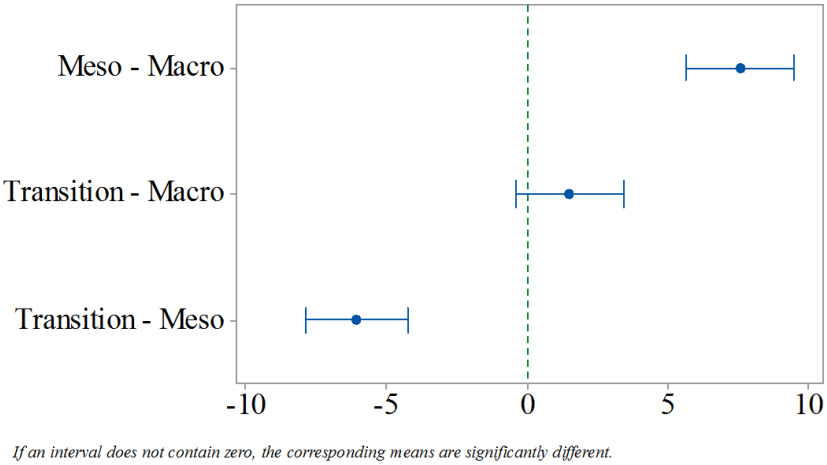

b) Fisher test.

Figure 7.16 – Comparison tests of the F_z force for spindle speed range of 0 to 1,000 rpm.

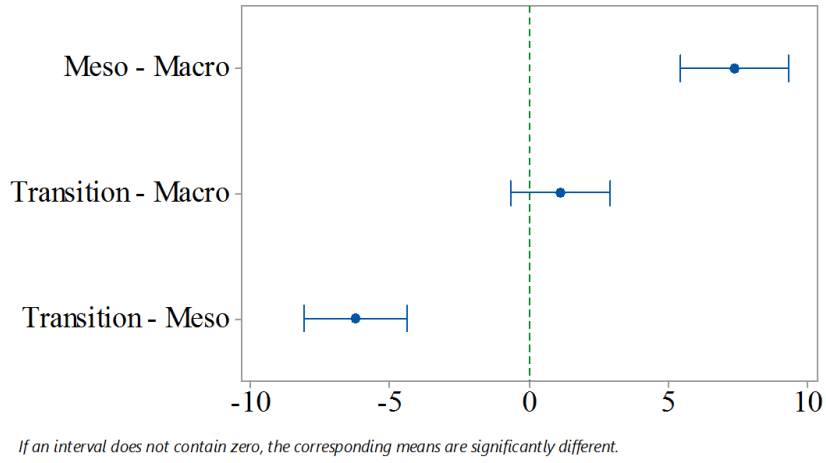

a) Tukey test.

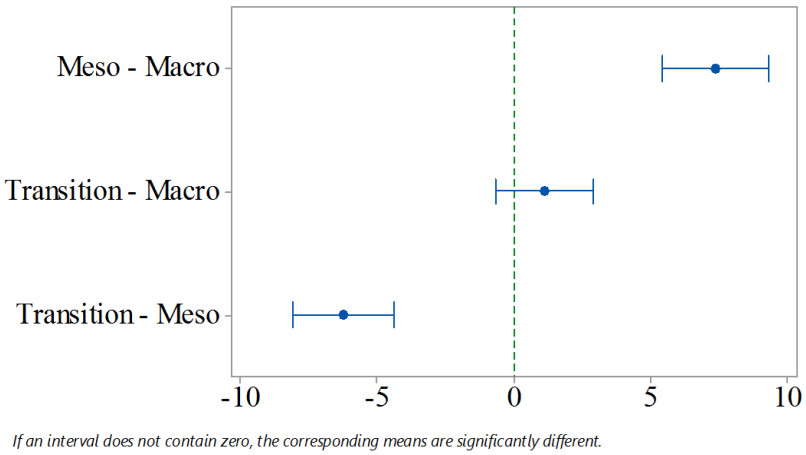

b) Fisher test.

Figure 7.17 – Comparison tests of the F_z force for spindle speed range of 1,000 to 2,000 rpm.

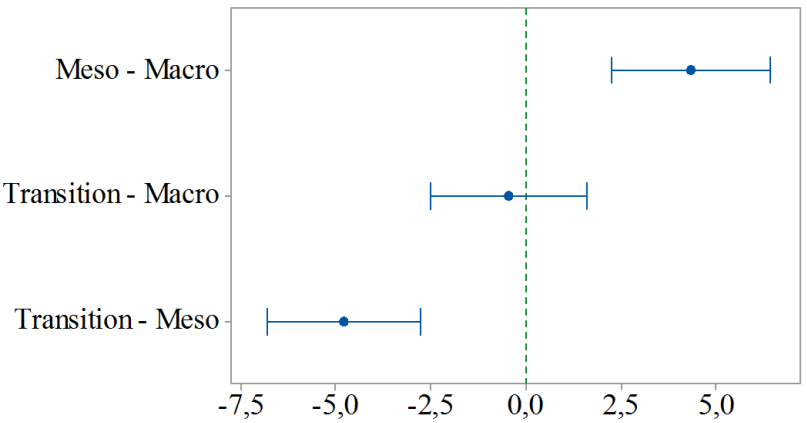

a) Tukey test.

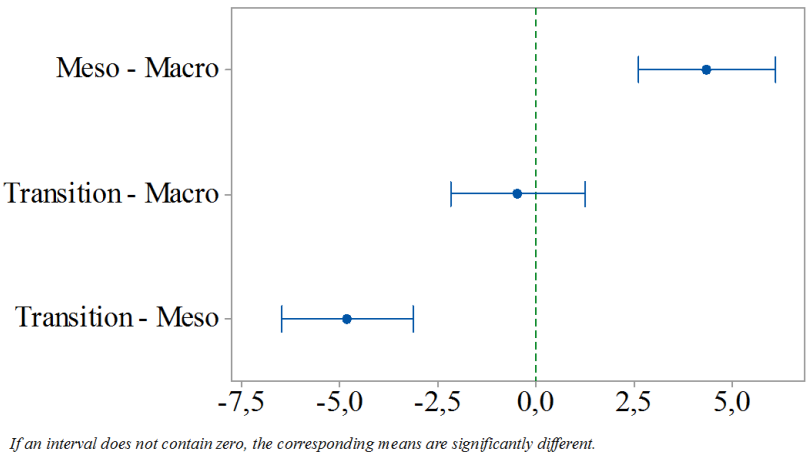

b) Fisher test.

Figure 7.18 – Comparison tests of the F_z force for spindle speed range of 2,000 to 3,000 rpm.

7.2. Surface roughness in the micro-cutting

7.2.1. R_a surface roughness

The Figure 7.19 shows the R_a surface roughness for flat inserts with spindle speed range of 0-1,000, 1,000-2,000, and 2,000-3,000 rpm. The increase of the depth of cut caused an increase, on average, for macro (0.9%), transitions (1.5%), and meso (3.4%) scales. The increase of the feed rate provided a rise sharply the R_a surface roughness more in the meso scale, 107.1%, than the transition, 103.4%, and macro, 101.4%, scales. The rise of the spindle speed range caused increase of the R_a surface roughness in all scales, macro, 0.9%, transition, 1.5%, and meso, 3.5%, on average.

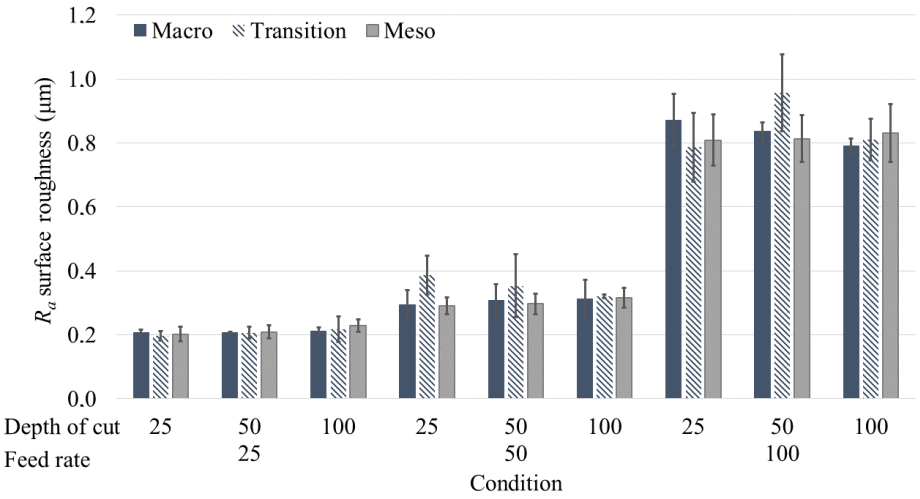

a) Spindle speed range of 0 to 1,000 rpm.

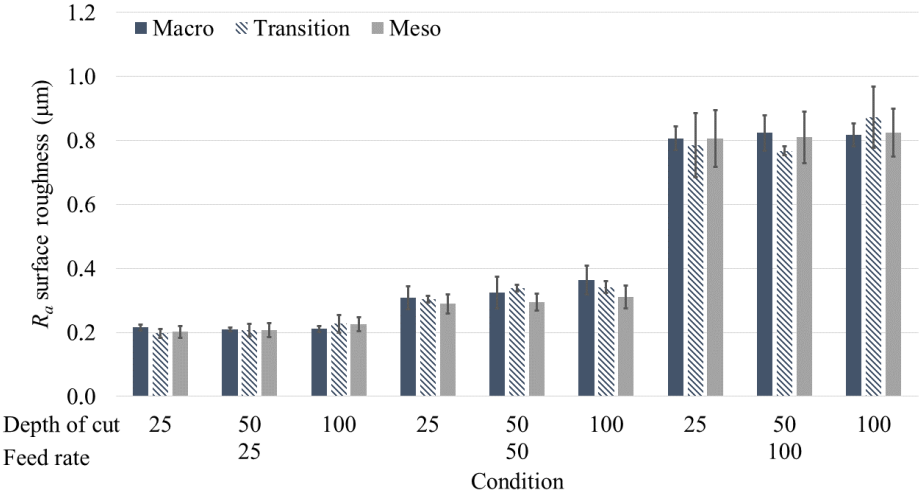

b) Spindle speed range of 1,000 to 2,000 rpm.

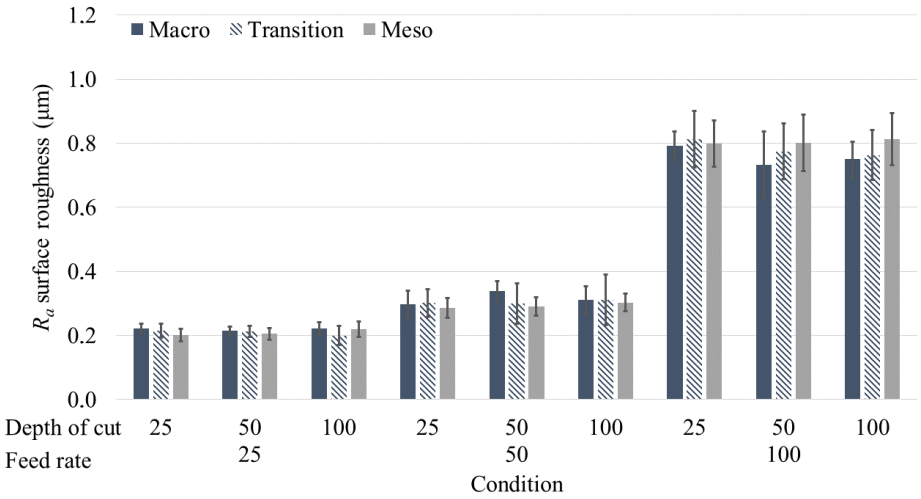

c) Spindle speed range of 2,000 to 3,000 rpm.

Figure 7.19 – R_a surface roughness for the flat inserts.

The R_a surface roughness for the chip-breaker insert in spindle speed range of 0-1,000, 1,000-2,000, and 2,000-3,000 rpm are presented in the Figure 7.20. The increase of the depth of cut provided increase for macro (1.2%) and transition (3.8%) scales, on average, when used spindle speed range of 0-1,000 and 1,000-2,000. A reduction was observed for the increase of the depth of cut in macro (2.4%) and transition (1.0%) scales for the spindle speed range of 2,000-3,000 and for the meso scale, 1.3% on average, in all spindle speed range. The rise of the spindle speed range increased the R_a surface roughness in 4.7% (macro), 0.7% (transition), and 6.7% (meso), on average. The increase of the feed rate caused a similar rise steeply in all scales, which was slightly larger in transition scale, 112.0%, than in macro, 109.4%, and meso, 110.0%.

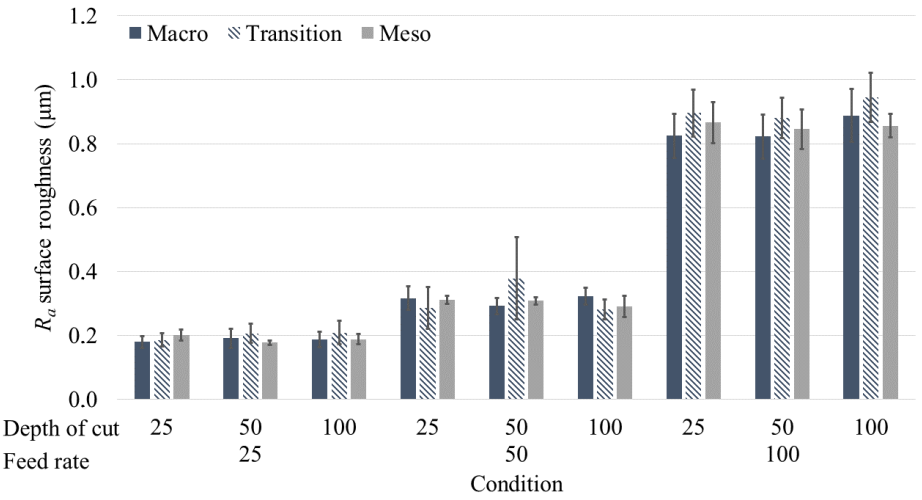

a) Spindle speed range of 0 to 1,000 rpm.

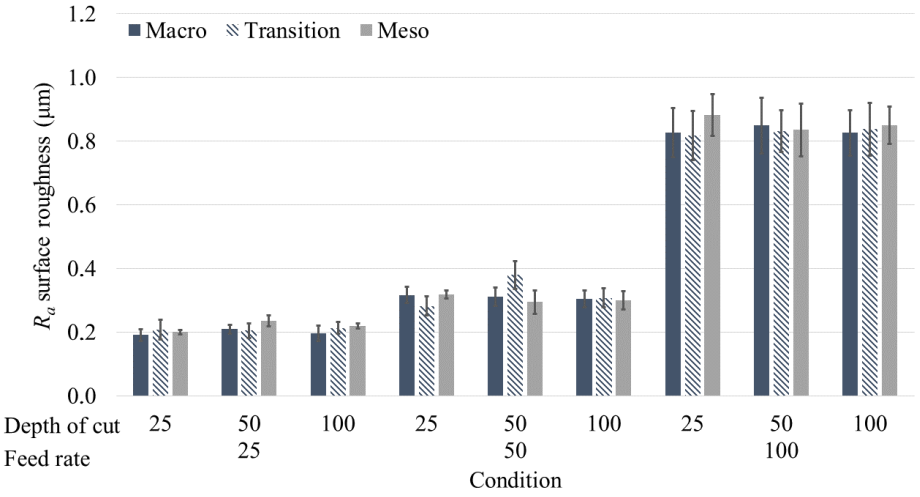

b) Spindle speed range of 1,000 to 2,000 rpm.

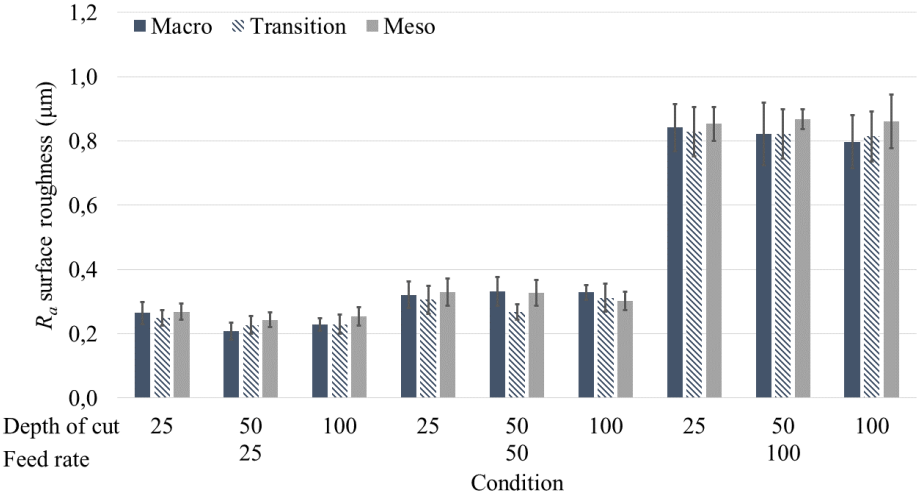

c) Spindle speed range of 2,000 to 3,000 rpm.

Figure 7.20 – R_a surface roughness for the chip-breaker inserts.

The results of R_a surface roughness for dual negative inserts are shown in the Figure 7.21 for spindle speed range of 0-1,000, 1,000-2,000, and 2,000-3,000 rpm. The increase of the feed rate went up the R_a surface roughness in all scales, 120.4% for the macro, 119.9% for the transition, and 100.7% for the macro, on average. The increase of the depth of cut caused a reduction in the macro (1.4%) and transition (0.3%) scales, and an increase in meso scale, 1.6%, on average. The rise of spindle speed range, in general, increased the values in macro (1.1%) and transition (4.6%), on average. For the meso scale, the rise of spindle speed range caused a reduction of 6.7% (0-1,000 to 1,000-2,000) or an increase of 5.0% (1,000-2,000 to 2,000-3,000), on average.

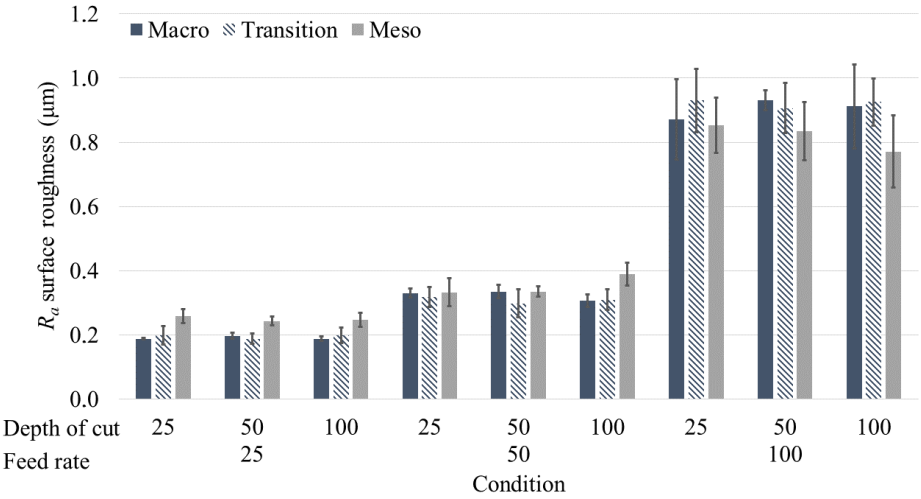

a) Spindle speed range of 0 to 1,000 rpm.

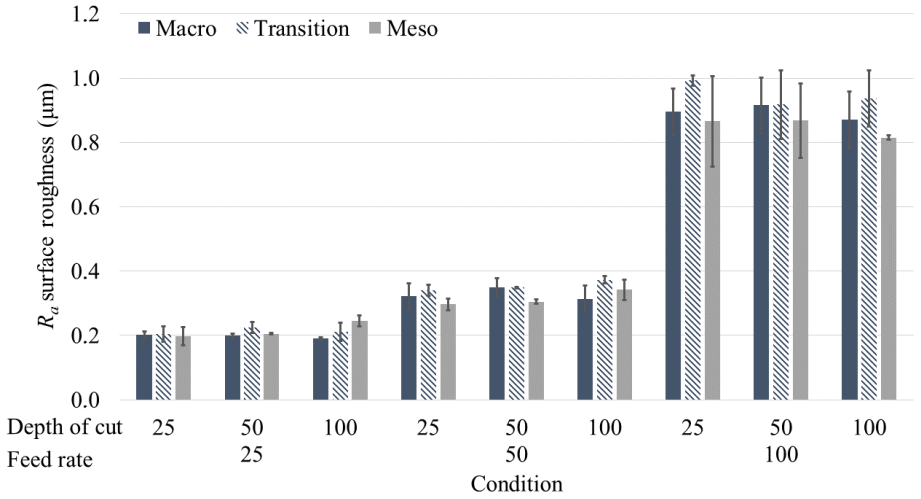

b) Spindle speed range of 1,000 to 2,000 rpm.

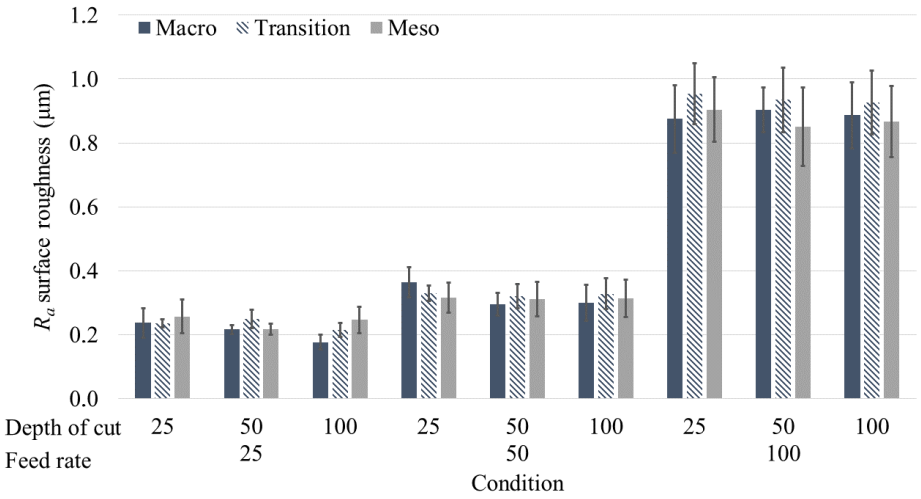

c) Spindle speed range of 2,000 to 3,000 rpm.

Figure 7.21 – R_a surface roughness for the dual negative inserts.

In the comparison between the scales, the reduction of the scale caused a decrease of the R_a surface roughness in the flat insert (1.9%) or an increase of 2.1% in the chip-breaker insert. For the dual negative inserts, in general, the reduction form macro to transition caused an increase of 4.7%, on average. For the reduction from transition to meso, in majority of case, in the low spindle speed range was observed increase, 10.3%, and other level of spindle speed range, a reduction, 4.6%, on average. Table 7.7 shows the ANOVA of the R_a surface roughness all scales, together and separately. The factor "scale" was not influence and the feed rate was the strongest influence factor for all scales.

Table 7.7 – ANOVA of R_a force for all and individual scales.

Source	All scales		Macro		Transition		Meso	
	F-Value	P-Value	F-Value	P-Value	F-Value	P-Value	F-Value	P-Value
Spindle speed range	0.01	0.989	0.06	0.937	0.72	0.490	1.91	0.150
Feed rate	*8667.64*	*0.000*	*3661.23*	*0.000*	*2844.15*	*0.000*	*3316.37*	*0.000*
Depth of cut	0.17	0.840	0.17	0.843	0.16	0.856	1.03	0.359
Chip-breaker	*5.66*	*0.018*	1.74	0.188	1.66	0.198	*4.55*	*0.034*
Inclination angle	*19.86*	*0.000*	*5.31*	*0.022*	*14.70*	*0.000*	1.11	0.294
Scale	1.67	0.189						
	R^2	R^2_{adj}	R^2	R^2_{adj}	R^2	R^2_{adj}	R^2	R^2_{adj}
	95.50%	95.45%	96.02%	95.92%	94.82%	94.68%	96.88%	96.76%

The ANOVA of R_a surface roughness for same cutting speed and spindle speed range are shown in the Table 7.8. The factor "scale" was not significant for any spindle speed range or cutting speed of 30 m/min. The feed rate and inclination angle were significant for all spindle speed range and the cutting speed analysed.

Table 7.8 – ANOVA for the R_a surface roughness for spindle speed range and cutting speed.

Source	v_c 30 m/min		n 0-1,000 rpm		n 1,000-2,000 rpm		n 2,000-3,000 rpm	
	F-Value	P-Value	F-Value	P-Value	F-Value	P-Value	F-Value	P-Value
Feed rate	*3090.53*	*0.000*	*3446.76*	*0.000*	*3340.34*	*0.000*	*2852.58*	*0.000*
Depth of cut	0.39	0.680	0.14	0.873	0.83	0.437	2.27	0.105
Chip-breaker	1.14	0.288	0.10	0.753	0.16	0.692	*11.32*	*0.001*
Inclination angel	*9.55*	*0.002*	*3.89*	*0.049*	*13.44*	*0.000*	*5.80*	*0.017*
Scale	0.83	0.437	2.48	0.086	0.75	0.475	0.37	0.689
	R^2	R^2_{adj}	R^2	R^2_{adj}	R^2	R^2_{adj}	R^2	R^2_{adj}
	95.84%	95.71%	96.22%	96.10%	96.32%	96.21%	94.99%	94.85%

7.2.2. R_z surface roughness

In the Figure 7.22 are exhibited the response surface for the flat inserts with spindle speed range of 0-1,000, 1,000-2,000, and 2,000-3,000 rpm. The rise of the spindle speed provided an increase in the macro scale, 1.9 on average, and, for the transition and meso scales, the reduction of 1.3% and 0.4% was observed, respectively. For the macro scale, the increase of the depth of cut caused increase of 0.6% (0-1,000 rpm) and 2.0% (1,000-2,000 rpm), or a decrease of 3.8% (2,000-3,000 rpm). In the transition and meso scales, the R_z surface roughness increased in 4.9% and 2.0%, respectively. The increase of the feed rate caused a similar increase in the macro (57.0%), transition (59.6%), and meso (55.8%) scales.

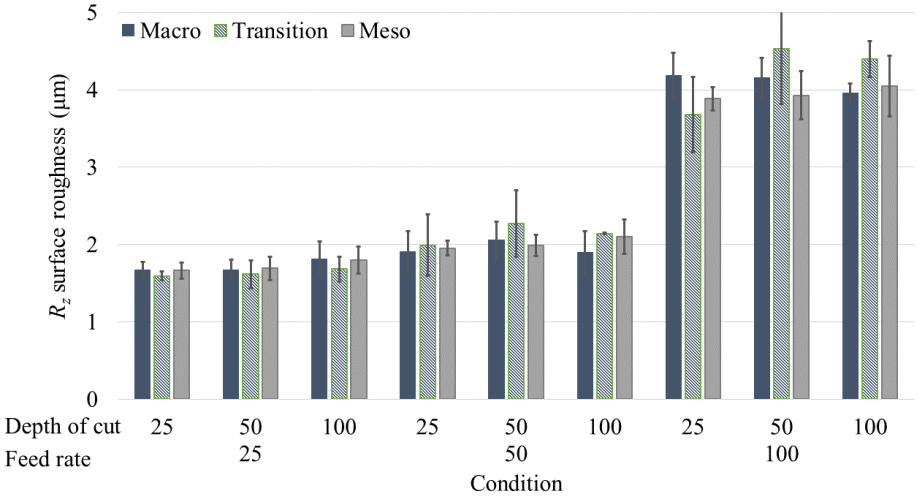

a) Spindle speed range of 0 to 1,000 rpm.

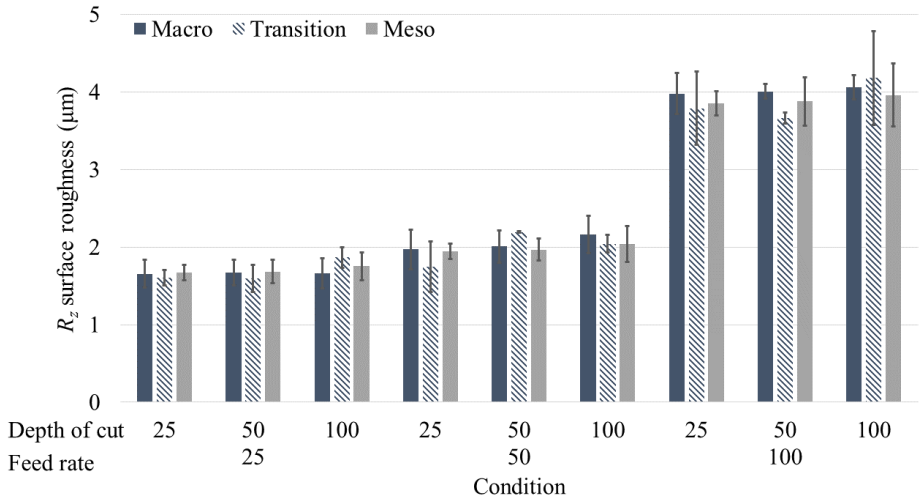

b) Spindle speed range of 1,000 to 2,000 rpm.

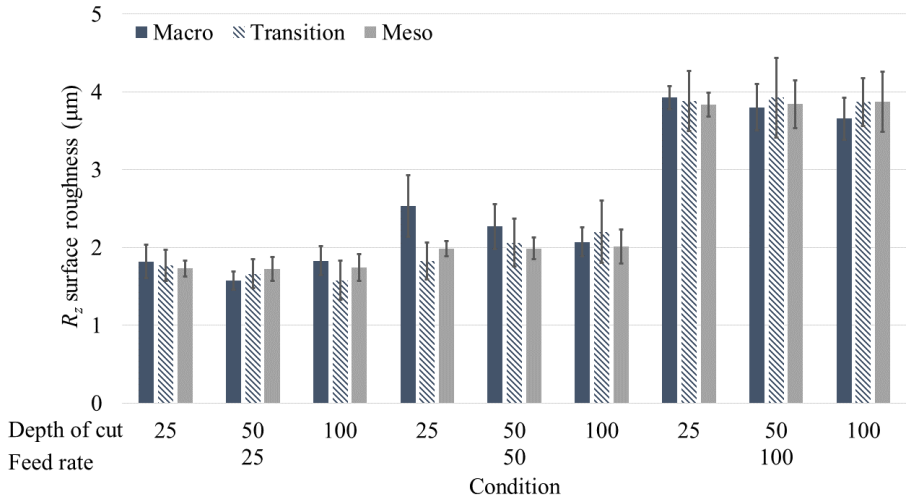

c) Spindle speed range of 2,000 to 3,000 rpm.

Figure 7.22 – R_z surface roughness for the flat inserts.

For the chip-breaker inserts, the Figure 7.23 shows the results of the R_z surface roughness for spindle speed range of 0-1,000, 1,000-2,000, and 2,000-3,000 rpm. The increase of the feed rate caused similar evolution in the R_z surface roughness, increase of 73.3% (macro), 73.9% (transition), and 70.8% (meso). The increase of the depth of cut caused reduction of 0.9% for the macro, on average. For the transition and meso, an increase of 0.7% and 1.4% were observed. For the rise of the spindle speed, in general, was observed an increase of 5.1% for the macro, 3.4% for transition, and 5.4% for meso scales, on average.

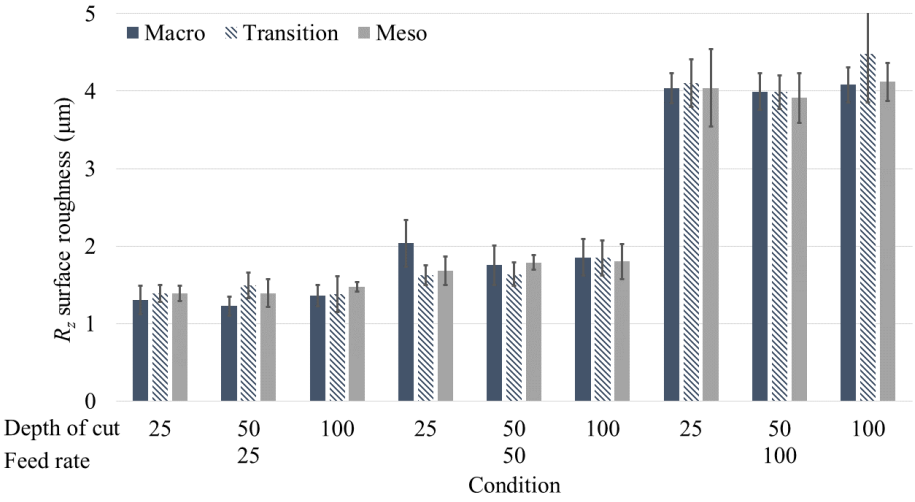

a) Spindle speed range of 0 to 1,000 rpm.

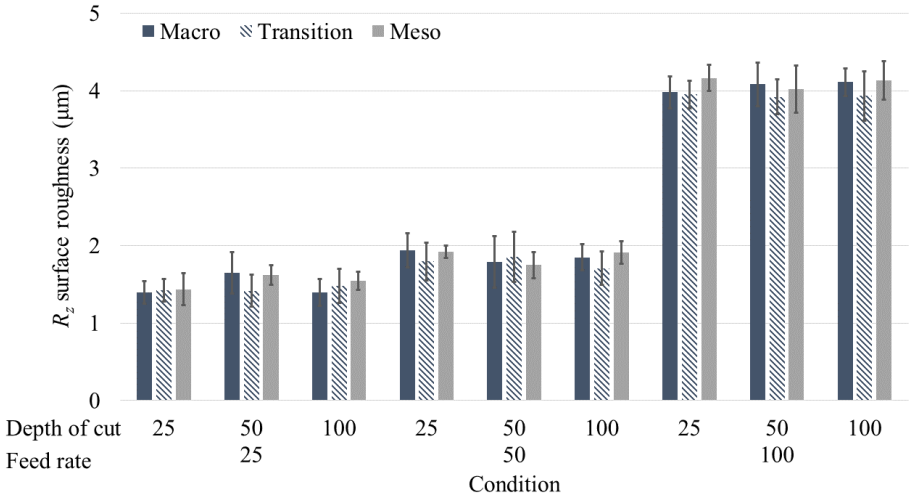

b) Spindle speed range of 1,000 to 2,000 rpm.

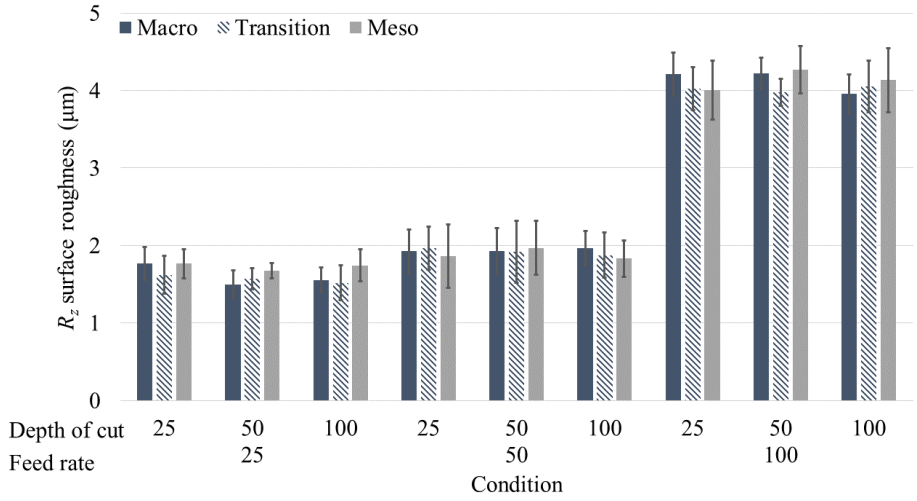

c) Spindle speed range of 2,000 to 3,000 rpm.

Figure 7.23 – R_z surface roughness for the chip-breaker inserts.

The values of the R_z surface roughness for spindle speed range of 0-1,000, 1,000-2,000, and 2,000-3,000 rpm are shown in the Figure 7.24, when used the dual negative inserts. The rise of the spindle speed range in the transition and meso scales caused a reduction of 0.8% and 1.9 for macro and meso scales, on average, respectively, and increase of 2.3% for the transition scale. The increase of the depth of cut reduced the R_z surface roughness in macro (1.3%) and transition (2.3%), on average. For the meso scale, the increase of the depth of cut caused an increase of 3.2, on average. The increase of the feed rate went up the R_z surface roughness in 71.9% (macro), 65.7% (transition), and 55.0% (meso).

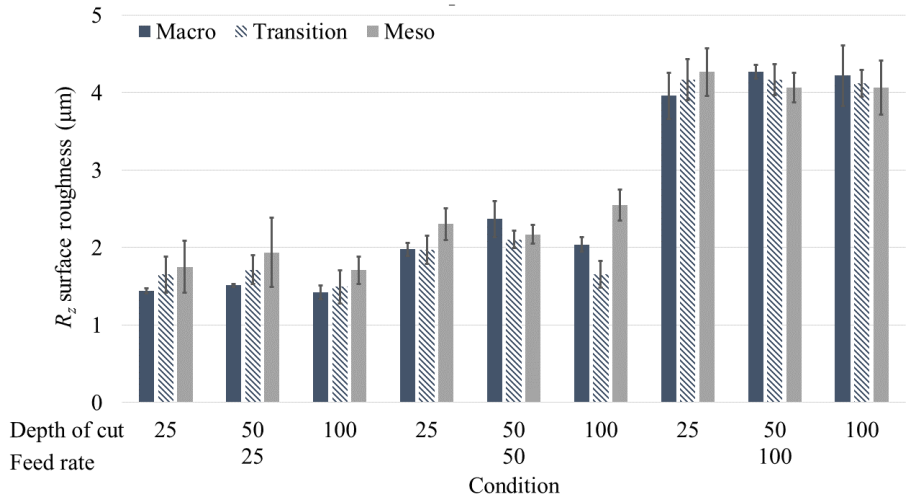

a) Spindle speed range of 0 to 1,000 rpm.

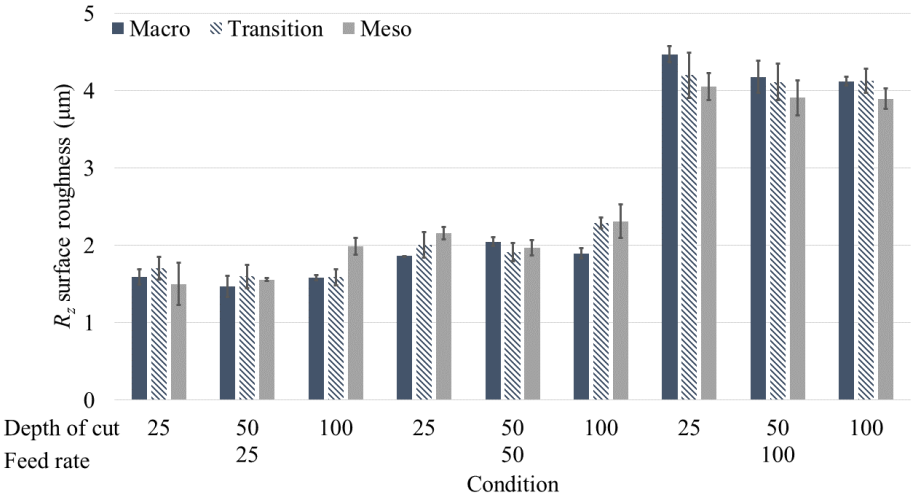

b) Spindle speed range of 1,000 to 2,000 rpm.

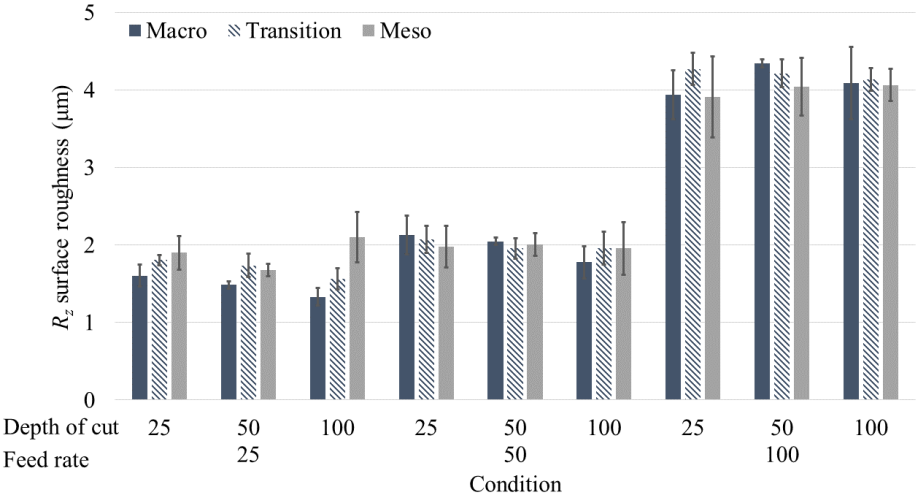

c) Spindle speed range of 2,000 to 3,000 rpm.

Figure 7.24 – R_z surface roughness for the dual negative inserts.

When compared the scales, a decrease was observed for the flat inserts (0.6%) and an increase for dual negative inserts, 4.1%, on average. For the chip-breaker inserts, in the reduction from macro to transition, a decrease of 1.1%, and in the reduction from transition to meso, an increase of 2.9% were observed. The Table 7.9 the ANOVA for the all and individual scales. For the analysis in all scales, the factor "scale" did not present significance. The feed rate and inclination angle were significant for all scales, together and separately.

Table 7.9 – ANOVA of R_z force for all and individual scales.

Source	All scales		Macro		Transition		Meso	
	F-Value	P-Value	F-Value	P-Value	F-Value	P-Value	F-Value	P-Value
Spindle speed range	2.40	0.091	1.61	0.202	1.42	0.242	0.29	0.750
Feed rate	*7321.40*	*0.000*	*3219.99*	*0.000*	*2782.34*	*0.000*	*1804.19*	*0.000*
Depth of cut	0.15	0.864	1.23	0.294	0.52	0.593	1.64	0.196
Chip-breaker	*18.65*	*0.000*	9.24	0.003	7.70	0.006	0.59	0.444
Inclination angle	*42.90*	*0.000*	*4.46*	*0.036*	*20.42*	*0.000*	*19.89*	*0.000*
Scale	2.50	0.083						
	R^2	R^2_{adj}	R^2	R^2_{adj}	R^2	R^2_{adj}	R^2	R^2_{adj}
	94.50%	94.44%	95.41%	95.29%	94.34%	94.21%	94.30%	94.09%

The ANOVA for the R_z surface roughness is shown in the Table 7.10. The factor "scale" was significant only in the micro-cutting for same the cutting speed. The feed rate has stronger significance for all spindle speed and same cutting speed. The chip-breaker and inclination angle were not significant only in the spindle speed range of 2,000-3,000. The Tukey and Fisher tests are show in the Figure 7.25. The transition and meso scales showed significant difference among themselves.

Table 7.10 – ANOVA for the R_z surface roughness for spindle speed range and cutting speed

Source	v_c 30 m/min		n 0-1,000 rpm		n 1,000-2,000 rpm		n 2,000-3,000 rpm	
	F-Value	P-Value	F-Value	P-Value	F-Value	P-Value	F-Value	P-Value
Feed rate	*2468.57*	*0.000*	*2545.85*	*0.000*	*3229.35*	*0.000*	*2377.50*	*0.000*
Depth of cut	0.48	0.622	1.24	0.292	1.48	0.228	1.61	0.201
Chip-breaker	*7.76*	*0.006*	*21.54*	*0.000*	*8.85*	*0.003*	0.02	0.901
Inclination angel	*15.86*	*0.000*	*33.88*	*0.000*	*22.59*	*0.000*	2.15	0.143
Scale	*3.55*	*0.030*	0.90	0.406	1.83	0.162	0.40	0.672
	R^2	R^2_{adj}	R^2	R^2_{adj}	R^2	R^2_{adj}	R^2	R^2_{adj}
	94.52%	94.37%	94.80%	94.65%	95.92%	95.80%	93.90%	93.75%

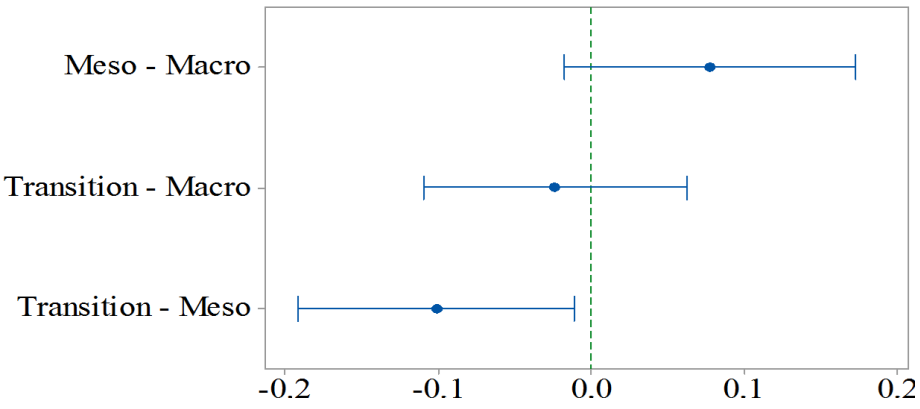

a) Tukey test.

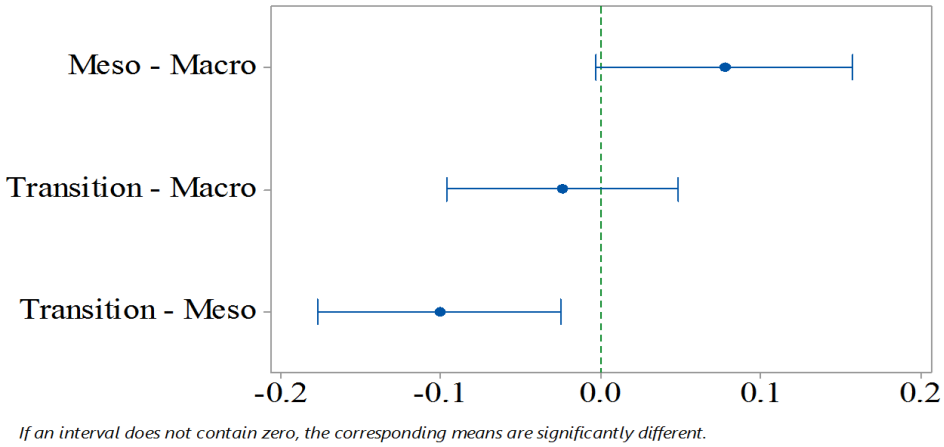

b) Fisher test.

Figure 7.25 – Comparison tests of the R_z surface roughness for cutting speed of 30 m/min.

7.3. Deflection

In the Figure 7.26 is shown the minimum deflection of the workpiece for the flat insert in the micro-cutting of titanium alloy. The increase of the feed rate and the depth of cut caused an increase, on average, in macro (15.3% and 46.8%), transition (34.0% and 106.2%), an meso (104.5% and 266.0%) scales, respectively. However, the rise of the spindle speed range caused a reduction of the deflection, on average, in macro (20.6%) and transition (48.2%). For the meso scale, the rise from 0-1,000 to 1,000-2,000 caused an increase and the rise from 1,000-2,000 to 2,000-3,000 cause a reduction in the deflection.

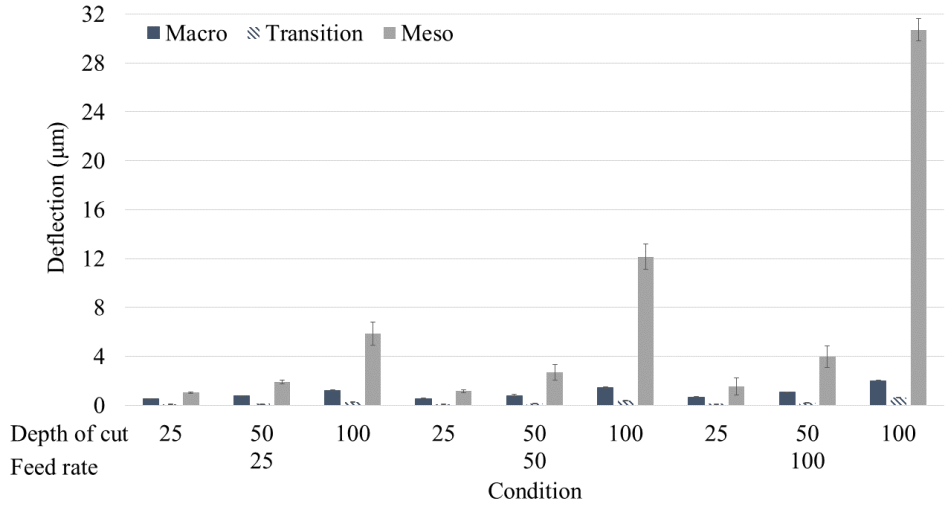

a) Spindle speed range of 0 to 1,000 rpm.

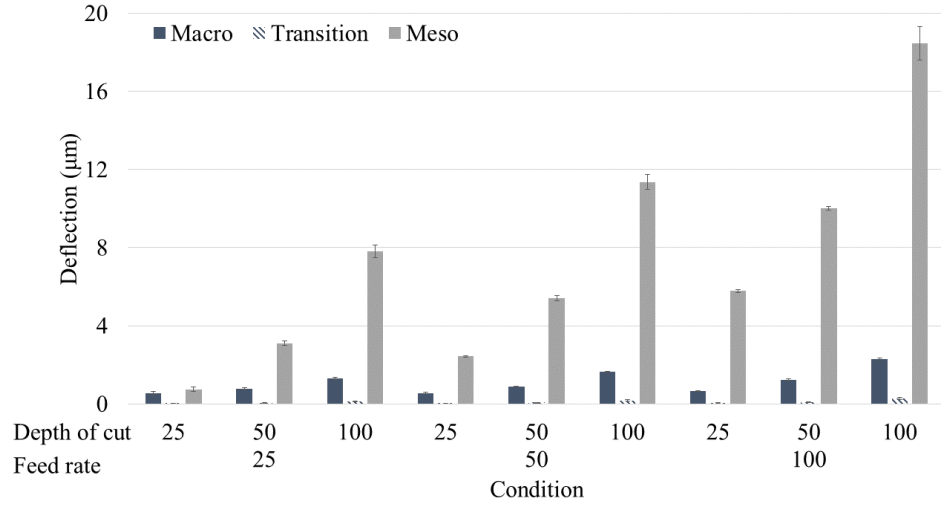

b) Spindle speed range of 1,000 to 2,000 rpm.

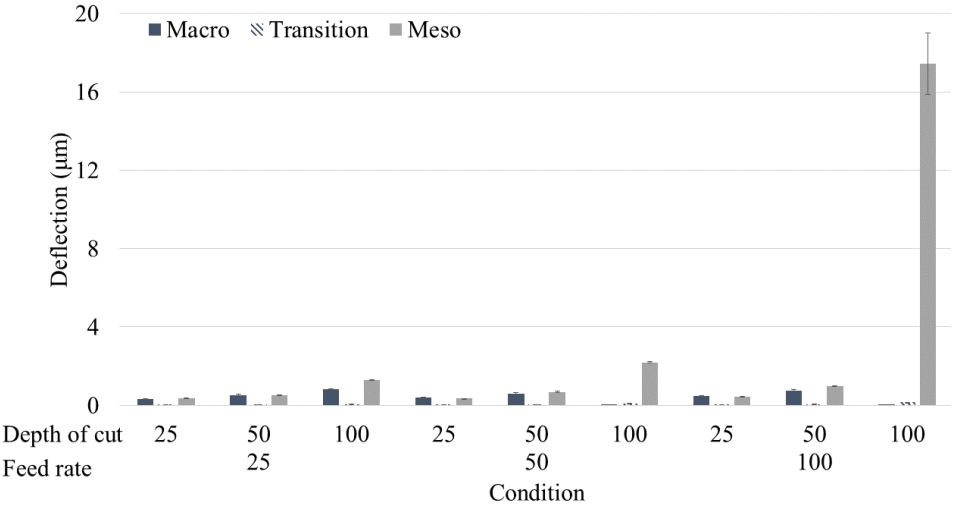

c) Spindle speed range of 2,000 to 3,000 rpm.

Figure 7.26 – Deflection of workpiece for the flat inserts.

The Figure 7.27 shows the minimum deflection of the workpiece during the micro-cutting. The increase of the depth of cut rose steeply the deflection in 63.0%, macro, 104.4%, transition, and 244.2%, meso scales. The deflection increase 21.8%, 35.7%, and 68.5%, on average, when the feed rate was increased, for the macro, transition, and meso scales respectively. The rise of the spindle speed range reduced the deflection in macro, 16.8%, transition, 49.2%, and meso, 49,0%, scales.

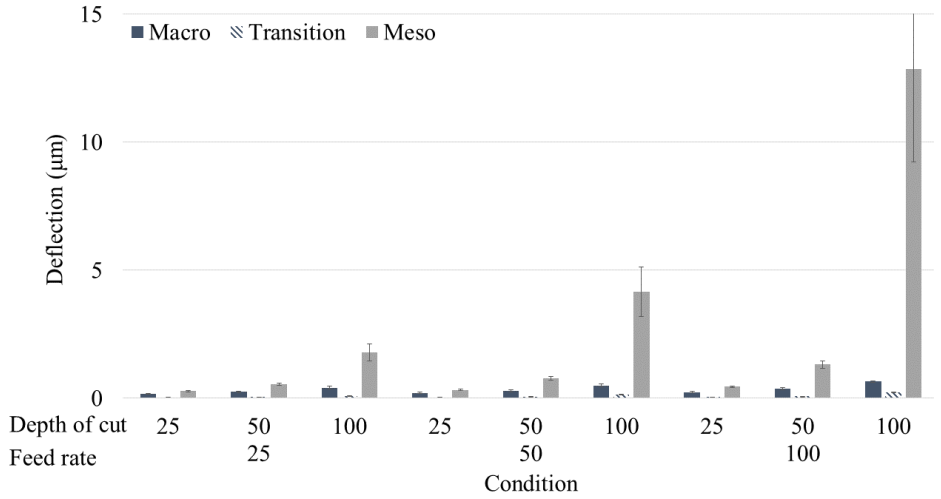

a) Spindle speed range of 0 to 1,000 rpm.

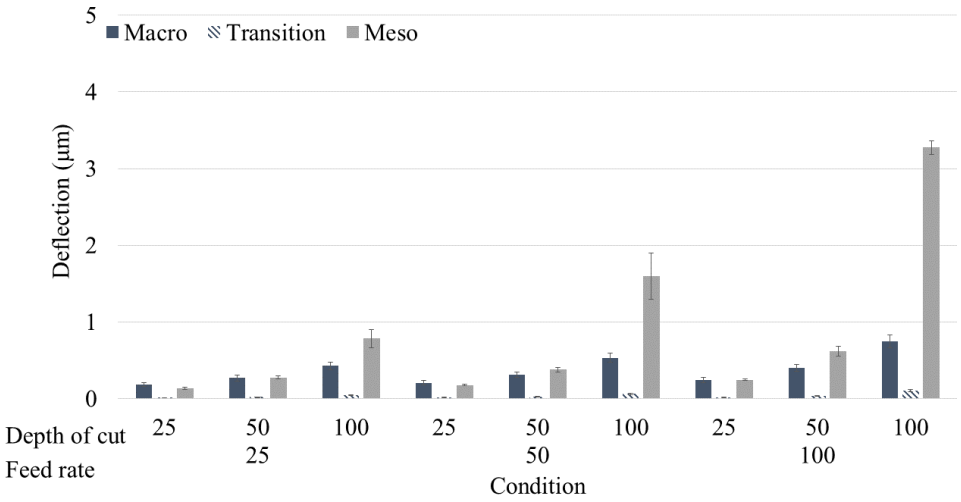

b) Spindle speed range of 1,000 to 2,000 rpm.

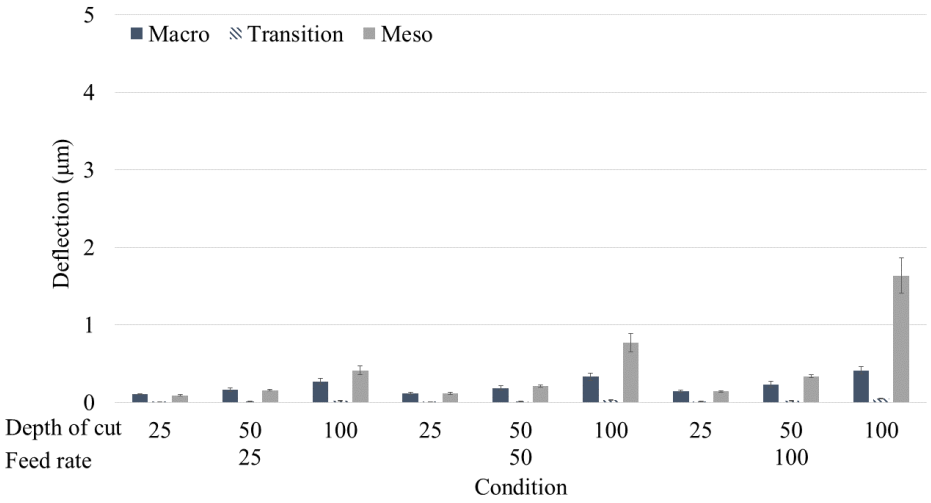

c) Spindle speed range of 2,000 to 3,000 rpm.

Figure 7.27 – Deflection of workpiece for the chip-breaker inserts.

The results of minimum deflection of the workpiece are shown in the Figure 7.28 when used the dual negative inserts. The rise of the spindle speed range presented a similar reduction of the deflection, on average, for transition (48.2%) and meso (48.6%). For the macro scale, the reduction, on average, had less impact, 18.6%. The increase of the feed rate went up the deflection in 26.0%, 36.8%, and 64.4%, on average, for the macro, transition, and meso scales, respectively.

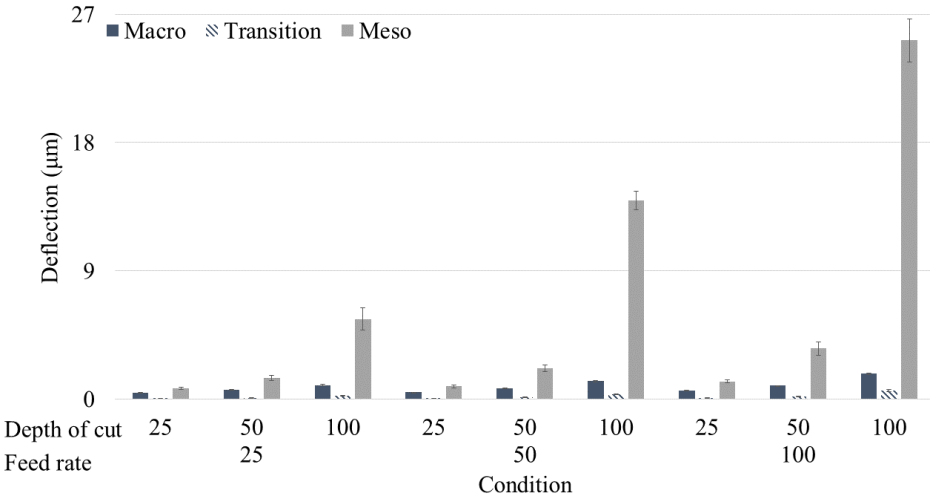

a) Spindle speed range of 0 to 1,000 rpm.

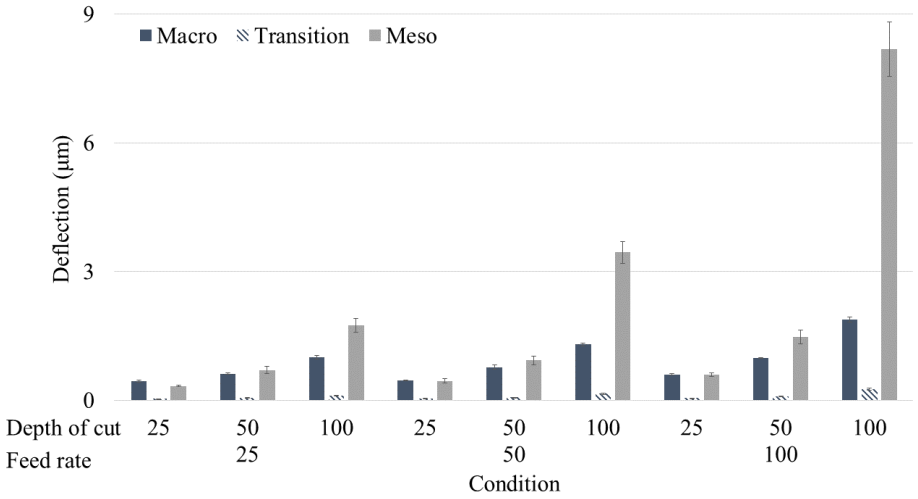

b) Spindle speed range of 1,000 to 2,000 rpm.

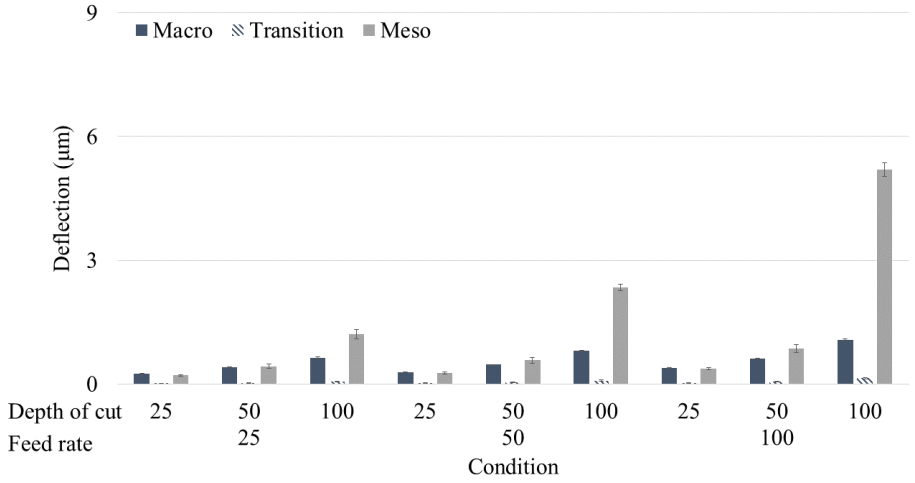

c) Spindle speed range of 2,000 to 3,000 rpm.

Figure 7.28 – Deflection of workpiece for the dual negative inserts.

The reduction of the scale caused a reduction in the minimum deflection, from macro to transition scale, in 87.5%, 86.9% and 87.2%, or a rise steeply, from transition to meso scale, in 3574.3%, 1722.5%, and 1817.0%, on average, for flat, chip-breaker and dual-negative inserts, respectively. Among the scales, the meso scale was more affected by the deflection, which, although the F_x force were lower for the meso scale than the macro and transition, the reduction of the diameter was about 74.3%, while the F_x force reduced in about 9.0%, on average. In the Table 7.11 is exhibited the ANOVA for the minimum deflection, all and individual scales. The scale was significant factor for the deflection during the micro-cutting.

Table 7.11 – ANOVA of vibration in the tangential direction for all and individual scales

Source	All scales		Macro		Transition		Meso	
	F-Value	P-Value	F-Value	P-Value	F-Value	P-Value	F-Value	P-Value
Spindle speed range (n)	*13.50*	*0.000*	*37.57*	*0.000*	*107.17*	*0.000*	*20.94*	*0.000*
Feed rate (f)	*9.50*	*0.000*	*14.02*	*0.000*	*32.87*	*0.000*	*15.11*	*0.000*
Depth of cut (a_p)	*32.36*	*0.000*	*62.69*	*0.000*	*137.26*	*0.000*	*44.80*	*0.000*
Chip-breaker (CB)	*10.70*	*0.001*	*103.95*	*0.000*	*83.19*	*0.000*	*5.78*	*0.021*
Inclination angle (λ_s)	*7.17*	*0.008*	*78.27*	*0.000*	*55.19*	*0.000*	*9.65*	*0.004*
Scale	*35.85*	*0.000*						
n*f	1.92	0.108	1.74	0.156	*5.46*	*0.001*	*3.06*	*0.028*
n* a_p	*6.76*	*0.000*	*7.21*	*0.000*	*22.89*	*0.000*	*11.63*	*0.000*
n*CB	1.34	0.265	*9.40*	*0.000*	*12.67*	*0.000*	1.65	0.206
n* λ_s	1.11	0.332	1.70	0.193	*8.08*	*0.001*	2.11	0.135
n*Scale	*9.85*	*0.000*						
f* a_p	*5.44*	*0.000*	1.61	0.187	*12.75*	*0.000*	*11.91*	*0.000*
f*CB	1.22	0.298	0.94	0.399	*3.44*	*0.040*	2.75	0.076
f* λ_s	0.54	0.581	2.02	0.143	2.99	0.060	0.90	0.413
f*Scale	*6.87*	*0.000*						
a_p*CB	*4.06*	*0.019*	*4.22*	*0.021*	*15.90*	*0.000*	*6.58*	*0.003*
a_p* λ_s	2.58	0.078	*6.54*	*0.003*	*11.54*	*0.000*	*4.52*	*0.017*
a_p*Scale	*21.70*	*0.000*						
CB*Scale	*4.89*	*0.009*						
λ_s *Scale	*3.34*	*0.038*						
	R^2	R^2_{adj}	R^2	R^2_{adj}	R^2	R^2_{adj}	R^2	R^2_{adj}
	69.68%	61.39%	89.72%	82.86%	94.68%	91.13%	89.99%	81.78%

In the Figure 7.29 is shown the comparison tests, Tukey and Fisher, for the minimum deflection during the micro-cutting. When compared the macro and transition scales, the average were not differing among themselves for both tests.

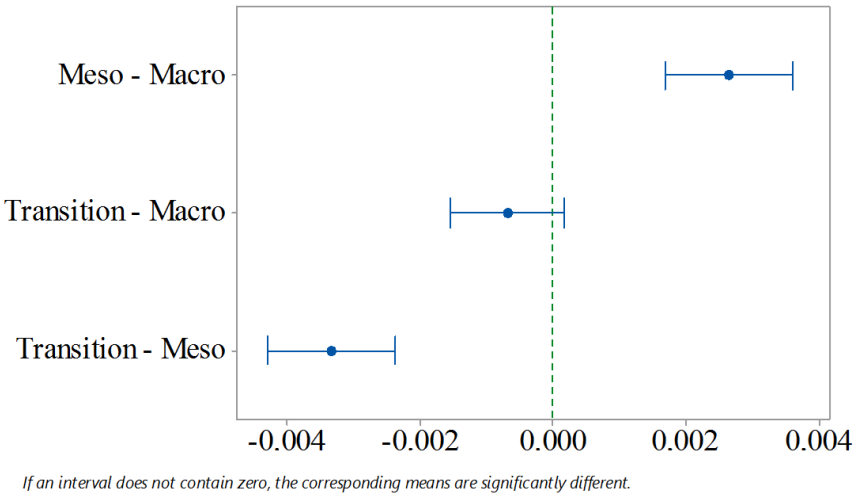

a) Tukey test.

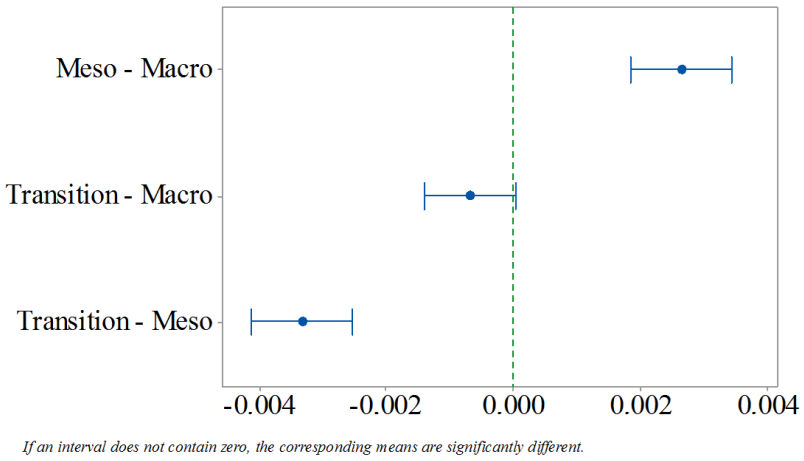

b) Fisher test.

Figure 7.29 – Comparison tests of the minimum deflection for all scales.

The ANOVA for the minimum deflection during the micro-cutting with cutting speed of 30 m/min and same spindle speed for all scales are presented Table 7.12. The scale was significant for the same cutting speed and spindle speed. In the Figure 7.30, Figure 7.31, Figure 7.32, and Figure 7.33 are shown the comparison tests for v_c of 30 m/min and different spindle speed range, respectively. For the v_c of 30 m/min and spindle speed range of 1,000-2,000 rpm, the macro and meso scales was not differ among themselves. For the spindle speed range of 0-1,000 rpm, the difference between macro and transition was not significant. When used the spindle speed range of 1,000-2,000 rpm, all scales were differed themselves.

Table 7.12 – ANOVA for the minimum deflection in spindle speed range and cutting speed.

Source	v_c 30 m/min		n 0-1,000 rpm		n 1,000-2,000 rpm		n 2,000-3,000 rpm	
	F-Value	P-Value	F-Value	P-Value	F-Value	P-Value	F-Value	P-Value
Feed rate (f)	*10.17*	*0.000*	*6.32*	*0.004*	*8.22*	*0.001*	*4.23*	*0.020*
Depth of cut (a_p)	*43.48*	*0.000*	*22.89*	*0.000*	*26.42*	*0.000*	*18.80*	*0.000*
Chip-breaker (CB)	*21.93*	*0.000*	*6.03*	*0.018*	3.33	0.076	*6.89*	*0.012*
Inclination angle (λ_s)	*23.89*	*0.000*	*4.22*	*0.045*	*13.00*	*0.001*	*13.33*	*0.001*
Scale	*44.09*	*0.000*	*32.43*	*0.000*	*15.35*	*0.000*	*32.92*	*0.000*
f*a_p	*4.35*	*0.005*	*4.50*	*0.004*	*3.24*	*0.022*	1.67	0.173
f*CB	0.33	0.722	0.63	0.537	0.43	*0.651*	*0.00*	0.996
f*λ_s	1.91	0.159	0.28	0.758	1.32	0.279	1.27	0.290
f*Scale	*3.36*	*0.017*	*5.35*	*0.001*	*3.87*	*0.010*	*3.05*	*0.026*
a_p*CB	2.87	0.067	2.27	0.114	1.56	0.223	0.24	0.785
a_p* λ_s	*6.46*	*0.003*	1.76	0.183	*3.46*	*0.041*	*4.17*	*0.021*
a_p*Scale	*13.32*	*0.000*	*17.69*	*0.000*	*11.46*	*0.000*	*12.81*	*0.000*
CB*Scale	*4.09*	*0.023*	*3.55*	*0.036*	1.53	0.230	2.35	0.106
λ_s *Scale	*5.47*	*0.007*	2.53	0.090	*3.92*	*0.028*	*4.68*	*0.014*
	R^2	R^2_{adj}	R^2	R^2_{adj}	R^2	R^2_{adj}	R^2	R^2_{adj}
	86.29%	76.95%	83.96%	73.26%	84.92%	72.85%	80.75%	67.65%

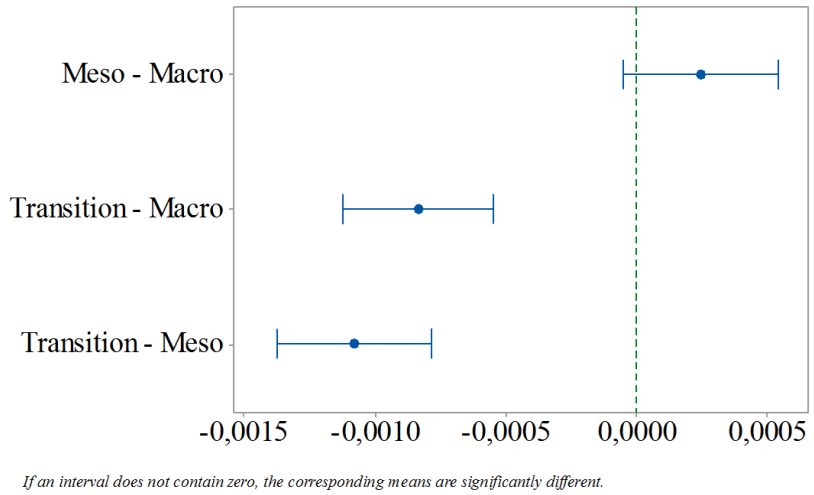

a) Tukey test.

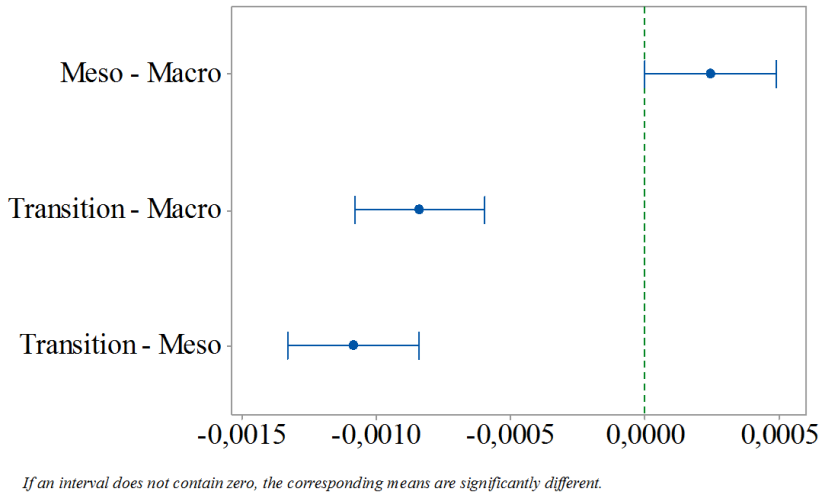

b) Fisher test.

Figure 7.30 – Comparison tests of the minimum deflection for cutting speed of 30 m/min.

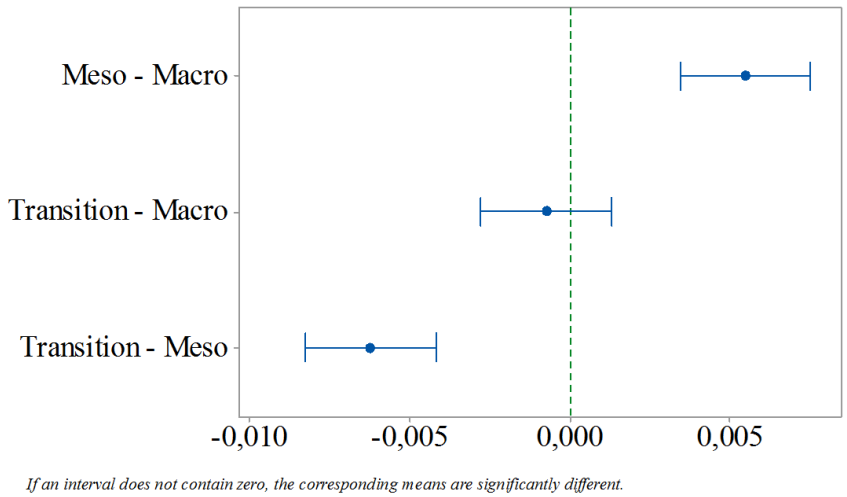

a) Tukey test.

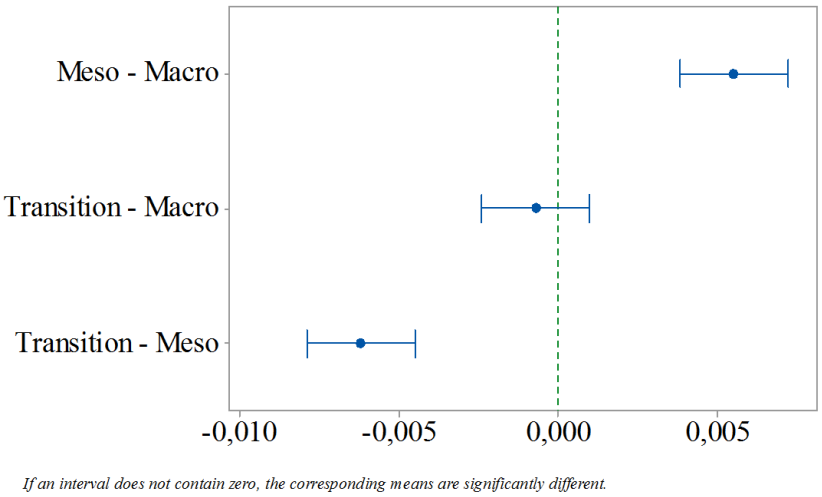

b) Fisher test.

Figure 7.31 – Comparison tests of the minimum deflection for spindle speed range of 0-1,000 rpm.

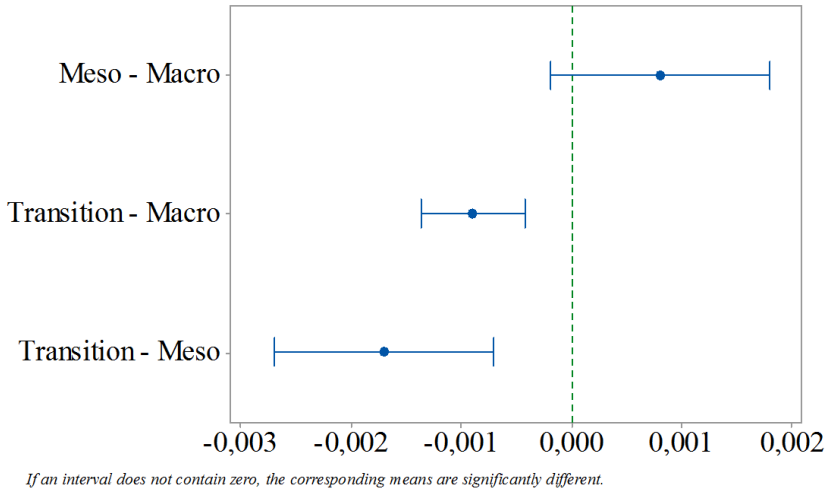

a) Tukey test.

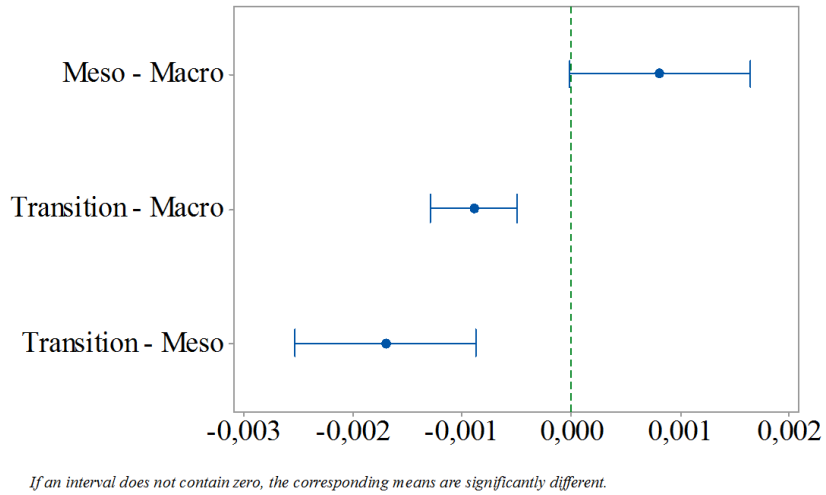

b) Fisher test.

Figure 7.32 – Comparison tests of the minimum deflection for spindle speed range of 1,000-2,000 rpm.

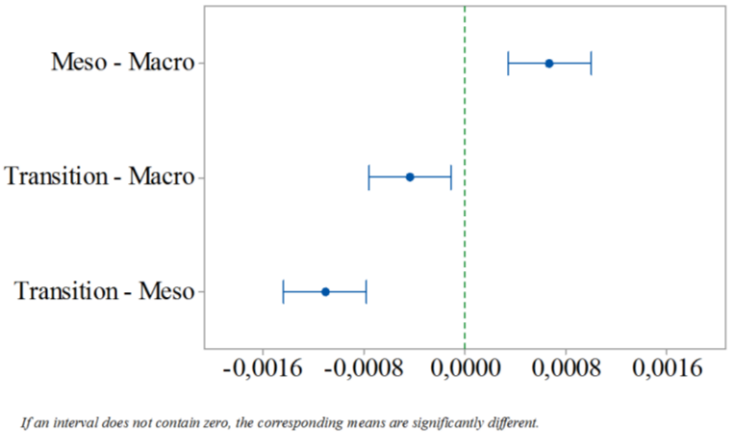

a) Tukey test.

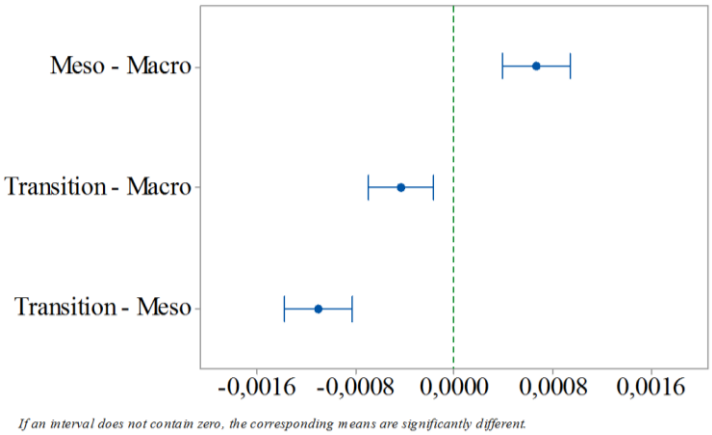

b) Fisher test.

Figure 7.33 – Comparison tests of the minimum deflection for spindle speed range of 2,000-3,000 rpm.

7.4. Vibration in the micro-cutting (Time domain)

7.4.1. Vibration in the axial direction

The vibration in the axial direction in the micro-cutting with flat inserts are shown in the Figure 7.34 for spindle speed range of 0-1,000, 1,000-2,000, and 2,000-3,000. The feed rate increased of the vibration, on average, in macro (33.1%), transition (16.9%), and meso (17.9%) scales. The increased of the depth of cut caused a similar increase in the transition and meso scales, 17.9% and 17.3% on average, respectively. For the macro scale, the increase was a slightly larger, 20.4% on average. The rise of spindle speed range from 0-1,000 to 1,000-2,000 presented smaller increase than the rise of spindle speed range from 1,000-2,000 to 2,000-3,000, 1.6% and 28.0%, respectively. The more variation, on average, was observed in the macro scale (22.2%) than in the transition (6.6%) and meso (15.4%) scales.

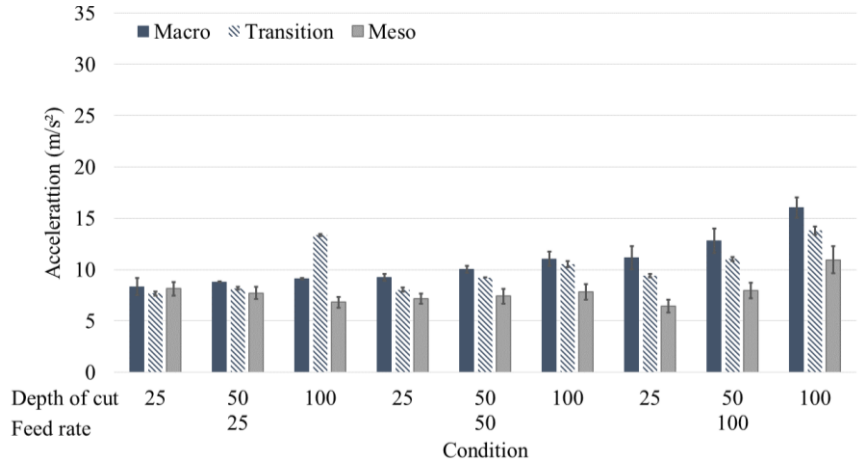

a) Spindle speed range of 0 to 1,000 rpm.

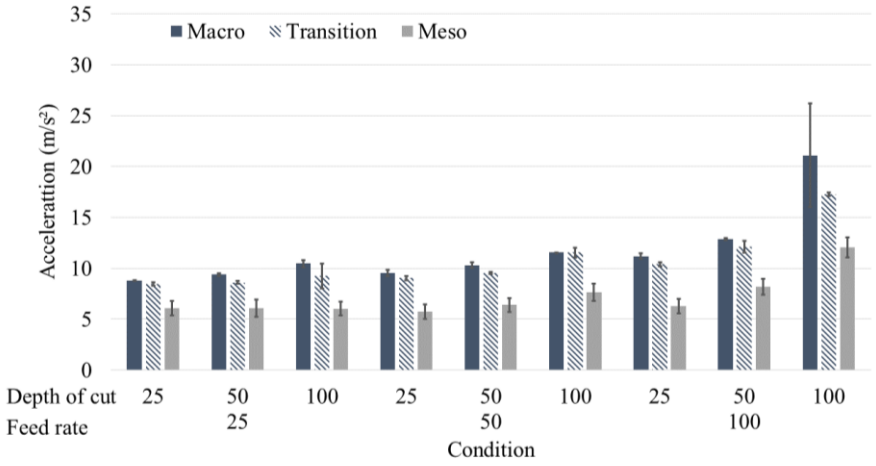

b) Spindle speed range of 1,000 to 2,000 rpm.

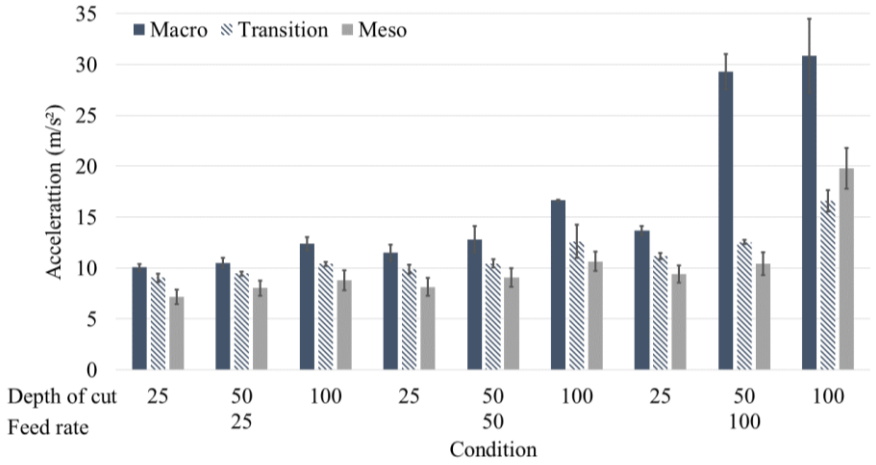

c) Spindle speed range of 2,000 to 3,000 rpm.

Figure 7.34 – Vibration in the axial direction with flat inserts.

The vibration for the spindle speed range of 0-1,000, 1,000-2,000, and 2,000-3,000 rpm are exhibited in the Figure 7.35 using the chip-breaker inserts. For the increase of the feed rate, it was observed that an increase in macro scale, on average, was almost twice as the transition

and meso scale, 16.5%, 9.9%, and 9.5%, respectively. The increase of the depth of cut caused a similar increase for all scales, 10.0% on average. The rise of the spindle speed range went up the vibration in 10.5%, 6.4%, and 3.8% for macro, transition and meso scales.

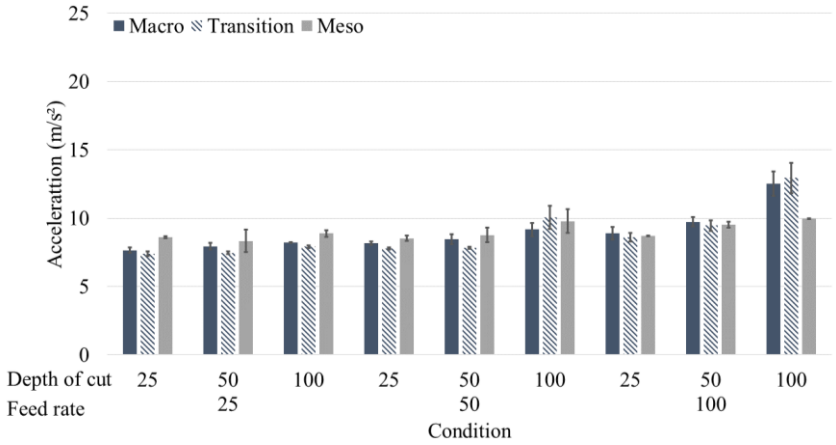

a) Spindle speed range of 0 to 1,000 rpm.

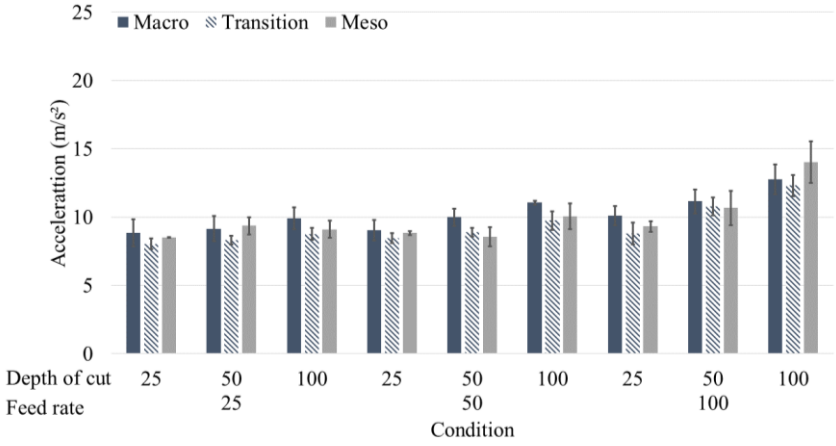

b) Spindle speed range of 1,000 to 2,000 rpm.

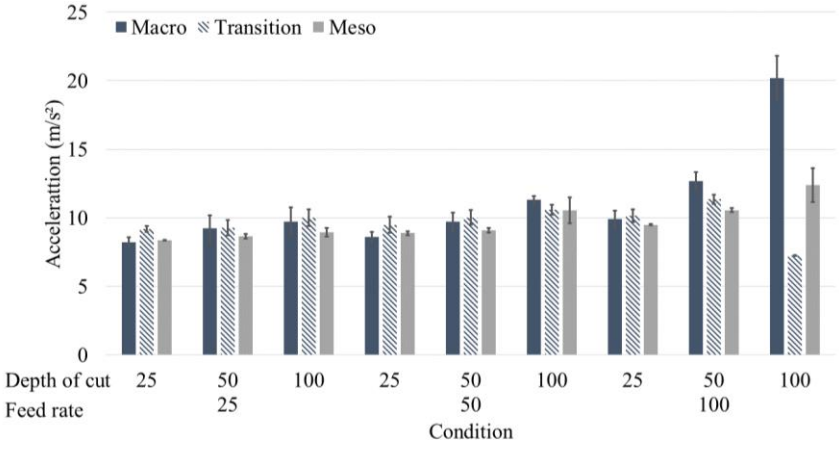

c) Spindle speed range of 2,000 to 3,000 rpm.

Figure 7.35 – Vibration in the axial direction with chip-breaker inserts.

For the dual negative inserts, the vibration is shown in the Figure 7.36 for the spindle speed range of 0-1,000, 1,000-2,000, and 2,000-3,000 rpm. The rise of the spindle speed range increased the vibration in 11.1% (macro), 13.6% (transition) and 18.8% (meso), on average. The increase of the feed rate and the depth of cut increased the vibration more in the macro (29.1% and 21.8%) than the transition (13.3% and 9.9%) and meso (10.3% and 11.2%).

When compared the reduction of scale, the vibration trended to reduce for flat (17.3%), chip-breaker (0.9%), and dual negative (15.8%) inserts, on average. Table 7.13 shows the ANOVA of the vibration in axial direction for the different scales, together and separately. The factor "scale" was significant for the vibration in the axial direction in the micro-cutting.

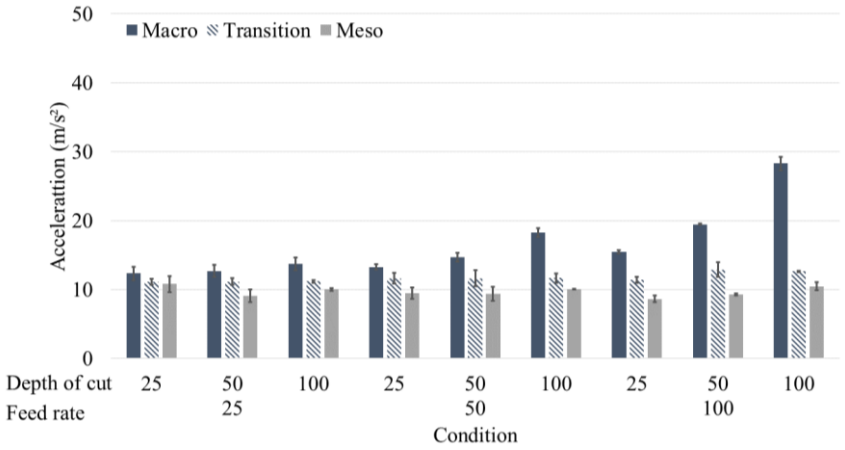

a) Spindle speed range of 0 to 1,000 rpm.

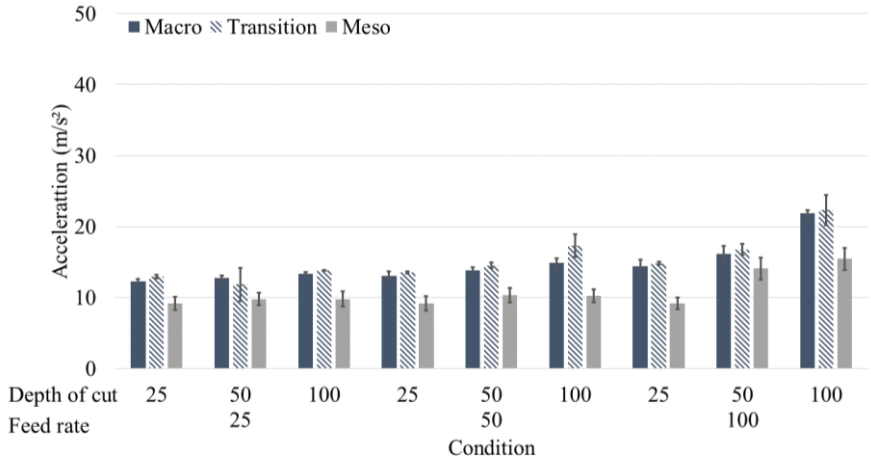

b) Spindle speed range of 1,000 to 2,000 rpm.

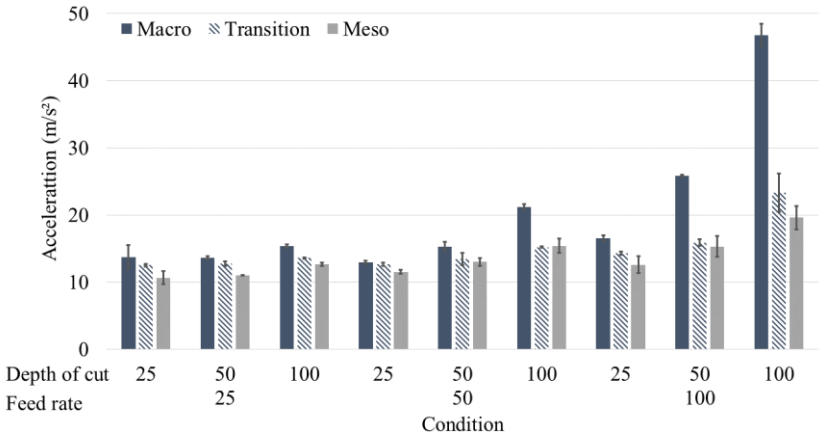

c) Spindle speed range of 2,000 to 3,000 rpm.

Figure 7.36 – Vibration in the axial direction with dual negative inserts.

Table 7.13 – ANOVA of vibration in axial direction all and individual scales.

Source	All scales		Macro		Transition		Meso	
	F-Value	P-Value	F-Value	P-Value	F-Value	P-Value	F-Value	P-Value
Spindle speed range (*n*)	*62.46*	*0.000*	*67.31*	*0.000*	*43.81*	*0.000*	*84.85*	*0.000*
Feed rate (*f*)	*145.07*	*0.000*	*169.02*	*0.000*	*95.23*	*0.000*	*51.34*	*0.000*
Depth of cut (a_p)	*98.19*	*0.000*	*87.81*	*0.000*	*83.12*	*0.000*	*52.91*	*0.000*
Chip-breaker (*CB*)	*10.23*	*0.001*	*58.14*	*0.000*	*47.98*	*0.000*	*31.47*	*0.000*
Inclination angle (λ_s)	*406.00*	*0.000*	*364.55*	*0.000*	*436.43*	*0.000*	*88.34*	*0.000*
Scale	*84.50*	*0.000*						
*n*f*	*11.52*	*0.000*	*19.87*	*0.000*	*3.98*	*0.004*	*13.84*	*0.000*
*n** a_p	*5.16*	*0.000*	*10.23*	*0.000*	0.54	0.704	*7.45*	*0.000*
*n*CB*	*6.48*	*0.002*	*10.75*	*0.000*	0.08	0.927	*17.14*	*0.000*
*n** λ_s	*10.85*	*0.000*	*12.82*	*0.000*	*17.18*	*0.000*	*27.40*	*0.000*
*n**Scale	*9.06*	*0.000*						
*f** a_p	*26.48*	*0.000*	*29.66*	*0.000*	*8.36*	*0.000*	*16.96*	*0.000*
*f*CB*	*12.80*	*0.000*	*13.61*	*0.000*	*6.34*	*0.002*	*3.24*	*0.044*
*f** λ_s	*18.13*	*0.000*	*25.95*	*0.000*	*6.79*	*0.001*	0.46	0.635
*f**Scale	*18.80*	*0.000*						
a_p**CB*	*6.99*	*0.001*	*3.46*	*0.034*	*12.45*	*0.000*	3.00	0.055
a_p* λ_s	*12.53*	*0.000*	*15.41*	*0.000*	*5.63*	*0.004*	1.54	0.220
a_p*Scale	*6.76*	*0.000*						
*CB**Scale	*10.65*	*0.000*						
λ_s *Scale	*43.51*	*0.000*						
	R^2	R^2_{adj}	R^2	R^2_{adj}	R^2	R^2_{adj}	R^2	R^2_{adj}
	80.59%	78.40%	89.33%	87.14%	86.04%	83.42%	90.21%	86.53%

The Tukey and Fisher tests for the vibration in the axial direction is shown in the Figure 7.37. In these tests, it was possible observe that the vibration for the scales differ among themselves.

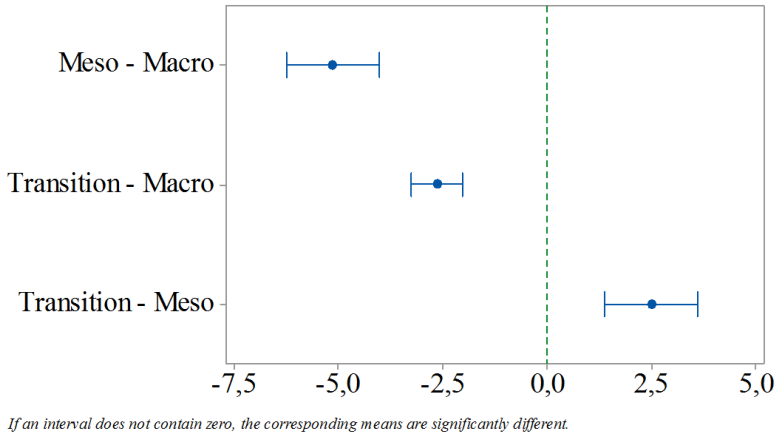

a) Tukey test.

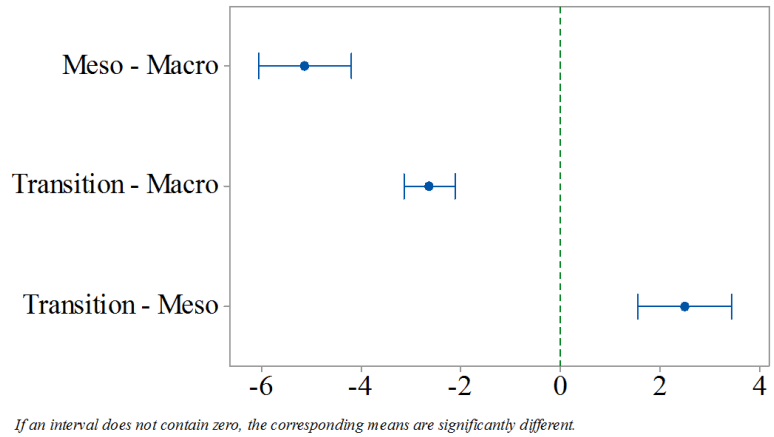

b) Fisher test.

Figure 7.37 – Comparison tests of the vibration in axial direction for all scales.

The ANOVA for same cutting speed and spindle speed range are shown in the Table 7.14. The factor “scale was significant for all spindle speed range and the cutting speed of 30 m/min. In the Figure 7.38, Figure 7.39, Figure 7.40, and Figure 7.41 are exhibited the Tukey and Fisher tests of same cutting speed and spindle speed range for different scales. Only for the spindle speed range of 1,000-2,000 and 2,000-3,000 rpm, the average between “macro and transition” and “transition and meso”, respectively, did not present significant difference.

Table 7.14 – ANOVA for the vibration in axial direction for spindle speed range and cutting speed.

Source	v_c 30 m/min		n 0-1,000 rpm		n 1,000-2,000 rpm		n 2,000-3,000 rpm	
	F-Value	P-Value	F-Value	P-Value	F-Value	P-Value	F-Value	P-Value
Feed rate (f)	*271.49*	*0.000*	*38.16*	*0.000*	*166.68*	*0.000*	*119.49*	*0.000*
Depth of cut (a_p)	*180.63*	*0.000*	*39.09*	*0.000*	*101.64*	*0.000*	*73.31*	*0.000*
Chip-breaker (CB)	*42.08*	*0.000*	*5.24*	*0.024*	0.25	0.617	*30.57*	*0.000*
Inclination angle (λ_s)	*1097.04*	*0.000*	*219.23*	*0.000*	*388.38*	*0.000*	*209.78*	*0.000*
Scale	*22.49*	*0.000*	*95.00*	*0.000*	*129.30*	*0.000*	*75.98*	*0.000*
f*a_p	*41.68*	*0.000*	*6.80*	*0.000*	*32.50*	*0.000*	*19.61*	*0.000*
f*CB	*15.68*	*0.000*	1.05	0.353	*15.78*	*0.000*	*13.07*	*0.000*
f*λ_s	*36.87*	*0.000*	2.25	0.109	*13.95*	*0.000*	*20.28*	*0.000*
f*Scale	2.21	0.071	*13.00*	*0.000*	1.61	0.176	*22.61*	*0.000*
a_p*CB	*7.52*	*0.001*	2.89	0.059	*8.87*	*0.000*	*5.33*	*0.006*
a_p* λ_s	*30.09*	*0.000*	1.52	0.223	*6.55*	*0.002*	*15.74*	*0.000*
a_p*Scale	0.22	0.926	*3.07*	*0.018*	0.87	0.485	*11.40*	*0.000*
CB*Scale	*3.58*	*0.030*	*10.17*	*0.000*	*39.45*	*0.000*	*12.08*	*0.000*
λ_s *$Scale$	*34.12*	*0.000*	*69.40*	*0.000*	*48.45*	*0.000*	*13.78*	*0.000*
	R^2	R^2_{adj}	R^2	R^2_{adj}	R^2	R^2_{adj}	R^2	R^2_{adj}
	94.81%	93.59%	86.69%	83.56%	92.90%	91.18%	84.49%	80.49%

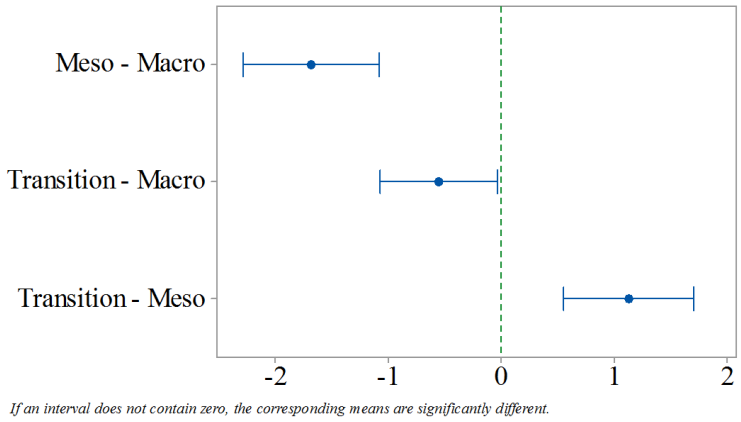

a) Tukey test.

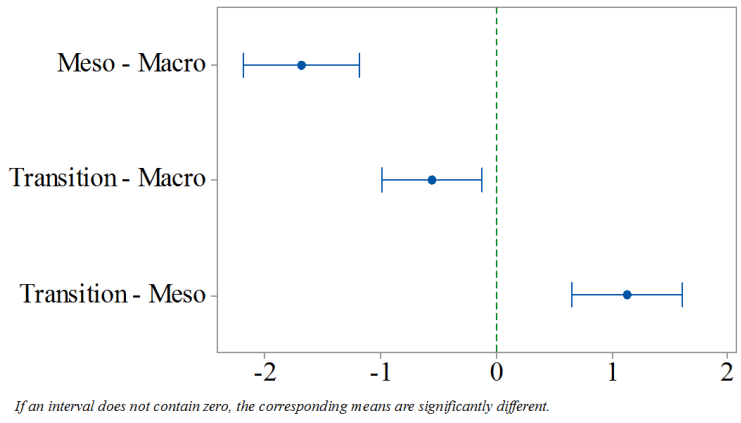

b) Fisher test.

Figure 7.38 – Comparison tests of the vibration in axial direction for same cutting speed.

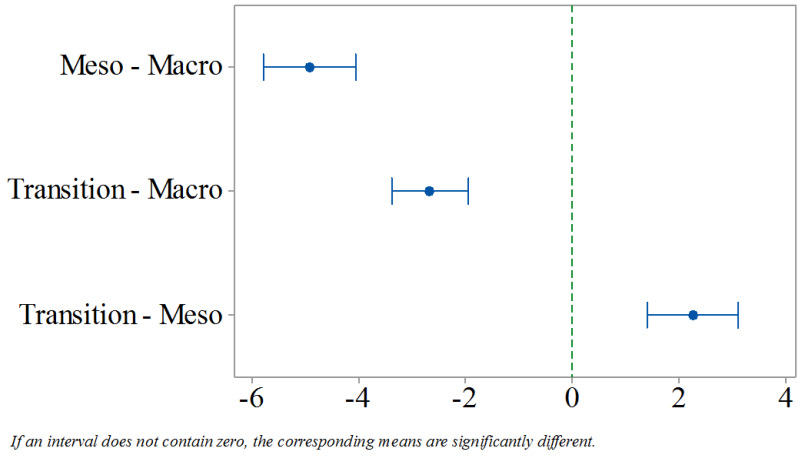

a) Tukey test.

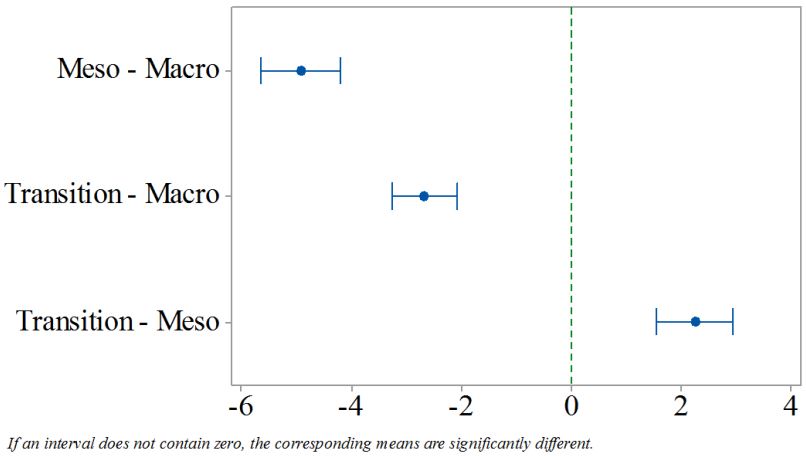

b) Fisher test.

Figure 7.39 – Comparison tests of the vibration in axial direction for spindle speed range of 0-1,000 rpm.

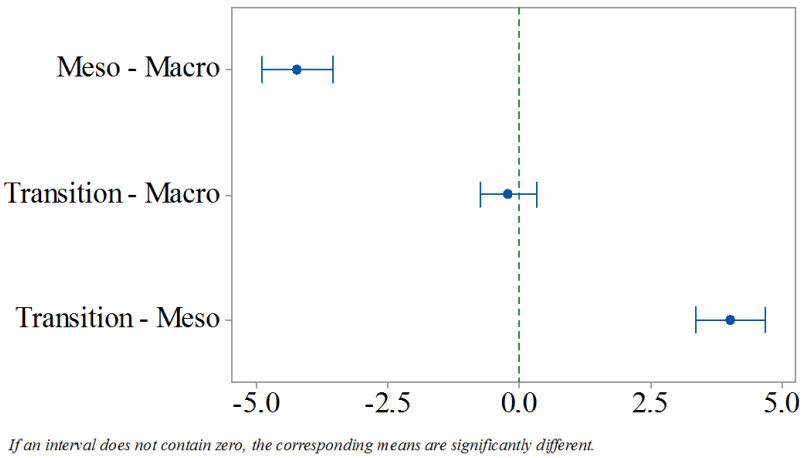

a) Tukey test.

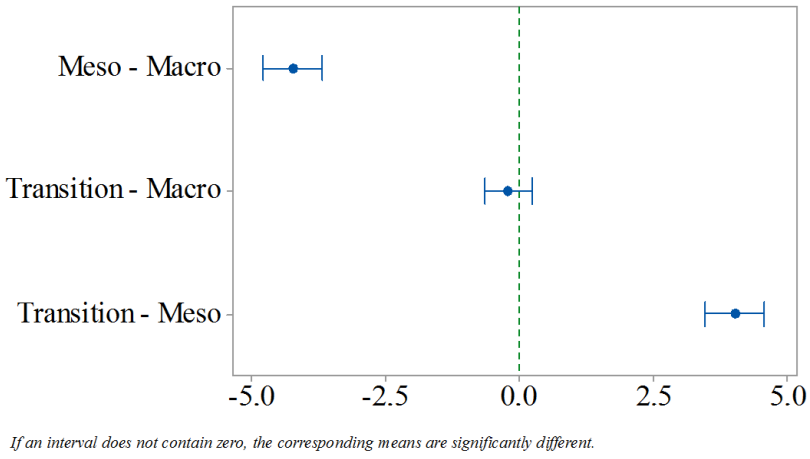

b) Fisher test.

Figure 7.40 – Comparison tests of the vibration in axial direction for spindle speed range of 1,000-2,000 rpm.

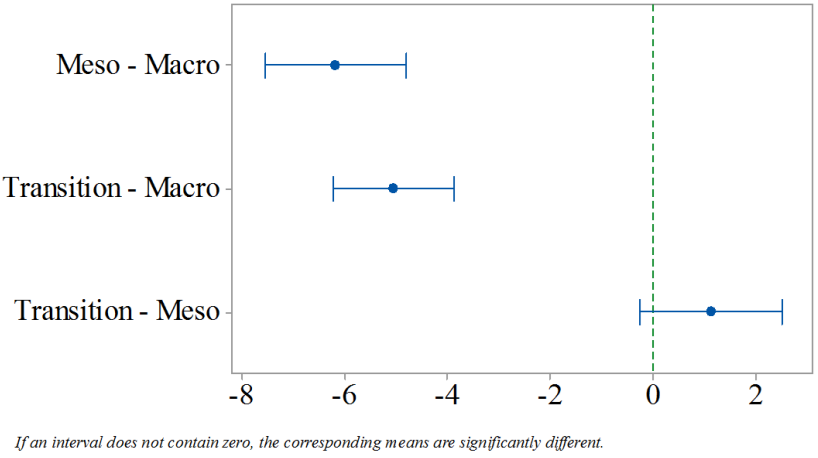

a) Tukey test.

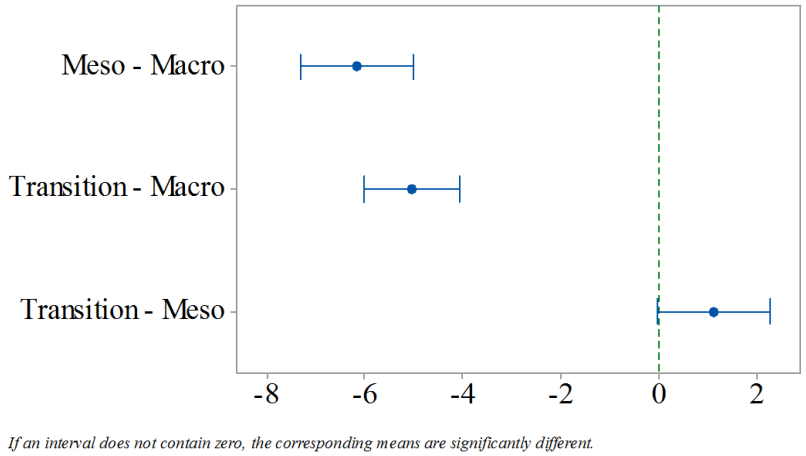

b) Fisher test.

Figure 7.41 – Comparison tests of the vibration in axial direction for spindle speed range of 2,000-3,000 rpm.

7.4.2. Vibration in the tangential direction

The Figure 7.42 shows the vibration in the tangential direction for the micro-cutting of Ti-6Al-7Nb with flat inserts for the spindle speed range of 0-1,000, 1,000-2,000, and 2,000-3,000 rpm. The increase of the feed rate and the depth of cut increased, respectively, the vibration in tangential direction in macro (64.0% and 46.6%), transition (32.5% and 27.0%), and meso (44.6% and 43.9%) scales, on average. For the rise of the spindle speed range caused increase of 36.5% (macro), 27.7% (transition), and 43.7% (meso), on average.

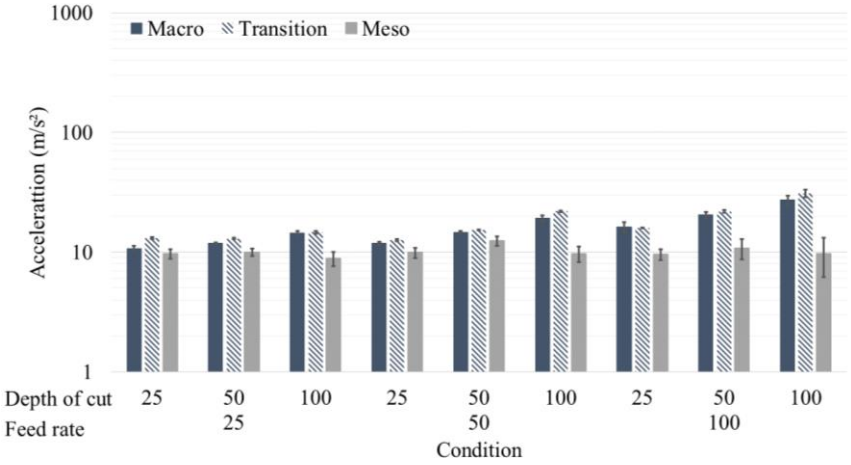

a) Spindle speed range of 0 to 1,000 rpm.

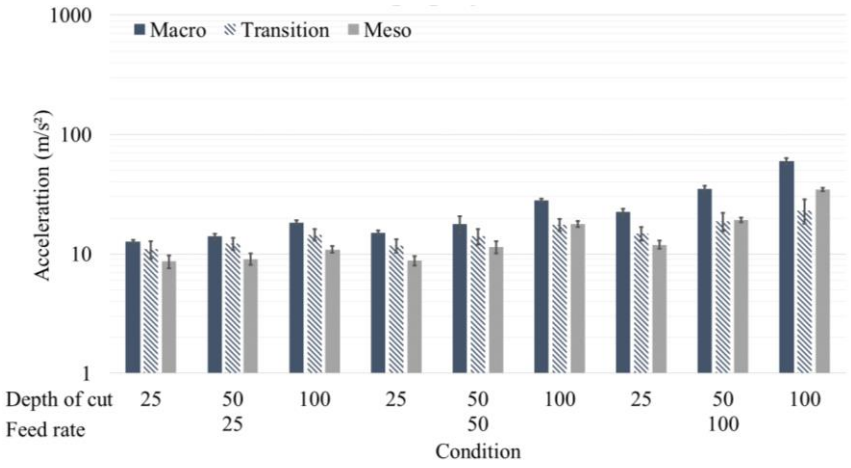

b) Spindle speed range of 1,000 to 2,000 rpm.

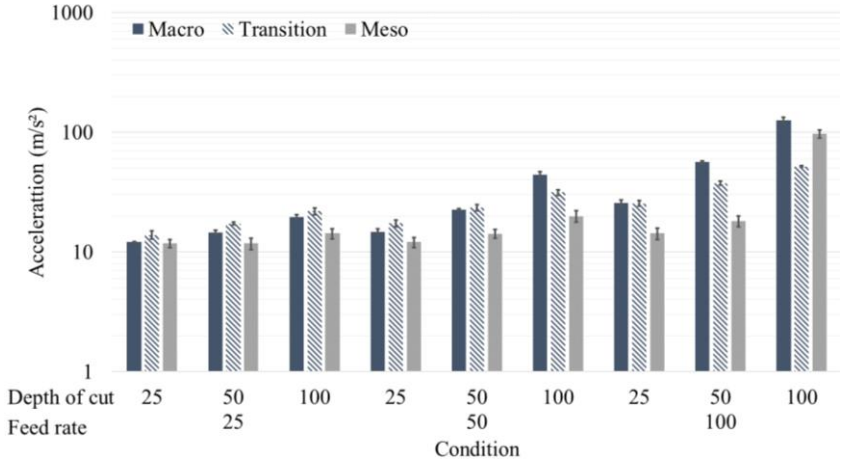

c) Spindle speed range of 2,000 to 3,000 rpm.

Figure 7.42 – Vibration in the tangential direction with flat inserts.

For the chip-breaker inserts, the surface for the vibration in the tangential direction for the spindle speed range of 1,000, 2,000, and 3,000 rpm are shown in the Figure 7.43. For the tangential direction, the increase of the feed rate and depth of cut increased, on average, the vibration in the macro (47.6% and 25.3%), transition (25.4% and 15.3%) and meso-scale (28.8% and 28.8%) scales, respectively. The rise in the spindle speed range increased in macro and transition, on average, 25.6% and 18.3%, respectively.

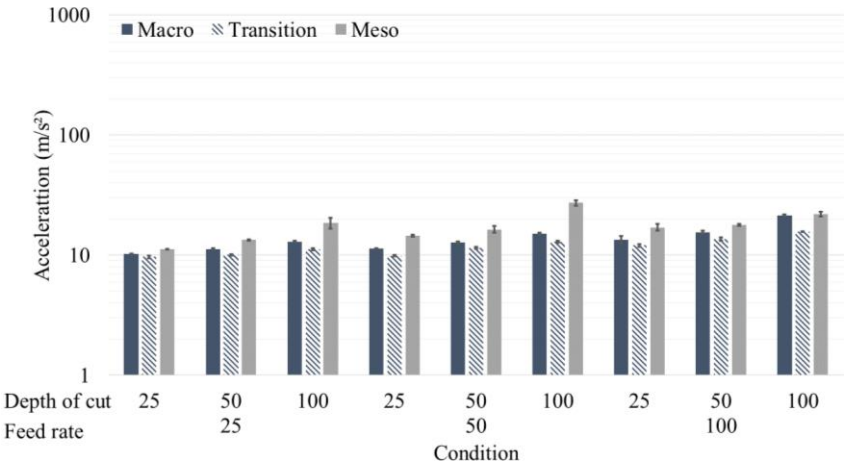

a) Spindle speed range of 0 to 1,000 rpm.

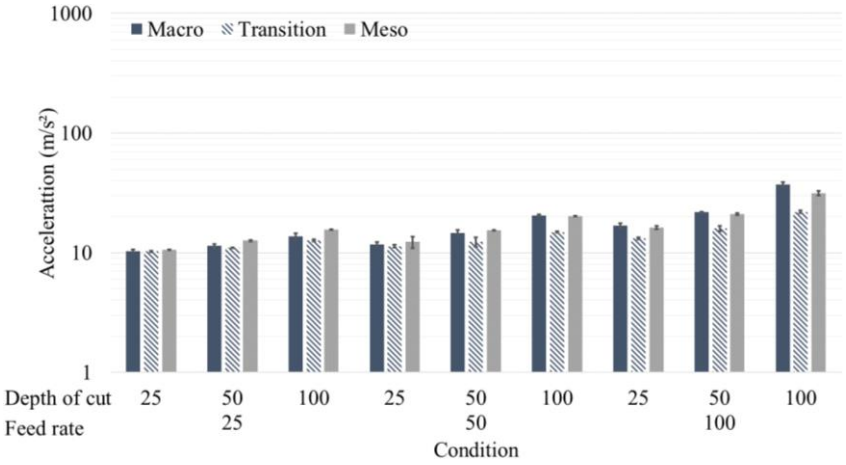

b) Spindle speed range of 1,000 to 2,000 rpm.

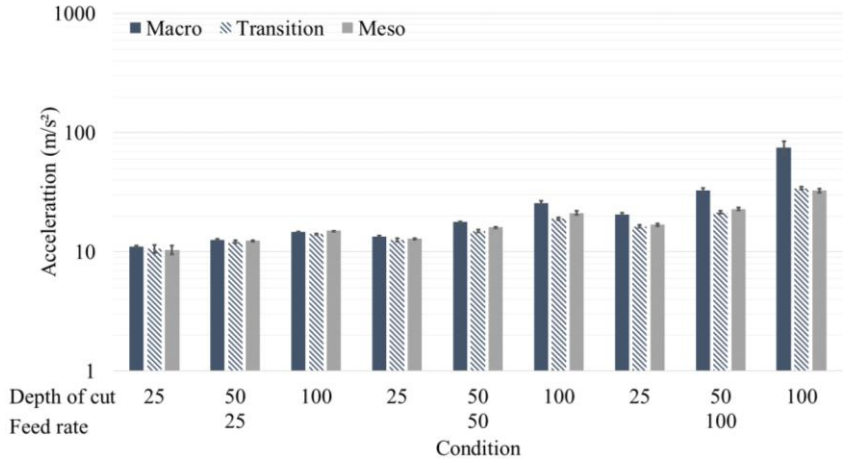

c) Spindle speed range of 2,000 to 3,000 rpm.

Figure 7.43 – Vibration in the tangential direction with chip-breaker inserts.

Figure 7.44 shows the vibration in the tangential direction for the spindle speed range of 1,000, 2,000, and 3,000 rpm employing the dual negative inserts. The increase of the feed rate and depth of cut caused a similar increase of the vibration, on average, in the tangential direction in transition (19.6% and 15.6%) meso (13.25 and 14.5%) scales, respectively. For the macro scale, it was observed a rose steeply of the vibration in the cutting for the increase of the feed rate and depth of cut, on average, 50.1% and 45.9%, respectively. For the rise of the spindle speed range, the rise from 1,000-2,000 to 2,000-3,000 caused an increase almost twice the rise from 0-1,000 to 1,000-2,000 in transition (11.6% and 6.3%) and meso (0.6% and 1.4%), on average. For the macro scale, the increase observed was greater than three times for the rise from 1,000-2,000 to 2,000-3,000 than the rise from 0-1,000 to 1,000-2,000, 111.1% and 33.0%, respectively, on average.

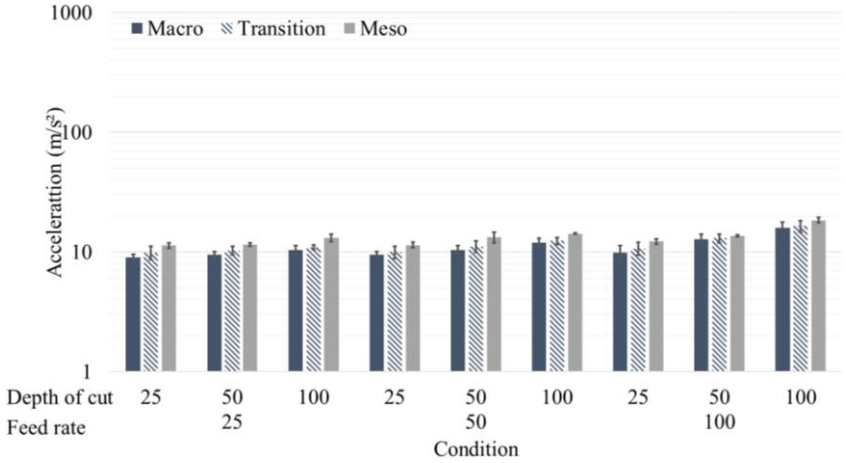

a) Spindle speed range of 0 to 1,000 rpm.

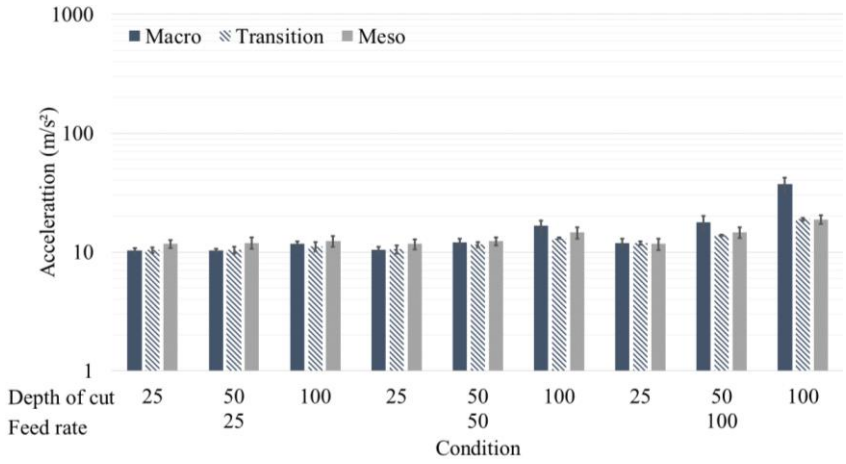

b) Spindle speed range of 1,000 to 2,000 rpm.

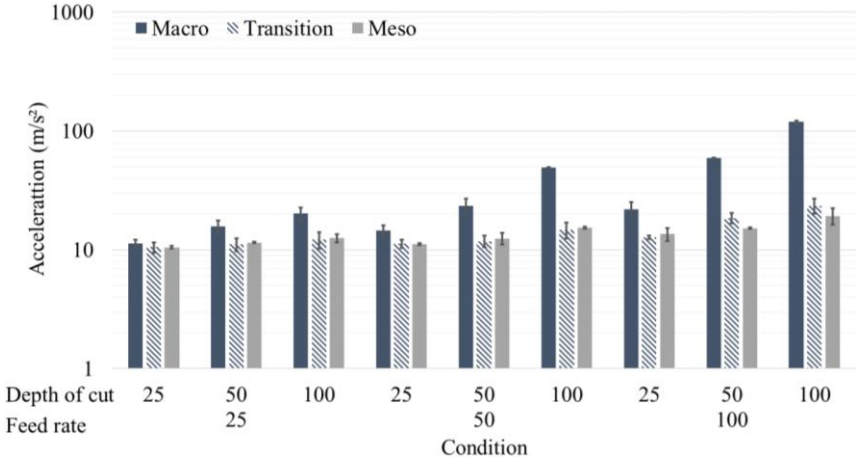

c) Spindle speed range of 2,000 to 3,000 rpm.

Figure 7.44 – Vibration in the tangential direction with dual negative inserts.

For the comparison of the reduction of the scale, the decrease from macro to transition scale caused a reduction, on average, in the vibration in the tangential direction for flat (11.1%), chip-breaker (16.0%), and dual negative (16.9%) inserts. However, the reduction from transition to meso scale, it was observed, on average, a reduction for the use of the flat insert, 23.1%, and an increase for the use of the chip-breaker (24.8%) and dual negative (6.7%) inserts. In the Table 7.15 is exhibited the ANOVA for all and individual scales. The factor "scale" was significant for the vibration in the tangential direction. The Tukey and Fisher tests are shown in the Figure 7.45. The transition and meso did not present significant difference among themselves.

Table 7.15 – ANOVA of vibration in the tangential direction for all and individual scales.

Source	All scales		Macro		Transition		Meso	
	F-Value	P-Value	F-Value	P-Value	F-Value	P-Value	F-Value	P-Value
Spindle speed range (*n*)	*78.89*	*0.000*	*144.28*	*0.000*	*132.13*	*0.000*	*6.80*	*0.002*
Feed rate (*f*)	*114.43*	*0.000*	*173.64*	*0.000*	*222.94*	*0.000*	*11.57*	*0.000*
Depth of cut (a_p)	*84.50*	*0.000*	*127.73*	*0.000*	*155.45*	*0.000*	*10.91*	*0.000*
Chip-breaker (*CB*)	*24.13*	*0.000*	*44.81*	*0.000*	*355.98*	*0.000*	0.63	0.428
Inclination angle (λ_s)	3.35	0.068	3.80	0.053	*24.13*	*0.000*	*9.49*	*0.003*
Scale	*49.43*	*0.000*						
*n*f*	*39.20*	*0.000*	*58.06*	*0.000*	*41.70*	*0.000*	*2.65*	*0.038*
n a_p*	*24.11*	*0.000*	*37.78*	*0.000*	*20.60*	*0.000*	1.38	0.246
*n*CB*	*11.03*	*0.000*	*6.42*	*0.002*	*57.55*	*0.000*	*6.41*	*0.003*
n λ_s*	*3.71*	*0.025*	*17.72*	*0.000*	*8.33*	*0.000*	0.01	0.994
*n**Scale	*21.21*	*0.000*						
f a_p*	*32.97*	*0.000*	*44.25*	*0.000*	*34.96*	*0.000*	*3.43*	*0.012*
*f*CB*	*11.61*	*0.000*	*12.67*	*0.000*	*25.71*	*0.000*	2.23	0.113
f λ_s*	0.14	0.866	1.53	0.219	2.88	0.059	1.41	0.249
*f**Scale	*22.78*	*0.000*						
*a_p*CB*	*8.37*	*0.000*	*9.17*	*0.000*	*19.64*	*0.000*	1.43	0.244
a_p λ_s*	0.10	0.904	2.54	0.081	1.64	0.197	1.32	0.272
*a_p**Scale	*14.33*	*0.000*						
*CB**Scale	*9.51*	*0.000*						
λ_s *Scale	*5.79*	*0.003*						
	R^2	R^2_{adj}	R^2	R^2_{adj}	R^2	R^2_{adj}	R^2	R^2_{adj}
	77.15%	74.92%	89.19%	87.46%	94.50%	93.51%	61.67%	47.88%

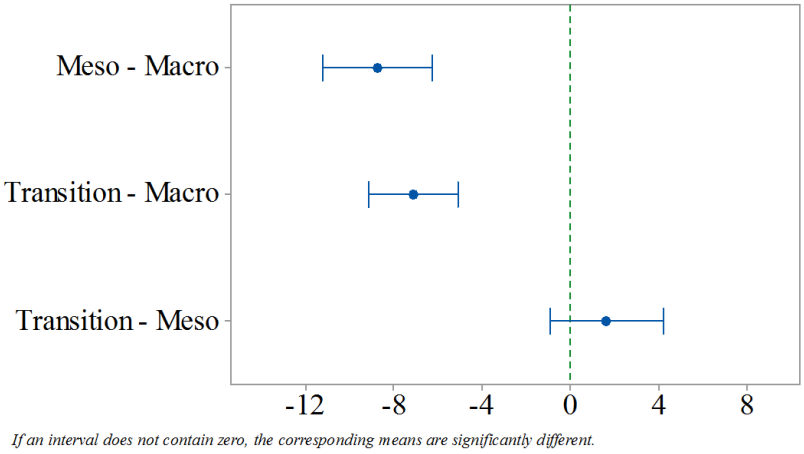

a) Tukey test.

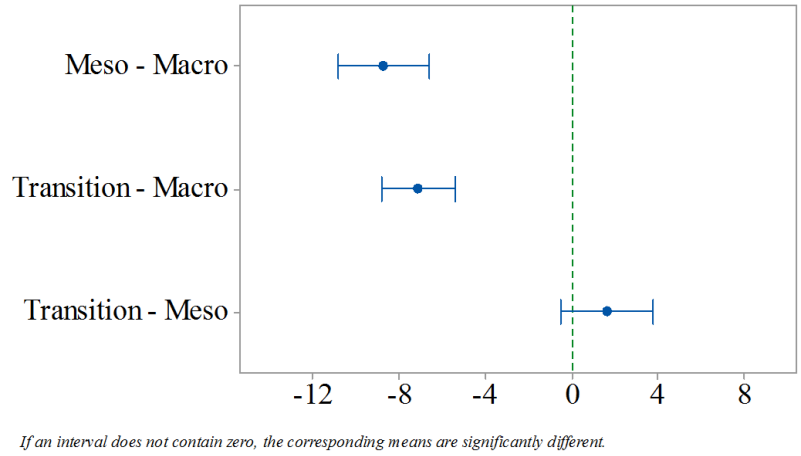

b) Fisher test.

Figure 7.45 – Comparison tests of the vibration in tangential direction for all scales.

The ANOVA of the same cutting speed and spindle speed range for all scales is exhibited in the Table 7.16. The factor “scale” was significant for all spindle speed range and the same cutting speed. The Figure 7.46, Figure 7.47, Figure 7.48, and Figure 7.49 are shown the Tukey and Fisher test for cutting speed of 30 m/min and spindle speed of 0-1,000, 1,000-2,000, and 2,000-3,000, respectively. For cutting speed of 30 m/min, the macro and transition was not differing among themselves. In the spindle speed range of 1,000-2,000, and 2,000-3,000, the meso and transition was not differing among themselves.

Table 7.16 – ANOVA for the vibration in tangential direction for spindle speed range and cutting speed.

Source	v_c 30 m/min		n 0-1,000 rpm		n 1,000-2,000 rpm		n 2,000-3,000 rpm	
	F-Value	P-Value	F-Value	P-Value	F-Value	P-Value	F-Value	P-Value
Feed rate (f)	*33.47*	*0.000*	*73.72*	*0.000*	*144.57*	*0.000*	*111.68*	*0.000*
Depth of cut (a_p)	*28.57*	*0.000*	*67.87*	*0.000*	*103.78*	*0.000*	*76.25*	*0.000*
Chip-breaker (CB)	*14.87*	*0.000*	0.78	0.380	*16.50*	*0.000*	*33.23*	*0.000*
Inclination angle (λ_s)	*11.53*	*0.001*	*49.76*	*0.000*	*23.29*	*0.000*	*0.46*	*0.500*
Scale	*9.71*	*0.000*	*18.82*	*0.000*	*82.53*	*0.000*	*57.51*	*0.000*
f*a_p	*6.60*	*0.000*	*9.77*	*0.000*	*45.03*	*0.000*	*35.62*	*0.000*
f*CB	*3.66*	*0.028*	*8.81*	*0.000*	*11.25*	*0.000*	*12.28*	*0.000*
f*λ_s	1.61	0.203	2.13	0.123	2.78	0.065	0.78	0.458
f*Scale	*4.65*	*0.001*	*4.00*	*0.004*	*34.38*	*0.000*	*27.88*	*0.000*
a_p*CB	*3.59*	*0.030*	2.69	0.071	*6.22*	*0.003*	*10.98*	*0.000*
a_p* λ_s	1.02	0.363	2.18	0.117	1.36	0.259	0.75	0.476
a_p*Scale	*4.65*	*0.001*	0.09	0.986	*19.93*	*0.000*	*19.99*	*0.000*
CB*Scale	1.80	0.169	*96.58*	*0.000*	*33.46*	*0.000*	1.52	0.222
λ_s *Scale	1.03	0.361	*11.39*	*0.000*	2.24	0.110	*13.82*	*0.000*
	R^2	R^2_{adj}	R^2	R^2_{adj}	R^2	R^2_{adj}	R^2	R^2_{adj}
	65.63%	58.88%	85.07%	82.10%	92.35%	90.74%	87.98%	85.45%

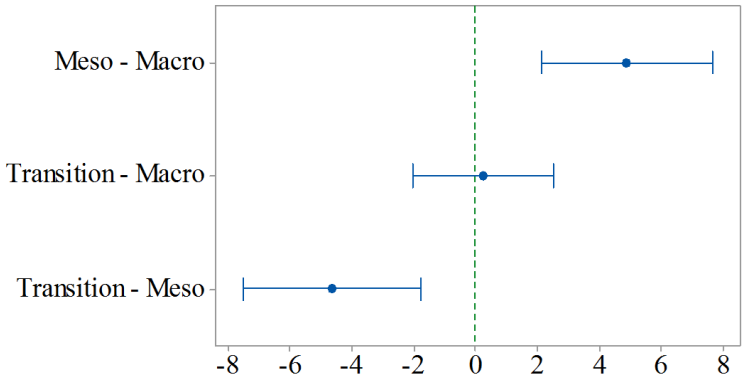

a) Tukey test.

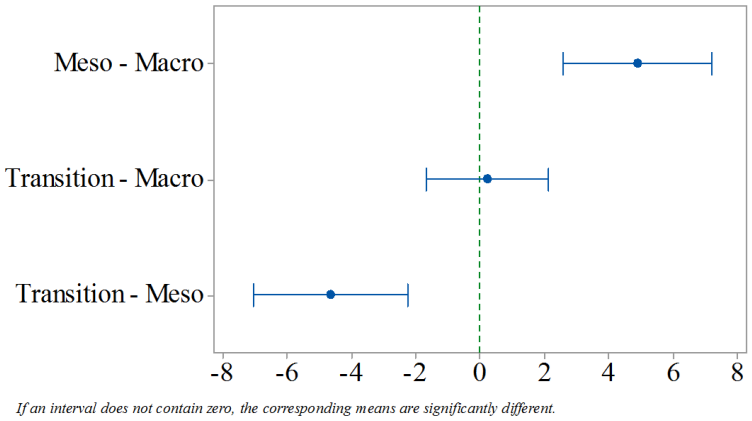

b) Fisher test.

Figure 7.46 – Comparison tests of the vibration in tangential direction for cutting speed of 30 m/min.

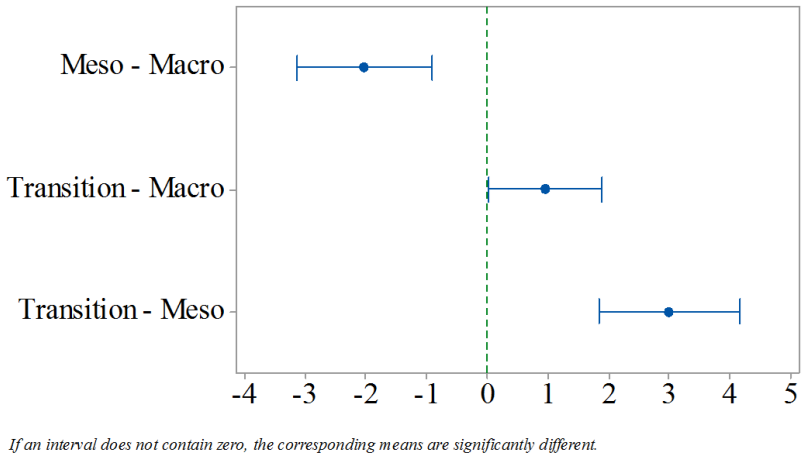

a) Tukey test.

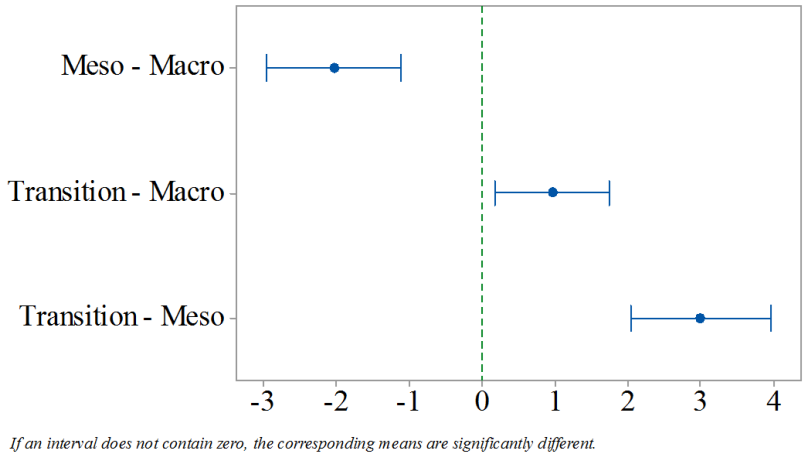

b) Fisher test.

Figure 7.47 – Comparison tests of the vibration in tangential direction for spindle speed range of 0 to 1,000.

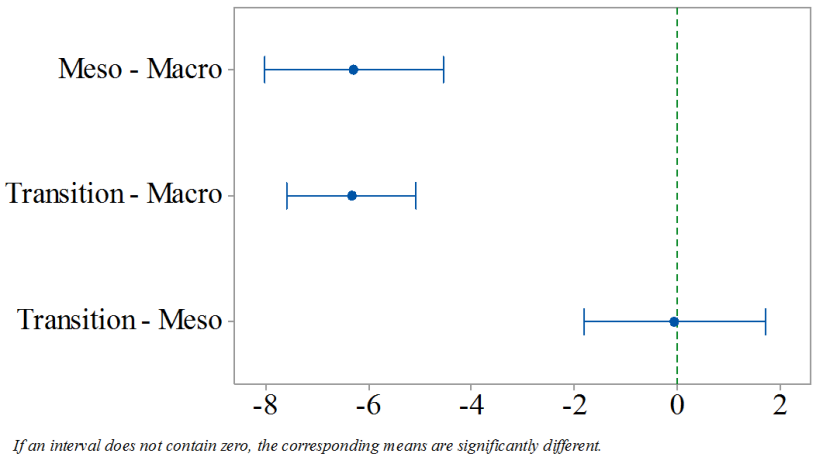

a) Tukey test.

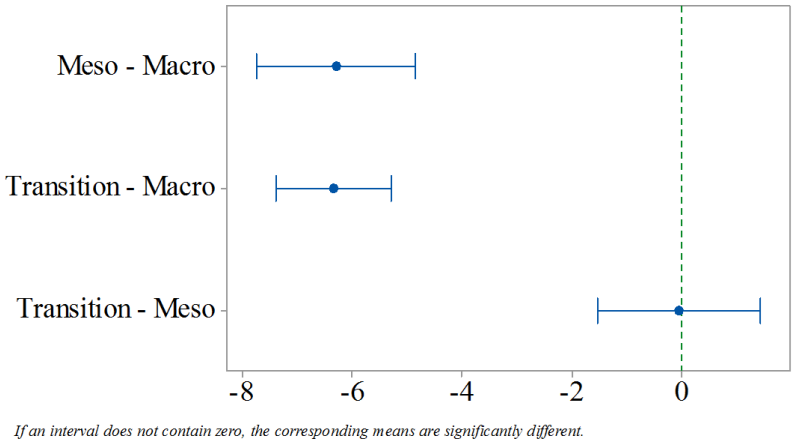

b) Fisher test.

Figure 7.48 – Comparison tests of the vibration in tangential direction for spindle speed range of 1,000 to 2,000.

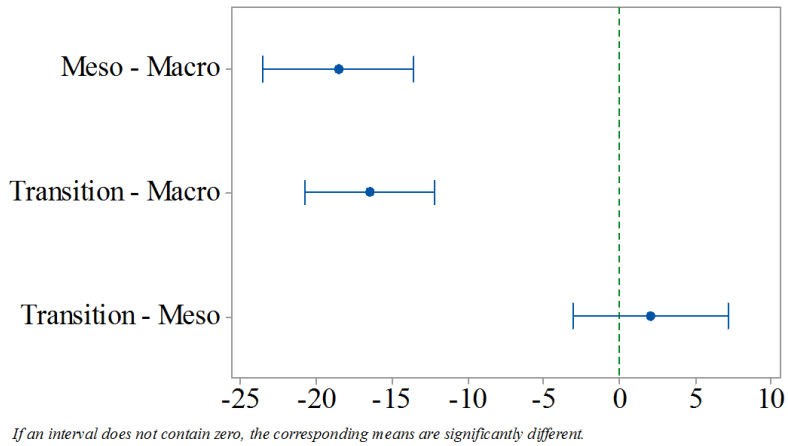

a) Tukey test.

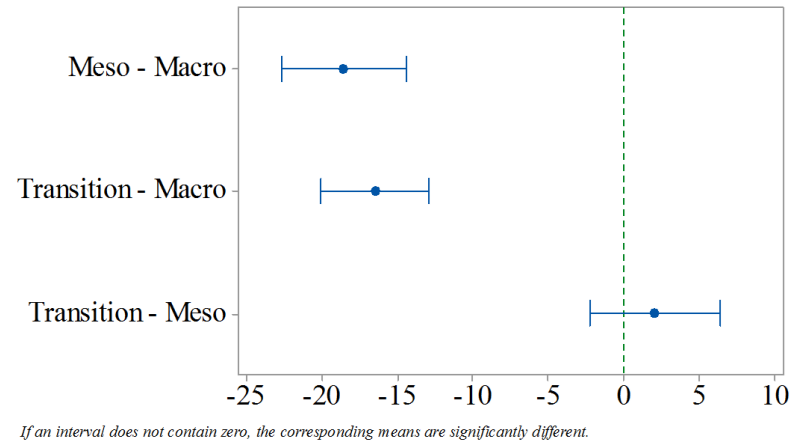

b) Fisher test.

Figure 7.49 – Comparison tests of the vibration in tangential direction for spindle speed range of 2,000 to 3,000.

7.5. Vibration in the micro-cutting (Frequency Domain)

When observed the spectrum of vibration, the higher peaks were between 0 and 25 Hz for all conditions. However, the behaviour for each condition presented a specific curve for each scale. In the Figure 7.50 and Figure 7.51 are shown the condition with lower variation between the scales for axial and tangential directions, respectively. It is obvious that the scales affected the magnitude of the vibration in the frequency domain.

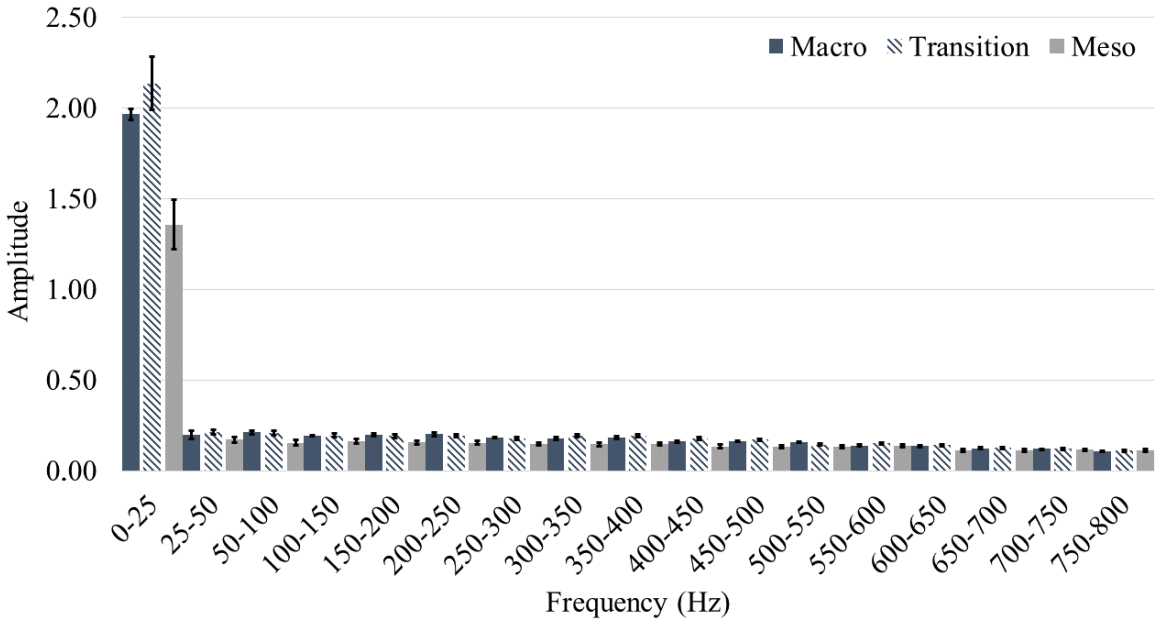

Figure 7.50 – Condition with lower variation of vibration in frequency domain for axial direction.

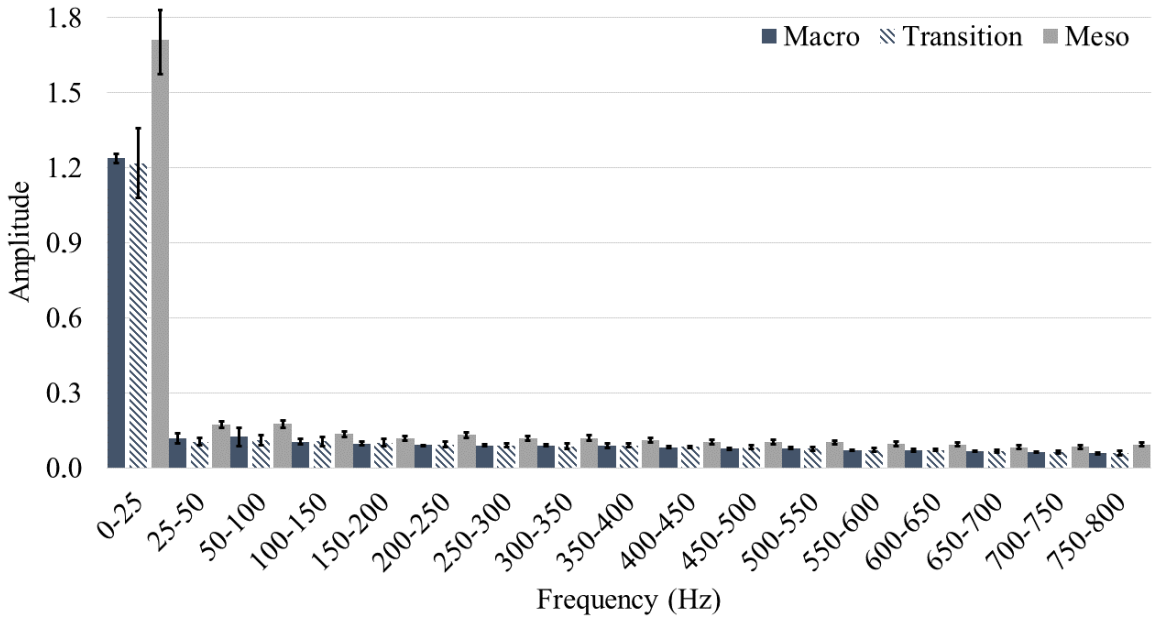

Figure 7.51 – Condition with lower variation of vibration in frequency domain for tangential direction.

7.6. Discussion

In this study, the influence of the tool wear was disregarded, although it was monitored. It is because the tool wear observed for one repetition was so small that did not affect the process, although some evidences that can be observed, Figure 7.52. Analysing the wear for V-insert, Ezugwu and Okeke (2001) observed that the wear along the nose region with adhering flake-like oxide debris was the dominant tool failure mode while micro/macro-adhesion and abrasion wear as well as plastic deformation of the sharp cutting edge are the wear mechanisms affecting tool performance, particularly at higher cutting conditions.

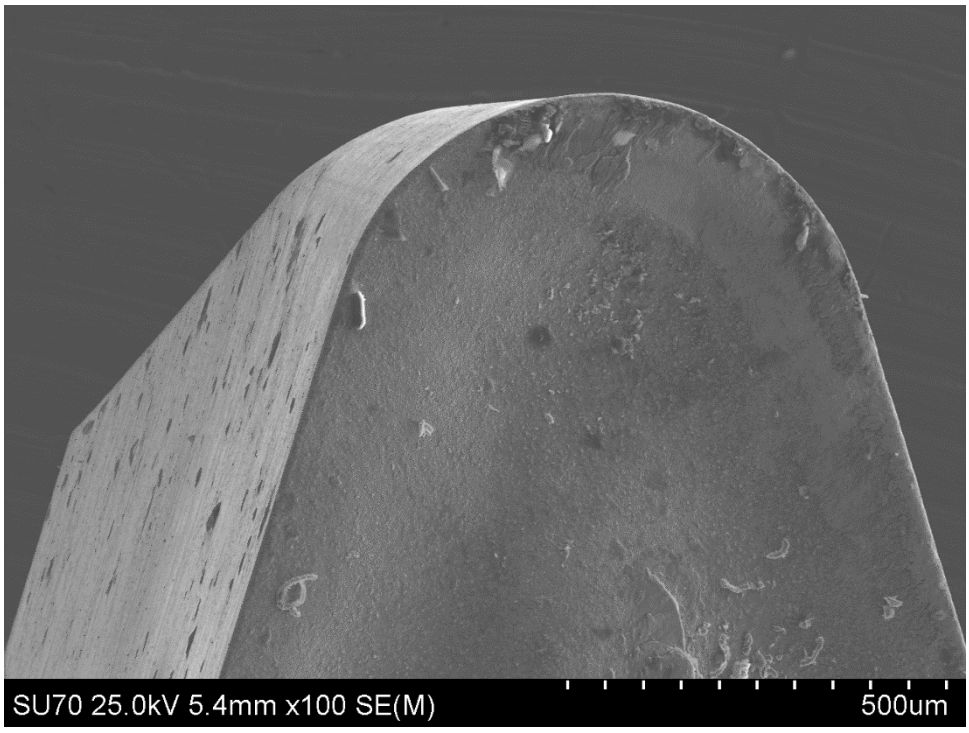

Figure 7.52 – Tool condition after one repetition.

The reduction of the cutting forces can be based on Jagadesh and Samuel (2014), which observed that the increase of the cutting speed, in the micro-turning of the Ti-6Al-4V titanium alloy, caused a reduction in the cutting forces when the uncut chip thickness was higher than the cutting edge radius because the temperature in the tool chip interface increased. The values of the F_x more than F_z can be justified based on Ducobu *et al.* (2016). These authors, in the analysis of the micro-cutting in Ti-6Al-4V titanium alloy with an uncut

chip thickness of 1 μm, observed that the thrust force is larger than the cutting force, which go against the conventional cutting theory.

The values of the surface roughness for the dual negative inserts can be influenced by the rake angle. Schneider *et al*. (2016) used the orthogonal micro-cutting to study the influence of the rake angle in micro-cutting of titanium commercial pure. They observed that an increase of the rake angle can improve the quality of the surface due to it reduce the plastic deformation in chip formation, independent of the uncut chip thickness. The dimension of texture in cutting direction was influenced by the rake angle and can be reduced with increasing rake angle.

When compared with Nogueira (2015), that analysed the finishing using the conventional parameters and MQL system, the use of micro-cutting in the finishing of Ti-6Al-7Nb titanium alloy, although the R_a values did not show perceivable difference, the cutting forces fell steeply for the F_x, between 68.7% and 71.3%, F_y, between 93.3% and 94.5%, and F_x, between 71.5% and 83.0%.

In the Table 7.17 is shown the Spearman's ρ correlation for responses. The F_x force presented a correlation with the vibration in feed direction, which can be justified because the deflection in the workpiece caused by the F_x force. For the inclination angle, the correlation can be justified due to more length of the dual negative cutting edge in contact with the workpiece.

Hessainia *et al*. (2013) analysed the vibration in hard turning, observed a strong relation between surface roughness and cutting parameters, mainly feed rate, was found, while vibrations were found to be non-significant in the Analysis of Variance performed. According to Carou *et al*. (2016)[5], the relation between surface roughness and the vibrations measured is clear in the dry machining tests, i.e., when higher vibrations are observed also higher surface roughness is measured.

[5] Self-citation

Table 7.17 – Spearman's ρ correlation for the responses of the micro-cutting in titanium alloy.

	Spindle speed	Feed rate	Depth of cut	Chip-breaker	Inclination angle	Diameter	
R_a	0.029	*0.943*	0.015	0.083	-0.101	-0.002	
R_z	0.030	*0.916*	0.024	-0.044	-0.097	-0.023	
F_x	-0.013	*0.196*	*0.482*	*-0.538*	*-0.270*	0.099	
F_y	-0.021	0.077	*0.794*	*-0.307*	*-0.221*	0.013	
F_z	-0.104	*0.314*	*0.522*	*-0.178*	*-0.475*	*-0.222*	
Deflection	*-0.270*	*0.132*	*0.339*	*-0.191*	-0.115	*-0.196*	
Vibration (tang)	*0.331*	*0.543*	*0.466*	*-0.160*	*0.243*	*0.150*	
Vibration (axial)	*0.266*	*0.381*	*0.319*	*0.189*	*-0.555*	*0.361*	

	R_a	R_z	F_x	F_y	F_z	Deflection	Vibration (tang)
R_a							
R_z	*0.938*						
F_x	*0.190*	*0.295*					
F_y	0.092	*0.182*	*0.858*				
F_z	*0.341*	*0.418*	*0.810*	*0.822*			
Deflection	0.102	*0.194*	*0.440*	*0.486*	*0.541*		
Vibration (tang)	*0.497*	*0.505*	*0.302*	*0.417*	*0.326*	*0.142*	
Vibration (axial)	*0.425*	*0.421*	*0.487*	*0.486*	*0.550*	0.053	*0.426*

7.7. Conclusion of the chapter

Based on the results of the experiments, main conclusions for the use of the micro-cutting in the finishing operation in the biomaterial are the following:

✓ Among the cutting forces components in micro-cutting, the F_x was more significant by the diameter scale. However, the F_y was not influenced by the diameter scale.

✓ For the both surface roughness profile, R_a and R_z, the scale was not significant.

✓ For the vibration in time domain in axial and tangential direction, generally, the reduction of the scale reduced the amplitudes, which can be justified due to the reduction of workpiece mass. The vibration in frequency domain indicated that each scale, the micro-cutting presents a specific behaviour.

✓ This process offers great results for the cutting forces, until one-fifteenth compared to conventional, and the tool life. The values of surface roughness in dry micro-cutting provides similar values to the conventional parameters using MQL. Thus, this process can be

classified as sustainable, reducing cost, time, and environment impact, because it presents a reduction in the consumption of oil, energy, complementary proceedings, and other.

CHAPTER 8 – CORROSION BEHAVIOUR OF MICRO-MACHINED SURFACE IN THE DENTAL APPLICATIONS

In this chapter, the quality of the micro-cutting as finished operation for the implants was analysed *in vitro* tests. The influence of finishing operation was analysed in body environment, through the corrosion using simulated of body fluid (SBF), for workpiece applied the optimum and worse condition of micro-cutting.

8.1. Machining modelling

The results of tests for the cutting forces (F_x, F_y, and F_z) and surface roughness (R_a and R_z) obtained for the diameter at meso-scale, lower than 5 mm, were modelled employed the Response Surface Method aided by the Minitab™ 17. The models obtained are presented in the Equation 8.1, 8.2, 8.3, 8.4, and 8.5 for the F_x, F_y, F_z, R_a, and R_z responses, respectively.

$$\begin{aligned} F_x = {} & 24.07 - 0.400 \cdot v_c - 0.1165 \cdot f + 0.1510 \cdot a_p - 13.58 \cdot CB - 0.298 \cdot \lambda_s \\ & + 6.51\times10^{-3} \cdot v_c^{\,2} + 0.567\times10^{-3} \cdot f^{\,2} - 0.595\times10^{-3} \cdot a_p^{\,2} + 1.066\times10^{-3} \cdot v_c \cdot f \\ & + 1.008\times10^{-3} \cdot v_c \cdot a_p - 9.1\times10^{-3} \cdot v_c \cdot CB - 1.65\times10^{-3} \cdot v_c \cdot \lambda_s + 0.698\times10^{-3} \cdot f \cdot a_p \\ & + 23.0\times10^{-3} \cdot f \cdot CB - 2.60 \cdot f \cdot \lambda_s - 50.6\times10^{-3} \cdot a_p \cdot CB - 5.22\times10^{-3} \cdot a_p \cdot \lambda_s \end{aligned} \quad \text{Equation 8.1}$$

$R^2 = 86.51\%$; $R^2_{adj} = 85.28\%$

$$\begin{aligned} F_y = {} & 5.087 - 89.4\times10^{-3} \cdot v_c - 65.5\times10^{-3} \cdot f + 46.2\times10^{-3} \cdot a_p - 2.488 \cdot CB + 12.2\times10^{-3} \cdot \lambda_s \\ & + 1.287\times10^{-3} \cdot v_c^{\,2} + 75\times10^{-6} \cdot f^{\,2} + 0.10\times10^{-3} \cdot a_p^{\,2} + 0.558\times10^{-3} \cdot v_c \cdot f \\ & + 0.754\times10^{-3} \cdot v_c \cdot a_p - 43.5\times10^{-3} \cdot v_c \cdot CB - 0.926\times10^{-3} \cdot v_c \cdot \lambda_s + 0.286\times10^{-3} \cdot f \cdot a_p \\ & + 37.53\times10^{-3} \cdot f \cdot CB - 0.143\times10^{-3} \cdot f \cdot \lambda_s - 32.34\times10^{-3} \cdot a_p \cdot CB - 3.769\times10^{-3} \cdot a_p \cdot \lambda_s \end{aligned} \quad \text{Equation 8.2}$$

$R^2 = 95.99\%$, $R^2_{adj} = 95.63\%$

$$F_z = 16.11 - 0.411 \cdot v_c - 0.1078 \cdot f + 17.4 \times 10^{-3} \cdot a_p - 7.07 \cdot CB - 0.4192 \cdot \lambda_s + 8.05 \times 10^{-3} \cdot v_c^2 + 0.168 \times 10^{-3} \cdot f^2 - 0.186 \times 10^{-3} \cdot a_p + 0.741 \times 10^{-3} \cdot v_c \cdot f + 12 \times 10^{-6} \cdot v_c \cdot a_p - 22.7 \times 10^{-3} \cdot v_c \cdot CB + 12.64 \times 10^{-3} \cdot v_c \cdot \lambda_s + 2.237 \times 10^{-3} \cdot f \cdot a_p + 54.7 \times 10^{-3} \cdot f \cdot CB - 4.379 \times 10^{-3} \cdot f \cdot \lambda_s + 26.7 \times 10^{-3} \cdot a_p \cdot CB - 10.014 \times 10^{-3} \cdot a_p \cdot \lambda_s$$ Equation 8.3

$R^2 = 95.32\%$; $R^2_{adj} = 94.90\%$

$$R_a = 0.2471 - 0.94 \times 10^{-3} \cdot v_c - 3.678 \times 10^{-3} \cdot f - 0.168 \times 10^{-3} \cdot a_p - 6.4 \times 10^{-3} \cdot CB - 2.75 \times 10^{-3} \cdot \lambda_s + 19 \times 10^{-6} \cdot v_c^2 + 96 \times 10^{-6} \cdot f^2 + 6 \times 10^{-6} \cdot a_p^2 + 1 \times 10^{-6} \cdot v_c \cdot f - 3 \times 10^{-6} \cdot v_c \cdot a_p + 1.722 \times 10^{-3} \cdot v_c \cdot CB + 86 \times 10^{-6} \cdot v_c \cdot \lambda_s - 5 \times 10^{-6} \cdot f \cdot a_p + 0.474 \times 10^{-3} \cdot f \cdot CB + 25 \times 10^{-6} \cdot f \cdot \lambda_s - 0.461 \times 10^{-3} \cdot a_p \cdot CB - 11 \times 10^{-6} \cdot a_p \cdot \lambda_s$$ Equation 8.4

$R^2 = 97.27\%$; $R^2_{adj} = 97.08\%$

$$R_z = 1.916 + 1.3 \times 10^{-3} \cdot v_c - 16.47 \times 10^{-3} \cdot f - 2.81 \times 10^{-3} \cdot a_p - 0.438 \cdot CB - 44.83 \times 10^{-3} \cdot \lambda_s + 61 \times 10^{-6} \cdot v_c^2 + 0.381 \times 10^{-3} \cdot f^2 + 33 \times 10^{-6} \cdot a_p^2 - 96 \times 10^{-6} \cdot v_c \cdot f + 11 \times 10^{-6} \cdot v_c \cdot a_p + 8.99 \times 10^{-3} \cdot v_c \cdot CB + 0.972 \times 10^{-3} \cdot v_c \cdot \lambda_s - 7 \times 10^{-6} \cdot f \cdot a_p + 4.77 \times 10^{-3} \cdot f \cdot CB + 0.323 \times 10^{-3} \cdot f \cdot \lambda_s - 0.65 \times 10^{-3} \cdot a_p \cdot CB - 69 \times 10^{-6} \cdot a_p \cdot \lambda_s$$ Equation 8.5

$R^2 = 97.27\%$; $R^2_{adj} = 97.08\%$

Where,

v_c	↔	cutting speed (7 to 30 m/min)
f	↔	feed rate (25 to 100 μm/rev)
a_p	↔	depth of cut (25 to 100 μm)
CB		chip-breaker (0 to flat and 1 to chip-breaker)
λ_s		cutting edge inclination angle (-13 or 0)

After the modelling of response, the LSM was employed to find the optimum and worse condition. In the Figure 8.1 is shown an example of the population generated to find the optimum and worse condition. The optimum and worse condition found by LSM are exhibited in the Table 8.1.

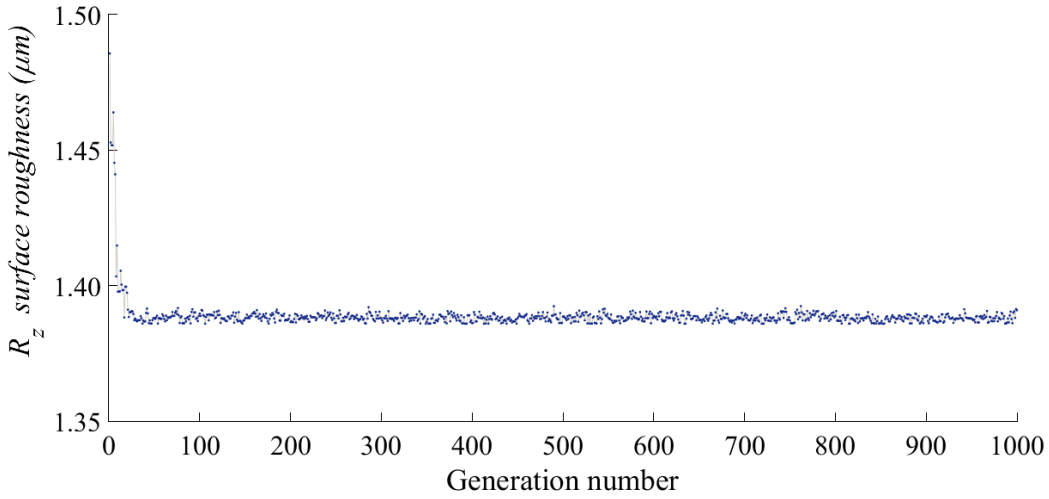

Figure 8.1 – Generation population to find the optimum condition for the R_z surface roughness.

Table 8.1 – Micro-cutting parameters for the finishing of dental implants.

Condition	Cutting speed (m/min)	Feed rate (µm/rev)	Depth of cut (µm)	Type of insert
Optimum	30	25	25	VBMT 16 04 04-UM H13A
Worse	7	100	100	VNMG 16 04 04-QM H13A

8.2. Corrosion behaviour

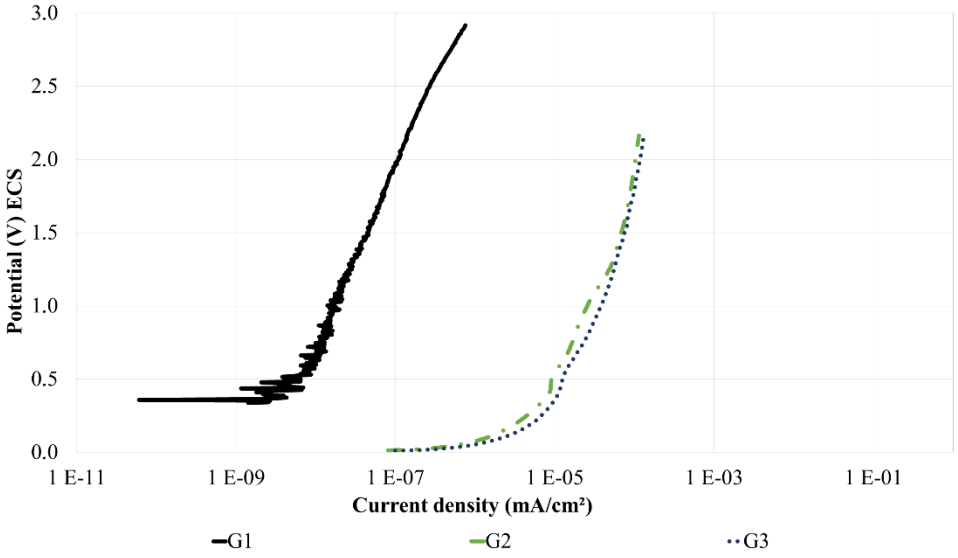

Figure 8.2 – Comparison between reference workpieces in the polarization tests.

The Figure 8.2 shows the results of the polarization to compare the reference workpieces geometry. The G1 geometry presented an initial passivation region being polarized about

0.40 V and can be observed a re-passivation of pits and the formation of the passive film, stabling a passive region about 0.50 V. The G2 and G3 geometries presented similar behaviour, passivation region being polarized about 0.00 V and did not occur the re-passivation of pits and the formation of the passive film. It can be justified because the G1 is a simple geometry, which is easier to machine.

According to Choe *et al*. (2009), in the bode analysis, a high impedance values (of 10^6 Ω cm^2) for the low and medium frequencies, indicates a high corrosion resistance. In the phase analysis, an approximating the 90º for middle and high frequency, indicating single and compact passive layer at the interface. The typical of passive materials occurs when the phase angles approaching 90º, indicating a high stable film formation (Al-Mobarak, Al-Swayih and Al-Rashoud, 2011). The Figure 8.3 and Figure 8.4 show the impedance spectra, bode (OCP) and phase (0.75 V) modulus respectively. In the bode modulus, a high impedance (> 10^5 Ω cm^2) was observed at low and medium frequencies that indicate a high corrosion resistance. In the phase modulus, the G1 curve closed to 90º at middle and high frequency, while the G2 and G3 curve approached 70º at low frequency.

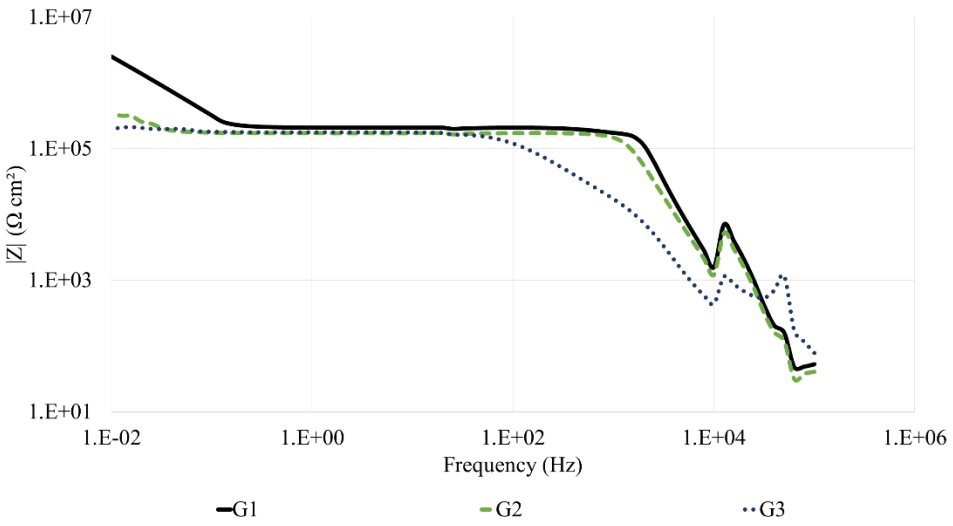

Figure 8.3 – Bode modulus for the references workpieces.

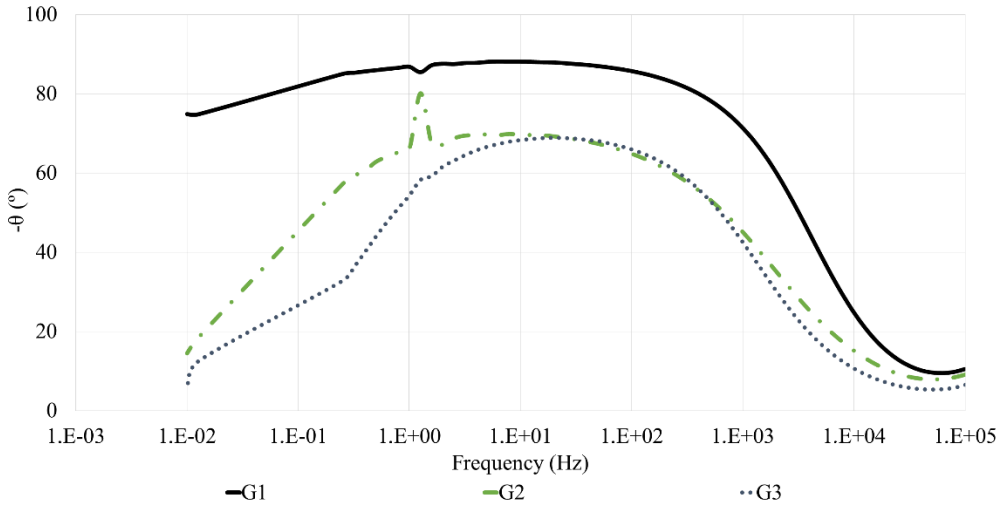

Figure 8.4 – Phase modulus for the references workpieces.

The results for the polarization, bode (OCP), and phase (0.75 V) tests for the G1 geometry are showed in the Figure 8.5, Figure 8.6, and Figure 8.7, respectively. In the impedance tests, all conditions, finished and unfinished, presented similar behaviour. In the polarization tests, the optimum finishing condition presented the worse corrosion behaviour. The worse finishing condition presented a corrosion potential higher than unfinished workpiece, after 0.7 V.

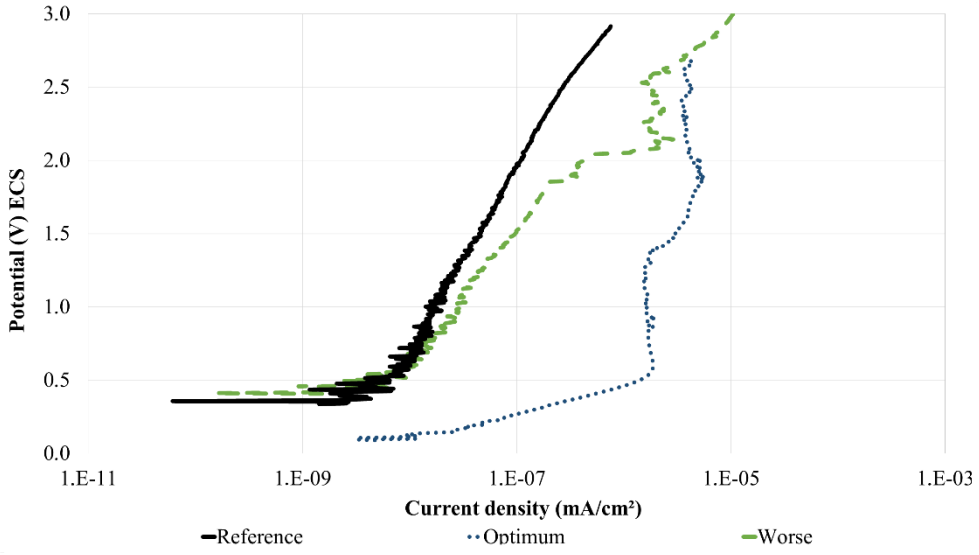

Figure 8.5 – Comparison of polarization tests for the G1 geometry.

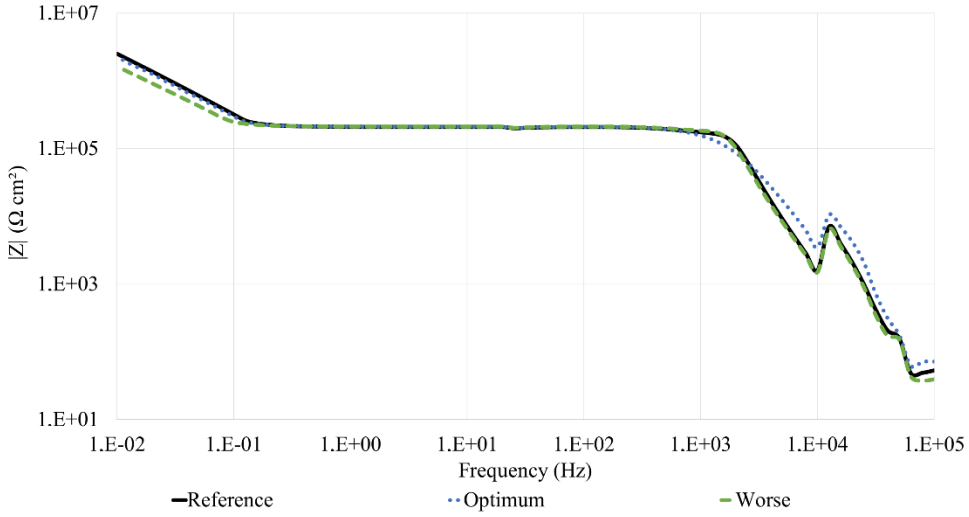

Figure 8.6 – Comparison of bode tests for the G1 geometry.

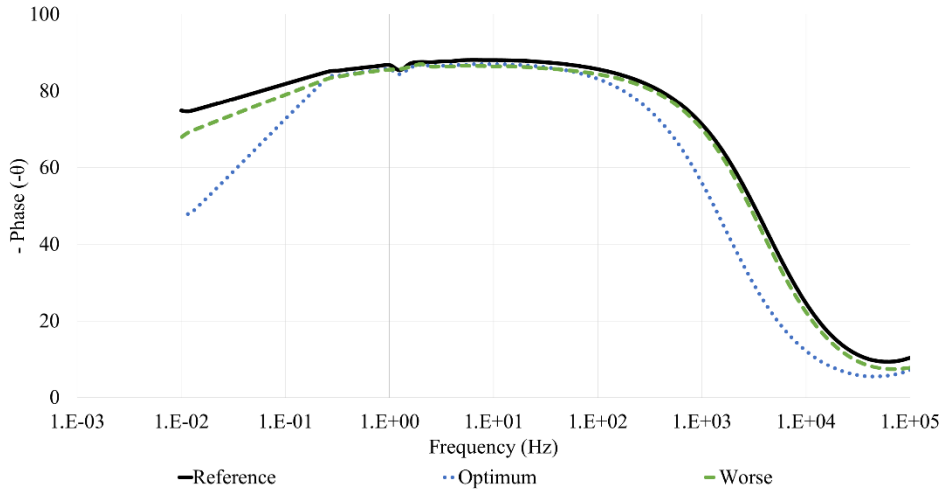

Figure 8.7 – Comparison of phase tests for the G1 geometry.

The Figure 8.8, Figure 8.9, and Figure 8.10 show the results of polarization, bode (OCP) and phase (0.75 V) tests for the G2 geometry, respectively. In the polarization tests, the finished workpieces presented re-passivation of pits and the formation of the passive film. The optimum finishing condition improved the corrosion behaviour. For the worse finishing condition, the results were better than unfinished workpiece before 0.7 V. In the bode tests, the conditions had similar corrosion behaviour. In the phase tests, an increase of the angle, about 70º, at high frequency was observed for the worse finishing condition.

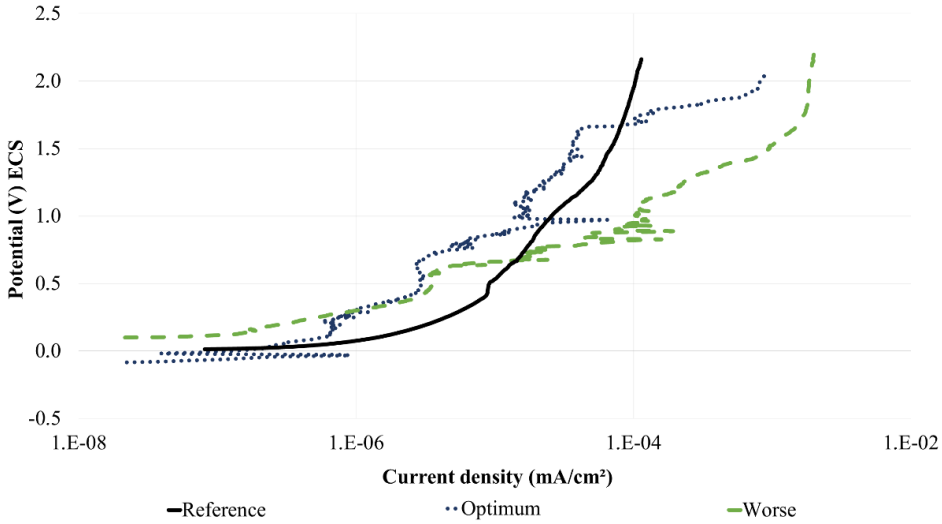

Figure 8.8 – Comparison of the polarization tests for the G2 geometry.

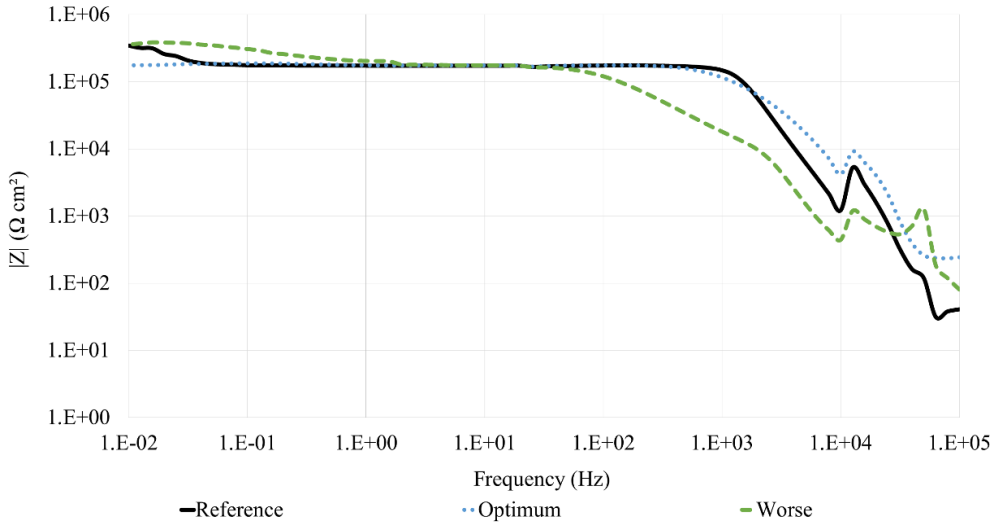

Figure 8.9 – Comparison of bode tests for the G2 geometry.

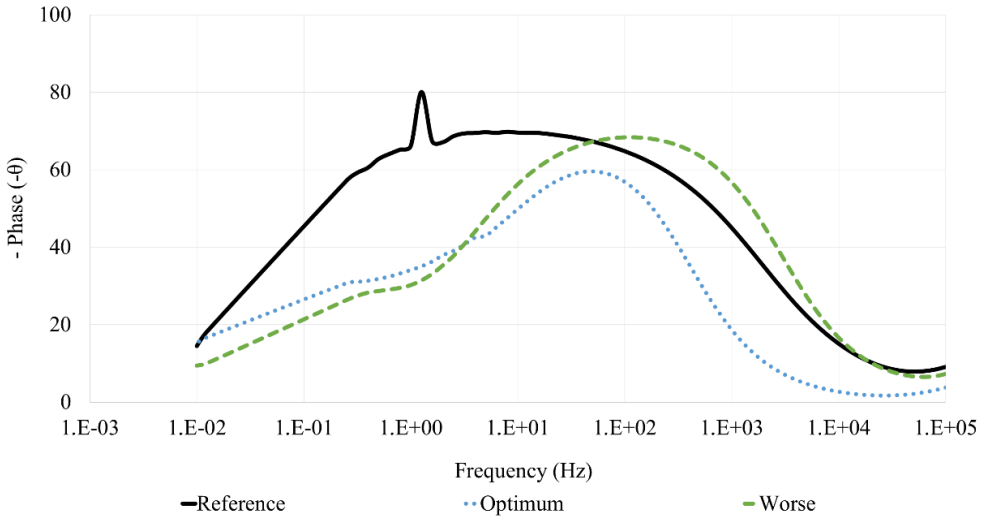

Figure 8.10 – Comparison of phase tests for the G2 geometry.

The results for the polarization, bode (OCP), and phase (0.75 V) tests for the G3 geometry are showed in the Figure 8.11, Figure 8.12, and Figure 8.13, respectively. In all tests, the worse finishing condition improved the corrosion aspects, significantly. In the bode tests can be observed a high corrosion resistance for both finished workpiece. In the phase modulus, an increase of the angle could be observed at high frequency.

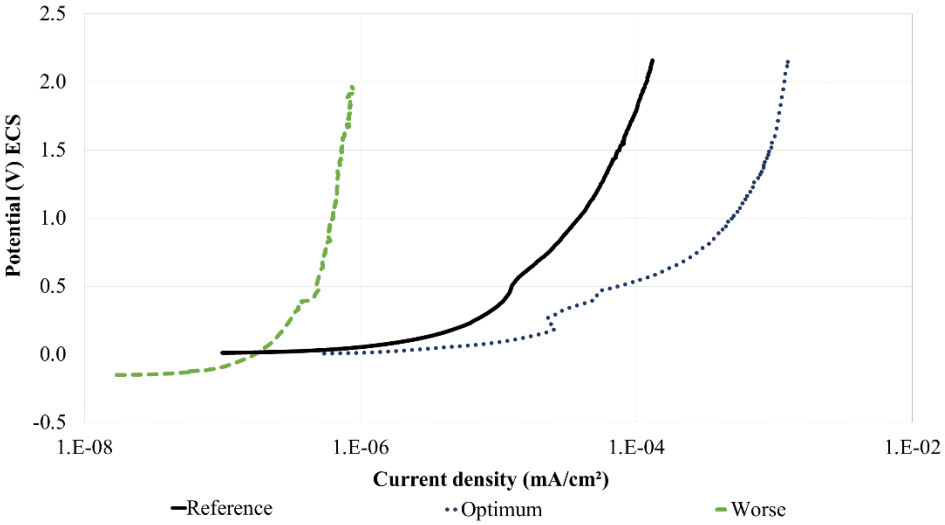

Figure 8.11 – Comparison between G3 geometry in the polarization tests.

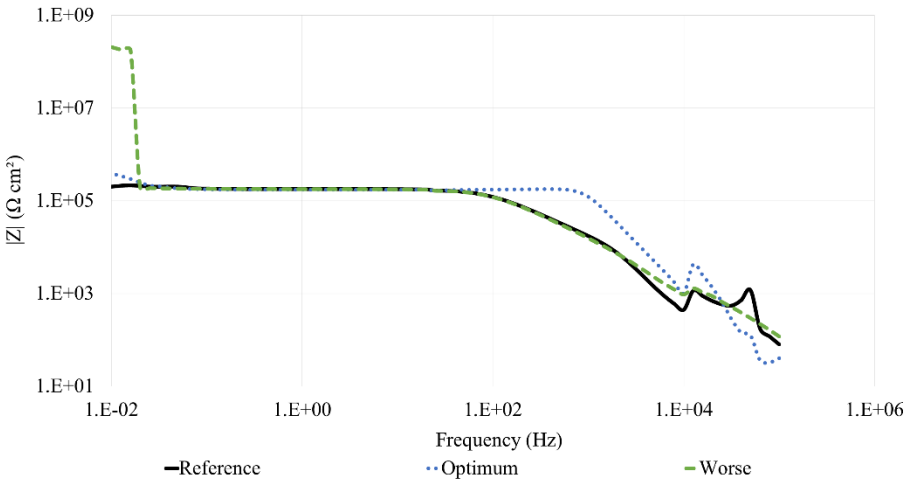

Figure 8.12 – Comparison of bode tests for the G3 geometry.

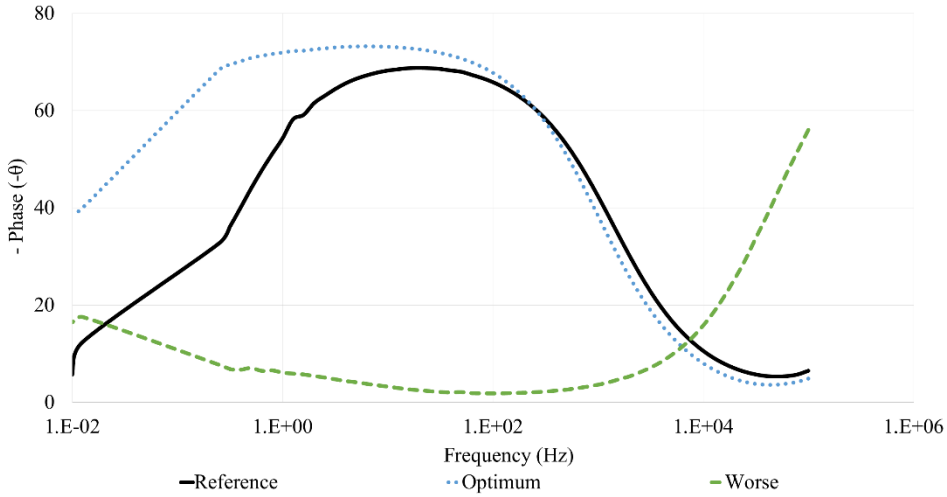

Figure 8.13 – Comparison of phase tests for the G3 geometry.

8.3. Discussion

Firstly, it is important emphasize that surface did not receive any preparation after micro-cutting. Although Basiaga *et al*. (2015) recommend the special surface preparation and low surface roughness (R_a < 0.16 µm), this study focused, only, in the influence of the micro-cutting in the Ti-6Al-7Nb titanium alloy.

For the G1 geometry, the results can be justified based on cutting forces in the section 7.3, Asad *et al*. (Asad *et al.*, 2007) and Lu and Yoneyama (1999). Because of G1 geometry has a small diameter and larger length that cause a high deflection and vibration at the furthest extremity of the chuck jaw, which affected the surface quality. Thus, the use of sharp edge tool can improve the corrosion behaviour due to it reduces the vibration and deflection in the workpiece.

The titanium and its alloys are characterized by the poor machinability, for instance, the Ti-6Al-4V has machinability of 22% (Froes, 2015). During the titanium cutting, the low area of contact produced chips very thin, stresses very high, and a very high cutting temperature (Sharma, Singh and Sørby, 2014), which can cause micro-cracks in the machined surface. When employed the optimum finishing condition, the small depth of cut may not be sufficient to remove the micro-cracks produced um the roughness machining in one pass.

Based in the section 6.3, the justification for the optimum condition present a worse corrosion behaviour can be the residual stress. The feed rate of 25 µm/rev can present a

tractive residual stress in the surface. The polishing of the workpiece can improve the corrosion behaviour for this condition.

8.4. Conclusion of the chapter

The results of the experiments for the usage of the micro-cutting as finishing operation in dental applications drawn from the study are the following:

✓ The results for the simple geometry, G1, the use of the micro-cutting did not present great efficiency, however, the use of sharp edge tool can improve the results.

✓ For the geometry "no cylindrical", G2 and G3, the use of the micro-cutting as finishing operation presented great results.

✓ The worse condition improved the corrosion behaviour in the biocomponents. The results for worse condition were better than optimum condition. It can be justified due to the depth of cut of optimum condition was so small that did not the crack and damage caused in the rough operation. The results can be improved employing the polishing and more pass in the manufacture of biocomponents.

CHAPTER 9 – CONCLUSIONS

In this chapter it is shown the conclusion and debated future work about the use of the micro-cutting as finishing operation.

9.1. Conclusions

This study provides a contribution to understanding the micro-cutting process, mainly for biocomponents that is usual components in small size. When analysed and compared all chapters, the following conclusions can be drawn:

✓ Although the high spindle speed is used in the micro-machining, the use of tools with smaller dimension result in lower values of cutting speed. Thus, in the literature, the use of the "rpm" as cutting speed is commonly found. However, these factors cause a discussion about the high speed cutting in the micromachining. The comparison in the orthogonal micro-cutting showed that, for same cutting speed, the increase of the spindle speed improved the cutting phenomena, such as specific cutting energy, shear plane angle, friction coefficient, temperature. For the oblique micro-cutting in different size scales, the surface roughness (R_a and R_z) presented the same values for same spindle speed range. The cutting force, except the *Fy* force, and vibration varied for different size scales, but, it is related to deflection of the workpiece.

✓ The use of the micro-cutting in the finishing operation can be classified as environmentally friendly machining technique. It is because the better results were obtained in dry condition. The use of the MQL system, although it reduced the burr formation, caused adherence of micro-chip and slip of the tool damaging the micro-machined surface. Furthermore, the micro-cutting caused lower deflection of the workpiece than the finishing operation using conventional conditions, besides, the cutting forces were lower than the conventional conditions. The values of surface roughness were much lower than the conventional, which would result in low polishing costs and time.

✓ The titanium and its alloy are widely used in several applications due to they provided a high mechanical property with low density. In the biomedical sector, the titanium and its alloy are widely used because the high compatibility with the body environment, however, in this sector, the components require fullest possible surface quality, smallest burr and surface roughness. However, the titanium and its alloy are poor machinability material, in other words, the cutting in the titanium and its alloy requires high cutting power and can occur metallurgic alterations in the machined surface.

✓ The micro-cutting used for finishing operation in bioapplications can prolong the life of the components and ensure patient health. The analysis developed in this study, the finishing operation with one pass and without polishing, caused a great improvement in the corrosion behaviour of the workpieces.

9.2. Future works

Although this study tried to develop all analysis to understand the influence of the micro-cutting in the finishing of the Ti-6Al-7Nb titanium alloy, others analysis will able to improve this understanding.

✓ The characterization of the wear and the influence of the worn tool.

✓ The corrosion behaviour for the implants machined with the sharp edge tool due to it reduces the vibration, surface roughness, and deflection in the micro-cutting.

✓ The analysis of the corrosion behaviour using simulated of salivary, normal and smoker, as "*in vivo*" analysis.

✓ The improvement of the material modelling to development of this micro-cutting using the 3D model FEM to analyse the residual stresses and the temperatures, for example.

✓ The analysis of the adherence of biomedical coating in the micro-machined surface, such as tantalum oxide.

✓ Furthermore, the study of this technique employed in hardness material, like AISI H13 and D2, to prolong the life of the mould and die.

REFERENCES

ABELLAN-NEBOT, J. V.; SUBIRÓN, F. R. - A review of machining monitoring systems based on artificial intelligence process models. **The International Journal of Advanced Manufacturing Technology**. . ISSN 0268-3768. 47:1–4 (2010) 237–257. doi: 10.1007/s00170-009-2191-8.

ABU-ZAHRA, N. H.; LANGE, J. H. - Tool chatter monitoring in turning operations using wavelet analysis of ultrasound waves. **The International Journal of Advanced Manufacturing Technology**. . ISSN 0268-3768. 20:4 (2002) 248–254. doi: 10.1007/s001700200149.

AFAZOV, S. M. *et al.* - Effects of micro-milling conditions on the cutting forces and process stability. **Journal of Materials Processing Technology**. . ISSN 09240136. 213:5 (2013) 671–684. doi: 10.1016/j.jmatprotec.2012.12.001.

AGARWAL, R.; GARCÍA, A. J. - Biomaterial strategies for engineering implants for enhanced osseointegration and bone repair. **Advanced Drug Delivery Reviews**. . ISSN 1872-8294. 94:2015) 53–62. doi: 10.1016/j.addr.2015.03.013.

AGUSTINA, B. De *et al.* - Experimental analysis of the cutting forces obtained in dry turning processes of UNS A97075 aluminium alloys. **Procedia Engineering**. . ISSN 18777058. 63:2004 (2013) 694–699. doi: 10.1016/j.proeng.2013.08.248.

AKKUŞ, H.; ASILTURK, İ. - Predicting surface roughness of AISI 4140 steel in hard turning process through artificial neural network, fuzzy logic and regression models. **Scientific Research and Essays**. . ISSN 1992-2248. 6:13 (2011) 2729–2736. doi: 10.5897/SRE11.120.

AL-MOBARAK, N. A.; AL-SWAYIH, A. A.; AL-RASHOUD, F. A. - Corrosion behavior of Ti-6Al-7Nb alloy in biological solution for dentistry applications. **International**

Journal of Electrochemical Science. ISSN 1452-3981. 6:June (2011) 2031–2042.

ALTAN, T.; LILLY, Blaine; YEN, Y. C. - Manufacturing of dies and molds. **CIRP Annals - Manufacturing Technology**. . ISSN 0007-8506. 50:2 (2001) 404–422. doi: 10.1016/S0007-8506(07)62988-6.

ANDRADE, D. P. De *et al.* - Titanium-35niobium alloy as a potential material for biomedical implants: In vitro study. **Materials Science & Engineering. C, Materials for Biological Applications**. . ISSN 1873-0191. 56:2015) 538–44. doi: 10.1016/j.msec.2015.07.026.

ANEIRO, F. M.; COELHO, R. T.; BRANDÃO, L. C. - Turning hardened steel using coated carbide at high cutting speeds. **Journal of the Brazilian Society of Mechanical Sciences and Engineering**. . ISSN 1678-5878. 30:2 (2008) 104–109. doi: 10.1590/S1678-58782008000200002.

ARAMCHAROEN, A.; MATIVENGA, P. T. - Size effect and tool geometry in micromilling of tool steel. **Precision Engineering**. . ISSN 01416359. 33:4 (2009) 402–407. doi: 10.1016/j.precisioneng.2008.11.002.

ARRAZOLA, P. J.; ARRIOLA, I.; DAVIES, M. A. - Analysis of the influence of tool type, coatings, and machinability on the thermal fields in orthogonal machining of AISI 4140 steels. **CIRP Annals - Manufacturing Technology**. . ISSN 00078506. 58:1 (2009) 85–88. doi: 10.1016/j.cirp.2009.03.085.

ARRAZOLA, P. J.; ÖZEL, T. - Investigations on the effects of friction modeling in finite element simulation of machining. **International Journal of Mechanical Sciences**. . ISSN 00207403. 52:1 (2010) 31–42. doi: 10.1016/j.ijmecsci.2009.10.001.

ARSECULARATNE, J. A. - On tool - Chip interface stress distributions, ploughing force and size effect in machining. **International Journal of Machine Tools & Manufacture. ISSN: 0890-6955**. 37:7 (1997) 885–899. doi: 10.1016/S0890-6955(97)00001-1.

ASAD, A. B. M. A. *et al.* - Tool-based micro-machining. **Journal of Materials Processing Technology**. . ISSN 09240136. 192–193:2007) 204–211. doi: 10.1016/j.jmatprotec.2007.04.038.

ASHIDA, M. *et al.* - Superplasticity in the Ti–6Al–7Nb alloy processed by high-pressure torsion. **Materials Science and Engineering: A**. . ISSN 09215093. 640:2015) 449–453. doi: 10.1016/j.msea.2015.06.020.

ASILTÜRK, İ.; AKKUŞ, H. - Determining the effect of cutting parameters on surface roughness in hard turning using the Taguchi method. **Measurement**. . ISSN 02632241. 44:9 (2011) 1697–1704. doi: 10.1016/j.measurement.2011.07.003.

ASTAKHOV, Viktor P.; SHVETS, S. - The assessment of plastic deformation in metal cutting. **Journal of Materials Processing Technology**. . ISSN 09240136. 146:2 (2004) 193–202. doi: 10.1016/j.jmatprotec.2003.10.015.

ATT, W.; STAPPERT, C. - Implant therapy to improve quality of life. **Quintessence International**. 34:8 (2003) 573–581.

ATTANASIO, A. *et al.* - Tool wear effects on white and dark layer formation in hard turning of AISI 52100 steel. **Wear**. . ISSN 00431648. 286–287:2012) 98–107. doi: 10.1016/j.wear.2011.07.001.

AXINTE, D. A.; DEWES, R. C. - Surface integrity of hot work tool steel after high speed milling-experimental data and empirical models. **Journal of Materials Processing Technology**. . ISSN 09240136. 127:3 (2002) 325–335. doi: 10.1016/S0924-0136(02)00282-0.

AZO MATERIAL - **Titanium Alloys** [Em linha], atual. 2016. [Consult. 21 dez. 2016]. Disponível em WWW:<URL:http://www.azom.com/properties.aspx?ArticleID=2064>.

BABU, M. K.; CHETTY, O. V. K. - A study on the use of single mesh size abrasives in abrasive waterjet machining. **The International Journal of Advanced Manufacturing Technology**. . ISSN 0268-3768. 29:5 (2006) 532–540. doi: 10.1007/s00170-005-2536-x.

BAGCI, E.; OZCELIK, B. - Analysis of temperature changes on the twist drill under different drilling conditions based on Taguchi method during dry drilling of Al 7075-T651. **The International Journal of Advanced Manufacturing Technology**. . ISSN 0268-3768. 29:7–8 (2005) 629–636. doi: 10.1007/s00170-005-2569-1.

BALAMURUGAN, A. *et al.* - Corrosion aspects of metallic implants - An overview. **Materials and Corrosion**. . ISSN 09475117. 59:11 (2008) 855–869. doi: 10.1002/maco.200804173.

BALDO, D. *et al.* - Analysis of Surface Roughness in Micro Milling of Ti-6Al-4V Titanium Alloy. **Advanced Materials Research**. . ISSN 1662-8985. 1079–1080:2015) 3–6. doi: 10.4028/www.scientific.net/AMR.1079-1080.3.

BALOGUN, V. A. *et al.* - Specific energy based evaluation of machining efficiency. **Journal of Cleaner Production**. 116:2016) 187–197. doi: 10.1016/j.jclepro.2015.12.106.

BARREIROS, I. D. *et al.* - Five-year survey of the activities of the course in implant prosthodontics from the UFMG School of Dentistry. **Arquivos em Odontologia**. . ISSN 1516-0939. 47:2011) 114–118.

BASIAGA, M. *et al.* - Impact of Surface Modification of Ti-6Al-7Nb Alloy on Electrochemical Properties in the Environment of Artificial Blood Plasma. **Solid State Phenomena**. . ISSN 1662-9779. 227:2015) 491–494. doi: 10.4028/www.scientific.net/SSP.227.491.

BASSIUNY, A. M.; LI, Xiaoli - Flute breakage detection during end milling using Hilbert–Huang transform and smoothed nonlinear energy operator. **International Journal of Machine Tools & Manufacture**. . ISSN 08906955. 47:6 (2007) 1011–1020. doi: 10.1016/j.ijmachtools.2006.06.016.

BENARDOS, P. G.; VOSNIAKOS, G. C. - Predicting surface roughness in machining: a review. **International Journal of Machine Tools & Manufacture**. . ISSN 08906955. 43:8 (2003) 833–844. doi: 10.1016/S0890-6955(03)00059-2.

BERUVIDES, Gerardo *et al.* - Sensoring systems and signal analysis to monitor tool wear in microdrilling operations on a sintered tungsten–copper composite material. **Sensors and Actuators A: Physical**. . ISSN 09244247. 199:2013) 165–175. doi: 10.1016/j.sna.2013.05.021.

BHASKARAN, J. *et al.* - Monitoring of hard turning using acoustic emission signal. **Journal of Mechanical Science and Technology**. . ISSN 1738-494X. 26:2 (2012) 609–

615. doi: 10.1007/s12206-011-1036-1.

BHATTACHARYA, A. *et al.* - Estimating the effect of cutting parameters on surface finish and power consumption during high speed machining of AISI 1045 steel using Taguchi design and ANOVA. **Production Engineering**. . ISSN 0944-6524. 3:1 (2008) 31–40. doi: 10.1007/s11740-008-0132-2.

BHENDE, A. R.; AWARI, G. K.; UNTAWALE, S. P. - Assessment of bearing fault detection using vibration signal analysis. **VSRD Technical & Non-Technical Journal**. 2:5 (2011) 249–261.

BHOWMICK, S.; LUKITSCH, M. J.; ALPAS, A. T. - Tapping of Al–Si alloys with diamond-like carbon coated tools and minimum quantity lubrication. **Journal of Materials Processing Technology**. . ISSN 09240136. 210:15 (2010) 2142–2153. doi: 10.1016/j.jmatprotec.2010.07.032.

BISSACCO, G.; HANSEN, H. N.; CHIFFRE, L. DE - Micromilling of hardened tool steel for mould making applications. **Journal of Materials Processing Technology**. . ISSN 09240136. 167:2–3 (2005) 201–207. doi: 10.1016/j.jmatprotec.2005.05.029.

BISU, C. F. *et al.* - Envelope dynamic analysis: a new approach for milling process monitoring. **The International Journal of Advanced Manufacturing Technology**. . ISSN 0268-3768. 62:5–8 (2011) 471–486. doi: 10.1007/s00170-011-3814-4.

BODZIAK, S. *et al.* - Surface integrity of moulds for microcomponents manufactured by micromilling and electro-discharge machining. **Journal of the Brazilian Society of Mechanical Sciences and Engineering**. . ISSN 1678-5878. 36:3 (2014) 623–635. doi: 10.1007/s40430-013-0108-9.

BORN, D. K.; GOODMAN, W. A. - An empirical survey on the influence of machining parameters on tool wear in diamond turning of large single-crystal silicon optics. **Precision Engineering**. 25:4 (2001) 247–257.

BOUZAKIS, K. D.; AICHOUH, P.; EFSTATHIOU, K. - Determination of the chip geometry, cutting force and roughness in free form surfaces finishing milling, with ball end tools. **International Journal of Machine Tools & Manufacture**. . ISSN 08906955. 43:5

(2003) 499–514. doi: 10.1016/S0890-6955(02)00265-1.

BRANDÃO, L. C. *et al.* - Influence of Different Cooling Systems on Surface Roughness in the Turning of the Ti-6Al-4V Alloy Used as Biomaterial. **Advanced Materials Research**. . ISSN 1662-8985. 704:2013) 155–160. doi: 10.4028/www.scientific.net/AMR.704.155.

BRANDÃO, L. C.; COELHO, R. T. - Temperature and heat flow when tapping of the hardened steel using different cooling systems. **Revista chilena de ingeniería**. 17:2 (2009) 267–274.

BRANDÃO, L. C.; COELHO, R. T.; LAURO, C. H. - Contribution to dynamic characteristics of the cutting temperature in the drilling process considering one dimension heat flow. **Applied Thermal Engineering**. . ISSN 13594311. 31:17–18 (2011) 3806–3813. doi: 10.1016/j.applthermaleng.2011.07.024.

BUCHKREMER, S. *et al.* - FE-Simulation of Machining Processes with a New Material Model. **Journal of Materials Processing Technology**. . ISSN 09240136. 2013). doi: 10.1016/j.jmatprotec.2013.10.014.

BURG, K. J. L.; PORTER, S.; KELLAM, J. F. - Biomaterial developments for bone tissue engineering. **Biomaterials**. . ISSN 01429612. 21:23 (2000) 2347–2359. doi: 10.1016/S0142-9612(00)00102-2.

BYRNE, G. - Thermoelectric signal characteristics and average interfacial temperatures in the machining of metals under geometrically defined conditions. **International Journal of Machine Tools & Manufacture**. 27:2 (1987) 215–224.

BYRNE, G.; DORNFELD, D.; DENKENA, B. - Advancing Cutting Technology. **CIRP Annals - Manufacturing Technology**. . ISSN 00078506. 52:2 (2003) 483–507. doi: 10.1016/S0007-8506(07)60200-5.

CALLISTER, W. D.; RETHWISCH, D. G. - **Fundamentals of Materials Science and Engineering: An Integrated Approach**. [S.l.] : John Wiley & Sons, 2012. ISBN 978-1-118-32269-7.

CÂMARA, M. A. *et al.* - State of the Art on Micromilling of Materials , a Review.

Journal of Materials Science & Technology. . ISSN 10050302. 28:8 (2012) 673–685. doi: 10.1016/S1005-0302(12)60115-7.

CAMPOS, P. H. S. *et al.* - Modeling and optimization techniques in machining of hardened steels: A brief review. **Reviews on Advanced Materials Science**. 34:2 (2013) 141–147.

CAO, H.; LEI, Y.; HE, Z. - Chatter identification in end milling process using wavelet packets and Hilbert–Huang transform. **International Journal of Machine Tools & Manufacture**. . ISSN 08906955. 69:2013) 11–19. doi: 10.1016/j.ijmachtools.2013.02.007.

CAROU, D. *et al.* - Experimental investigation on finish intermittent turning of UNS M11917 magnesium alloy under dry machining. **The International Journal of Advanced Manufacturing Technology**. . ISSN 0268-3768. 75:2014) 1417–1429. doi: 10.1007/s00170-014-6215-7.

CAROU, D. *et al.* - The effect of minimum quantity lubrication in the intermittent turning of magnesium based on vibration signals. **Measurement**. . ISSN 02632241. 2016). doi: 10.1016/j.measurement.2016.08.016.

CARVALHO, A. O. *et al.* - Analysis of form threads using fluteless taps in cast magnesium alloy (AM60). **Journal of Materials Processing Technology**. . ISSN 09240136. 212:8 (2012) 1753–1760. doi: 10.1016/j.jmatprotec.2012.03.018.

CHAE, J.; PARK, S. S.; FREIHEIT, T. - Investigation of micro-cutting operations. **International Journal of Machine Tools & Manufacture**. . ISSN 08906955. 46:3–4 (2006) 313–332. doi: 10.1016/j.ijmachtools.2005.05.015.

CHEN, F. M.; LIU, X. - Advancing biomaterials of human origin for tissue engineering. **Progress in Polymer Science**. . ISSN 00796700. 53:2016) 86–168. doi: 10.1016/j.progpolymsci.2015.02.004.

CHENG, Kai - **Machining Dynamics - Fundamentals, Applications and Practices**. London : Springer, 2009. ISBN 9781846283673.

CHILDS, T. H. C. *et al.* - **Metal Machining Theory and Applications**. London : Arnold,

2000. ISBN 034069159X.

CHILDS, T. H. C. - Friction modelling in metal cutting. **Wear**. . ISSN 00431648. 260:3 (2006) 310–318. doi: 10.1016/j.wear.2005.01.052.

CHLEBUS, E. *et al.* - Microstructure and mechanical behaviour of Ti-6Al-7Nb alloy produced by selective laser melting. **Materials Characterization**. . ISSN 10445803. 62:5 (2011) 488–495. doi: 10.1016/j.matchar.2011.03.006.

CHOE, H. C.; SAJI, V. S.; KO, Y. M. - Mechanical properties and corrosion resistance of low rigidity quaternary titanium alloy for biomedical applications. **Transactions of Nonferrous Metals Society of China**. . ISSN 10036326. 19:4 (2009) 862–865. doi: 10.1016/S1003-6326(08)60365-9.

CHOI, Y.; NARAYANASWAMI, R.; CHANDRA, A. - Tool wear monitoring in ramp cuts in end milling using the wavelet transform. **The International Journal of Advanced Manufacturing Technology**. . ISSN 0268-3768. 23:5–6 (2004) 419–428. doi: 10.1007/s00170-003-1898-1.

COLDWELL, H. *et al.* - Rapid machining of hardened AISI H13 and D2 moulds, dies and press tools. **Journal of Materials Processing Technology**. . ISSN 09240136. 135:2–3 (2003) 301–311. doi: 10.1016/S0924-0136(02)00861-0.

COTRIM-FERREIRA, F. A. *et al.* - Metallographic analysis of the internal microstructure of orthodontic mini-implants. **Brazilian Oral Research**. . ISSN 1806-8324. 24:4 (2010) 438–442. doi: 10.1590/S1806-83242010000400011.

COZ, G. L. *et al.* - Measuring temperature of rotating cutting tools: Application to MQL drilling and dry milling of aerospace alloys. **Applied Thermal Engineering**. . ISSN 13594311. 36:2012) 434–441. doi: 10.1016/j.applthermaleng.2011.10.060.

CRISTOFARO, S. D. *et al.* - High-speed micro-milling: Novel coatings for tool wear reduction. **International Journal of Machine Tools & Manufacture**. . ISSN 08906955. 63:2012) 16–20. doi: 10.1016/j.ijmachtools.2012.07.005.

DĄBROWSKI, R. - Investigations of $\alpha + \beta \rightarrow \beta$ Phase Transformation in Monotonically

Heated Ti6Al7Nb Alloy / Badania Przemiany Fazowej α + β → β W Stopie Ti6Al7Nb Przy Nagrzewaniu Ciągłym. **Archives of Metallurgy and Materials**. . ISSN 2300-1909. 57:4 (2012) 995–1000. doi: 10.2478/v10172-012-0111-7.

DAVOODI, B.; HOSSEINZADEH, H. - A new method for heat measurement during high speed machining. **Measurement**. . ISSN 02632241. 45:8 (2012) 2135–2140. doi: 10.1016/j.measurement.2012.05.020.

DEB, K. *et al.* - A fast and elitist multiobjective genetic algorithm: NSGA-II. **IEEE Transactions on Evolutionary Computation**. . ISSN 1089778X. 6:2 (2002) 182–197. doi: 10.1109/4235.996017.

DENG, W. J. *et al.* - Study on the cutting force of cylindrical turning with novel restricted contact tools. **The International Journal of Advanced Manufacturing Technology**. . ISSN 0268-3768. 2013). doi: 10.1007/s00170-013-5137-0.

DEPARTAMENTO DE ENGENHARIA DE MATERIAIS E CERÂMICA - DEMAC - **Equipamentos Integrados na Rede e sua Utilização** [Em linha], atual. 2015. [Consult. 6 set. 2016]. Disponível em WWW:<URL:http://www.ua.pt/demac/PageText.aspx?id=7327>.

DEVILLEZ, A. *et al.* - Dry machining of Inconel 718, workpiece surface integrity. **Journal of Materials Processing Technology**. . ISSN 09240136. 211:10 (2011) 1590–1598. doi: 10.1016/j.jmatprotec.2011.04.011.

DEVILLEZ, A.; DUDZINSKI, D. - Tool vibration detection with eddy current sensors in machining process and computation of stability lobes using fuzzy classifiers. **Mechanical Systems and Signal Processing**. . ISSN 08883270. 21:1 (2007) 441–456. doi: 10.1016/j.ymssp.2005.11.007.

DEY, S.; STORI, J. A. - A Bayesian network approach to root cause diagnosis of process variations. **International Journal of Machine Tools and Manufacture**. . ISSN 08906955. 45:1 (2005) 75–91. doi: 10.1016/j.ijmachtools.2004.06.018.

DIMLA, D. E. - The Correlation of Vibration Signal Features to Cutting Tool Wear in a Metal Turning Operation. **The International Journal of Advanced Manufacturing**

Technology. . ISSN 0268-3768. 19:10 (2002) 705–713. doi: 10.1007/s001700200080.

DING, H. *et al.* - Experimental study on machinability improvement of hardened tool steel using two dimensional vibration-assisted micro-end-milling. **International Journal of Machine Tools & Manufacture**. . ISSN 08906955. 50:12 (2010) 1115–1118. doi: 10.1016/j.ijmachtools.2010.08.010.

DOMINGO, J. L. - Vanadium and tungsten derivatives as antidiabetic agents: a review of their toxic effects. **Biological trace element research**. . ISSN 0163-4984. 88:2 (2002) 97–112. doi: 10.1385/BTER:88:2:097.

DUAN, C. *et al.* - Modeling of white layer thickness in high speed machining of hardened steel based on phase transformation mechanism. **The International Journal of Advanced Manufacturing Technology**. . ISSN 0268-3768. 69:1–4 (2013) 59–70. doi: 10.1007/s00170-013-5005-y.

DUCOBU, F.; RIVIÈRE-LORPHÈVRE, E.; FILIPPI, E. - Material constitutive model and chip separation criterion influence on the modeling of Ti6Al4V machining with experimental validation in strictly orthogonal cutting condition. **International Journal of Mechanical Sciences**. . ISSN 00207403. 107:2016) 136–149. doi: 10.1016/j.ijmecsci.2016.01.008.

DUCOBU, F.; RIVIÈRE-LORPHÈVRE, E.; FILIPPI, E. - Experimental and numerical investigation of the uncut chip thickness reduction in Ti6Al4V orthogonal cutting. **Meccanica**. . ISSN 0025-6455. 2016) 1–16. doi: 10.1007/s11012-016-0499-7.

EE, K. C.; DILLON, O. W.; JAWAHIR, I. S. - Finite element modeling of residual stresses in machining induced by cutting using a tool with finite edge radius. **International Journal of Mechanical Sciences**. . ISSN 00207403. 47:10 (2005) 1611–1628. doi: 10.1016/j.ijmecsci.2005.06.001.

ELIAS, C. N. *et al.* - Biomedical applications of titanium and its alloys. **JOM**. . ISSN 1047-4838. 60:3 (2008) 46–49. doi: 10.1007/s11837-008-0031-1.

ENGINEERING VILLAGE - **Number of papers about titanium-based biomaterial**, atual. 2016.

ENGINEERING VILLAGE - **Type of analysis in the biomaterial**, atual. 2016.

EZUGWU, E. O.; OKEKE, C. I. - Tool life and wear mechanisms of TiN coated tools in an intermittent cutting operation. **Journal of Materials Processing Technology**. . ISSN 09240136. 116:1 (2001) 10–15. doi: 10.1016/S0924-0136(01)00852-4.

FALLBÖHMER, P. *et al.* - High-speed machining of cast iron and alloy steels for die and mold manufacturing. **Journal of Materials Processing Technology**. 98:1 (2000) 104–115. doi: 10.1016/S0924-0136(99)00311-8.

FANG, F. Z.; LIU, Y. C. - On minimum exit-burr in micro cutting. **Journal of Micromechanics and Microengineering**. . ISSN 0960-1317. 14:7 (2004) 984–988. doi: 10.1088/0960-1317/14/7/020.

FERNANDES, D. J.; ELIAS, C. N.; VALIEV, R. Z. - Properties and Performance of Ultrafine Grained Titanium for Biomedical Applications. **Materials Research**. . ISSN 1980-5373. 18:6 (2015) 1163–1175. doi: 10.1590/1516-1439.005615.

FILIZ, S. *et al.* - Micromilling of microbarbs for medical implants. **International Journal of Machine Tools & Manufacture**. . ISSN 08906955. 48:3–4 (2008) 459–472. doi: 10.1016/j.ijmachtools.2007.08.020.

FROES, F. H. - **Titanium: Physical Metallurgy, Processing, and Applications**. Ohio : ASM International, 2015. ISBN 978-1-62708-079-8.

FROMENTIN, G. *et al.* - An experimental study on the effects of lubrication in form tapping. **Tribology International**. . ISSN 0301679X. 43:9 (2010) 1726–1734. doi: 10.1016/j.triboint.2010.04.005.

FROMENTIN, G. *et al.* - Development of a precision machine to perform and study orthogonal micro-cutting. **Production Engineering**. . ISSN 0944-6524. 10:2 (2016) 217–226. doi: 10.1007/s11740-016-0657-8.

GAITONDE, V. N. *et al.* - Machinability analysis in turning tungsten–copper composite for application in EDM electrodes. **International Journal of Refractory Metals and Hard Materials**. . ISSN 02634368. 28:2 (2010) 221–227. doi:

10.1016/j.ijrmhm.2009.10.002.

GALLEGO, J. *et al.* - Microstructural characterization of Ti-6Al-7Nb alloy after severe plastic deformation. **Materials Research**. . ISSN 1516-1439. 15:5 (2012) 786–791. doi: 10.1590/S1516-14392012005000100.

GARCÍA-PLAZA, E. *et al.* - Surface Finish Monitoring in Taper Turning CNC Using Artificial Neural Network and Multiple Regression Methods. **Procedia Engineering**. . ISSN 18777058. 63:2013) 599–607. doi: 10.1016/j.proeng.2013.08.245.

GINTING, A.; NOUARI, M. - Surface integrity of dry machined titanium alloys. **International Journal of Machine Tools & Manufacture**. . ISSN 08906955. 49:3–4 (2009) 325–332. doi: 10.1016/j.ijmachtools.2008.10.011.

GOK, A.; GOLOGLU, C.; DEMIRCI, H. I. - Cutting parameter and tool path style effects on cutting force and tool deflection in machining of convex and concave inclined surfaces. **The International Journal of Advanced Manufacturing Technology**. . ISSN 0268-3768. 3 (2013). doi: 10.1007/s00170-013-5075-x.

GOPALSAMY, B. M.; MONDAL, B.; GHOSH, S. - Optimisation of machining parameters for hard machining: grey relational theory approach and ANOVA. **The International Journal of Advanced Manufacturing Technology**. . ISSN 0268-3768. 45:11–12 (2009) 1068–1086. doi: 10.1007/s00170-009-2054-3.

GUOHE, L.; CAI, Y.; BING, Y. - Experimental Study of Adiabatic Shear Critical Conditions in Orthogonal Cutting of AISI 1045 Steel. Em **2010 International Conference on Electrical and Control Engineering**. [S.l.] : IEEE, Jun. 2010. ISBN 978-1-4244-6880-5

HABIB, S. S. - Study of the parameters in electrical discharge machining through response surface methodology approach. **Applied Mathematical Modelling**. . ISSN 0307904X. 33:12 (2009) 4397–4407. doi: 10.1016/j.apm.2009.03.021.

HADAD, M.; SADEGHI, B. - Minimum quantity lubrication-MQL turning of AISI 4140 steel alloy. **Journal of Cleaner Production**. . ISSN 09596526. 54:2013) 332–343. doi: 10.1016/j.jclepro.2013.05.011.

HAMDAN, A.; SARHAN, A. A. D.; HAMDI, M. - An optimization method of the machining parameters in high-speed machining of stainless steel using coated carbide tool for best surface finish. **The International Journal of Advanced Manufacturing Technology**. . ISSN 0268-3768. 58:1–4 (2012) 81–91. doi: 10.1007/s00170-011-3392-5.

HESSAINIA, Z. *et al.* - On the prediction of surface roughness in the hard turning based on cutting parameters and tool vibrations. **Measurement**. . ISSN 02632241. 46:5 (2013) 1671–1681. doi: 10.1016/j.measurement.2012.12.016.

HISBERGUES, M.; VENDEVILLE, S.; VENDEVILLE, P. - Zirconia: Established facts and perspectives for a biomaterial in dental implantology. **Journal of biomedical materials research. Part B, Applied biomaterials**. . ISSN 1552-4981. 88:2 (2009) 519–29. doi: 10.1002/jbm.b.31147.

HONG, Y. C.; HA, S. J.; CHO, M. W. - Predicting of cutting forces in a micromilling process based on frequency analysis of sensor signals and modified polynomial neural network algorithm. **International Journal of Precision Engineering and Manufacturing**. . ISSN 1229-8557. 13:1 (2012) 17–23. doi: 10.1007/s12541-012-0003-9.

HOWELL, D. C. - **Statistical Methods for Psychology**. 7. ed. Belmont : Cengage Learning, 2010. ISBN 978-0-495-59784-1.

HUA, J.; UMBRELLO, D.; SHIVPURI, R. - Investigation of cutting conditions and cutting edge preparations for enhanced compressive subsurface residual stress in the hard turning of bearing steel. **Journal of Materials Processing Technology**. . ISSN 09240136. 171:2 (2006) 180–187. doi: 10.1016/j.jmatprotec.2005.06.087.

HUANG, L. *et al.* - Comparison of Fourier transform, windowed Fourier transform, and wavelet transform methods for phase extraction from a single fringe pattern in fringe projection profilometry. **Optics and Lasers in Engineering**. . ISSN 01438166. 48:2 (2010) 141–148. doi: 10.1016/j.optlaseng.2009.04.003.

HWANG, Y. K.; LEE, C. M. - Surface roughness and cutting force prediction in MQL and wet turning process of AISI 1045 using design of experiments. **Journal of Mechanical Science and Technology**. . ISSN 1738-494X. 24:8 (2010) 1669–1677. doi:

10.1007/s12206-010-0522-1.

JAFFERY, S. I.; MATIVENGA, P. T. T. - Assessment of the machinability of Ti-6Al-4V alloy using the wear map approach. **The International Journal of Advanced Manufacturing Technology**. . ISSN 0268-3768. 40:7–8 (2009) 687–696. doi: 10.1007/s00170-008-1393-9.

JAGADESH, T.; SAMUEL, G. L. - Investigations into Cutting Forces and Surface Roughness in Micro Turning of Titanium Alloy Using Coated Carbide Tool. **Procedia Materials Science**. . ISSN 22118128. 5:2014) 2450–2457. doi: 10.1016/j.mspro.2014.07.496.

JAHANMIR, S. - Surface Integrity in Ultrahigh Speed Micromachining. **Procedia Engineering**. . ISSN 18777058. 19:2011) 156–161. doi: 10.1016/j.proeng.2011.11.095.

JAWAHIR, I. S. *et al.* - Surface integrity in material removal processes: Recent advances. **CIRP Annals - Manufacturing Technology**. . ISSN 00078506. 60:2 (2011) 603–626. doi: 10.1016/j.cirp.2011.05.002.

KAJARIA, S. *et al.* - Micromilling in minimum quantity lubrication. **Machining Science and Technology**. 16:4 (2012) 524–546. doi: 10.1080/10910344.2012.730848.

KALVODA, T.; HWANG, Y. R. - A cutter tool monitoring in machining process using Hilbert–Huang transform. **International Journal of Machine Tools & Manufacture**. . ISSN 08906955. 50:5 (2010) 495–501. doi: 10.1016/j.ijmachtools.2010.01.006.

KALVODA, T.; HWANG, Y. R. - Analysis of signals for monitoring of nonlinear and non-stationary machining processes. **Sensors and Actuators A: Physical**. . ISSN 09244247. 161:1–2 (2010) 39–45. doi: 10.1016/j.sna.2010.05.032.

KANG, I. S. *et al.* - Tool condition and machined surface monitoring for micro-lens array fabrication in mechanical machining. **Journal of Materials Processing Technology**. . ISSN 09240136. 201:1–3 (2008) 585–589. doi: 10.1016/j.jmatprotec.2007.11.187.

KANG, M. C.; KIM, J. S.; KIM, J. H. - A monitoring technique using a multi-sensor in high speed machining. **Journal of Materials Processing Technology**. . ISSN 09240136.

113:1–3 (2001) 331–336. doi: 10.1016/S0924-0136(01)00698-7.

KIM, Gi D.; CHU, Chong N. - Indirect Cutting Force Measurement Considering Frictional Behaviour in a Machining Centre Using Feed Motor Current. **The International Journal of Advanced Manufacturing Technology**. . ISSN 0268-3768. 15:7 (1999) 478–484. doi: 10.1007/s001700050092.

KIM, J. D.; KIM, D. S. - Development of a combined-type tool piezo-film accelerometer for an ultra-precision lathe. **Journal of Materials Processing Technology**. 71:3 (1997) 360–366.

KITAGAWA, T.; KUBO, A.; MAEKAWA, K. - Temperature and wear of cutting tools in high-speed machining of Inconel 718 and Ti-6A1-6V-2Sn. **Wear**. 202:2 (1997) 142–148.

KLOCKE, F.; GERSCHWILER, K.; ABOURIDOUANE, M. - Size effects of micro drilling in steel. **Production Engineering**. . ISSN 0944-6524. 3:1 (2009) 69–72. doi: 10.1007/s11740-008-0144-y.

KOKUBO, T.; TAKADAMA, H. - How useful is SBF in predicting in vivo bone bioactivity? **Biomaterials**. . ISSN 0142-9612. 27:15 (2006) 2907–15. doi: 10.1016/j.biomaterials.2006.01.017.

KONDO, E.; SHIMANA, K. - Monitoring of Prefailure Phase and Detection of Tool Breakage in Micro-Drilling Operations. **Procedia CIRP**. . ISSN 22128271. 1:2012) 581–586. doi: 10.1016/j.procir.2012.05.003.

KONO, D. *et al.* - High-precision machining by measurement and compensation of motion error. **International Journal of Machine Tools and Manufacture**. . ISSN 08906955. 48:10 (2008) 1103–1110. doi: 10.1016/j.ijmachtools.2008.02.005.

KRAJNIK, P.; KOPAČ, J. - Modern machining of die and mold tools. **Journal of Materials Processing Technology**. . ISSN 09240136. 157–158:2004) 543–552. doi: 10.1016/j.jmatprotec.2004.07.146.

KRIMPENIS, A.; FOUSEKIS, A.; VOSNIAKOS, G. - Assessment of sculptured surface milling strategies using design of experiments. **The International Journal of Advanced**

Manufacturing Technology. . ISSN 0268-3768. 25:5–6 (2004) 444–453. doi: 10.1007/s00170-003-1881-x.

KULJANIC, E.; TOTIS, G.; SORTINO, M. - Development of an intelligent multisensor chatter detection system in milling. **Mechanical Systems and Signal Processing**. . ISSN 08883270. 23:5 (2009) 1704–1718. doi: 10.1016/j.ymssp.2009.01.003.

KUMAR, K. V. B. S. K.; CHOUDHURY, S. K. - Investigation of tool wear and cutting force in cryogenic machining using design of experiments. **Journal of Materials Processing Technology**. . ISSN 09240136. 203:1–3 (2008) 95–101. doi: 10.1016/j.jmatprotec.2007.10.036.

LAHIFF, C.; GORDON, S.; PHELAN, P. - PCBN tool wear modes and mechanisms in finish hard turning. **Robotics and Computer-Integrated Manufacturing**. . ISSN 07365845. 23:6 (2007) 638–644. doi: 10.1016/j.rcim.2007.02.008.

LAMRAOUI, M. *et al.* - Indicators for monitoring chatter in milling based on instantaneous angular speeds. **Mechanical Systems and Signal Processing**. . ISSN 08883270. 44:1–2 (2014) 72–85. doi: 10.1016/j.ymssp.2013.05.002.

LAMRAOUI, M.; THOMAS, M.; BADAOUI, M. EL - Cyclostationarity approach for monitoring chatter and tool wear in high speed milling. **Mechanical Systems and Signal Processing**. 44:1 (2014) 177–198.

LAURO, C. H. *et al.* - Influência da variação do tamanho de grão austenítico na qualidade superficial no processo de microfresamento do aço AISI H13 endurecido. **Matéria (Rio de Janeiro)**. . ISSN 1517-7076. 19:3 (2014) 235–246. doi: 10.1590/S1517-70762014000300007.

LAURO, C. H. *et al.* - Monitoring And Processing Signal Applied In Machining Processes – A Review. **Measurement**. . ISSN 02632241. 58:2014) 73–86. doi: 10.1016/j.measurement.2014.08.035.

LAURO, C. H. *et al.* - Specific cutting energy employed to study the influence of the grain size in the micro-milling of the hardened AISI H13 steel. **The International Journal of Advanced Manufacturing Technology**. . ISSN 0268-3768. 81:9 (2015) 1591–1599. doi:

10.1007/s00170-015-7321-x.

LAURO, C. H. *et al.* - Optimization of Micro Milling of Hardened Steel with Different Grain Sizes using Multi-Objective Evolutionary Algorithm. **Measurement**. . ISSN 02632241. 85:2016) 88–99. doi: 10.1016/j.measurement.2016.02.011.

LAURO, C. H.; BRANDÃO, L. C.; RIBEIRO FILHO, S. L. M. - Monitoring the temperature of the milling process using infrared camera. **Scientific Research and Essays**. 8:23 (2013) 1112–1120. doi: 10.5897/SRE12.579.

LEE, D. E. *et al.* - Precision manufacturing process monitoring with acoustic emission. **International Journal of Machine Tools & Manufacture**. . ISSN 08906955. 46:2 (2006) 176–188. doi: 10.1016/j.ijmachtools.2005.04.001.

LEE, K. S.; LEE, L. C.; TEO, S. C. - On-line tool-wear monitoring using a PC. **Journal of Materials Processing Technology**. . ISSN 09240136. 29:1–3 (1992) 3–13. doi: 10.1016/0924-0136(92)90421-N.

LEE, W. S.; CHEN, C. W. - Dynamic mechanical properties and microstructure of Ti–6Al–7Nb biomedical alloy as function of strain rate. **Materials Science and Technology**. . ISSN 0267-0836. 29:9 (2013) 1055–1064. doi: 10.1179/1743284713Y.0000000252.

LEKKALA, R. *et al.* - Characterization and modeling of burr formation in micro-end milling. **Precision Engineering**. . ISSN 01416359. 35:4 (2011) 625–637. doi: 10.1016/j.precisioneng.2011.04.007.

LEPPERT, T. - Effect of cooling and lubrication conditions on surface topography and turning process of C45 steel. **International Journal of Machine Tools and Manufacture**. . ISSN 08906955. 51:2 (2011) 120–126. doi: 10.1016/j.ijmachtools.2010.11.001.

LI, K. M.; CHOU, S. Y. - Experimental evaluation of minimum quantity lubrication in near micro-milling. **Journal of Materials Processing Technology**. . ISSN 09240136. 210:15 (2010) 2163–2170. doi: 10.1016/j.jmatprotec.2010.07.031.

LI, R.; SHIH, A. J. - Spiral point drill temperature and stress in high-throughput drilling of titanium. **International Journal of Machine Tools and Manufacture**. . ISSN 08906955.

47:12–13 (2007) 2005–2017. doi: 10.1016/j.ijmachtools.2007.01.014.

LI, X.; OUYANG, G.; LIANG, Z. - Complexity measure of motor current signals for tool flute breakage detection in end milling. **International Journal of Machine Tools & Manufacture**. . ISSN 08906955. 48:3–4 (2008) 371–379. doi: 10.1016/j.ijmachtools.2007.09.008.

LIAO, T. W. *et al.* - A wavelet-based methodology for grinding wheel condition monitoring. **International Journal of Machine Tools & Manufacture**. . ISSN 08906955. 47:3–4 (2007) 580–592. doi: 10.1016/j.ijmachtools.2006.05.008.

LIAO, Z.; AXINTE, D. A. - On chip formation mechanism in orthogonal cutting of bone. **International Journal of Machine Tools and Manufacture**. . ISSN 08906955. 102:2016) 41–55. doi: 10.1016/j.ijmachtools.2015.12.004.

LIN, Y. C. *et al.* - Optimization of machining parameters in magnetic force assisted EDM based on Taguchi method. **Journal of Materials Processing Technology**. . ISSN 09240136. 209:7 (2009) 3374–3383. doi: 10.1016/j.jmatprotec.2008.07.052.

LIU, K.; MELKOTE, S. N. - Effect of plastic side flow on surface roughness in micro-turning process. **International Journal of Machine Tools & Manufacture**. . ISSN 08906955. 46:14 (2006) 1778–1785. doi: 10.1016/j.ijmachtools.2005.11.014.

LIU, K.; MELKOTE, S. N. - Finite element analysis of the influence of tool edge radius on size effect in orthogonal micro-cutting process. **International Journal of Mechanical Sciences**. . ISSN 00207403. 49:5 (2007) 650–660. doi: 10.1016/j.ijmecsci.2006.09.012.

LIU, X. *et al.* - Adaptive interpolation scheme for NURBS curves with the integration of machining dynamics. **International Journal of Machine Tools and Manufacture**. . ISSN 08906955. 45:4–5 (2005) 433–444. doi: 10.1016/j.ijmachtools.2004.09.009.

LOPES, L. G. D. *et al.* - A multivariate surface roughness modeling and optimization under conditions of uncertainty. **Measurement**. . ISSN 02632241. 46:8 (2013) 2555–2568. doi: 10.1016/j.measurement.2013.04.031.

LU, C. - Study on prediction of surface quality in machining process. **Journal of**

Materials Processing Technology. . ISSN 09240136. 205:1–3 (2008) 439–450. doi: 10.1016/j.jmatprotec.2007.11.270.

LU, M. C.; KANNATEY-ASIBU, E. - Analysis of Sound Signal Generation Due to Flank Wear in Turning. **Journal of Manufacturing Science and Engineering**. . ISSN 10871357. 124:4 (2002) 799. doi: 10.1115/1.1511177.

LU, Z.; YONEYAMA, T. - Micro cutting in the micro lathe turning system. **International Journal of Machine Tools & Manufacture**. . ISSN 08906955. 39:7 (1999) 1171–1183. doi: 10.1016/S0890-6955(98)00092-3.

MADYIRA, D. M. *et al.* - High speed machining induced residual stresses in grade 5 titanium alloy. **Journal of Materials : Design and Applications**. 227:2013) 208–215.

MAHDAVINEJAD, R. A.; SAEEDY, S. - Investigation of the influential parameters of machining of AISI 304 stainless steel. **SADHANA**. 36:6 (2011) 963–970.

MAIYAR, L. M. *et al.* - Optimization of Machining Parameters for end Milling of Inconel 718 Super Alloy Using Taguchi based Grey Relational Analysis. **Procedia Engineering**. . ISSN 18777058. 64:2013) 1276–1282. doi: 10.1016/j.proeng.2013.09.208.

MAKADIA, A. J.; NANAVATI, J. I. - Optimisation of machining parameters for turning operations based on response surface methodology. **Measurement**. . ISSN 02632241. 46:4 (2013) 1521–1529. doi: 10.1016/j.measurement.2012.11.026.

MALEKIAN, M.; PARK, S. S.; JUN, M. B. G. - Modeling of dynamic micro-milling cutting forces. **International Journal of Machine Tools & Manufacture**. . ISSN 08906955. 49:7–8 (2009) 586–598. doi: 10.1016/j.ijmachtools.2009.02.006.

MANDAL, N.; DOLOI, B.; MONDAL, B. - Predictive modeling of surface roughness in high speed machining of AISI 4340 steel using yttria stabilized zirconia toughened alumina turning insert. **International Journal of Refractory Metals and Hard Materials**. . ISSN 02634368. 38:2013) 40–46. doi: 10.1016/j.ijrmhm.2012.12.007.

MANDAL, S.; KUMAR, A.; NAGAHANUMAIAH - Assessment of micro turning machine stiffness response and material characteristics by fuzzy rule based pattern

matching of cutting force plots. **Journal of Manufacturing Systems**. . ISSN 02786125. 32:1 (2013) 228–237. doi: 10.1016/j.jmsy.2012.11.007.

MANIKANDAN, G.; UTHAYAKUMAR, M.; ARAVINDAN, S. - Machining and simulation studies of bimetallic pistons. **The International Journal of Advanced Manufacturing Technology**. . ISSN 0268-3768. 66:5–8 (2012) 711–720. doi: 10.1007/s00170-012-4359-x.

MARANHÃO, C.; DAVIM, J. P. - An overview on commmercial software's in FEM. **International Journal of Engineering: Annals of Faculty of Engineering Hunedoara**. 10:1 (2012) 137–139.

MASUZAWA, T. - State of the Art of Micromachining. **Annals of the ClRP**. 49:1 (2000) 473–488. doi: 10.1016/S0007-8506(07)63451-9.

MEYER, P. A.; VELDHUIS, S. C.; ELBESTAWI, M. A. - Predicting the effect of vibration on ultraprecision machining surface finish as described by surface finish lobes. **International Journal of Machine Tools and Manufacture**. . ISSN 08906955. 49:15 (2009) 1165–1174. doi: 10.1016/j.ijmachtools.2009.08.006.

MHAMDI, M. B. *et al.* - Surface Integrity of Titanium Alloy Ti-6Al-4V in Ball end Milling. **Physics Procedia**. . ISSN 18753892. 25:0 (2012) 355–362. doi: 10.1016/j.phpro.2012.03.096.

MIN, S. *et al.* - A study on initial contact detection for precision micro-mold and surface generation of vertical side walls in micromachining. **CIRP Annals - Manufacturing Technology**. . ISSN 00078506. 57:1 (2008) 109–112. doi: 10.1016/j.cirp.2008.03.068.

MINITAB - Minitab 17 Support. 2016).

MISCH, C. E. - **Implantes Dentais Contemporâneos**. 3th. ed. Rio de Janeiro : Elsevier Health Sciences Brazil, 2009. ISBN 978-85-352-3088-8.

MISCH, C. E. - **Dental Implant Prosthetics**. [S.l.] : Elsevier, 2014. ISBN 9780323078450.

MOHAMED, A. M. O.; WARKENTIN, A.; BAUER, R. - Variable heat flux in numerical simulation of grinding temperatures. **The International Journal of Advanced Manufacturing Technology**. . ISSN 0268-3768. 63:5–8 (2012) 549–554. doi: 10.1007/s00170-012-3948-z.

MOHD ADNAN, M. R. H. *et al.* - Fuzzy logic for modeling machining process: a review. **Artificial Intelligence Review**. 43:3 (2015) 345–379. doi: 10.1007/s10462-012-9381-8.

MONTGOMERY, D. C. - **Design and Analysis of Experiments**. 5th. ed. [S.l.] : Jonh Wiley and Sons, 2001. ISBN 9780471316497.

MONTGOMERY, D. C. - **Design and Analysis of Experiments** [Em linha]. [S.l.] : John Wiley & Sons, 2008 [Consult. 9 jul. 2014]. Disponível em WWW:<URL:http://books.google.com/books?id=kMMJAm5bD34C&pgis=1>. ISBN 0470128666.

MONTGOMERY, Douglas C.; RUNGER, George C. - **Applied statistics and probability for engineers**. 3. ed. [S.l.] : Wiley, 2003. ISBN 0470053046.

MORALA-ARGÜELLO, P.; BARREIRO, J.; ALEGRE, E. - A evaluation of surface roughness classes by computer vision using wavelet transform in the frequency domain. **The International Journal of Advanced Manufacturing Technology**. . ISSN 0268-3768. 59:1–4 (2011) 213–220. doi: 10.1007/s00170-011-3480-6.

MORI, K. *et al.* - Prediction of small drill bit breakage by wavelet transforms and linear discriminant functions. **International Journal of Machine Tools & Manufacture**. . ISSN 08906955. 39:9 (1999) 1471–1484. doi: 10.1016/S0890-6955(99)00004-8.

MORSKA, A.; MATUSZAK, M.; WASZCZUK, P. - Zeszyty Naukowe Experimental sensor system implementation for selected micromilling-related parameters. **Scientific Journals Maritime University of Szczecin**. 31:103 (2012) 134–139.

MUKHERJEE, I.; RAY, P. K. - A review of optimization techniques in metal cutting processes. **Computers & Industrial Engineering**. . ISSN 03608352. 50:1–2 (2006) 15–34. doi: 10.1016/j.cie.2005.10.001.

MUSTAPHA, K. B.; ZHONG, Z. W. - A hybrid analytical model for the transverse vibration response of a micro-end mill. **Mechanical Systems and Signal Processing**. . ISSN 08883270. 34:1–2 (2013) 321–339. doi: 10.1016/j.ymssp.2012.07.006.

MUTHUKRISHNAN, N.; DAVIM, J. P. - Optimization of machining parameters of Al/SiC-MMC with ANOVA and ANN analysis. **Journal of Materials Processing Technology**. . ISSN 09240136. 209:1 (2009) 225–232. doi: 10.1016/j.jmatprotec.2008.01.041.

NATIONAL INSTRUMENTS - How to Choose the Right DAQ Hardware for Your Measurement System. 2012) 1–5.

NEŞELI, S.; YALDIZ, S.; TÜRKEŞ, E. - Optimization of tool geometry parameters for turning operations based on the response surface methodology. **Measurement**. . ISSN 02632241. 44:3 (2011) 580–587. doi: 10.1016/j.measurement.2010.11.018.

NG, C. K. *et al.* - Experimental study of micro- and nano-scale cutting of aluminum 7075-T6. **International Journal of Machine Tools & Manufacture**. . ISSN 08906955. 46:9 (2006) 929–936. doi: 10.1016/j.ijmachtools.2005.08.004.

NIINOMI, M. - Fatigue performance and cyto-toxicity of low rigidity titanium alloy, Ti–29Nb–13Ta–4.6Zr. **Biomaterials**. . ISSN 01429612. 24:16 (2003) 2673–2683. doi: 10.1016/S0142-9612(03)00069-3.

NISHIKAWA, F.; YOSHIMOTO, S.; SOMAYA, K. - Ultrahigh-Speed Micro-Milling End Mill with Shank Directly Supported by Aerostatic Bearings. **Journal of Advanced Mechanical Design, Systems, and Manufacturing**. . ISSN 1881-3054. 6:6 (2012) 979–988. doi: 10.1299/jamdsm.6.979.

NOGUEIRA, J. C. C. - **Análise da maquinabilidade da liga de titânio Ti6Al7Nb**. [S.l.] : University of Aveiro, 2015

NOR, I. *et al.* - Monitoring drill conditions with wavelet encoding and neural networks based. **International Journal of Machine Tools & Manufacture**. 33:4 (1993) 559–575.

NOVOTNY, M.; SEDLACEK, M. - Measurement of active power by time domain digital

signal processing. **Measurement**. . ISSN 02632241. 42:8 (2009) 1139–1152. doi: 10.1016/j.measurement.2008.02.002.

NUNOME, S. *et al.* - In vitro evaluation of biocompatibility of Ti-Mo-Sn-Zr superelastic alloy. **Journal of biomaterials applications**. . ISSN 1530-8022. 30:1 (2015) 119–30. doi: 10.1177/0885328215569892.

O'SULLIVAN, D.; COTTERELL, M. - Temperature measurement in single point turning. **Journal of Materials Processing Technology**. . ISSN 09240136. 118:1–3 (2001) 301–308. doi: 10.1016/S0924-0136(01)00853-6.

ÖZEL, T.; ZEREN, E. - Finite element modeling the influence of edge roundness on the stress and temperature fields induced by high-speed machining. **The International Journal of Advanced Manufacturing Technology**. . ISSN 0268-3768. 35:3–4 (2007) 255–267. doi: 10.1007/s00170-006-0720-2.

PAIVA, A. P. *et al.* - A multivariate robust parameter design approach for optimization of AISI 52100 hardened steel turning with wiper mixed ceramic tool. **International Journal of Refractory Metals and Hard Materials**. . ISSN 02634368. 30:1 (2012) 152–163. doi: 10.1016/j.ijrmhm.2011.08.001.

PALANI, S.; NATARAJAN, U.; CHELLAMALAI, M. - On-line prediction of micro-turning multi-response variables by machine vision system using adaptive neuro-fuzzy inference system (ANFIS). **Machine Vision and Applications**. . ISSN 0932-8092. 24:1 (2013) 19–32. doi: 10.1007/s00138-011-0378-0.

PARK, S. J.; KIM, D. H.; LEE, C. M. - A study determining the optimal machining conditions for a 40,000rpm ultra high speed spindle system. **Precision Engineering**. . ISSN 01416359. 36:3 (2012) 451–457. doi: 10.1016/j.precisioneng.2012.02.003.

PARK, S. S.; RAHNAMA, R. - Robust chatter stability in micro-milling operations. **CIRP Annals - Manufacturing Technology**. . ISSN 00078506. 59:1 (2010) 391–394. doi: 10.1016/j.cirp.2010.03.023.

PAWADE, R. S. *et al.* - An investigation of cutting forces and surface damage in high-speed turning of Inconel 718. **Journal of Materials Processing Technology**. . ISSN

09240136. 192–193:2007) 139–146. doi: 10.1016/j.jmatprotec.2007.04.049.

PENCHEV, P. *et al.* - Generic integration tools for reconfigurable laser micromachining systems. **Journal of Manufacturing Systems**. . ISSN 02786125. 38:2016) 27–45. doi: 10.1016/j.jmsy.2015.10.006.

PEREIRA, R. B. D. *et al.* - Analysis of surface roughness and cutting force when turning AISI 1045 steel with grooved tools through Scott–Knott method. **The International Journal of Advanced Manufacturing Technology**. . ISSN 0268-3768. 69:5–8 (2013) 1431–1441. doi: 10.1007/s00170-013-5126-3.

PILEHVA, F. *et al.* - High-Temperature Deformation Behavior of a Ti-6Al-7Nb Alloy in Dual-Phase (α + β) and Single-Phase (β) Regions. **Journal of Materials Engineering and Performance**. . ISSN 1059-9495. 25:1 (2016) 46–58. doi: 10.1007/s11665-015-1813-6.

PRABHU, S.; UMA, M.; VINAYAGAM, B. K. - Adaptive neuro-fuzzy interference system modelling of carbon nanotube-based electrical discharge machining process. **Journal of the Brazilian Society of Mechanical Sciences and Engineering**. . ISSN 1678-5878. 35:4 (2013) 505–516. doi: 10.1007/s40430-013-0047-5.

PU, Z. *et al.* - Enhanced surface integrity of AZ31B Mg alloy by cryogenic machining towards improved functional performance of machined components. **International Journal of Machine Tools & Manufacture**. . ISSN 08906955. 56:2012) 17–27. doi: 10.1016/j.ijmachtools.2011.12.006.

RAHMAN, M. A. *et al.* - Development of micropin fabrication process using tool based micromachining. **The International Journal of Advanced Manufacturing Technology**. . ISSN 0268-3768. 27:9–10 (2005) 939–944. doi: 10.1007/s00170-004-2270-9.

RAMESH, A.; MELKOTE, S. N. - Modeling of white layer formation under thermally dominant conditions in orthogonal machining of hardened AISI 52100 steel. **International Journal of Machine Tools & Manufacture**. . ISSN 08906955. 48:3–4 (2008) 402–414. doi: 10.1016/j.ijmachtools.2007.09.007.

RAMESH, R.; JYOTHIRMAI, S.; LAVANYA, K. - Intelligent automation of design and manufacturing in machine tools using an open architecture motion controller. **Journal of**

Manufacturing Systems. . ISSN 02786125. 32:1 (2013) 248–259. doi: 10.1016/j.jmsy.2012.11.004.

RAO, G. K. M. *et al.* - Development of hybrid model and optimization of surface roughness in electric discharge machining using artificial neural networks and genetic algorithm. **Journal of Materials Processing Technology**. . ISSN 09240136. 209:3 (2009) 1512–1520. doi: 10.1016/j.jmatprotec.2008.04.003.

REN, Q. *et al.* - Type-2 Fuzzy Tool Condition Monitoring System Based on Acoustic Emission in Micromilling. **Information Sciences**. . ISSN 00200255. 255:2014) 121–134. doi: 10.1016/j.ins.2013.06.010.

RIBEIRO FILHO, S. L. M. *et al.* - Effects of the Dynamic Tapping Process on the Biocompatibility of Ti-6Al-4V Alloy in Simulated Human Body Environment. **Arabian Journal for Science and Engineering**. . ISSN 2193-567X. 41:11 (2016) 4313–4326. doi: 10.1007/s13369-016-2089-3.

RIBEIRO FILHO, S. L. M. *et al.* - Influence cutting parameters on the surface quality and corrosion behavior of Ti–6Al–4V alloy in synthetic body environment (SBF) using Response Surface Method. **Measurement**. . ISSN 02632241. 88:2016) 223–237. doi: 10.1016/j.measurement.2016.03.047.

RITOU, M. *et al.* - Angular approach combined to mechanical model for tool breakage detection by eddy current sensors. **Mechanical Systems and Signal Processing**. . ISSN 08883270. 44:1–2 (2014) 211–220. doi: 10.1016/j.ymssp.2013.02.004.

RIZZUTI, S. *et al.* - FINITE ELEMENT ANALYSIS OF RESIDUAL STRESSES IN MACHINING. **International Journal of Material Forming**. 3:1 (2010) 431–434. doi: 10.1007/s12289-010-0799-.

ROBINSON, G. M.; JACKSON, M. J.; WHITFIELD, M. D. - A review of machining theory and tool wear with a view to developing micro and nano machining processes. **Journal of Materials Science**. . ISSN 0022-2461. 42:6 (2007) 2002–2015. doi: 10.1007/s10853-006-0171-z.

ROWE, W. B. - **Principles of Modern Grinding Technology**. [S.l.] : Elsevier, 2009.

ISBN 9780815520184.

RUBIO, E. M.; TETI, R.; BACIU, I. L. - Advanced signal processing in acoustic emission monitoring systems for machining technology. Em **Intelligent Production Machines and Systems**. Cardiff : Elsevier, 2006

SAEDON, J. B. *et al.* - Prediction and Optimization of Tool Life in Micromilling AISI D2 (~62 HRC) Hardened Steel. **Procedia Engineering - International Symposium on Robotics and Intelligent Sensors 2012 (IRIS 2012)**. 41:2012) 1674–1683. doi: 10.1016/j.proeng.2012.07.367.

SANDVIK COROMANT - **Turning tools**. [S.l.] : Sandvik Coromant, 2012

SANTOS, P. F. *et al.* - Fabrication of low-cost beta-type Ti-Mn alloys for biomedical applications by metal injection molding process and their mechanical properties. **Journal of the mechanical behavior of biomedical materials**. . ISSN 1878-0180. 59:2016) 497–507. doi: 10.1016/j.jmbbm.2016.02.035.

SAYUTI, M. *et al.* - Enhancement and verification of a machined surface quality for glass milling operation using CBN grinding tool - Taguchi approach. **The International Journal of Advanced Manufacturing Technology**. . ISSN 0268-3768. 60:9–12 (2011) 939–950. doi: 10.1007/s00170-011-3657-z.

SCHNEIDER, F. *et al.* - Investigation of Chip Formation and Surface Integrity when Micro-cutting cp-Titanium with Ultra-fine Grain Cemented Carbide. **Procedia CIRP**. . ISSN 22128271. 45:2016) 115–118. doi: 10.1016/j.procir.2016.02.257.

SCHUELER, G. M. *et al.* - Burr Formation and Surface Characteristics in Micro-End Milling of Titanium Alloys. Em AURICH, J. C.; DORNFELD, D. (Eds.) - **Burrs - Analysis, Control and Removal**. Berlin, Heidelberg : Springer Berlin Heidelberg, 2010. ISBN 978-3-642-00567-1. p. 129–138.

SCHULZ, H.; MORIWAKI, T. - High-speed Machining. **Annals of the ClRP**. 41:1992) 637–643.

SEVILLA-CAMACHO, P. Y. *et al.* - FPGA-based reconfigurable system for tool

condition monitoring in high-speed machining process. **Measurement**. . ISSN 02632241. 64:2015) 81–88. doi: 10.1016/j.measurement.2014.12.037.

SHAH, F. A. *et al.* - Commercially pure titanium (cp-Ti) versus titanium alloy (Ti6Al4V) materials as bone anchored implants — Is one truly better than the other? **Materials Science and Engineering: C**. . ISSN 09284931. 62:2016) 960–966. doi: 10.1016/j.msec.2016.01.032.

SHAO, H.; SHI, X.; LI, L. - Power signal separation in milling process based on wavelet transform and independent component analysis. **International Journal of Machine Tools & Manufacture**. . ISSN 08906955. 51:9 (2011) 701–710. doi: 10.1016/j.ijmachtools.2011.05.006.

SHARMA, V. S.; SINGH, G.; SØRBY, K. - A Review on Minimum Quantity Lubrication for Machining Processes. **Materials and Manufacturing Processes**. . ISSN 1042-6914. 30:8 (2014) 935–953. doi: 10.1080/10426914.2014.994759.

SHAW, M. C. - **Metal Cutting Principles**. 2ª ed. New York : Oxford University Press., 2004

SHIN, B. C. *et al.* - Indirect cutting force measurement in the micro end-milling process based on frequency analysis of sensor signals. **Journal of Mechanical Science and Technology**. . ISSN 1738-494X. 24:1 (2010) 165–168. doi: 10.1007/s12206-009-1121-x.

SHIN, S. H. *et al.* - Cutting performance of CrN and Cr-Si–N coated end-mill deposited by hybrid coating system for ultra-high speed micro machining. **Surface and Coatings Technology**. . ISSN 02578972. 202:22–23 (2008) 5613–5616. doi: 10.1016/j.surfcoat.2008.06.128.

SIENIAWSKI, J. *et al.* - Microstructure and Mechanical Properties of High Strength Two-Phase Titanium Alloys. Em **Titanium Alloys - Advances in Properties Control**. [S.l.] : InTech, 2013. ISBN 978-953-51-1110-8

SILVA, L. R. Da *et al.* - Machinability aspects concerning micro-turning of PA66-GF30-reinforced polyamide. **The International Journal of Advanced Manufacturing Technology**. . ISSN 0268-3768. 41:9–10 (2008) 839–845. doi: 10.1007/s00170-008-1537-

y.

SILVA, L. R. Da *et al.* - Machinability study of steels in precision orthogonal cutting. **Materials Research**. . ISSN 1516-1439. 15:4 (2012) 589–595. doi: 10.1590/S1516-14392012005000071.

SILVA, Marcos Aurélio Bomfim Da *et al.* - Associação entre implantes odontológicos e próteses parciais removíveis: revisão de literatura. **RSBO (Online)**. . ISSN 1984-5685. 8:1 (2011) 97–101.

SILVA, R. B. Da *et al.* - Tool life and wear mechanisms in high speed machining of Ti-6Al-4V alloy with PCD tools under various coolant pressures. **Journal of Materials Processing Technology**. . ISSN 09240136. 213:8 (2013) 1459–1464. doi: 10.1016/j.jmatprotec.2013.03.008.

SILVA, S. P.; RIBEIRO FILHO, S. L. M.; BRANDÃO, L. C. - Particle swarm optimization for achieving the minimum profile error in honing process. **Precision Engineering**. . ISSN 01416359. 38:4 (2014) 759–768. doi: 10.1016/j.precisioneng.2014.04.003.

SIMONEAU, A.; NG, E.; ELBESTAWI, M. A. - Chip formation during microscale cutting of a medium carbon steel. **International Journal of Machine Tools & Manufacture**. . ISSN 08906955. 46:5 (2006) 467–481. doi: 10.1016/j.ijmachtools.2005.07.019.

SIMUNOVIC, K.; SIMUNOVIC, G.; SARIC, T. - Single and multiple goal optimization of structural steel face milling process considering different methods of cooling/lubricating. **Journal of Cleaner Production**. . ISSN 09596526. 94:2015) 321–329. doi: 10.1016/j.jclepro.2015.02.015.

SINGARAVEL, B.; SELVARAJ, T. - Experimental investigation on cutting forces, specific cutting pressure, co-efficient of friction and shear energy in turning of hsla steel. **Management and Production Engineering Review**. 7:1 (2016) 71–76. doi: 10.1515/mper-2016-0008.

SINGH, R.; MELKOTE, S. N. - Characterization of a hybrid laser-assisted mechanical micromachining (LAMM) process for a difficult-to-machine material. **International**

Journal of Machine Tools & Manufacture. . ISSN 08906955. 47:7–8 (2007) 1139–1150. doi: 10.1016/j.ijmachtools.2006.09.004.

SIVASAKTHIVEL, P. S.; SUDHAKARAN, R. - Optimization of machining parameters on temperature rise in end milling of Al 6063 using response surface methodology and genetic algorithm. **The International Journal of Advanced Manufacturing Technology**. . ISSN 0268-3768. 67:9–12 (2012) 2313–2323. doi: 10.1007/s00170-012-4652-8.

SOSHI, M. *et al.* - A study on cubic boron nitride (CBN) milling of hardened cast iron for productive and quality manufacturing of machine tool structural components. **The International Journal of Advanced Manufacturing Technology**. . ISSN 0268-3768. 65:9–12 (2012) 1485–1491. doi: 10.1007/s00170-012-4272-3.

SOUTO-LEBEL, A. *et al.* - Characterization and influence of defect size distribution induced by ball-end finishing milling on fatigue life. **Procedia Engineering**. . ISSN 18777058. 19:2011) 343–348. doi: 10.1016/j.proeng.2011.11.123.

STARR, P. *et al.* - Evolution of micromachined pressure transducers for cardiovascular applications. **Sensors and Actuators A: Physical**. . ISSN 09244247. 225:2015) 8–19. doi: 10.1016/j.sna.2015.01.026.

SUBRAMANIAN, M. *et al.* - Optimization of end mill tool geometry parameters for Al7075-T6 machining operations based on vibration amplitude by response surface methodology. **Measurement**. . ISSN 02632241. 46:10 (2013) 4005–4022. doi: 10.1016/j.measurement.2013.08.015.

SURESH, R. *et al.* - State-of-the-art research in machinability of hardened steels. **Proceedings of the Institution of Mechanical Engineers, Part B: Journal of Engineering Manufacture**. . ISSN 0954-4054. 227:2 (2013) 191–209. doi: 10.1177/0954405412464589.

SURMANN, T.; KREBS, E. - Optimization of Micromilling by Adjustment of Inclination Angles. **Procedia CIRP**. . ISSN 22128271. 2:2012) 87–91. doi: 10.1016/j.procir.2012.05.046.

TANG, W. X. *et al.* - Prediction of chatter stability in high-speed finishing end milling

considering multi-mode dynamics. **Journal of Materials Processing Technology**. . ISSN 09240136. 209:5 (2009) 2585–2591. doi: 10.1016/j.jmatprotec.2008.06.003.

TANIGUCHI, N. - Current Status in and Future Trends of Ultraprecision Machining and Ultrafine Materials Processing. **CIRP Annals - Manufacturing Technology**. 32:2 (1983) 573–582.

TARNG, Y. S.; LEE, B. Y. - Amplitude demodulation of the induction motor current for the tool breakage detection in drilling operations. **Robotics and Computer-Integrated Manufacturing**. . ISSN 07365845. 15:4 (1999) 313–318. doi: 10.1016/S0736-5845(99)00015-0.

TETI, R. *et al.* - Advanced monitoring of machining operations. **CIRP Annals - Manufacturing Technology**. . ISSN 00078506. 59:2 (2010) 717–739. doi: 10.1016/j.cirp.2010.05.010.

THAKUR, D. G.; RAMAMOORTHY, B.; VIJAYARAGHAVAN, L. - Study on the machinability characteristics of superalloy Inconel 718 during high speed turning. **Materials & Design**. . ISSN 02613069. 30:5 (2009) 1718–1725. doi: 10.1016/j.matdes.2008.07.011.

TLUSTY, J. - High-Speed Machining. **CIRP Annals - Manufacturing Technology**. . ISSN 00078506. 42:2 (1993) 733–738. doi: 10.1016/S0007-8506(07)62536-0.

TRENT, E.; WRIGHT, P. - **Metal Cutting**. 4. ed. Woburn : Butterworth–Heinemann, 2000. ISBN 075067069X.

UCUN, I.; ASLANTAS, K.; BEDIR, F. - The effect of minimum quantity lubrication and cryogenic pre-cooling on cutting performance in the micro milling of Inconel 718. **Proceedings of the Institution of Mechanical Engineers, Part B: Journal of Engineering Manufacture**. . ISSN 0954-4054. 229:12 (2014) 2134–2143. doi: 10.1177/0954405414546144.

UEDA, T. *et al.* - Measurement of Grinding Temperature of Active Grains Using Infrared Radiation Pyrometer with Optical Fiber. **CIRP Annals - Manufacturing Technology**. 42:1 (1993) 405–408.

ULUTAN, D.; ÖZEL, T. - Machining induced surface integrity in titanium and nickel alloys: A review. **International Journal of Machine Tools & Manufacture**. . ISSN 08906955. 51:3 (2011) 250–280. doi: 10.1016/j.ijmachtools.2010.11.003.

UMBRELLO, D.; M'SAOUBI, R.; OUTEIRO, J. C. - The influence of Johnson–Cook material constants on finite element simulation of machining of AISI 316L steel. **International Journal of Machine Tools & Manufacture**. . ISSN 08906955. 47:3–4 (2007) 462–470. doi: 10.1016/j.ijmachtools.2006.06.006.

UPADHYAY, V.; JAIN, P. K.; MEHTA, N. K. - In-process prediction of surface roughness in turning of Ti–6Al–4V alloy using cutting parameters and vibration signals. **Measurement**. . ISSN 02632241. 46:1 (2013) 154–160. doi: 10.1016/j.measurement.2012.06.002.

VALIORGUE, F. *et al.* - 3D modeling of residual stresses induced in finish turning of an AISI304L stainless steel. **International Journal of Machine Tools & Manufacture**. 53:2012) 77–90. doi: 10.1016/j.ijmachtools.2011.09.011.

VELAYUDHAM, A.; KRISHNAMURTHY, R.; SOUNDARAPANDIAN, T. - Acoustic emission based drill condition monitoring during drilling of glass/phenolic polymeric composite using wavelet packet transform. **Materials Science and Engineering: A**. . ISSN 09215093. 412:1–2 (2005) 141–145. doi: 10.1016/j.msea.2005.08.036.

VÉR, I. L.; BERANEK, L. L. - **Noise and Vibration Control Engineering - Principles and Aplications**. New Jersey : Wiley, 2006. ISBN 0471449423.

VOSNIAKOS, G. C.; KRIMPENIS, A. - Optimisation of Multiple Tool CNC Rough Machining of a Hemisphere as a Genetic Algorithm Paradigm Application. **The International Journal of Advanced Manufacturing Technology**. . ISSN 0268-3768. 20:10 (2002) 727–734. doi: 10.1007/s001700200230.

WANG, L.; LIANG, M. - Chatter detection based on probability distribution of wavelet modulus maxima. **Robotics and Computer-Integrated Manufacturing**. . ISSN 07365845. 25:6 (2009) 989–998. doi: 10.1016/j.rcim.2009.04.011.

WANG, Q.; LIU, F.; WANG, X. - Multi-objective optimization of machining parameters

considering energy consumption. **The International Journal of Advanced Manufacturing Technology**. . ISSN 0268-3768. 71:5–8 (2013) 1133–1142. doi: 10.1007/s00170-013-5547-z.

WANG, W.; KWEON, S. H.; YANG, S. H. - A study on roughness of the micro-end-milled surface produced by a miniatured machine tool. **Journal of Materials Processing Technology**. . ISSN 09240136. 162–163:2005) 702–708. doi: 10.1016/j.jmatprotec.2005.02.141.

WANG, X. *et al.* - Transformations in machining. Part 1. enhancement of wavelet transformation neural network (WT-NN) combination with a preprocessor. **International Journal of Machine Tools & Manufacture**. . ISSN 08906955. 46:1 (2006) 36–42. doi: 10.1016/j.ijmachtools.2005.04.010.

WANG, X. *et al.* - Tool wear of coated drills in drilling CFRP. **Journal of Manufacturing Processes**. . ISSN 15266125. 15:1 (2013) 127–135. doi: 10.1016/j.jmapro.2012.09.019.

WEI, C. J. *et al.* - Temperature modeling in end grinding of coated workpieces. **Journal of Shanghai Jiaotong University (Science)**. . ISSN 1007-1172. 15:3 (2010) 319–322. doi: 10.1007/s12204-010-1010-6.

WEINERT, K.; SCHNEIDER, M. - Simulation of Tool-Grinding with Finite Element Method. **CIRP Annals - Manufacturing Technology**. 49:1 (2000) 253–256. doi: 10.1016/S0007-8506(07)62940-0.

WEULE, H.; HUNTRUP, V.; TRITSCHLER, H. - Micro-Cutting of Steel to Meet New Requirements in Miniaturization. **CIRP Annals - Manufacturing Technology**. 50:1 (2001) 61–64.

YAN, J.; LI, L. - Multi-objective optimization of milling parameters – the trade-offs between energy, production rate and cutting quality. **Journal of Cleaner Production**. . ISSN 09596526. 52:2013) 462–471. doi: 10.1016/j.jclepro.2013.02.030.

YANG, Z. *et al.* - Application of Hilbert–Huang Transform to acoustic emission signal for burn feature extraction in surface grinding process. **Measurement**. . ISSN 02632241. 47:2014) 14–21. doi: 10.1016/j.measurement.2013.08.036.

YANG, Z.; YU, Z. - Grinding wheel wear monitoring based on wavelet analysis and support vector machine. **The International Journal of Advanced Manufacturing Technology**. . ISSN 0268-3768. 62:1–4 (2011) 107–121. doi: 10.1007/s00170-011-3797-1.

YAP, Tze Chuen; EL-TAYEB, N. S. M.; BREVERN, Peter - Cutting forces, friction coefficient and surface roughness in machining Ti-5Al-4V-0.6Mo-0.4Fe using carbide tool K313 under low pressure liquid nitrogen. **Journal of the Brazilian Society of Mechanical Sciences and Engineering**. . ISSN 1678-5878. 35:1 (2013) 11–15. doi: 10.1007/s40430-013-0001-6.

YAZID, M. Z. A. *et al.* - Surface integrity of Inconel 718 when finish turning with PVD coated carbide tool under MQL. **Procedia Engineering**. . ISSN 18777058. 19:2011) 396–401. doi: 10.1016/j.proeng.2011.11.131.

YU, P. H. *et al.* - Improvement of wire electrical discharge machining efficiency in machining polycrystalline silicon with auxiliary-pulse voltage supply. **The International Journal of Advanced Manufacturing Technology**. . ISSN 0268-3768. 57:9–12 (2011) 991–1001. doi: 10.1007/s00170-011-3350-2.

YUN, H. T. *et al.* - Ploughing detection in micromilling processes using the cutting force signal. **International Journal of Machine Tools & Manufacture**. . ISSN 0890-6955. 51:5 (2011) 377–382. doi: 10.1016/j.ijmachtools.2011.01.003.

ZENG, S. *et al.* - A novel approach to fixture design on suppressing machining vibration of flexible workpiece. **International Journal of Machine Tools & Manufacture**. . ISSN 08906955. 58:2012) 29–43. doi: 10.1016/j.ijmachtools.2012.02.008.

ZHANG, E.; LIU, C. - Effect of surface treatments on the surface morphology, corrosion property, and antibacterial property of Ti-10Cu sintered alloy. **Biomedical materials (Bristol, England)**. . ISSN 1748-605X. 10:4 (2015) 45009. doi: 10.1088/1748-6041/10/4/045009.

ZHANG, J. *et al.* - Fundamental investigation of ultra-precision ductile machining of tungsten carbide by applying elliptical vibration cutting with single crystal diamond. **Journal of Materials Processing Technology**. . ISSN 09240136. 214:11 (2014) 2644–

2659. doi: 10.1016/j.jmatprotec.2014.05.024.

ZHANG, J. Z.; CHEN, J. C. - Tool condition monitoring in an end-milling operation based on the vibration signal collected through a microcontroller-based data acquisition system. **The International Journal of Advanced Manufacturing Technology**. . ISSN 0268-3768. 39:1–2 (2007) 118–128. doi: 10.1007/s00170-007-1186-6.

ZHANG, T. *et al.* - Size effect on surface roughness in micro turning. **International Journal of Precision Engineering and Manufacturing**. . ISSN 2234-7593. 14:3 (2013) 345–349. doi: 10.1007/s12541-013-0048-4.

ZHONG, W.; ZHAO, D.; WANG, X. - A comparative study on dry milling and little quantity lubricant milling based on vibration signals. **International Journal of Machine Tools & Manufacture**. . ISSN 08906955. 50:12 (2010) 1057–1064. doi: 10.1016/j.ijmachtools.2010.08.011.

ZHU, K.; WONG, Y. S.; HONG, G. S. - Multi-category micro-milling tool wear monitoring with continuous hidden Markov models. **Mechanical Systems and Signal Processing**. . ISSN 08883270. 23:2 (2009) 547–560. doi: 10.1016/j.ymssp.2008.04.010.

ZHU, K.; WONG, Y. S.; HONG, G. S. - Wavelet analysis of sensor signals for tool condition monitoring: A review and some new results. **International Journal of Machine Tools & Manufacture**. . ISSN 08906955. 49:7–8 (2009) 537–553. doi: 10.1016/j.ijmachtools.2009.02.003.

ANNEXES

ANNEX A

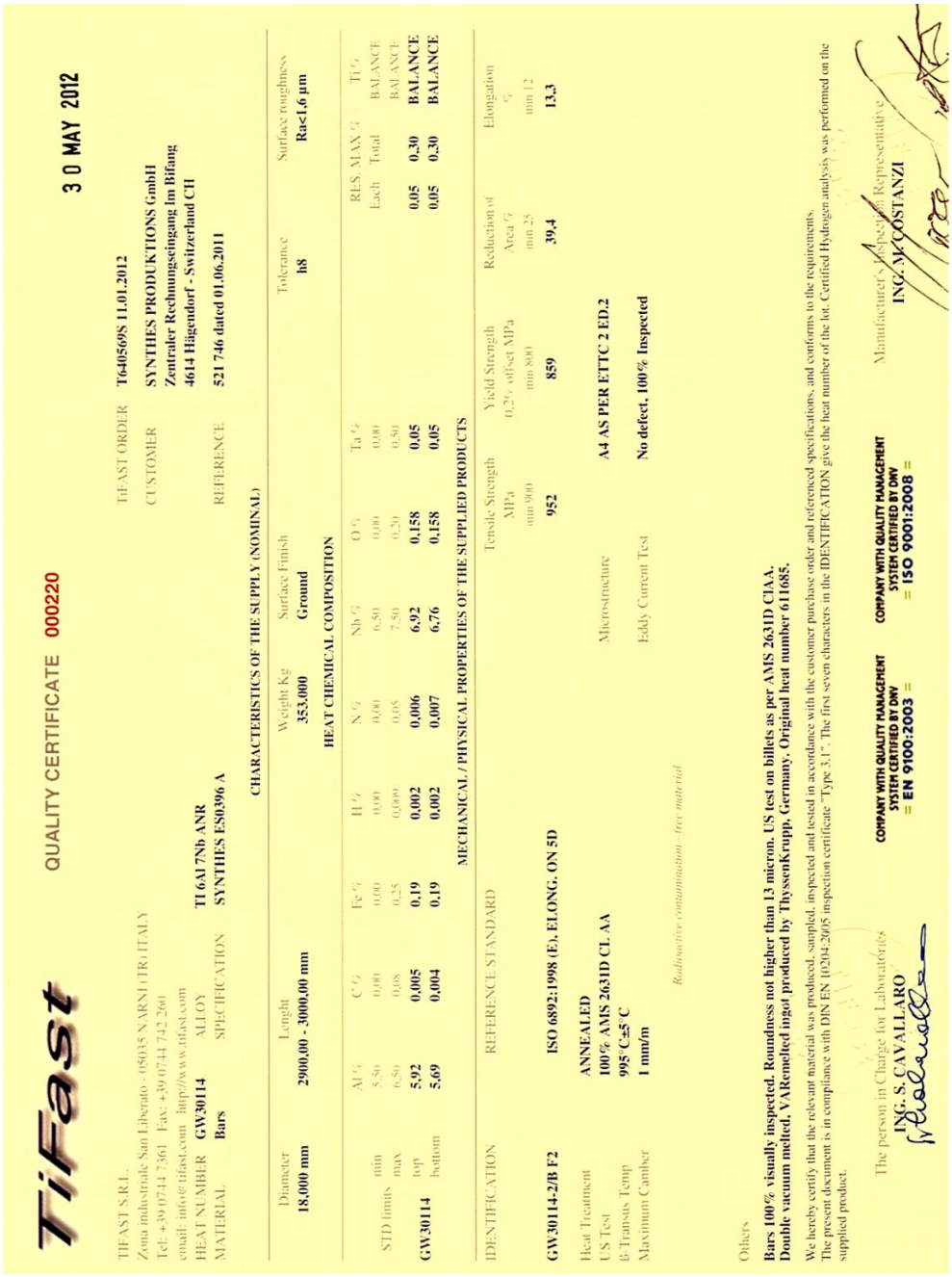

TiFast

QUALITY CERTIFICATE 000220

30 MAY 2012

TIFAST S.R.L.
Zona industriale San Liberato - 65035 NARNI (TR) ITALY
Tel. +39 0744 7361 Fax +39 0744 742 260
email: info@tifast.com http://www.tifast.com

HEAT NUMBER GW30114 ALLOY TI 6Al 7Nb ANR
MATERIAL Bars SPECIFICATION SYNTHES ES0396 A

TIFAST ORDER T6405698 11.01.2012
CUSTOMER SYNTHES PRODUKTIONS GmbH
Zentraler Rechnungseingang Im Bifang
4614 Hägendorf - Switzerland CH
REFERENCE 521 746 dated 01.06.2011

CHARACTERISTICS OF THE SUPPLY (NOMINAL)

Diameter	Lenght	Weight Kg	Surface Finish	Tolerance	Surface roughness
18.000 mm	2900,00 - 3000,00 mm	353.000	Ground	h8	Ra<1.6 µm

HEAT CHEMICAL COMPOSITION

		Al %	C %	Fe %	H %	N %	Nb %	O %	Ta %	RES. MAX % Each	RES. MAX % Total	Ti %
STD limits	min	5,50	0,00	0,00	0,00	0,00	6,50	0,00	0,00			BALANCE
	max	6,50	0,08	0,25	0,009	0,05	7,50	0,20	0,50			BALANCE
GW30114	top	5,92	0,005	0,19	0,002	0,006	6,92	0,158	0,05	0,05	0,30	BALANCE
	bottom	5,69	0,004	0,19	0,002	0,007	6,76	0,158	0,05	0,05	0,30	BALANCE

MECHANICAL / PHYSICAL PROPERTIES OF THE SUPPLIED PRODUCTS

IDENTIFICATION	REFERENCE STANDARD	Tensile Strength MPa min 900	Yield Strength 0,2% offset MPa min 800	Reduction of Area % min 25	Elongation % min 12
GW30114-2/B F2	ISO 6892:1998 (E), ELONG. ON 5D	952	859	39.4	13.3

Heat Treatment	ANNEALED
US Test	100% AMS 2631D CL AA
E-Transus Temp	995°C±5°C
Maximum Camber	1 mm/m
Microstructure	A4 AS PER ETTC 2 ED.2
Eddy Current Test	No defect. 100% Inspected

Radioactive contamination - free material

Others

Bars 100% visually inspected. Roundness not higher than 13 micron. US test on billets as per AMS 2631D CIAA.
Double vacuum melted, VARemelted ingot produced by ThyssenKrupp, Germany. Original heat number 611685.

We hereby certify that the relevant material was produced, sampled, inspected and tested in accordance with the customer purchase order and referenced specifications, and conforms to the requirements.
The present document is in compliance with DIN EN 10204:2005 inspection certificate "Type 3.1". The first seven characters in the IDENTIFICATION give the heat number of the lot. Certified Hydrogen analysis was performed on the supplied product.

The person in Charge for Laboratories
ING. S. CAVALLARO

COMPANY WITH QUALITY MANAGEMENT SYSTEM CERTIFIED BY DNV = EN 9100:2003 =

COMPANY WITH QUALITY MANAGEMENT SYSTEM CERTIFIED BY DNV = ISO 9001:2008 =

Manufacturer's Inspection Representative
ING. M. COSTANZI

Figure B.1 - Quality certificate of the Ti-6Al-7Nb titanium alloy used in the micro-cutting (chemical and mechanical properties).

TiFast

COMPANY WITH QUALITY MANAGEMENT SYSTEM CERTIFIED BY DNV = EN 9100:2003 =

COMPANY WITH QUALITY MANAGEMENT SYSTEM CERTIFIED BY DNV = ISO 9001:2008 =

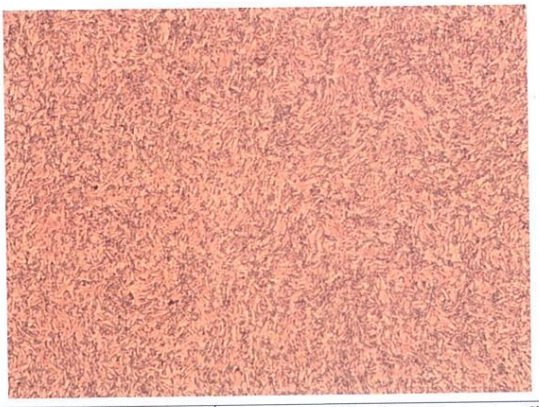

29 MAY 2012

Fig. N°	Material Identification	Nominal diameter Ø [mm]
1	GW30114-2/B F2	18

Structure composed by a fine dispersion of the α and β phases resulting from processing within the α-β field. No continuous α network at prior grain boundaries. No coarse, elongated α platelets. Inclusion free.

Section		Structure as per ETTC 2 Ed 2	Magnification
Transverse		A4	200×

The Person in charge for Laboratories	Manufacturer's Inspection Representative

Modello 116 rev 1 del 12-03-2012

Figure B.2 - Quality certificate of the Ti-6Al-7Nb titanium alloy used in the micro-cutting (metallography analysis).

ANNEX B

In this section is shown the results of the experimental tests.

B.1. Development of measurements techniques and analysis

B.1.1. Cutting Forces

Table B.1 - Thrust force in the orthogonal micro cutting.

Cutting speed (m/min)	Feed rate (µm/rev)	Spindle speed (rev)	Thrust force (N)			
			Maximum		Minimum	
			Average	Standard deviation	Average	Standard deviation
30	10	1,500	20.03	0.31	19.82	0.28
30	10	735	26.09	0.02	25.83	0.03
30	50	735	44.06	3.24	43.51	3.23
60	10	3,000	18.73	0.58	18.57	0.58
60	10	1,500	23.18	0.16	22.82	0.18
120	10	3,000	25.35	1.24	25.13	1.21
120	25	3,000	33.05	0.16	32.75	0.18
120	50	3,000	37.50	0.15	37.19	0.02

Table B.2 - Cutting force in the orthogonal micro cutting.

Cutting speed (m/min)	Feed rate (µm/rev)	Spindle speed (rev)	Cutting force (N)			
			Maximum		Minimum	
			Average	Standard deviation	Average	Standard deviation
30	10	1,500	23.18	0.52	22.49	0.53
30	10	735	27.68	0.09	26.64	0.07
30	50	735	83.16	1.33	82.23	1.27
60	10	3,000	20.36	0.57	19.88	0.62
60	10	1,500	25.46	0.05	24.27	0.20
120	10	3,000	25.62	1.19	24.95	1.15
120	25	3,000	49.12	0.51	48.05	0.46
120	50	3,000	81.07	0.24	80.30	0.17

B.1.2. Specific cutting energy

Table B.3 – Specific cutting energy in the orthogonal micro cutting.

Cutting speed (m/min)	Feed rate (µm/rev)	Spindle speed (rev)	Specific cutting energy (J/mm^3)	
			Average	Standard deviation
30	10	1,500	4.29	0.08
30	10	735	5.00	0.00
30	50	735	2.49	0.07
60	10	3,000	3.89	0.12
60	10	1,500	4.66	0.17
120	10	3,000	4.76	0.23
120	25	3,000	3.12	0.02
120	50	3,000	2.37	0.01

B.1.3. Friction coefficient

Table B.4 – Friction coefficient in the orthogonal micro cutting.

Cutting speed (m/min)	Feed rate (µm/rev)	Spindle speed (rev)	Friction coefficient	
			Average	Standard deviation
30	10	1,500	0.90	0.01
30	10	735	0.96	0.00
30	50	735	0.60	0.03
60	10	3,000	0.94	0.00
60	10	1,500	0.94	0.00
120	10	3,000	1.00	0.00
120	25	3,000	0.73	0.01
120	50	3,000	0.54	0.00

B.1.4. Temperature

Table B.5 – Temperature in the insert during the orthogonal micro cutting.

Cutting speed (m/min)	Feed rate (µm/rev)	Spindle speed (rev)	Temperature (ºC)	
			Average	Standard deviation
30	10	1,500	88.91	2.83
30	10	735	104.75	1.86
30	50	735	84.17	0.25
60	10	3,000	85.02	2.16
60	10	1,500	94.75	2.43
120	10	3,000	78.31	12.97
120	25	3,000	58.75	9.25
120	50	3,000	61.29	2.94

B.1.5. Chip

Table B.6 – Chip compression ratio and chip deformation in the orthogonal micro cutting.

Cutting speed (m/min)	Feed rate (µm/rev)	Spindle speed (rev)	Chip compression ratio		Chip deformation	
			Average	Standard deviation	Average	Standard deviation
30	10	1,500	2.34	0.03	2.57	0.02
30	10	735	2.47	0.08	2.68	0.07
30	50	735	1.71	0.03	2.10	0.02
60	10	3,000	2.25	0.11	2.50	0.09
60	10	1,500	2.26	0.04	2.50	0.03
120	10	3,000	2.10	0.03	2.38	0.02
120	25	3,000	1.67	0.03	2.07	0.02
120	50	3,000	1.58	0.02	2.01	0.01

B.1.6. Shear plane angle

Table B.7 – Shear plane angle in the orthogonal micro cutting.

Cutting speed (m/min)	Feed rate (µm/rev)	Spindle speed (rev)	Experimental shear plane angle (º)		Merchant shear plane angle (º)		Lee-Shaffer shear plane angle (º)	
			Average	Standard deviation	Average	Standard deviation	Average	Standard deviation
30	10	1,500	23.98	0.27	27.08	0.09	9.16	0.19
30	10	735	22.81	0.73	26.02	0.00	7.04	0.00
30	50	735	31.76	0.43	32.50	0.56	19.99	1.12
60	10	3,000	24.94	1.09	26.38	0.03	7.75	0.06
60	10	1,500	24.82	0.36	26.40	0.02	7.81	0.04
120	10	3,000	26.49	0.32	25.52	0.03	6.04	0.05
120	25	3,000	32.46	0.47	29.94	0.15	14.89	0.29
120	50	3,000	34.02	0.41	33.78	0.00	22.56	0.01

B.2. Influence of the HSM and MQL in the micro-cutting

B.2.1. Cutting Forces

Table B.8 – Shear plane angle in the orthogonal micro cutting.

Cutting speed (m/min)	Feed rate (µm/rev)	Colling	Thrust force (N)		Cutting force (N)	
			Average	Standard deviation	Average	Standard deviation
30	10	Dry	40.81	0.83	41.55	0.48
30	50	Dry	71.36	1.34	124.30	2.52
120	10	Dry	33.51	0.28	34.38	0.21
120	50	Dry	52.86	3.21	121.16	0.88
30	10	MQL	30.60	1.81	33.47	0.79
30	50	MQL	62.22	1.20	124.45	0.28
120	10	MQL	34.10	1.51	32.35	0.51
120	50	MQL	55.36	9.30	118.48	4.15

B.2.2. Specific cutting energy and Friction coefficient

Table B.9 – Specific cutting energy and Friction coefficient in the orthogonal micro cutting.

Cutting speed (m/min)	Feed rate (µm/rev)	Colling	Specific cutting energy (J/mm^3)		Friction coefficient	
			Average	Standard deviation	Average	Standard deviation
30	10	Dry	5.75	0.04	0.99	0.03
30	50	Dry	2.84	0.05	0.64	0.00
120	10	Dry	4.74	0.04	0.98	0.00
120	50	Dry	2.60	0.03	0.52	0.02
30	10	MQL	4.47	0.19	0.93	0.02
30	50	MQL	2.74	0.00	0.57	0.01
120	10	MQL	4.57	0.09	1.03	0.02
120	50	MQL	2.57	0.15	0.55	0.06

B.2.3. Shear plane angle

Table B.10 – Specific cutting energy and Friction coefficient in the orthogonal micro cutting.

Cutting speed (m/min)	Feed rate (µm/rev)	Colling	Lee-Shaffer shear plane angle (º)	
			Average	Standard deviation
30	10	Dry	6.39	0.80
30	50	Dry	18.39	0.05
120	10	Dry	6.66	0.09
120	50	Dry	23.63	1.10
30	10	MQL	8.05	0.65
30	50	MQL	21.25	0.40
120	10	MQL	5.04	0.48
120	50	MQL	22.40	2.64

B.2.4. Chips

Table B.11 – Chip compression in the orthogonal micro cutting.

Cutting speed (m/min)	Feed rate (µm/rev)	Colling	Chip compression	
			Average	Standard deviation
30	10	Dry	2.66	0.00
30	50	Dry	1.71	0.07
120	10	Dry	2.09	0.05
120	50	Dry	1.44	0.00
30	10	MQL	2.45	0.02
30	50	MQL	1.74	0.01
120	10	MQL	2.17	0.06
120	50	MQL	1.60	0.04

B.2.5. Surface roughness

Table B.12 – Surface roughness in the orthogonal micro cutting.

Cutting speed (m/min)	Feed rate (µm/rev)	Colling	R_a (µm)		R_t (µm)		R_z (µm)	
			Average	Standard deviation	Average	Standard deviation	Average	Standard deviation
30	10	Dry	0.176	0.018	0.863	0.254	1.282	0.443
30	50	Dry	0.115	0.001	0.725	0.046	1.306	0.338
120	10	Dry	0.078	0.006	0.569	0.107	1.179	0.564
120	50	Dry	0.048	0.007	0.374	0.093	0.576	0.232
30	10	MQL	0.162	0.074	0.975	0.148	1.529	0.249
30	50	MQL	0.158	0.011	0.929	0.049	1.475	0.356
120	10	MQL	0.305	0.233	1.522	0.300	3.396	0.651
120	50	MQL	0.096	0.000	0.750	0.102	0.828	0.262

B.2.6. Burr

Table B.11 – Burr in the orthogonal micro cutting.

Cutting speed (m/min)	Feed rate (µm/rev)	Colling	Burr (µm)	
			Average	Standard deviation
30	10	Dry	100.57	3.83
30	50	Dry	127.46	12.40
120	10	Dry	29.18	0.70
120	50	Dry	94.26	12.75
30	10	MQL	17.21	1.16
30	50	MQL	53.28	3.48
120	10	MQL	9.10	1.04
120	50	MQL	8.28	2.20

B.3. The micro-cutting in the finishing operation of biomaterial

B.3.1. F_x force

Table B.12 – F_x force in the micro cutting for flat insert.

Spindle Speed range (rpm)	Scale	Feed rate (μm/rev)	Depth of cut (μm)					
			25		50		100	
			Average	Standard deviation	Average	Standard deviation	Average	Standard deviation
0 - 1,000	Macro	25	16.86	2.76	24.13	2.08	30.09	4.13
		50	18.36	1.73	25.88	2.43	33.44	4.58
		100	21.62	3.08	29.15	3.95	40.69	5.31
	Transition	25	18.65	1.23	23.67	1.95	31.55	2.56
		50	21.16	3.25	25.48	2.20	34.21	2.50
		100	21.93	1.70	29.58	2.49	39.79	2.98
	Meso	25	22.29	0.60	25.17	0.71	32.49	0.93
		50	21.32	0.57	26.83	0.78	34.39	1.02
		100	23.22	0.67	29.69	0.95	41.77	1.30
1.000 - 2,000	Macro	25	16.52	2.37	24.97	2.45	34.74	3.65
		50	18.26	2.73	25.00	3.73	39.21	4.21
		100	21.36	2.24	31.57	4.76	45.89	7.20
	Transition	25	17.30	1.89	22.32	1.68	29.28	2.02
		50	17.56	1.16	24.02	2.05	32.88	2.57
		100	20.96	1.73	28.92	2.52	39.99	3.50
	Meso	25	17.81	0.50	23.09	0.71	30.43	0.91
		50	18.68	0.55	24.54	0.76	33.05	1.04
		100	21.46	0.67	28.48	0.95	39.31	1.31
2,000 - 3,000	Macro	25	18.27	2.60	28.80	3.11	36.52	5.65
		50	17.71	1.52	29.08	5.19	42.78	4.63
		100	25.61	3.24	36.68	3.47	47.79	6.97
	Transition	25	13.55	1.63	21.90	1.77	29.01	1.53
		50	16.46	1.61	24.47	1.89	34.38	2.53
		100	20.86	1.63	30.26	2.78	42.86	3.43
	Meso	25	21.33	0.49	22.20	0.67	30.21	0.90
		50	18.04	0.64	24.25	0.75	32.81	1.03
		100	20.73	0.66	28.65	0.95	39.09	1.31

Table B.13 – F_x force in the micro cutting for chip-breaker insert.

Spindle Speed range (rpm)	Scale	Feed rate (μm/rev)	Depth of cut (μm)					
			25		50		100	
			Average	Standard deviation	Average	Standard deviation	Average	Standard deviation
0 - 1,000	Macro	25	6.77	1.27	8.69	1.36	11.48	1.51
		50	6.98	1.22	9.19	1.37	12.48	1.51
		100	8.21	1.06	10.93	1.47	15.01	1.76
	Transition	25	7.25	1.19	9.12	1.58	11.72	1.72
		50	7.17	1.22	9.57	1.59	12.56	1.78
		100	8.24	1.06	11.08	1.65	14.91	1.98
	Meso	25	5.98	0.10	7.14	0.04	9.26	0.00
		50	5.69	0.07	7.83	0.31	10.20	0.11
		100	6.66	0.02	9.49	0.10	12.96	0.16
1.000 - 2,000	Macro	25	6.43	1.09	8.98	1.46	11.90	1.62
		50	7.13	1.18	9.59	1.38	13.25	1.72
		100	8.19	1.20	11.66	1.76	16.50	2.04
	Transition	25	6.15	0.88	8.27	1.29	10.74	1.53
		50	6.68	1.03	8.70	1.43	11.92	1.60
		100	7.76	1.05	10.45	1.43	14.38	1.84
	Meso	25	5.03	0.18	7.06	0.01	9.09	0.01
		50	5.50	0.07	7.64	0.08	10.45	0.30
		100	6.72	0.03	9.54	0.04	13.06	0.17
2,000 - 3,000	Macro	25	5.88	0.82	8.75	1.47	12.87	2.03
		50	6.28	0.75	9.96	1.52	14.38	2.26
		100	8.21	0.95	12.18	1.97	16.32	2.39
	Transition	25	5.46	1.29	8.43	1.26	10.57	1.46
		50	6.23	1.10	8.84	1.27	11.81	1.62
		100	7.78	1.08	10.43	1.44	14.76	2.03
	Meso	25	4.89	0.37	6.73	0.01	8.97	0.03
		50	6.36	1.77	7.50	0.15	10.28	0.15
		100	6.63	0.31	9.48	0.03	13.08	0.03

Table B.14 – F_x force in the micro cutting for dual negative insert.

Spindle Speed range (rpm)	Scale	Feed rate (μm/rev)	Depth of cut (μm)					
			25		50		100	
			Average	Standard deviation	Average	Standard deviation	Average	Standard deviation
0 - 1,000	Macro	25	15.93	0.46	21.31	0.30	27.68	1.06
		50	16.98	0.02	23.40	0.42	31.28	1.29
		100	20.67	0.13	28.43	0.40	39.24	1.42
	Transition	25	15.86	1.47	19.85	1.58	26.43	2.08
		50	15.77	1.15	21.64	1.58	29.35	2.01
		100	18.92	1.41	26.37	1.84	36.48	2.36
	Meso	25	17.37	1.39	18.58	1.20	23.39	1.13
		50	16.14	1.19	19.76	1.14	24.72	1.09
		100	17.57	1.10	22.98	1.30	31.49	1.80
1.000 - 2,000	Macro	25	15.84	0.70	20.60	0.17	27.93	1.42
		50	16.90	0.13	24.07	1.81	32.39	1.81
		100	20.85	0.45	29.73	0.50	41.65	1.93
	Transition	25	15.79	0.63	18.91	1.60	26.02	1.62
		50	15.05	1.72	20.77	1.66	28.88	2.29
		100	18.33	1.45	25.63	1.93	36.35	2.58
	Meso	25	14.21	1.08	17.89	2.00	23.29	2.25
		50	14.34	1.43	19.01	1.82	25.46	1.79
		100	16.59	1.17	22.73	1.90	32.93	2.26
2,000 - 3,000	Macro	25	14.38	0.72	22.45	0.54	30.19	1.65
		50	17.05	0.09	25.37	0.40	34.68	1.57
		100	22.39	0.35	30.88	0.25	41.49	1.41
	Transition	25	13.01	2.01	18.28	1.65	25.09	2.13
		50	14.40	1.30	20.72	1.73	29.43	2.52
		100	18.02	1.82	26.19	2.27	38.20	3.03
	Meso	25	14.53	1.37	17.55	1.61	23.30	1.27
		50	13.72	1.42	18.97	1.43	25.78	1.56
		100	16.55	0.95	23.36	1.11	33.99	1.49

B.3.2. F_y force

Table B.15 – F_y force in the micro cutting for flat insert.

Spindle Speed range (rpm)	Scale	Feed rate (µm/rev)	Depth of cut (µm)					
			25		50		100	
			Average	Standard deviation	Average	Standard deviation	Average	Standard deviation
0 - 1,000	Macro	25	2.75	0.48	5.49	0.74	11.05	1.38
		50	2.44	0.43	5.53	0.73	11.87	1.49
		100	2.31	0.37	5.66	0.73	13.18	1.80
	Transition	25	2.76	0.22	5.58	0.71	11.54	1.49
		50	2.62	0.37	5.55	0.75	11.75	1.17
		100	2.30	0.33	5.63	0.72	12.36	1.16
	Meso	25	4.01	0.16	5.59	0.26	10.94	0.51
		50	2.91	0.13	5.33	0.28	10.54	0.55
		100	2.32	0.13	5.10	0.29	10.01	0.61
1.000 - 2,000	Macro	25	2.61	0.39	5.91	1.01	12.62	2.22
		50	2.51	0.33	5.95	0.95	13.35	2.23
		100	2.21	0.39	6.35	1.02	14.77	2.40
	Transition	25	2.63	0.53	5.38	0.58	10.83	0.96
		50	2.36	0.27	5.29	0.65	11.65	1.07
		100	2.20	0.38	5.55	0.63	12.72	1.42
	Meso	25	2.95	0.13	5.50	0.23	10.91	0.46
		50	2.58	0.12	5.38	0.25	11.27	0.52
		100	1.99	0.12	5.27	0.28	12.14	0.59
2,000 - 3,000	Macro	25	2.50	0.43	6.36	0.85	13.48	2.18
		50	2.42	0.47	6.77	0.86	14.00	2.34
		100	2.52	0.35	6.90	0.72	14.76	2.08
	Transition	25	1.73	0.53	5.41	0.63	8.14	1.50
		50	2.29	0.42	5.44	0.55	12.27	1.13
		100	2.30	0.42	5.75	0.75	13.86	1.07
	Meso	25	4.79	0.10	5.36	0.23	11.41	0.45
		50	2.48	0.11	5.31	0.25	11.49	0.52
		100	2.05	0.12	5.19	0.28	12.65	0.64

Table B.16 – F_y force in the micro cutting for chip-breaker insert.

Spindle Speed range (rpm)	Scale	Feed rate (μm/rev)	Depth of cut (μm)					
			25		50		100	
			Average	Standard deviation	Average	Standard deviation	Average	Standard deviation
0 - 1,000	Macro	25	1.02	0.21	1.96	0.27	4.25	0.57
		50	0.96	0.19	2.08	0.37	4.59	0.60
		100	0.96	0.16	2.34	0.37	5.22	0.69
	Transition	25	1.07	0.16	2.07	0.42	4.12	0.56
		50	0.98	0.17	2.18	0.45	4.46	0.60
		100	0.96	0.12	2.27	0.48	5.02	0.68
	Meso	25	1.59	0.28	2.59	0.46	5.11	0.75
		50	1.32	0.22	2.76	0.39	5.50	0.67
		100	1.33	0.23	2.87	0.21	6.09	0.14
1.000 - 2,000	Macro	25	1.05	0.25	2.17	0.40	4.48	0.64
		50	0.97	0.20	2.13	0.41	4.93	0.67
		100	1.00	0.20	2.39	0.46	5.74	0.75
	Transition	25	0.96	0.17	1.90	0.34	3.85	0.54
		50	0.93	0.15	1.93	0.36	4.37	0.54
		100	0.92	0.13	2.20	0.36	5.39	0.77
	Meso	25	1.30	0.37	2.31	0.32	4.61	0.63
		50	1.17	0.21	2.45	0.32	5.15	0.36
		100	1.23	0.20	2.77	0.23	5.90	0.13
2,000 - 3,000	Macro	25	0.88	0.12	2.18	0.45	4.90	0.80
		50	0.87	0.12	2.34	0.42	5.33	0.88
		100	0.95	0.17	2.60	0.48	6.01	0.90
	Transition	25	0.79	0.09	1.91	0.34	3.89	0.52
		50	0.79	0.12	2.03	0.37	4.37	0.60
		100	0.89	0.14	2.21	0.32	5.69	0.44
	Meso	25	0.96	0.22	2.29	0.34	4.48	0.63
		50	1.12	0.23	2.47	0.31	5.23	0.63
		100	1.18	0.18	2.85	0.31	6.40	0.52

Table B.17 – F_y force in the micro cutting for dual negative insert.

Spindle Speed range (rpm)	Scale	Feed rate (µm/rev)	Depth of cut (µm)					
			25		50		100	
			Average	Standard deviation	Average	Standard deviation	Average	Standard deviation
0 - 1,000	Macro	25	2.47	0.13	5.24	0.56	10.19	1.03
		50	2.50	0.27	5.37	0.48	11.12	1.08
		100	2.59	0.21	5.91	0.56	12.98	1.28
	Transition	25	2.91	0.43	5.04	0.36	10.57	0.99
		50	2.52	0.16	5.37	0.44	11.39	0.95
		100	2.56	0.16	6.05	0.34	13.29	1.04
	Meso	25	3.98	0.33	4.88	0.20	9.58	0.22
		50	2.98	0.20	5.09	0.21	9.69	0.17
		100	2.68	0.17	5.27	0.14	10.47	0.37
1.000 - 2,000	Macro	25	2.52	0.44	4.95	0.43	10.34	1.17
		50	2.43	0.28	5.54	1.08	11.40	1.28
		100	2.41	0.42	5.91	0.58	13.63	1.87
	Transition	25	2.91	0.31	4.92	0.45	10.25	1.09
		50	2.32	0.23	5.12	0.40	11.13	1.04
		100	2.51	0.13	5.87	0.35	13.03	1.06
	Meso	25	2.55	0.00	4.68	0.26	9.67	0.61
		50	2.36	0.11	4.85	0.36	10.02	0.54
		100	2.37	0.18	5.24	0.42	11.72	0.54
2,000 - 3,000	Macro	25	2.11	0.21	5.43	0.60	10.96	1.16
		50	2.11	0.14	5.46	0.61	11.58	1.32
		100	2.41	0.46	5.88	0.84	12.80	1.88
	Transition	25	2.19	0.59	4.79	0.51	10.07	1.08
		50	2.21	0.30	5.03	0.43	11.18	1.12
		100	2.44	0.17	5.78	0.44	14.18	1.17
	Meso	25	2.41	0.58	4.79	0.33	9.93	0.26
		50	2.36	0.28	4.90	0.25	10.30	0.41
		100	2.33	0.20	5.37	0.12	13.35	0.34

B.3.3. F_z force

Table B.18 – F_z force in the micro cutting for flat insert.

Spindle Speed range (rpm)	Scale	Feed rate (μm/rev)	Depth of cut (μm)					
			25		50		100	
			Average	Standard deviation	Average	Standard deviation	Average	Standard deviation
0 - 1,000	Macro	25	9.13	0.39	12.56	0.23	18.39	0.19
		50	9.93	0.36	15.02	0.25	23.29	0.04
		100	13.35	0.24	20.49	0.38	33.81	0.71
	Transition	25	9.53	0.21	13.03	0.46	19.53	1.09
		50	10.58	0.19	15.85	0.54	24.53	0.72
		100	13.70	0.30	21.40	0.71	34.24	0.54
	Meso	25	11.92	0.69	13.83	0.89	19.96	1.37
		50	12.19	0.78	16.31	1.19	23.78	1.84
		100	14.49	1.01	21.11	1.65	31.36	2.72
1,000 - 2,000	Macro	25	8.57	1.48	11.47	0.43	17.49	0.60
		50	9.07	0.40	14.16	0.67	22.78	1.08
		100	11.88	0.29	20.38	0.54	32.43	2.16
	Transition	25	8.77	0.27	11.79	0.39	17.26	0.43
		50	9.50	0.11	14.22	0.63	22.23	0.29
		100	12.48	0.03	20.03	0.35	32.55	0.99
	Meso	25	4.94	0.53	9.52	0.80	17.57	1.26
		50	6.82	0.67	12.60	1.06	23.05	1.76
		100	11.17	0.95	19.35	1.58	34.62	2.68
2,000 - 3,000	Macro	25	7.46	0.43	11.77	0.39	17.24	0.96
		50	9.43	1.31	14.49	0.56	23.64	0.62
		100	12.60	0.23	20.45	0.50	33.46	0.68
	Transition	25	7.01	1.28	10.63	0.38	15.75	0.01
		50	8.52	0.33	13.17	0.33	19.57	2.63
		100	10.51	1.44	19.00	0.48	30.48	2.61
	Meso	25	2.14	0.46	11.21	0.72	16.90	1.15
		50	9.32	0.61	13.69	0.96	21.38	1.58
		100	11.77	0.87	18.52	1.46	31.97	2.51

Table B.19 – F_z force in the micro cutting for chip-breaker insert.

Spindle Speed range (rpm)	Scale	Feed rate (μm/rev)	Depth of cut (μm)					
			25		50		100	
			Average	Standard deviation	Average	Standard deviation	Average	Standard deviation
0 - 1,000	Macro	25	1.96	0.21	2.85	0.20	4.44	0.24
		50	2.33	0.21	3.61	0.23	6.03	0.20
		100	3.33	0.17	5.45	0.20	9.44	0.24
	Transition	25	2.07	0.18	2.92	0.17	4.51	0.18
		50	2.44	0.21	3.85	0.14	6.28	0.20
		100	3.47	0.15	5.65	0.13	9.72	0.22
	Meso	25	6.94	0.19	8.88	0.39	13.66	1.14
		50	7.82	0.53	11.94	1.19	18.40	1.57
		100	10.13	0.61	16.52	1.62	27.23	3.85
1,000 - 2,000	Macro	25	1.77	0.23	2.59	0.19	4.07	0.23
		50	2.15	0.17	3.27	0.21	5.76	0.25
		100	3.14	0.15	5.17	0.32	9.37	0.20
	Transition	25	1.82	0.15	2.62	0.16	4.10	0.11
		50	2.27	0.13	3.32	0.46	5.93	0.14
		100	3.21	0.07	5.35	0.08	9.22	0.71
	Meso	25	5.30	0.33	8.02	0.54	12.62	1.05
		50	6.69	0.27	10.60	0.80	17.56	2.05
		100	9.46	0.61	15.77	1.54	26.77	3.61
2,000 - 3,000	Macro	25	1.53	0.10	2.39	0.18	3.95	0.25
		50	1.89	0.11	3.35	0.17	5.92	0.26
		100	3.00	0.12	5.37	0.21	9.69	0.30
	Transition	25	1.56	0.08	2.43	0.11	3.81	0.08
		50	1.96	0.11	3.28	0.07	5.52	0.08
		100	2.93	0.07	5.10	0.04	9.52	0.23
	Meso	25	4.64	0.11	7.16	0.48	11.46	0.98
		50	6.14	0.25	9.60	0.73	15.83	1.32
		100	8.66	0.58	14.58	1.19	25.14	2.73

Table B.20 – F_z force in the micro cutting for dual negative insert.

Spindle Speed range (rpm)	Scale	Feed rate (μm/rev)	Depth of cut (μm)					
			25		50		100	
			Average	Standard deviation	Average	Standard deviation	Average	Standard deviation
0 - 1,000	Macro	25	9.57	0.56	13.55	0.01	19.64	0.33
		50	10.83	0.14	16.41	0.04	25.24	0.45
		100	14.61	0.14	22.83	0.06	37.29	0.46
	Transition	25	12.60	1.01	16.63	1.12	25.02	1.16
		50	13.33	0.73	20.11	1.07	31.34	1.39
		100	17.49	0.83	27.70	1.28	45.14	1.81
	Meso	25	19.14	1.75	21.63	1.83	31.59	2.27
		50	18.81	1.64	25.14	1.75	37.85	2.45
		100	21.83	1.62	32.18	1.83	55.53	3.50
1,000 - 2,000	Macro	25	8.72	0.23	11.91	0.08	17.94	0.51
		50	9.81	0.06	15.41	1.05	23.80	0.70
		100	13.34	0.35	21.82	0.10	37.24	1.50
	Transition	25	11.61	0.60	14.58	0.94	22.08	0.94
		50	11.80	1.13	17.73	0.97	28.09	1.36
		100	15.73	0.72	24.93	0.98	41.11	1.38
	Meso	25	13.36	0.87	18.19	1.81	27.13	2.42
		50	14.57	1.19	21.35	1.73	33.59	1.89
		100	18.24	1.00	28.85	1.70	50.69	2.20
2,000 - 3,000	Macro	25	7.03	0.07	11.94	0.18	18.03	0.80
		50	8.96	0.23	15.06	0.11	24.25	0.90
		100	13.23	0.36	21.62	0.44	35.78	1.26
	Transition	25	8.62	1.49	12.79	0.84	19.28	1.13
		50	10.14	0.69	15.93	0.84	25.61	1.27
		100	13.85	1.04	22.92	0.98	40.39	1.74
	Meso	25	12.96	1.81	16.56	1.45	24.70	1.33
		50	12.96	1.24	19.54	1.36	30.79	1.72
		100	17.11	0.75	26.85	0.98	47.77	1.66

B.3.4. R_a surface roughness

Table B.21 – R_a surface roughness in the micro cutting for flat insert.

Spindle Speed range (rpm)	Scale	Feed rate (µm/rev)	Depth of cut (µm)					
			25		50		100	
			Average	Standard deviation	Average	Standard deviation	Average	Standard deviation
0 - 1,000	Macro	25	0.21	0.01	0.21	0.00	0.21	0.01
		50	0.30	0.05	0.31	0.05	0.31	0.06
		100	0.87	0.08	0.84	0.03	0.79	0.02
	Transition	25	0.20	0.01	0.21	0.02	0.22	0.03
		50	0.39	0.01	0.35	0.01	0.32	0.02
		100	0.79	0.10	0.96	0.01	0.81	0.10
	Meso	25	0.20	0.02	0.21	0.02	0.23	0.02
		50	0.29	0.03	0.30	0.03	0.32	0.03
		100	0.81	0.09	0.81	0.08	0.83	0.07
1,000 - 2,000	Macro	25	0.22	0.01	0.21	0.01	0.21	0.01
		50	0.31	0.04	0.32	0.05	0.36	0.04
		100	0.81	0.04	0.82	0.06	0.82	0.04
	Transition	25	0.20	0.02	0.21	0.02	0.23	0.04
		50	0.30	0.06	0.34	0.10	0.34	0.00
		100	0.78	0.11	0.77	0.12	0.87	0.07
	Meso	25	0.20	0.02	0.21	0.02	0.23	0.02
		50	0.29	0.03	0.29	0.03	0.31	0.03
		100	0.81	0.08	0.81	0.07	0.82	0.09
2,000 - 3,000	Macro	25	0.22	0.02	0.21	0.01	0.22	0.02
		50	0.30	0.04	0.34	0.03	0.31	0.04
		100	0.79	0.04	0.73	0.10	0.75	0.05
	Transition	25	0.22	0.02	0.21	0.02	0.20	0.03
		50	0.30	0.04	0.30	0.06	0.31	0.08
		100	0.81	0.09	0.77	0.09	0.76	0.08
	Meso	25	0.20	0.02	0.20	0.02	0.22	0.02
		50	0.29	0.03	0.29	0.03	0.30	0.03
		100	0.80	0.07	0.80	0.09	0.81	0.08

Table B.22 – R_a surface roughness in the micro cutting for chip-breaker insert.

Spindle Speed range (rpm)	Scale	Feed rate (μm/rev)	Depth of cut (μm)					
			25		50		100	
			Average	Standard deviation	Average	Standard deviation	Average	Standard deviation
0 - 1,000	Macro	25	0.18	0.02	0.19	0.03	0.19	0.02
		50	0.32	0.04	0.29	0.03	0.32	0.03
		100	0.82	0.07	0.82	0.07	0.89	0.08
	Transition	25	0.19	0.02	0.21	0.03	0.21	0.04
		50	0.29	0.07	0.38	0.13	0.28	0.03
		100	0.90	0.07	0.88	0.06	0.94	0.08
	Meso	25	0.20	0.02	0.18	0.01	0.19	0.02
		50	0.31	0.01	0.31	0.01	0.29	0.03
		100	0.87	0.06	0.85	0.06	0.86	0.04
1,000 - 2,000	Macro	25	0.19	0.02	0.21	0.01	0.20	0.02
		50	0.32	0.03	0.31	0.03	0.30	0.03
		100	0.83	0.08	0.85	0.09	0.83	0.07
	Transition	25	0.21	0.03	0.20	0.02	0.21	0.02
		50	0.28	0.03	0.38	0.04	0.31	0.03
		100	0.82	0.08	0.83	0.07	0.84	0.08
	Meso	25	0.20	0.01	0.24	0.02	0.22	0.01
		50	0.32	0.01	0.29	0.04	0.30	0.03
		100	0.88	0.07	0.84	0.08	0.85	0.06
2,000 - 3,000	Macro	25	0.27	0.03	0.21	0.03	0.23	0.02
		50	0.32	0.04	0.33	0.04	0.33	0.02
		100	0.84	0.07	0.82	0.10	0.80	0.08
	Transition	25	0.25	0.02	0.23	0.03	0.23	0.03
		50	0.31	0.04	0.27	0.02	0.31	0.04
		100	0.83	0.08	0.82	0.08	0.81	0.08
	Meso	25	0.27	0.03	0.24	0.02	0.26	0.03
		50	0.33	0.04	0.33	0.04	0.30	0.03
		100	0.85	0.05	0.87	0.03	0.86	0.08

Table B.23 – R_a surface roughness in the micro cutting for dual negative insert.

Spindle Speed range (rpm)	Scale	Feed rate (μm/rev)	Depth of cut (μm)					
			25		50		100	
			Average	Standard deviation	Average	Standard deviation	Average	Standard deviation
0 - 1,000	Macro	25	0.19	0.00	0.20	0.01	0.19	0.01
		50	0.33	0.01	0.34	0.02	0.31	0.02
		100	0.87	0.12	0.93	0.03	0.91	0.13
	Transition	25	0.20	0.03	0.19	0.02	0.20	0.02
		50	0.32	0.03	0.30	0.04	0.31	0.03
		100	0.93	0.10	0.91	0.08	0.93	0.07
	Meso	25	0.26	0.02	0.24	0.01	0.25	0.02
		50	0.33	0.04	0.34	0.02	0.39	0.04
		100	0.85	0.09	0.84	0.09	0.77	0.11
1,000 - 2,000	Macro	25	0.20	0.01	0.20	0.00	0.19	0.00
		50	0.32	0.04	0.35	0.03	0.31	0.04
		100	0.90	0.07	0.92	0.09	0.87	0.09
	Transition	25	0.21	0.02	0.23	0.02	0.21	0.03
		50	0.34	0.02	0.35	0.00	0.37	0.01
		100	0.99	0.02	0.92	0.11	0.94	0.09
	Meso	25	0.20	0.03	0.21	0.00	0.25	0.02
		50	0.30	0.02	0.31	0.01	0.34	0.03
		100	0.87	0.14	0.87	0.12	0.82	0.01
2,000 - 3,000	Macro	25	0.24	0.05	0.22	0.01	0.18	0.02
		50	0.36	0.05	0.30	0.04	0.30	0.06
		100	0.88	0.11	0.90	0.07	0.89	0.10
	Transition	25	0.24	0.01	0.25	0.03	0.21	0.02
		50	0.33	0.02	0.32	0.04	0.33	0.05
		100	0.95	0.10	0.93	0.10	0.93	0.10
	Meso	25	0.26	0.05	0.22	0.02	0.25	0.04
		50	0.32	0.05	0.31	0.05	0.31	0.06
		100	0.90	0.10	0.85	0.12	0.87	0.11

B.3.5. R_z surface roughness

Table B.24 – R_z surface roughness in the micro cutting for flat insert.

Spindle Speed range (rpm)	Scale	Feed rate (μm/rev)	Depth of cut (μm)					
			25		50		100	
			Average	Standard deviation	Average	Standard deviation	Average	Standard deviation
0 - 1,000	Macro	25	1.67	0.11	1.67	0.12	1.81	0.23
		50	1.91	0.26	2.06	0.23	1.90	0.28
		100	4.18	0.30	4.16	0.26	3.96	0.12
	Transition	25	1.59	0.09	1.62	0.17	1.68	0.13
		50	1.99	0.33	2.27	0.01	2.14	0.11
		100	3.68	0.47	4.53	0.07	4.40	0.61
	Meso	25	1.66	0.10	1.69	0.15	1.79	0.18
		50	1.95	0.10	1.99	0.14	2.10	0.23
		100	3.88	0.16	3.93	0.31	4.05	0.40
1,000 - 2,000	Macro	25	1.65	0.18	1.67	0.17	1.66	0.19
		50	1.97	0.25	2.01	0.21	2.16	0.24
		100	3.98	0.27	4.01	0.09	4.06	0.16
	Transition	25	1.60	0.06	1.59	0.18	1.87	0.16
		50	1.74	0.40	2.19	0.43	2.04	0.01
		100	3.79	0.49	3.66	0.72	4.18	0.23
	Meso	25	1.67	0.10	1.68	0.15	1.75	0.18
		50	1.95	0.10	1.97	0.14	2.04	0.22
		100	3.85	0.15	3.88	0.31	3.96	0.40
2,000 - 3,000	Macro	25	1.82	0.21	1.57	0.12	1.83	0.18
		50	2.54	0.39	2.27	0.28	2.07	0.18
		100	3.93	0.15	3.80	0.30	3.65	0.27
	Transition	25	1.77	0.20	1.66	0.18	1.58	0.25
		50	1.83	0.24	2.06	0.31	2.20	0.40
		100	3.88	0.39	3.93	0.51	3.87	0.30
	Meso	25	1.73	0.10	1.73	0.16	1.74	0.17
		50	1.99	0.10	1.99	0.14	2.01	0.22
		100	3.84	0.15	3.84	0.31	3.87	0.39

Table B.25 – R_z surface roughness in the micro cutting for chip-breaker insert.

Spindle Speed range (rpm)	Scale	Feed rate (µm/rev)	Depth of cut (µm)					
			25		50		100	
			Average	Standard deviation	Average	Standard deviation	Average	Standard deviation
0 - 1,000	Macro	25	1.30	0.18	1.22	0.12	1.36	0.14
		50	2.04	0.30	1.75	0.25	1.85	0.24
		100	4.04	0.19	3.99	0.24	4.08	0.22
	Transition	25	1.39	0.11	1.49	0.17	1.38	0.23
		50	1.62	0.13	1.64	0.15	1.85	0.23
		100	4.10	0.30	3.99	0.21	4.48	0.63
	Meso	25	1.39	0.10	1.39	0.18	1.47	0.06
		50	1.68	0.18	1.79	0.09	1.80	0.22
		100	4.04	0.50	3.91	0.32	4.12	0.25
1,000 - 2,000	Macro	25	1.40	0.15	1.65	0.27	1.40	0.17
		50	1.94	0.22	1.79	0.33	1.85	0.17
		100	3.98	0.21	4.08	0.28	4.11	0.18
	Transition	25	1.42	0.15	1.42	0.20	1.48	0.22
		50	1.80	0.24	1.85	0.32	1.71	0.22
		100	3.95	0.17	3.92	0.23	3.93	0.32
	Meso	25	1.43	0.21	1.62	0.13	1.55	0.12
		50	1.92	0.08	1.75	0.17	1.91	0.15
		100	4.16	0.17	4.02	0.30	4.14	0.25
2,000 - 3,000	Macro	25	1.77	0.21	1.50	0.18	1.56	0.16
		50	1.92	0.28	1.93	0.29	1.97	0.22
		100	4.21	0.28	4.22	0.20	3.96	0.25
	Transition	25	1.62	0.24	1.57	0.14	1.52	0.23
		50	1.96	0.28	1.92	0.40	1.88	0.29
		100	4.03	0.28	3.98	0.17	4.05	0.33
	Meso	25	1.77	0.19	1.68	0.10	1.74	0.21
		50	1.86	0.41	1.97	0.35	1.83	0.24
		100	4.01	0.38	4.27	0.31	4.13	0.41

Table B.26 – R_z surface roughness in the micro cutting for dual negative insert.

Spindle Speed range (rpm)	Scale	Feed rate (μm/rev)	Depth of cut (μm)					
			25		50		100	
			Average	Standard deviation	Average	Standard deviation	Average	Standard deviation
0 - 1,000	Macro	25	1.44	0.03	1.51	0.02	1.43	0.09
		50	1.98	0.08	2.37	0.23	2.04	0.09
		100	3.96	0.30	4.27	0.09	4.22	0.39
	Transition	25	1.65	0.23	1.72	0.18	1.49	0.21
		50	1.97	0.19	2.11	0.11	1.65	0.17
		100	4.17	0.26	4.17	0.20	4.12	0.17
	Meso	25	1.75	0.34	1.94	0.45	1.71	0.18
		50	2.30	0.20	2.17	0.12	2.55	0.20
		100	4.27	0.31	4.06	0.19	4.06	0.35
1,000 - 2,000	Macro	25	1.59	0.10	1.47	0.14	1.58	0.03
		50	1.86	0.00	2.05	0.06	1.90	0.06
		100	4.47	0.10	4.18	0.21	4.12	0.06
	Transition	25	1.71	0.15	1.60	0.15	1.59	0.11
		50	2.01	0.16	1.91	0.12	2.29	0.07
		100	4.20	0.30	4.11	0.23	4.13	0.16
	Meso	25	1.50	0.27	1.56	0.02	1.99	0.11
		50	2.16	0.08	1.97	0.10	2.31	0.22
		100	4.05	0.17	3.91	0.23	3.90	0.13
2,000 - 3,000	Macro	25	1.60	0.14	1.49	0.05	1.33	0.12
		50	2.13	0.25	2.05	0.05	1.78	0.21
		100	3.94	0.31	4.34	0.05	4.09	0.47
	Transition	25	1.81	0.07	1.74	0.15	1.56	0.14
		50	2.07	0.17	1.96	0.13	1.96	0.21
		100	4.27	0.21	4.21	0.18	4.13	0.14
	Meso	25	1.90	0.22	1.67	0.08	2.10	0.33
		50	1.98	0.27	2.01	0.15	1.95	0.34
		100	3.91	0.52	4.04	0.38	4.06	0.21

B.3.6. Deflection

Table B.27 – Minimum deflection of workpiece during the micro cutting with flat insert.

Spindle Speed range (rpm)	Scale	Feed rate (µm/rev)	Depth of cut (µm)					
			25		50		100	
			Average	Standard deviation	Average	Standard deviation	Average	Standard deviation
0 - 1,000	Macro	25	0.53	0.03	0.75	0.03	1.18	0.05
		50	0.55	0.02	0.79	0.10	1.46	0.05
		100	0.68	0.03	1.06	0.03	1.99	0.07
	Transition	25	0.08	0.00	0.13	0.01	0.26	0.02
		50	0.09	0.00	0.15	0.01	0.39	0.04
		100	0.11	0.00	0.21	0.01	0.65	0.04
	Meso	25	1.03	0.10	1.90	0.11	5.86	0.32
		50	1.15	0.04	2.67	0.14	12.15	0.38
		100	1.54	0.08	3.97	0.10	30.71	0.87
1,000 - 2,000	Macro	25	0.55	0.09	0.78	0.03	1.30	0.04
		50	0.55	0.04	0.88	0.02	1.63	0.04
		100	0.64	0.02	1.22	0.06	2.29	0.05
	Transition	25	0.04	0.00	0.06	0.00	0.12	0.01
		50	0.04	0.00	0.07	0.00	0.17	0.01
		100	0.05	0.00	0.10	0.01	0.28	0.02
	Meso	25	0.75	0.07	3.10	0.16	7.80	0.94
		50	2.43	0.12	5.40	0.65	11.35	1.02
		100	5.78	0.69	10.00	0.90	18.45	0.92
2,000 - 3,000	Macro	25	0.32	0.02	0.52	0.03	0.83	0.03
		50	0.38	0.04	0.60	0.03	0.00	0.00
		100	0.47	0.03	0.75	0.03	0.01	0.00
	Transition	25	0.02	0.00	0.03	0.00	0.07	0.01
		50	0.02	0.00	0.04	0.00	0.10	0.01
		100	0.03	0.00	0.06	0.00	0.15	0.01
	Meso	25	0.38	0.01	0.52	0.02	1.30	0.02
		50	0.35	0.01	0.69	0.02	2.20	0.04
		100	0.44	0.02	0.97	0.01	17.45	1.57

Table B.28 – Minimum deflection of workpiece during the micro cutting with chip-breaker insert.

Spindle Speed range (rpm)	Scale	Feed rate (μm/rev)	Depth of cut (μm)					
			25		50		100	
			Average	Standard deviation	Average	Standard deviation	Average	Standard deviation
0 - 1,000	Macro	25	0.17	0.02	0.25	0.04	0.41	0.05
		50	0.20	0.03	0.29	0.04	0.50	0.06
		100	0.24	0.03	0.36	0.05	0.65	0.03
	Transition	25	0.03	0.00	0.05	0.01	0.09	0.01
		50	0.04	0.01	0.06	0.01	0.14	0.01
		100	0.04	0.01	0.07	0.01	0.23	0.02
	Meso	25	0.28	0.02	0.54	0.05	1.80	0.33
		50	0.32	0.02	0.77	0.08	4.16	0.97
		100	0.45	0.02	1.31	0.15	12.85	3.61
1,000 - 2,000	Macro	25	0.18	0.03	0.27	0.04	0.43	0.05
		50	0.21	0.03	0.31	0.04	0.53	0.06
		100	0.24	0.03	0.40	0.05	0.75	0.08
	Transition	25	0.01	0.00	0.02	0.00	0.04	0.00
		50	0.02	0.00	0.03	0.00	0.06	0.01
		100	0.02	0.00	0.03	0.00	0.11	0.02
	Meso	25	0.13	0.01	0.28	0.02	0.78	0.12
		50	0.18	0.01	0.38	0.03	1.60	0.30
		100	0.25	0.01	0.62	0.06	3.27	0.09
2,000 - 3,000	Macro	25	0.11	0.01	0.16	0.02	0.27	0.04
		50	0.12	0.01	0.19	0.03	0.33	0.05
		100	0.14	0.02	0.23	0.03	0.41	0.04
	Transition	25	0.01	0.00	0.01	0.00	0.02	0.00
		50	0.01	0.00	0.01	0.00	0.03	0.00
		100	0.01	0.00	0.02	0.00	0.05	0.00
	Meso	25	0.09	0.01	0.16	0.01	0.41	0.06
		50	0.11	0.01	0.21	0.01	0.77	0.12
		100	0.14	0.01	0.34	0.02	1.64	0.23

Table B.29 – Minimum deflection of workpiece during the micro cutting with dual negative insert.

Spindle Speed range (rpm)	Scale	Feed rate (μm/rev)	Depth of cut (μm)					
			25		50		100	
			Average	Standard deviation	Average	Standard deviation	Average	Standard deviation
0 - 1,000	Macro	25	0.43	0.02	0.64	0.02	0.99	0.03
		50	0.48	0.02	0.74	0.01	1.26	0.04
		100	0.60	0.02	0.95	0.01	1.78	0.04
	Transition	25	0.07	0.01	0.11	0.01	0.22	0.03
		50	0.07	0.01	0.13	0.01	0.34	0.04
		100	0.09	0.01	0.19	0.02	0.59	0.08
	Meso	25	0.75	0.07	1.49	0.20	5.62	0.77
		50	0.89	0.10	2.18	0.24	13.95	0.65
		100	1.25	0.12	3.55	0.46	25.17	1.52
1,000 - 2,000	Macro	25	0.44	0.02	0.62	0.01	1.00	0.04
		50	0.46	0.01	0.77	0.05	1.30	0.04
		100	0.60	0.02	0.99	0.01	1.88	0.06
	Transition	25	0.04	0.00	0.05	0.01	0.11	0.01
		50	0.04	0.00	0.06	0.01	0.15	0.02
		100	0.05	0.00	0.09	0.01	0.25	0.03
	Meso	25	0.33	0.02	0.70	0.08	1.75	0.16
		50	0.45	0.05	0.93	0.10	3.45	0.26
		100	0.60	0.04	1.47	0.16	8.18	0.64
2,000 - 3,000	Macro	25	0.25	0.00	0.40	0.01	0.63	0.02
		50	0.29	0.00	0.47	0.01	0.80	0.02
		100	0.39	0.01	0.61	0.01	1.07	0.03
	Transition	25	0.02	0.00	0.03	0.00	0.06	0.01
		50	0.02	0.00	0.04	0.00	0.08	0.01
		100	0.03	0.00	0.05	0.00	0.14	0.02
	Meso	25	0.21	0.02	0.42	0.05	1.21	0.12
		50	0.26	0.02	0.57	0.06	2.34	0.08
		100	0.37	0.03	0.86	0.10	5.19	0.17

B.3.7. Vibration in the time domain for the axial direction

Table B.30 – Vibration in the axial direction in the micro cutting for flat insert.

Spindle Speed range (rpm)	Scale	Feed rate (μm/rev)	Depth of cut (μm)					
			25		50		100	
			Average	Standard deviation	Average	Standard deviation	Average	Standard deviation
0 - 1,000	Macro	25	8.35	0.84	8.79	0.02	9.11	0.06
		50	9.26	0.31	10.06	0.33	11.06	0.71
		100	11.15	1.12	12.81	1.22	16.04	1.01
	Transition	25	7.68	0.17	8.18	0.15	13.34	1.23
		50	8.04	0.22	9.21	0.08	10.52	0.46
		100	9.41	0.20	11.04	0.55	13.81	0.17
	Meso	25	8.13	0.73	7.71	0.85	6.82	0.68
		50	7.17	0.72	7.40	0.67	7.80	0.86
		100	6.44	0.71	7.95	0.80	10.93	0.98
1,000 - 2,000	Macro	25	8.82	0.03	9.37	0.16	10.46	0.32
		50	9.54	0.28	10.32	0.30	11.55	0.01
		100	11.20	0.29	12.84	0.10	21.11	5.11
	Transition	25	8.46	0.20	8.61	0.15	9.25	0.10
		50	9.04	0.21	9.53	0.11	11.55	0.28
		100	10.41	0.19	12.13	0.18	17.27	0.39
	Meso	25	6.07	0.67	6.07	0.61	6.04	0.54
		50	5.74	0.52	6.39	0.70	7.64	0.76
		100	6.25	0.63	8.19	0.74	12.03	1.32
2,000 - 3,000	Macro	25	10.06	0.36	10.52	0.49	12.39	0.63
		50	11.54	0.78	12.81	1.28	16.65	0.05
		100	13.69	0.42	29.29	1.75	30.84	3.60
	Transition	25	9.03	0.39	9.45	0.20	10.40	0.21
		50	9.87	0.46	10.43	0.41	12.62	1.64
		100	11.17	0.30	12.54	0.21	16.58	1.05
	Meso	25	7.16	0.72	8.01	0.72	8.78	0.97
		50	8.15	0.90	9.08	0.91	10.64	0.96
		100	9.41	0.85	10.43	1.15	19.80	1.98

Table B.31 – Vibration in the axial direction in the micro cutting for chip-breaker insert.

Spindle Speed range (rpm)	Scale	Feed rate (µm/rev)	Depth of cut (µm)					
			25		50		100	
			Average	Standard deviation	Average	Standard deviation	Average	Standard deviation
0 - 1,000	Macro	25	7.64	0.19	7.93	0.24	8.23	0.00
		50	8.16	0.11	8.47	0.35	9.17	0.48
		100	8.89	0.45	9.72	0.34	12.53	0.90
	Transition	25	7.39	0.17	7.46	0.10	7.90	0.08
		50	7.78	0.09	7.84	0.07	10.07	0.85
		100	8.60	0.31	9.46	0.39	12.93	1.13
	Meso	25	8.59	0.08	8.33	0.83	8.88	0.24
		50	8.52	0.18	8.76	0.54	9.77	0.87
		100	8.70	0.02	9.50	0.21	9.96	0.04
1,000 - 2,000	Macro	25	8.85	0.98	9.16	0.92	9.91	0.81
		50	9.03	0.75	9.99	0.62	11.06	0.14
		100	10.10	0.72	11.14	0.89	12.76	1.11
	Transition	25	8.04	0.37	8.30	0.32	8.76	0.44
		50	8.46	0.36	8.87	0.32	9.74	0.68
		100	8.78	0.79	10.77	0.64	12.31	0.77
	Meso	25	8.50	0.03	9.35	0.61	9.10	0.63
		50	8.83	0.15	8.55	0.71	10.04	0.93
		100	9.30	0.39	10.67	1.26	14.01	1.54
2,000 - 3,000	Macro	25	8.22	0.35	9.22	0.94	9.74	1.05
		50	8.59	0.36	9.71	0.68	11.30	0.31
		100	9.93	0.60	12.69	0.64	20.22	1.59
	Transition	25	9.20	0.23	9.30	0.56	10.02	0.62
		50	9.50	0.57	10.03	0.52	10.60	0.37
		100	10.16	0.47	11.35	0.35	7.26	0.04
	Meso	25	8.35	0.02	8.66	0.18	8.96	0.32
		50	8.88	0.13	9.10	0.16	10.56	0.95
		100	9.49	0.05	10.55	0.15	12.38	1.24

Table B.32 – Vibration in the axial direction in the micro cutting for dual negative insert.

Spindle Speed range (rpm)	Scale	Feed rate (µm/rev)	Depth of cut (µm)					
			25		50		100	
			Average	Standard deviation	Average	Standard deviation	Average	Standard deviation
0 - 1,000	Macro	25	12.33	0.96	12.69	0.84	13.71	0.93
		50	13.28	0.40	14.67	0.65	18.24	0.62
		100	15.44	0.26	19.47	0.06	28.31	0.96
	Transition	25	11.13	0.43	11.16	0.48	11.17	0.23
		50	11.60	0.78	11.64	1.16	11.66	0.67
		100	11.40	0.42	12.86	1.07	12.65	0.10
	Meso	25	10.79	1.19	9.05	0.91	10.02	0.18
		50	9.47	0.85	9.34	1.03	10.04	0.02
		100	8.60	0.49	9.32	0.14	10.44	0.58
1,000 - 2,000	Macro	25	12.24	0.34	12.77	0.36	13.32	0.30
		50	13.05	0.65	13.77	0.50	14.89	0.65
		100	14.39	0.93	16.17	1.11	21.90	0.43
	Transition	25	12.95	0.27	11.85	2.33	13.82	0.05
		50	13.50	0.14	14.54	0.36	17.34	1.61
		100	14.84	0.21	16.76	0.80	22.31	2.10
	Meso	25	9.21	0.92	9.76	0.88	9.76	1.07
		50	9.17	1.01	10.32	1.03	10.27	0.92
		100	9.19	0.83	14.10	1.55	15.45	1.54
2,000 - 3,000	Macro	25	13.73	1.75	13.60	0.26	15.37	0.20
		50	12.98	0.25	15.31	0.66	21.17	0.42
		100	16.54	0.47	25.82	0.16	46.82	1.65
	Transition	25	12.53	0.20	12.75	0.38	13.59	0.09
		50	12.65	0.25	13.42	0.91	15.22	0.09
		100	14.30	0.25	15.88	0.47	23.35	2.84
	Meso	25	10.66	1.00	11.04	0.02	12.68	0.27
		50	11.54	0.26	13.00	0.56	15.40	1.08
		100	12.58	1.26	15.30	1.53	19.61	1.77

B.3.8. Vibration in the time domain for the tangential direction

Table B.33 – Vibration in the tangential direction in the micro cutting for flat insert.

Spindle Speed range (rpm)	Scale	Feed rate (µm/rev)	Depth of cut (µm)					
			25		50		100	
			Average	Standard deviation	Average	Standard deviation	Average	Standard deviation
0 - 1,000	Macro	25	10.76	0.45	11.92	0.14	14.53	0.49
		50	11.81	0.37	14.66	0.46	19.14	1.04
		100	16.29	1.61	20.56	1.20	27.22	2.54
	Transition	25	13.16	1.78	12.97	1.44	14.68	1.57
		50	12.64	1.54	15.31	2.08	22.03	2.08
		100	15.86	1.95	21.86	3.28	30.97	5.24
	Meso	25	9.67	1.06	9.97	1.00	8.88	0.71
		50	9.92	0.79	12.45	1.37	9.72	0.97
		100	9.59	0.96	10.80	0.86	9.69	1.07
1,000 - 2,000	Macro	25	12.65	0.46	14.00	0.78	18.37	0.64
		50	15.03	0.65	17.89	2.91	28.08	0.79
		100	22.38	1.57	35.07	2.19	60.01	3.54
	Transition	25	10.92	0.27	12.17	0.16	14.53	0.38
		50	11.81	0.23	14.04	0.06	17.59	0.30
		100	14.91	0.09	18.84	0.58	23.22	2.21
	Meso	25	8.67	0.87	9.09	0.73	10.91	1.20
		50	8.79	0.97	11.47	1.15	17.81	1.42
		100	11.96	0.96	19.16	2.11	34.54	3.45
2,000 - 3,000	Macro	25	12.03	0.22	14.53	0.70	19.62	0.77
		50	14.75	0.85	22.55	0.49	44.20	2.35
		100	25.67	1.58	56.14	0.96	125.16	7.64
	Transition	25	13.86	1.03	17.25	0.51	21.86	1.33
		50	17.35	1.10	23.37	1.43	31.43	1.64
		100	25.42	1.29	37.40	1.42	51.72	0.52
	Meso	25	11.73	0.94	11.78	1.30	14.25	1.42
		50	12.03	1.20	14.22	1.14	19.83	2.18
		100	14.26	1.57	18.06	1.81	96.75	7.74

Table B.34 – Vibration in the tangential direction in the micro cutting for chip-breaker insert.

Spindle Speed range (rpm)	Scale	Feed rate (μm/rev)	Depth of cut (μm)					
			25		50		100	
			Average	Standard deviation	Average	Standard deviation	Average	Standard deviation
0 - 1,000	Macro	25	10.19	0.17	11.22	0.16	12.96	0.16
		50	11.35	0.11	12.80	0.28	15.08	0.37
		100	13.48	0.96	15.54	0.36	21.42	0.26
	Transition	25	9.68	0.23	10.06	0.13	11.24	0.19
		50	9.85	0.12	11.52	0.21	12.95	0.21
		100	12.05	0.26	13.59	0.41	15.67	0.16
	Meso	25	11.21	0.02	13.39	0.19	18.54	1.85
		50	14.50	0.21	16.35	1.07	27.19	1.57
		100	17.05	1.14	17.84	0.37	21.88	1.01
1,000 - 2,000	Macro	25	10.35	0.26	11.42	0.33	13.61	0.84
		50	11.73	0.47	14.62	0.93	20.41	0.32
		100	16.80	0.71	21.77	0.28	37.14	1.64
	Transition	25	10.23	0.17	11.02	0.08	12.68	0.20
		50	11.30	0.31	12.29	1.13	14.86	0.15
		100	13.17	0.23	15.98	0.80	21.87	0.55
	Meso	25	10.58	0.06	12.61	0.19	15.57	0.08
		50	12.30	1.35	15.35	0.06	20.29	0.04
		100	16.26	0.54	21.01	0.45	31.35	1.35
2,000 - 3,000	Macro	25	11.07	0.19	12.54	0.21	14.64	0.24
		50	13.49	0.19	17.74	0.21	25.73	0.94
		100	20.56	0.78	32.66	1.48	75.02	9.27
	Transition	25	10.59	0.77	12.12	0.31	14.06	0.18
		50	12.58	0.41	14.93	0.37	18.94	0.49
		100	16.33	0.44	21.50	0.56	34.21	0.91
	Meso	25	10.42	0.83	12.39	0.14	15.05	0.01
		50	12.83	0.20	16.01	0.19	21.19	0.84
		100	16.83	0.36	22.90	0.66	32.70	1.25

Table B.35 – Vibration in the tangential direction in the micro cutting for dual negative insert.

Spindle Speed range (rpm)	Scale	Feed rate (µm/rev)	Depth of cut (µm)					
			25		50		100	
			Average	Standard deviation	Average	Standard deviation	Average	Standard deviation
0 - 1,000	Macro	25	8.99	0.53	9.51	0.55	10.37	0.94
		50	9.48	0.50	10.37	0.89	11.91	1.13
		100	9.86	1.35	12.70	1.30	15.89	1.79
	Transition	25	9.85	1.28	10.23	0.82	10.91	0.47
		50	9.99	1.16	11.09	1.17	12.39	0.86
		100	10.68	1.30	13.01	1.12	16.48	1.81
	Meso	25	11.32	0.59	11.46	0.38	13.12	0.99
		50	11.38	0.58	13.19	1.37	14.21	0.14
		100	12.23	0.60	13.56	0.25	18.38	0.96
1,000 - 2,000	Macro	25	10.33	0.45	10.30	0.30	11.70	0.56
		50	10.48	0.58	12.03	0.99	16.62	1.87
		100	11.95	1.02	17.73	2.50	37.24	5.18
	Transition	25	10.39	0.59	10.42	0.72	11.13	0.97
		50	10.55	0.83	11.52	0.56	13.07	0.15
		100	11.89	0.42	13.84	0.18	18.90	0.50
	Meso	25	11.71	0.94	11.94	1.31	12.32	1.23
		50	11.68	1.17	12.32	0.99	14.57	1.60
		100	11.73	1.29	14.60	1.46	18.75	1.50
2,000 - 3,000	Macro	25	11.30	0.90	15.69	2.02	20.12	2.64
		50	14.51	1.52	23.54	3.32	49.10	0.14
		100	21.91	3.31	59.30	0.15	118.93	3.38
	Transition	25	10.50	1.05	11.08	1.34	12.17	1.97
		50	11.25	0.90	11.83	1.36	14.72	2.26
		100	12.76	0.44	18.54	1.85	23.51	3.31
	Meso	25	10.49	0.26	11.52	0.17	12.57	1.01
		50	11.15	0.24	12.43	1.37	15.40	0.31
		100	13.53	1.71	15.19	0.19	19.32	2.98

ANNEX C

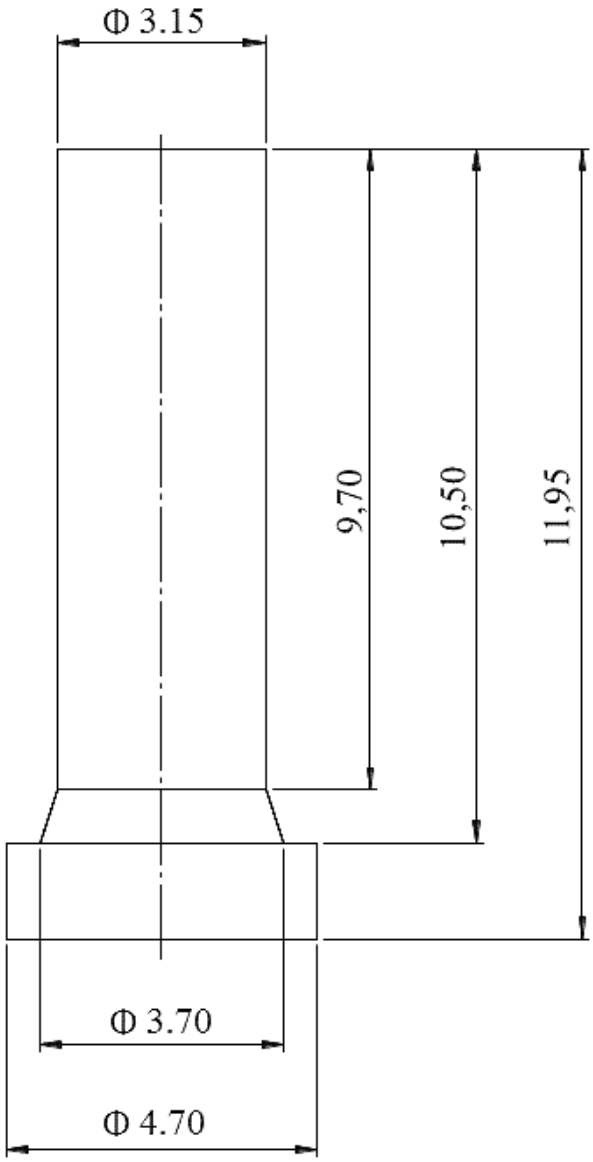

Figure C.1 – Details of workpiece used in the biocorrosion tests (Geometry 1).

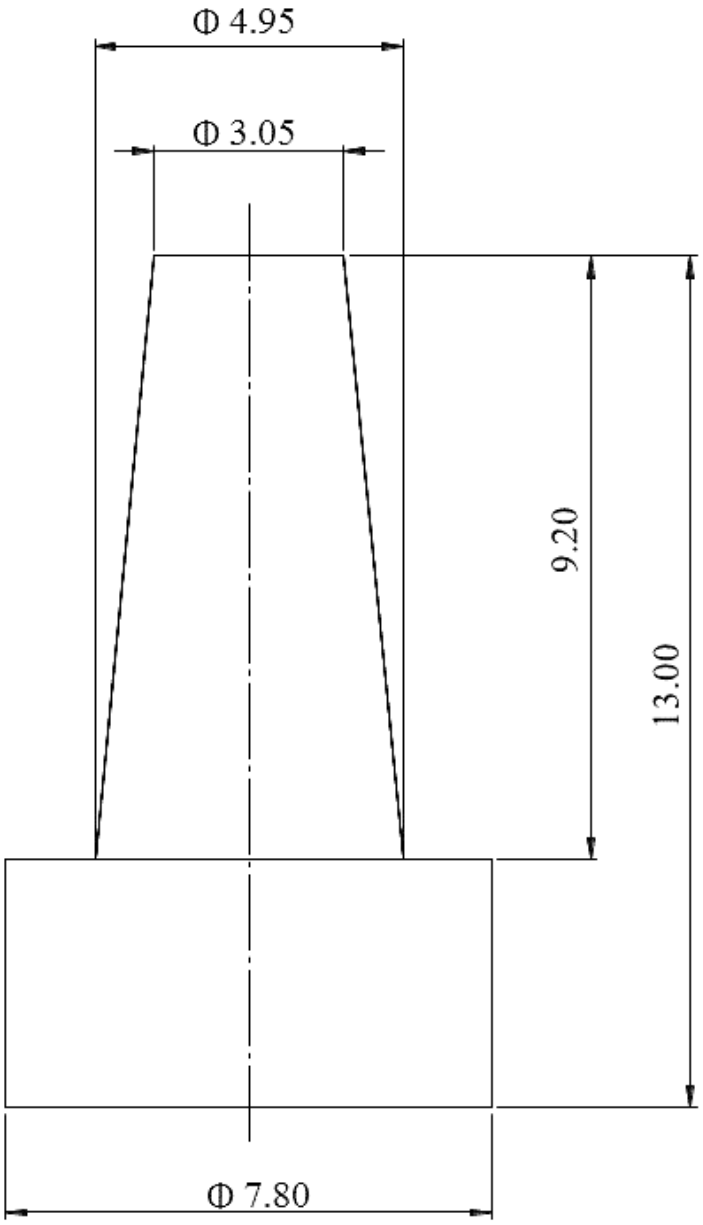

Figure C.2 – Details of workpiece used in the biocorrosion tests (Geometry 2).

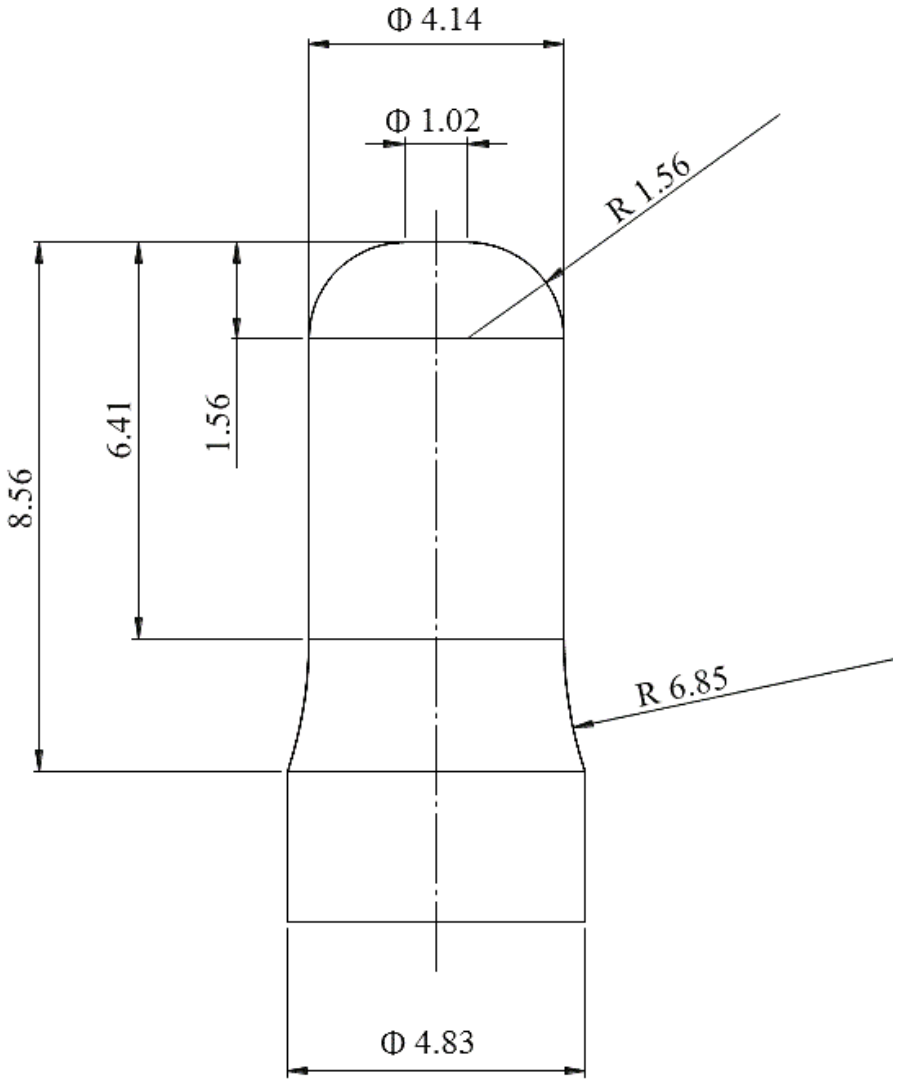

Figure C.3 – Details of workpiece used in the biocorrosion tests (Geometry 3).

ANNEX D

In this Annex is showed the list of publication developed during the doctoral course in scientific journals, book, and conference.

D.1. Articles in Scientific Journals

D.1.1. Monitoring and processing signal applied in machining processes – A review

Authors: C.H. Lauro; L.C. Brandão; D. Baldo; R.A. Reis; J.P. Davim

Journal: Measurement, V.58, 2014, p. 73 – 86.

Abstract: In machining processes several phenomena occur during material cutting. These phenomena can affect the production through the reduction of quality or accuracy, or by increasing costs (tools, materials, time). Thus, an understanding of machining phenomena is needed not only to define the cutting parameters for maximizing production, but also to ensure worker safety. An easy way to identify these phenomena is by monitoring machining processes, such as the measurement of cutting force, temperature and vibration. The acquired signal can have information about tool life, quality of cutting and defects in the workpiece. This review paper discusses the first steps involved in choosing and defining various techniques that may be used to monitor machining processes. Furthermore, this paper also outlines the techniques to acquire and process the signals of the monitoring processes. Hence, the objective of this paper is to help the reader understand the procedures for monitoring machining processes, and define methods, parameters, targets and other factors involved in doing so.

D.1.2. Surface integrity in the micromachining: a review

Authors: C. H. Lauro; L. C. Brandão; T.H. Panzera; J.P. Davim

Journal: Review on Advanced Material Science. Vol. 40, 2015, p. 227 - 234

Abstract: Increasingly, the manufacturing industry is concerned to produce the components with the great quality. This quality is correlated with desired surface integrity, accuracy of dimensions, burrs, and other defects in machining. Among these aspects, the surface integrity of the machined components can be complex to manage because it shows a stochastic behaviour or requires special equipment for measuring. Thus, the studies on surface integrity are necessary to understand the surface integrity phenomena and ensure the desired quality. However, if lower values for surface integrity are desired, the micromachining can be a solution because it exhibits closest matches the desired range. This paper shows a review about the surface integrity in conventional machining, but its main purpose is to discuss the results of the literature and the advantage of the surface integrity when the micromachining process is used.

D.1.3. Analysis of behaviour biocompatible titanium alloy (Ti-6Al-7Nb) in the micro-cutting

Authors: C. H. Lauro; S.L.M. Ribeiro Filho, L.C. Brandão; J.P. Davim

Journal: Measurement. Vol. 96, 2016, p. 529-540

Abstract: Among the several processes employed to manufacture components with reduced dimensions, the cutting in micro-scale is one of the most used in modern industries. Although the micro-cutting has been studied, there are still gaps about the process to be analysed. The comprehension of micro-cutting has great importance mainly in the biomedical industry, for instance, for the manufacturing of dental implants. In order to ensure patient safety, it was researched the behaviour of the Ti-6Al-7Nb titanium alloy during micro-cutting used for biomedical applications. For that, it was developed an orthogonal micro-cutting with the variation of the cutting speed, feed rate, and spindle speed. The monitoring and signals processing technique employed in this study, allowed observe the influence of the ploughing

effect in the chip, cutting forces, specific cutting energy, friction coefficient, temperature, and shear plane angle.

D.2. Chapter in Scientific Books

D.2.1. Quality in the Machining Characteristics and Techniques to Obtain Good Results

Authors: C.H. Lauro; L.C. Brandão; S.M. Ribeiro Filho; J.P. Davim

Book: Manufacturing Engineering: New Research ISBN: 978-1-63463-396-3

Abstract: To obtain great results in the machining of new materials, the manufacture industry required development of tools and techniques. Enhanced knowledge of these tools and techniques can offer a decreasing of cost, time, and risk to operator. This chapter debates the quality of the machined surface, the aspects and characteristics to analyse the desired quality. Furthermore, it presents some developments (tool and techniques) applied in the machining process to obtain the quality of surface.

D.2.2. Finite Element Method in Machining Processes: A Review

Authors: C.H. Lauro; L.C. Brandão; S.M. Ribeiro Filho; R.A.F. Valente; J.P. Davim

Book: Modern Manufacturing Engineering ISBN: 978-3-319-20151-1

Abstract: An ecological production and low cost is the target of several industries. Increasingly, the product development is critical stage to obtain a great quality and fair price. This stage will define shapes and parameters that will able to reduce wastes and improve the product. However, the expense of prototypes also should be reduced, because, in general, the prototypes are more expensive that final product. The use of finite element method (FEM) can avoid much tests that reduce number of prototypes, and consequently the project cost. In the machining processes simulation, several cutting conditions can be reproduced to define the best tool and parameters in function of analyzed forces, stress, damages and others. This paper debates the use of FEM in the machining processes, shows some

researches and indicates the main attributes to develop simulation studies for conventional machining and micromachining.

D.2.3. Design of Experiments - Statistical and Artificial Intelligence Analysis for the Improvement of Machining Processes: A Review

Authors: C.H. Lauro; R.B.D. Pereira; L.C. Brandão; J.P. Davim

Book: Design of Experiments in Production Engineering ISBN: 978-3-319-23837-1

Abstract: The modern industry needs that its manufacture process to be fast, efficient, low cost, ecologic, and other. It occurs because many consumers require that the products have great quality and a fair price. Furthermore, in sometimes, the industry has the sale price imposes by client. Thus, the industry develops news techniques, process, tools, and other to attain this goal. However, these new developments require great studies to obtain the best condition and avoid that become more a waste. The Statistical or Artificial Intelligence (AI) Analysis are great ways to understand the new developments and obtain the best conditions. This review chapter presents the techniques (Statistical and AI) that were applied to plan and analyse the machining processes. Aim of this chapter is to argue the planning and analysis importance in researches, as well as help researchers to choose a technique and define their machining experiments, optimising the time, material and other means.

D.3. Article in Conference

D.3.1. Analysis of the tool wear influence in the micro-cutting in the Ti-6Al-7Nb titanium alloy

Authors: C. H. Lauro, S. L. M. Ribeiro Filho, D. Baldo, D. Carou, L. C. Brandão, J. P. Davim

Conference: IX National Congress of Mechanical Engineering, Fortaleza - Brazil

Abstract: Several studies have been developed for the micro-cutting processes; however, many gaps still should be filled, mainly in the manufacturing of components that required great accuracy, like the dental implants. These studies gained importance due to the new materials that are developed to satisfy or improve the characteristics of their applications, for example, the density or the biocompatibility. This study analysed the behaviour of the

Ti-6Al-7Nb titanium alloy when employed the micro-cutting process using a tool with the flank wear of end tool live. A simplified way was employed to study this influence, the analysis of chip. A tool wear influence was observed, which caused a worsening in the analysed parameters.